ON THE BLAST INITIATION OF GASEOUS DETONATIONS

by

K. Ramamurthi

A thesis submitted to the Faculty of Graduate
Studies and Research in partial fulfillment
of the requirements for the degree of
Doctor of Philosophy

Department of Mechanical Engineering
McGill University
Montreal, Quebec
Canada

November 1976

TABLE OF CONTENTS

ABSTRACT

A phenomenological theory for blast initiation of gaseous detonations is developed by introducing the concept of the detonation kernel in analogy to the concept of the flame kernel used in the flame ignition theory. The critical size of the detonation kernel is obtained by equating the effects of the source energy and combustion energy on shock motion. It is shown that the detonation kernel theory gives good estimates for the minimum energy necessary for direct initiation of gaseous detonations. The propagation and limit characteristics are also shown to be closely related to the initiation behaviour and to be well predicted by the detonation kernel theory.

Experiments conducted with different explosive gas mixtures reveal a profound influence of the confinement on the initiation process. The explosion length (R_0) is found to be capable of identifying the geometry of initiation in the different experiments, i.e., for $R_0 >$ the characteristic source dimension L the geometry of initiation is governed by the confinement whilst for $R_0 < L$ the initiation geometry is characterized by the geometry of the source. The explosion length for a given explosive gas mixture is also found to be equivalent in the different geometries of initiation.

RESUME

Le concept de centre (kernel) de détonation est utilisé
en analogie avec le centre d'allumage de la théorie de l'ignition de
flamme pour développer une théorie phénoménologique sur l'initiation de
détonations en phase gazeuse par onde de choc.   On obtient la
dimension critique du centre de détonation en égalant l'énergie de
combustion à l'énergie de la source qui entretiennent effectivement
le choc.   La théorie du centre de détonation permet d'estimer d'une
manière satisfaisante l'énergie minimum nécessaire pour l'initiation
directe des détonations en phase gazeuse.   Cette théorie prédit
adéquatement les paramètres charactérisant la propagation et les limites
et démontre que ces derniers sont étroitement liés au comportement de
l'initiation.

Des expériences réalisées dans divers mélanges explosifs
gazeux montrent une influence marquée du confinement sur le processus
de l'initiation.   On démontre que la longueur charactéristique
d'explosion R_o permet d'identifier la géométrie d'initiation dans
différentes expériences, c'est-à-dire, si R_o est plus grand que la
dimension L charactéristique de la source, le confinement gouverne la
géométrie de l'initiation, alors que si $R_o < L$, la géométrie de la source
charactérise la géométrie de l'initiation.   On trouve que, pour un
mélange explosif gazeux donné, les différentes géométries d'initiation
ont des longueurs charactéristiques d'explosion équivalentes.

ACKNOWLEDGEMENTS

LIST OF SYMBOLS

A, B	numerical constants
C	local speed of sound; also specific heat of gases and capcitance of the condensers
C_0	speed of sound in the undisturbed medium
D	characteristic dimension
$\frac{D}{Dt}$	substantial derivative
E	activation energy
E_s	blast energy released by the source
e	internal energy
F	function
f	dimensionless pressure defined as $p/\rho_0 \dot{R}_s^2$
I	energy integral defined by Eq. 5.4 of Chapter 3
I_0	constant
i	current
j	numerical constant denoting wave symmetry; $j=0$ for planar, $j=1$ for cylindrical, and $j=2$ for spherical
k	constant
k_j	numerical constant which is 1, 2π and 4π in the planar, cylindrical and spherical geometries respectively
$\mathcal{L}$	gap between the electrodes
L	volumetric heat loss rate; also inductance of the electrical circuit; also characteristic dimension of igniter
l	height of the cylindrical chamber
M	third body in exothermic recombination reactions
M_s	shock Mach number

γ — specific heat ratio

δ — distance travelled by the shock front during the induction time; hydrodynamic thickness in Eq. 10.3 of Chapter 3

ε — perturbation parameter

Δ — non-dimensional induction zone thickness

$\frac{\partial [\,]}{\partial x}$ — partial differentiation with respect to x

η — $1/M_s^2$

θ — shock decay coefficient defined by Eq. A.2.23; also constant of integration in Eq. A.2

ξ — similarity coordinate r/R_s

ρ — density

τ — induction time

τ_D — duration of electrical discharge

τ_p — duration of electrical discharge up to the attainment of the peak average power

ϕ — dimensionless particle velocity ($u/\dot{R}_s$); also tube diameter and the detonation cell exit angle

χ — $\dot{R}_s^2/2$

ψ — dimensionless density ratio (ρ/ρ_0); detonation cell entrance angle

Ω — resistance in ohms

ω — angular frequency

Subscripts and superscripts

$(\ )_o$ undisturbed condition

$(\ )_{1,2}$ shocked condition / condition behind a detonation wave

$(\ )_{CJ}$ Chapman-Jouguet condition

$(\ )_p$ condition at the piston surface

$(\ )_s$ condition behind the shock wave

$(\ )_u$ unburned gas

$(\ ^\circ)$ differentiation with respect to time

$(\ ^{\circ\circ})$ second derivative with respect to time

$[i]$ mass concentration in moles/liter

LIST OF TABLES

LIST OF FIGURES

CHAPTER 1

INTRODUCTION

This thesis reports an investigation of the initiation of detonations in explosive gas mixtures. The main aim of this research is twofold: to develop a simple analytical theory which can determine, *a priori*, the conditions under which a detonation is likely to occur in a given explosive gas mixture, and to devise suitable laboratory experiments for generating meaningful quantitative results on initiation of detonations. The motivation for such an investigation stems primarily from a desire to further our understanding of the basic features of the detonation phenomenon. The recent upsurge in the number of accidental explosions and the need to evolve safety criterion to minimize their occurrence also warrant such an endeavour.

A detonation is a shock wave sustained by exothermic chemical reactions. The shock wave in passing through a gas, capable of reacting, heats it up to a level wherein spontaneous chemical reactions can occur and the energy liberated during the combustion process in turn goes to maintain the strength of the shock. Experiments reveal that there are two ways by which a detonation can be formed from the energy released by the ignition source. One mode involves the instantaneous or direct formation of the detonation by the ignition source. In the other mode of initiation, the ignition source merely serves to ignite

'the gas mixture. The gas dynamic processes associated with the acceleration of the flame and its interaction with the confinement results in the transition to a detonation. In the literature, the former mode of initiation is usually spoken of as direct or blast initiation, whilst the latter is known as indirect or transitional mode of initiation. This thesis deals mainly with the blast initiation of detonations.

A study of the blast initiation process should help us resolve the other characteristic features of a detonation such as the propagation, and limit behaviour. By propagation is meant the particular manner in which the detonation proceeds or propagates. The limits of detonability, on the other hand, denote the ability of the mixture to support a detonation wave. The initiation, propagation and limit characteristics of a detonation are intimately related and accrue out of the same basic mechanism, *viz.*, the coupling between the transient hydrodynamic flow structure behind the shock front with the kinetics of the chemical reactions. Detailed experiments (1-4) suggest that the propagation of a detonation is through a series of local periodic initiations whilst the inability to form such localized points of initiation is indicative of the approach to the limits of detonability. The key to the understanding of the propagation and limit characteristics therefore hinges on the initiation mechanism itself. Hence a study of the initiation process should contribute to discern the propagation and limit behaviour as well. In fact, theories developed to explain these individual features separately

such as the acoustic theory of Strehlow and Barthel (5-7) for the propagation behaviour, and the loss theory of Dove et al.(8), Tsuge (9) and Williams (10) for limit behaviour, have met with very limited success. The present work aims at resolving the basic characteristics of a detonation wave by a detailed study of its initiation behaviour.

The theoretical description of the initiation problem consists of depicting the coupling between the shock wave and the chemical reactions occurring in its wake. Analytical solution of this problem presents formidable difficulties because of the nonlinear nature of the coupling between the hydrodynamic flow structure generated by the shock and the chemistry of the combustion process. It is only under some limiting assumptions such as heat release at the plane of the shock front itself (the Jouguet, Taylor and Zel'dovich model (11,12) and the Reacting Blast Wave model (12,13)), or a complete decoupling of shock motion and heat release (the Finite Kinetic Rate model (14,15)), that analytical solutions have been shown to be possible. The perturbation schemes, such as those of Korobeinikov (16,17) which allow for a weak coupling between heat release and shock motion, are also inadequate to describe the strong coupling involved in the initiation process.

In view of the difficulties associated with an analytical description, many researchers have attempted a numerical analysis of the problem. Notable amongst these are Rajan (18), Kyong (19), Feay and Bowen (20), and Levin and Markov (21). It is important to realize that a detonation has a three-dimensional nonsteady character with

finite amplitude transverse waves moving laterally in the combustion zone, whereas it is only possible to describe a one-dimensional non-steady flow involving chemical reactions numerically with any degree of success. In addition, the detailed chemistry for most explosive gases of interest are not known, and even where known their application to the highly non-equilibrium conditions behind the shock is somewhat dubious (22). Consequently, it does not appear worthwhile to pursue a numerical approach and develop sophisticated computer codes which are expensive to run and reveal numerical data of questionable validity without providing any further insight into the physics of the problem.

Over the last two decades, however, a significant number of experiments (15,23-29) have been conducted on the blast initiation of detonations using a variety of ignition sources (e.g., electrical and laser sparks, exploding wires, solid explosive detonators, linear detonation from a tube, etc.) for a number of fuel oxygen mixtures at different initial thermodynamic states. Some detailed experiments (30,31) on the mechanism of coupling between the shock front and the combustion heat release have also been reported. On the basis of the experimentally observed dependence of the initiation process on the various parameters, it is possible to develop a phenomenological theory. Such an approach has been adopted in this thesis.

The use of phenomenological models is not new to the field of detonation research. As early as 1956, Zel'dovich (29), on the basis of the similarity in the behaviour of the chemical induction zone

thickness and the threshold energy required for direct initiation, proposed a phenomenological criterion linking the two together. Lee et al. (32) showed that this criterion works when an experimentally observed reaction zone thickness, *viz.*, the so-called "hydrodynamic thickness" of a detonation is used for the induction zone thickness. More recently Edwards (33) proposed a criterion very similar to that of Zel'dovich for the quantitative determination of the threshold energy required for direct initiation using the hydrodynamic thickness derived on the basis of the experiments of Vasiliev, Gavrilenko and Topchian (34).

Lee and Bach (35) employed a more sophisticated phenomenological theory in which the coupling between the hydrodynamic flow structure and the chemical heat release was modelled in terms of an effective heat release at the shock front. Their model recovered the experimentally observed features of propagation of spherical detonation waves. However, as in Zel'dovich's model, the prediction of the correct order of magnitude of the threshold energy was seen to be possible only by using the experimentally observed reaction zone thickness or the hydrodynamic thickness of a detonation.

Though the phenomenological models proposed so far have been able to predict the correct order of magnitude of the initiation energy, they suffer a serious defect in that they make use of the hydrodynamic thickness. The concept of the hydrodynamic thickness is undoubtedly very useful since it defines an equivalent one-dimensional reaction zone thickness for the three-dimensional nonsteady detonation wave (*viz.*, the distance between the shock front and an equivalent Chapman-Jouguet

surface). Soloukhin (36) gives an order of magnitude estimation of the hydrodynamic thickness as being about the characteristic cell size of a multiheaded detonation wave. Vasiliev *et al.* (34) determine experimentally the upper bound for the hydrodynamic thickness for a few gas mixtures at certain initial conditions. However, the estimation of this length is extremely fuzzy in view of the arbitrariness associated with defining a plane of completed reactions or an equivalent Chapman-Jouguet surface for a multiheaded detonation wave.

It is desirable that a theory should not rely on a parameter which has to be determined on the basis of experiments and which is ill-defined both experimentally and theoretically. Hence an attempt has been made in this thesis to develop a phenomenological theory which describes the initiation in terms of the physical and chemical properties of the explosive gas mixture alone. A novel concept of a critical detonation kernel is introduced to model the blast initiation of detonations in analogy to the well-established concept of the flame kernel used in the flame ignition theory. The development of this new concept in detonation initiation has primarily been possible by virtue of the more recent experimental results on blast initiations of detonations.

Concurrent with the development of the detonation kernel theory, an experimental investigation of the blast initiation process has also been carried out. The purpose of these experiments has been (i) to assist in the development of the phenomenological kernel theory

and (ii) to help deduce fundamental results of a generalized nature independent of the configurations and geometry of the initiation experiment. **The need for determining a set of generalized experimental** results is particularly necessary since the results on initiation reported so far in the literature by different investigators for the same explosive gas mixture at the same initial condition, differ considerably. The present experiments are conducted in different geometries with acetylene-oxygen and hydrogen-oxygen mixtures. Those experiments desiged to help in the formulation of the theory are mainly done with oxyhydrogen mixtures since their detailed chemical kinetics and autoignition characteristics are somewhat well understood.

The subject matter of this thesis is divided into six chapters. The second chapter is devoted to a critical survey of some recent experiments with a view to ascertain the role of ignition sources in blast initiation. Based on these experimental findings the concept of the detonation kernel is developed in Chapter 3 and using this concept a phenomenological theory of blast initiation is presented. The chemistry of the combustion processes is considered using a simplified chemical kinetics model based on shock tube induction time measurements.

The theoretical calculations of Chapter 3 yield results for planar, cylindrical and spherical geometries and take no account of the influence of confinement on the initiation process. In practice, since almost all laboratory experiments are performed on a small scale, the effect of confinement on detonation initiation can be profound. The

igniter sources are also of finite size and in no way conform to perfect
point, line or planar energy sources.   To achieve any meaningful
comparison between the initiation experiments done under different
conditions and to correlate the results with the theory, it becomes
necessary to independently assess the geometry of initiation and the
confinement effects.   Chapter 4 deals with the results of exploratory
experiments conducted in this regard.

In Chapter 5 the suitability of the initiation theory to model
the propagation and limit behaviour is demonstrated.   The phenomenon
of transverse wave spacing and limits of detonability are also examined
in the light of some recent experimental results.

Chapter 6 discusses the limitations and validity of the theory
and summarizes the main conclusions and opinions.

ROLE OF THE IGNITER IN BLAST INITIATION

2.1 Introduction

In this chapter the results of some experiments on blast initiation are reviewed in order to discern the basic function of the ignition source in the initiation process.   The majority of the experiments discussed herein have already been reported in the literature by various investigators using different ignition sources and different explosive gas mixtures.   The results of some additional experiments performed during this investigation, so as to extend the existing results over a wider range of conditions, are also included.   The description of these experiments is given in Appendix I.

2.2 Minimum Energy and Power Requirement

The early experiments of Laffitte (37) in 1923 showed that spherical detonations could be initiated in mixtures of CS_2+3O_2 and $2H_2+O_2$ with powerful detonators containing 1 gm of mercury fulminate. Theoretical considerations, however, led to considerable bickering on the very existence of spherical detonations and cast doubt on the validity of Laffitte's observations.   The experiments of Manson and Ferrie (38) in the early fifties with different ignition sources such

as hot wire, electrical sparks and detonators in the spherical symmetry,
followed by the work of Zel'dovich (29) in planar and spherical geometries,
conclusively established that the blast initiation of planar and
diverging waves is possible by the explosive release of finite quantities
of energy.   A threshold value of source energy was identifiable above
which instantaneous initiation of detonation was invariably obtained,
whilst with smaller source energies a deflagrative type of combustion
resulted.   This threshold value of energy, known as the critical energy
for direct initiation, was seen to be a function of the explosive gas
mixture and its initial conditions of temperature and pressure.   Subsequent
studies of the blast initiation of detonations have mostly been associated
with determining this critical energy requirement for a variety of gas
mixtures using different ignition sources.

Bach, Lee and Knystautas (39) pointed out that the magnitude
of the critical energy for the same gas mixture at the same pressure and
initial composition varied by several orders of magnitude when different
ignition sources were employed.   The practice of characterizing the
blast initiation by a source energy alone was shown to be inadequate.
Experiments conducted with laser and electrical sparks with a detailed
monitoring of the time history of the energy deposition process showed
the critical energy to increase in magnitude as the duration of the
energy release increased.   On the basis of these experiments Bach et al.
proposed that the average power density of the ignition source, i.e.,
source energy/(deposition time x source volume) should be a more realistic

parameter.   They demonstrated that for the particular case of,
stoichiometric acetylene-oxygen mixture at an initial pressure of
30 torr, for which the critical energy varied from 0.6 joules for the
rapid laser spark to 450 joules for a very slow electrical discharge,
the power density remained almost constant at 3×10^{17} watts/m^3.
Further experiments (39) at several pressures with the acetylene-oxygen
mixtures confirmed that the power density of the ignition source does
indeed uniquely characterize the blast initiation process.

From a physical point of view, the description of the initiation
process by the average power density of the source alone does not appear
to be meaningful since it admits the possibility of zero critical energy
in the limit of infinitesimally small energy deposition times or a
negligibly small source volume or both.   A finite amount of energy is
required even to initiate chemical reactions between two molecules and
it is therefore impossible to expect a vanishingly small amount of energy
to be capable of forming a chemical energy driven detonation wave.

Some very recent experiments (40,26) conducted with source
energy released from electrical sparks in the cylindrical geometry have
helped to resolve this quandary.   Figure 1 shows the results obtained
by Knystautas and Lee (26) for the variation of the critical initiation
energy with the duration of the effective energy release[†] for a

---

[†] Only a small portion of the total energy released by the electrical
spark contributes towards the formation of a detonation.   Knystautas
and Lee (26) showed this fraction to correspond to the energy released
by the spark till the attainment of the peak averaged power.   Details
of evaluating the effective energy of an electrical discharge forming
a detonation wave along with a theoretical model thereof are given in
Appendix II.

stoichiometric acetylene-oxygen mixture at an initial pressure of 100 torr. It is seen that the critical energy reaches a constant minimum value for energy release times less than a microsecond.

Experiments similar to the above were conducted for stoichiometric hydrogen-oxygen mixtures at an initial pressure of half atmosphere for which the critical energy is more than an order of magnitude greater than for the 100 torr oxyacetylene mixture. The results, also included in Figure 1, clearly confirm the observations of Knystautas and Lee of a constant minimum energy requirement for rapid energy release rates and a sharply increasing trend in the energy requirement for slower energy release rates. We can surmise on the basis of these experiments that no matter how rapid the energy deposition is, a limiting quantity of energy is always required for blast initiation.

Figure 2 shows the critical energy results of Figure 1 replotted as a function of the average power of the energy release. The dependence of the energy on the power and the existence of a limiting value of initiation energy is evident. It is also seen that there is a critical value of power below which initiation is not possible no matter how large the initiation energy is.

The above experiments suggest that both the energy and the power of the ignition source are related in the initiation process and that they must each exceed certain threshold values for direct initiation to occur. The implications of the existence of a minimum limiting power and a minimum energy requirement is examined in the next section.

2.3 Implications of a Minimum Energy and Power Requirement

The strength of the shock wave generated by an ignition

source depends on the rate at which the source energy is deposited in

the gaseous medium, *viz.*, the power of the energy source.   The subsequent

decay of the shock depends on the time rate of change of the total

energy bounded by the shock front and the origin.

The existence of a minimum limiting power for the initiation

of a detonation therefore suggests that a shock wave of a certain minimum

strength must be generated by the ignition source.   A minimum limiting

energy requirement, on the other hand, implies that the strength of the

shock wave must be maintained over a certain duration of time.

It is possible to derive an idea of the minimum shock strength

necessary on the basis of the results reported for the oxyacetylene and

oxyhydrogen mixtures in the previous section.   The energy released

corresponding to the minimum power requirement is modelled in terms of

the energy release from a constant velocity cylindrical piston.   For

simplicity, the approximate analytical solution of Guirao *et al.* (41)

which assumes a linear velocity profile behind the shock front, is used.

The details of this method are given in Appendix III.   The minimum

shock Mach number as implied by the minimum power requirement is seen

to correspond to about Mach 5 for both the mixtures. , This limiting

Mach number is slightly greater than the conventional autoignition limit

for most fuel oxygen mixtures as obtained in the shock tube experiments.

Since, in practice, the gas dynamic expansion associated with the
transient motion of the shock causes the temperature, pressure and
density of the shocked gases to be less than those corresponding to a
steady planar case, we can conjecture the minimum power requirement to
indicate the necessity for the initiation source to generate a shock,
wave of a certain minimum strength of the order of the autoignition
limit.   Physically this makes sense because the spontaneous chemical
reactions can occur behind the shock only if the conditions behind it
exceed the autoignition limit.

2.4 Mechanism of Shock Reaction Coupling in Blast Initiation

The coupling of the shock front with the chemical reactions
occurring in its wake can best be illustrated by subdividing them
according to Bach et al. (15) on the basis of their experiments on
spherical detonations.   Following reference (15), reactive shocks are
classified into three regimes of initiation, viz., supercritical, sub-
critical and critical regimes according to whether the source energy is
greater than, less than, or equal to a threshold value corresponding to
the critical energy discussed in section 2.2.

Figure 3, taken directly from the work of Knystautas (30), is
a streak schlieren photograph illustrating the supercritical, subcritical
and critical regimes from left to right respectively.   In the super-
critical regime, an overdriven detonation is formed by the energy released

from the ignition source.   The chemical reactions are observed to occur adjacent to the plane of the shock front itself (Fig. 3a). This overdriven detonation wave decays continuously to a multiheaded detonation front which propagates with a velocity corresponding to about the Chapman-Jouguet value.   A typical sequence of spark-schlieren photographs, shown in Figure 4, illustrates the strong coupling between the shock and the reaction front.

For the subcritical regime, an overdriven detonation is initially formed as in the supercritical mode.   However, as the wave moves away from the source, the zone of chemical reactions progressively recedes from the shock front as evidenced in Figure 3b, and in the framed spark schlieren pictures of Figure 5.   The reaction zone and the shock front become decoupled; the combustion zone propagates as a deflagration wave whilst the shock front decays as an unreactive blast wave.

Figure 6 illustrates the critical regime of initiation.   The reaction front and shock are seen to initially behave in a manner similar to the subcritical or decoupled mode in that the shock is observed to decouple from the chemical reaction zone.   But unlike the subcritical case wherein the reaction zone continually recedes from the shock, the decoupling in this case stops when their separation is a few millimeters.   Thereafter both the shock and the reaction front propagate together as a quasi-steady complex for several microseconds at a Mach number corresponding to about the autoignition limit.   This

is followed by localized explosions which grow and sweep around the shock front leading to the formation of a highly asymmetric multi-headed detonation wave.

The existence of a quasi-steady period of propagation around the autoignition Mach number, followed by the localized explosions which culminate in the formation of a multiheaded detonation front, has also been observed in the re-establishment process when an over-driven detonation in a tube is suddenly expanded (detonation diffraction) (31,30). The formation of the localized explosions is also manifested in the transitional mode of initiation when the turbulent flame transits violently into a detonation. Oppenheim (42) called these localized explosions in the transitional mode of initiation 'explosion in an explosion'.

The precise reasons for the occurrence of the localized explosions following a quasi-steady period of propagation is not under-stood. Lee et al. (43) point out that some instability generating mechanism in the shock reaction complex, such as the chemical instability of the autocatalytic reactions, could lead to the formation of localized reaction centres and hence to the localized explosions. This facet of the problem has, however, not been explored. We shall not dwell on this problem in this thesis other than realize that for the critical case of blast initiation the ignition source must be capable of generating conditions conducive to the formation of these localized explosions.

The necessity of forming a quasi-steady complex travelling at the autoignition conditions is in agreement with the conclusion derived from section 2.3 on the basis of a minimum power and energy requirement of the ignition source.

2.5 Parameters Influencing the Initiation of Detonations

Having studied the role of the ignition source in the initiation process, we briefly examine some experimental results in order to determine the influence of the common detonation properties on initiation. Such a survey should reveal the parameters affecting the ignition source requirements and would pave the way for the choice of pertinent parameters in the phenomenological theory.

We first note, on the basis of discussion in section 2.2, that the limiting minimum value of energy, under conditions of rapid energy release, is unique and can describe the blast initiation of the explosive gas mixture. We shall therefore address the problem of blast initiation in this thesis in terms of determining the minimum critical energy. In the following, unless otherwise stated, the critical energy will be taken to correspond to the limiting value under conditions of rapid energy deposition.

Figures 7 and 8, reproduced from the works of Lee and Matsui (28), show the experimental variation of the critical energy for acetylene-oxygen mixtures with composition and initial pressure. It is seen that

the critical energy increases sharply near the limits of detonability
and decreases with increasing pressure.   The dependence of the
induction zone thickness on composition and pressure is similar to that
of critical energy.   The Chapman-Jouguet velocity, on the other hand,
has an opposite behaviour in that this velocity increases with increasing
pressure and falls near the limits of detonability (Fig. 7).   It is also
of interest to note that the characteristic transverse wave spacing of a
detonation has a dependence on composition and pressure, very similar to
that of the critical energy for blast initiation.

Additional parameters like the ratio of specific heats γ, the
geometry of initiation j, and the overall activation energy for the
chemical reactions E, are also expected to affect the initiation process.
Levin and Markov (21) on the basis of dimensional considerations
postulated a functional relationship between these various parameters
and the initiation energy of the form

$$E_s = p_o Q^{\frac{j+1}{2}} \tau^{j+1} F \left(\frac{p_o}{\rho_o Q}, \frac{E}{Q}, \gamma, j \right)$$

CHAPTER 3

A DETONATION KERNEL THEORY FOR INITIATION

3.1 Introduction

In the preceding chapter the role of the source energy in
the initiation of a detonation was discussed and some parameters
involved in the initiation process were noted on the basis of experiments.
Using this information, a phenomenological theory of initiation of a
detonation is developed in this chapter.

The basic aspects of the theory are similar to the one recently
reported by Lee and the author (44).   The concept of a critical
detonation kernel is introduced in analogy to the concept of a flame
kernel in the ignition theory.   An equation for the kernel size is
formulated in blast wave coordinates and a simplified method of solution
is demonstrated.   The solution is in a generalized form wherein planar,
cylindrical and spherical waves are treated simultaneously.

The following section of this chapter recapitulates the notion
of the critical flame kernel in order to be able to constitute a clear
presentation of the concept of a detonation kernel.

3.2 Flame Ignition and Flame Kernel

The formation of a steady propagating flame is governed by
the transport processes of heat conduction and mass diffusion.   The

ignition source, *e.g.*, an electric spark, raises the temperature of a certain volume of gas and causes chemical reactions to occur within this volume.   Some of the heat and reactive species are also transferred out of this volume into adjacent regions of the unburnt gas, thereby leading to conditions conducive to the occurrence of chemical reactions in these neighbouring layers.   Thus the adjacent regions of the fresh gas begin to burn and a flame is propagated away from the ignition source.

The transport of heat and mass out of the volume of the chemically reacting gases into the adjacent regions of the unburnt gas also results in a decrease of temperature and a depletion in the concentration of reactive species.   The chemical reactions tend to offset the effect of these losses (due to transport) by generating heat and active radicals.   If, however, the rate of loss of heat and reactive species is greater than the rate at which these are produced by the chemical reactions, then the temperature and concentration of the active species decrease within the initial volume thereby inhibiting further chemical reactions and leading to the extinction of the flame.

Hence for a self-sustained flame to be formed (*i.e.*, successful ignition) it is necessary that the net rate of production of heat and activated radicals by the chemical reactions overrides the losses. The obvious way of achieving the above is to generate an adequate volume of burning gases.   In other words, for flame ignition, the energy source must be capable of forming a certain minimum volume of reacting gases so as to lead to a situation wherein the generation of heat and

activated radicals is in excess of their dissipation. Schlieren
photographs of Olsen, as given in Strehlow's book (45) and reproduced
in Figure. 9, clearly demonstrate the above reasoning. When the
magnitude of the source energy is less than the energy corresponding
to the ignition threshold (Fig.9b), an incipient volume of burning
gases is initially formed but soon collapses (around 100 μs) due to
losses. On the other hand, for the source energies greater than the
threshold value (Fig.9c) the initial volume of burning gas does not
decay with time due to losses but instead continues to form a well-
established flame.

Theoretical work on flame ignition has continually exploited
the necessity of forming an adequate volume of burning gases, *viz.*, a
flame kernel (46,47). Approximate estimations of ignition energies
have been made assuming the minimum flame kernel size to be about the
combustion wave thickness (*e.g.*, Williams (48)). The flame kernel
criterion has also been applied to combustion under turbulent flow
conditions (DeSoete (49), Ballal and Lefebvre (50)).

Yang (51) gives an elegant theory to determine the flame
kernel size by explicitly invoking the balance condition between the
production and dissipation of the heat and reactive species. He
expresses the minimum flame kernel size in terms of a critical mass flow
rate G*, for which the net rate of production of heat and active species
is identically equal to zero (generation equals losses). Mathematically,

his criterion reduces to

$$\int_0^\infty \rho C \frac{\partial T}{\partial t}\, dr = 0 \qquad\qquad 2.1$$

and

$$\int_0^\infty \rho \frac{\partial \alpha}{\partial t}\, dr = 0 \qquad\qquad 2.2$$

In deriving the phenomenological theory for detonation, a parallel approach has been adopted. A brief discussion of the methodology involved in the derivation of Yang's theory is given in Appendix IV.

3.3 Concept of a Detonation Kernel

In contrast to flames, the chemical reactions in case of detonations are brought about by the shock heating of the gas particles instead of by the transport processes of heat and mass.   It has also been seen on the basis of experiments in Chapter 2, that for the blast initiation of detonations it is necessary to

1. generate a shock wave above a minimum strength (say, M_s^*) corresponding to about the autoignition limit, and

2. maintain the shock strength above this minimum value over a certain distance of travel (say, R_s^*).

Since spontaneous chemical reactions take place above the autoignition limit, the above statements suggest that an adequate volume of spontaneous chemical reactions (corresponding to R_s^*) must be induced by the ignition source in order to generate a detonation. The significance of an adequate volume of burning gas can be interpreted as follows.

During the early phase of shock travel, the mass of the shocked particles is small so that the heat released from the chemical reactions of the shocked mass of gas will be insignificant as compared to the source energy. The shock motion will consequently be governed principally by the source energy, leading to the shock wave decaying as an unreactive blast wave. As the shock wave moves away from the source, it embraces an increasing volume of the gas and if the shock is sufficiently strong ($M_s \geq M_s^*$) the chemical energy released from their combustion progressively becomes more influential in determining the shock motion. If the chemical energy released is greater than the source energy, the decaying characteristics of a source dominated motion is arrested and a shock wave sustained by chemical reactions (viz., a detonation wave) is formed. However, if a domination of the chemical energy release over the source energy is not possible, say by the shock wave decaying below M_s^* before the shock embraces a sufficiently large mass of gas, then the shock front will continue to decay more or less like an unreactive blast wave, so that no self-sustained detonation can be formed. This line of reasoning is in conformity with the theoretical considerations of Nicholls et al. (52) and Korobeinikov (16).

Fry and Nicholls (23) used a mathematical regression model
to describe the initiation behaviour in terms of a strong blast decay
followed by a constant velocity detonation.   Specifically, they
presumed the shock wave time history to have a second order dependence
on the distance travelled for the early time shock motion and a linear
dependence on distance for later times in their experiments in a
cylindrical geometry.   They demonstrated that the value of R_s^* at which
the character of the wave changes from a strong blast decay to a constant
velocity detonation coincides with the radius at which the chemical
energy released by the shocked gas is about the same as the source
energy.   Lee et al., (53) also showed, on the basis of the experimentally
observed shock trajectories, that the shock motion transits from a
source driven decaying blast mode to a detonative mode when the chemical
energy of the shocked gas and the source energy are about equal.   The
transition was also demonstrated to be attended with the formation of
localized explosions as evidenced by the experiments in the critical
regime of initiation discussed in section 2.4 of Chapter 2.   These
observations substantiate the assertions made in the previous paragraph,
viz.,that for the formation of a detonation a certain volume of burning
gasses (R_s^*) must be created, the chemical energy release from which can
dominate over the source energy.

The analogy between the initiation of a flame and the initiation
of a detonation is now evident.   In section 3.2, we saw that the role
of the ignition source in flame ignition was to form a sizeable volume of

hot burning gases, *i.e.*, a flame kernel so that the generation of
heat and active species within this volume could compensate for the
losses.   In detonation initiation also, we find that the igniter
must be capable of forming an adequate volume (corresponding to R_s^*)
of strongly shocked gases so that the chemical energy release from
this volume can dominate over the decaying influence of the source
energy and maintain a detonation wave.   We shall call this volume
the detonation kernel in parallel to the flame kernel used in flame
ignition.

It is important to realize the clear distinction in the
manner in which the concept of the detonation kernel is derived in
relation to the flame kernel.   Unlike the latter, the formation of
an adequate volume of heat release in the case of a detonation
initiation (the detonation kernel of size R_s^*) is to mitigate the
decaying characteristic of a source-dominated shock motion and to
result in the formation of a strongly coupled shock-reaction complex
(*viz.*, a detonation wave).   If the size of the detonation kernel is
too small, the energy released by the chemical reactions in the kernel
is negligibly small as compared to the energy released by the source.
Hence the shock will decay further and the inflammed gas will grow as
a flame subsequently.   There is no question of losses here as in the
concept of the flame kernel.

In the following section we shall formulate the above notion
of a detonation kernel in terms of a simple theory and determine the
critical size of a detonation kernel required for the blast initiation
of detonations.   From the size of the kernel the threshold initiation
energy and other characteristics of a detonation wave will be derived.

3.4   Theoretical Formulation

In this section the concepts of section 3.3 are mathematically
described.   It is assumed that spherical, cylindrical and planar
symmetries exist.   The flow is taken to be one-dimensional.   Transport
losses of heat and mass are neglected.   The chemical reactions behind
the shock front are modelled in terms of an induction delay followed
by spontaneous exothermic reactions.

Consider the source energy E_s to be rapidly deposited at a
point, a line or a plane so as to generate a strong spherical, cylindrical
or planar shock wave respectively.   Let the shock be at a distance
$R_s(t)$ from the source at a certain instant of time t.

Let d be the induction zone thickness so that the plane of
heat release is at $(R_s(t)-d)$ as shown in sketch 1.   The energy released
by the source E_s and the energy from the chemical reactions go to increase
the kinetic and internal energy of the gas bounded by the shock at $R_s(t)$.
The conservation of the total energy enclosed by the moving boundary
(viz., the shock front) at some instant of time t is, therefore, given by
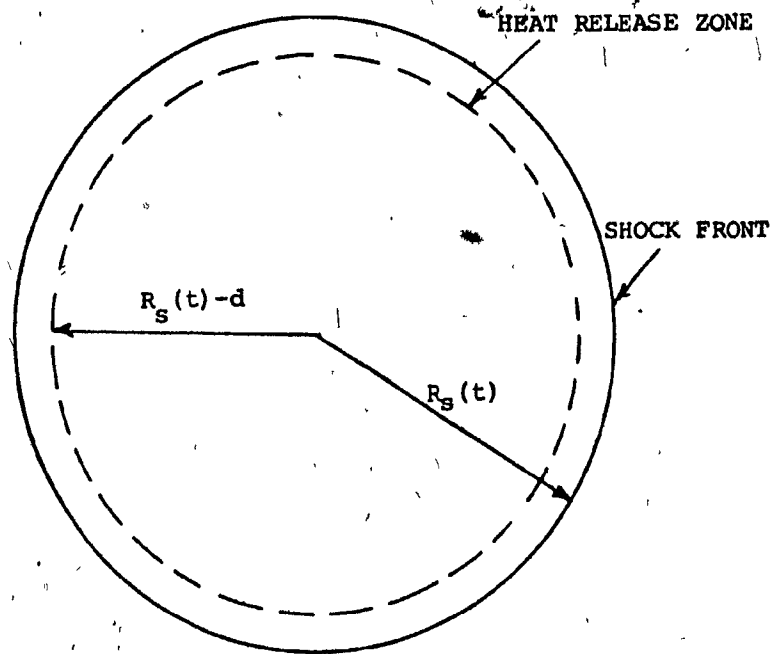
SKETCH 1: SCHEMATIC REPRESENTATION OF THE SHOCK AND
THE CHEMICAL REACTION FRONT

$$E_s + \int_0^{R_s(t)-d} Q\rho k_j r^j dr = \int_0^{R_s(t)} (\frac{u^2}{2} + e)\, \rho k_j r^j dr - \int_0^{R_s(t)} e_0 \rho k_j r^j dr \qquad 4.1$$

where $k_j = 4\pi$, 2π and 1 for $j = 2$, 1 and 0 corresponding to the spherical, cylindrical and planar geometries, respectively.

For convenience in analysis, we shall recast the above energy conservation equation in blast wave parameters by replacing the spatial coordinate r by ξ , where

$$\xi = \frac{r}{R_s(t)} \qquad 4.2$$

and the variables p, ρ and u by f, ψ and ϕ where

$$f(\xi,\eta) = \frac{p(r,t)}{\rho_0 \mathring{R}_s^2(t)}$$

$$\psi(\xi,\eta) = \frac{\rho(r,t)}{\rho_0} \qquad 4.3$$

and $\qquad \phi(\xi,\eta) = \dfrac{u(r,t)}{\mathring{R}_s(t)}$

Here $\overset{\circ}{R}_s(t)$ is the local shock velocity $\dfrac{dR_s(t)}{dt}$ and

$$\eta = \frac{1}{M_s^2} = \frac{C_0^2}{\overset{\bullet}{R}_s^2(t)}.$$ Substituting the values of p, ρ, u and γ

from Eqs. 4.2 and 4.3 in Eq. 4.1, and simplifying, we get

$$M_s^2 = \frac{\hbar 1}{I}\left[\frac{E_s}{\rho_0 C_0^2 k_j R_s(t)^{j+1}} + \frac{Q}{C_0^2}\int_0^{1-d/R_s(t)}\psi\xi^j d\xi + \frac{e_o}{C_0^2}\int_0^1\psi\xi^j d\xi\right] \qquad 4.4$$

where

$$I = \int_0^{1-d/R_s(t)}\left(\frac{f}{\gamma-1} + \frac{\psi\phi^2}{2}\right)\xi^j d\xi + \int_{1-d/R_s(t)}^1\left(\frac{f}{\gamma-1} + \frac{\psi\phi^2}{2}\right)\xi^j d\xi \qquad 4.5$$

Conserving the total mass enclosed by the shock at any

instant, we get

$$\int_0^{R_s(t)}\rho k_j r^j dr = \frac{\rho_o k_j}{j+1} R_s(t)^{j+1} \qquad 4.6$$

In blast wave coordinates, Eq. 4.6 reduces to

$$k_j R_s(t)^{j+1} \rho_0 \int_0^1 \psi \xi^j d\xi = \frac{\rho_0 k_j}{j+1} R_s(t)^{j+1}$$

giving

$$\int_0^1 \psi \xi^j d\xi = \frac{1}{j+1} \qquad\qquad 4.7$$

Substituting Eq. 4.7 in Eq. 4.4 leads to the global conservation of energy of the form

$$M_s^2 = \frac{1}{I} \left[\frac{E_s}{\rho_0 C_0^2 k_j R_s(t)^{j+1}} + \frac{Q}{C_0^2} \int_0^{1-d/R_s(t)} \psi \xi^j d\xi + \frac{e_0}{(j+1)C_0^2} \right] \qquad 4.8$$

The above equation is an exact statement of the conservation of energy. No assumptions, whatsoever, have been made in its derivation.

For small values of shock radius $R_s(t)$, *i.e.*, $d/R_s(t) \sim O[1]$, the integral term on the RHS of Eq. 4.8 and the initial internal energy term are small compared to the source energy term. Hence

$$M_s^2 = \frac{E_s}{\rho_0 C_0^2 k_j R_s(t)^{j+1} I} \qquad \text{for} \quad R_s(t) \sim d \qquad 4.9$$

This denotes that the shock strength M_s^2[†] is dependent on

the specific energy $\varepsilon = \dfrac{E_s}{\rho_0 k_j R_s(t)^{j+1}/(j+1)}$ of the source. As the

shock wave moves away from the source, the mass of shocked gases

$\left(\dfrac{\rho_0 k_j R_s(t)^{j+1}}{j+1} \right)$ increases. If $E_s = E_o$ (= constant), as in the ideal

blast wave theory, then the specific energy decreases with increasing

shock radius and consequently the shock strength decays. From Eq. 4.9

$M_s \sim R_s(t)^{-\frac{j+1}{2}}$ so that $R_s(t) \sim t^{2/(j+3)}$ (*i.e.*, $R_s(t) \sim t^N$

[†] The strength of a shock wave is usually expressed in terms of pressure ratio across it. For a perfect gas, the pressure ratio is a linear function of the square of the shock Mach number, so that M_s^2 is indicative of the strength of a shock wave.

where N = 2/3, 1/2 and 2/5 for j = 0, 1, 2) as given by the similarity

solution of Taylor, Sedov and von Neumann (54-56).

On the other hand, for large shock radius ($R_s(t) \to \infty$) the

source energy term in Eq. 4.8 becomes vanishingly small so that

$$M_s^2 = \frac{1}{I} \left[\frac{Q}{C_0^2} \int_0^1 \psi \xi^j d\xi + \frac{e_o}{(j+1)C_0^2} \right] \qquad 4.10$$

Using Eq. 4.7 the above expression can be rewritten as

$$M_s^2 = M_{CJ}^2 = \frac{1}{(j+1)C_0^2 I}(Q + e_o) \qquad 4.11$$

This implies that the wave is essentially driven at constant

velocity by the chemical energy at large radius, i.e, the shock wave

asymptotically approaches a Chapman-Jouguet detonation at large radius.

The above statement assumes that E_s is finite as t tends to infinity

which is true, in general, in initiation problems.

It is instructive to note that the early time motion described

by Eq. 4.9 and the asymptotic or late time motion given by Eq. 4.11, are

in good agreement with the experiments (Nicholls (52,23) and Lee (53))

and with the phenomenological theory of Lee and Bach (35).

From fairly general considerations, we thus see that the shock strength is a consequence of the competition between two terms: one is a decreasing function of time, or equivalently $R_s(t)$, i.e.,

$$\frac{E_s}{\rho_0 C_0^2 k_j R_s(t)^{j+1}}$$

whilst the other is an increasing function of time, or $R_s(t)$, i.e.,

$$\frac{Q}{C_0^2} \int_0^{1-d/R_s(t)} \psi \xi^j d\xi$$

We define the minimum size R_s^* for the detonation kernel, as discussed in section 3.3, by the condition of balance between the energy diminishing and energy production terms analogous to Eqs. 2.1 and 2.2 of Yang (51) for the critical flame kernel. We, therefore, write for $R_s(t) \to R_s^*$

$$\frac{E_s}{k_j \rho_0 C_0^2 R_s^{*\,j+1}} = \frac{Q}{C_0^2} \int_0^{1-d(R_s^*)/R_s^*} \psi \xi^j d\xi \qquad 4.12$$

$d(R_s^*)$ being the value of d when $R_s(t) = R_s^*$.

The shock Mach number M_s must at least be M_s^* when $R_s(t) \to R_s^*$ (section 3.3). Using this information along with Eq. 4.12 to replace the source energy term in Eq. 4.8, we get

$$M_s^{*2} = \frac{1}{I} \left[\frac{2Q}{C_0^2} \int_0^{1-\frac{d(R_s^*)}{R_s^*}} \psi \xi^j d\xi + \frac{e_o}{(j+1)C_0^2} \right] \qquad 4.13$$

Equation 4.13 gives an expression for the minimum size of the detonation kernel R_s^* in terms of M_s^*, I, Q and the induction zone thickness d. The evaluation of R_s^* from this expression, however, is not straightforward and section 3.5 deals with a simplified method of explicitly determining R_s^* from Eq. 4.13

It should be pointed out that once R_s^* is known, the source energy can be determined from Eq. 4.12.

3.5 Method of Solution

We require to know the distribution of density, pressure and velocity between the shock front and the source in order to determine the mass integral $\int_0^{1-d(R_s^*)/R_s^*} \psi \xi^j d\xi$ and the value of the energy integral I

in Equation 4.13. We also require a knowledge of the variation of the thermodynamic properties of pressure, temperature and density along a gas particle after it is processed by the shock so as to figure out the time taken for the induction reactions to go to completion and thus evaluate the induction distance d.

The mathematical relations governing the flow field behind the shock front are the basic conservation equations. For a perfect gas, we can write these conservation equations, in the absence of viscosity and heat conduction effects, as follows:

Conservation of mass:

$$\frac{\partial \rho}{\partial t} + u \frac{\partial \rho}{\partial r} + \rho \frac{\partial u}{\partial r} + \frac{j \rho u}{r} = 0 \qquad\qquad 5.1$$

Conservation of momentum:

$$\frac{D}{Dt} u + \frac{1}{\rho} \frac{\partial p}{\partial r} = 0 \qquad\qquad 5.2$$

Conservation of energy:

$$\frac{1}{\gamma - 1} \frac{D}{Dt} \left(\frac{p}{\rho}\right) + p \frac{D}{Dt} \left(\frac{1}{\rho}\right) = \frac{D}{Dt} Q \qquad\qquad 5.3$$

Analytical solutions of the above equations for the flow field are possible only for some particular cases such as a strong blast wave, a constant velocity shock driven by a piston, or a constant velocity detonation. The numerical solutions, though possible in

highly overdriven regimes (57) are, in general, plagued with mathe-

matical instabilities (Strehlow and Hartung (58),and Fickett and Wood

(59)) in view of the nonlinear feedback between the hydrodynamic flow

structure and the chemical reactions.   As already metioned in the

Introduction to this thesis, it is the purpose of this work to avoid

a detailed numerical description in view of the well-established three-

dimensional character of a detonation and the uncertainty in the chemical

kinetic data.   In this section, therefore, certain simplifying

assumptions will be made in order to develop a straightforward solution

of Eq. 4.13.   The simplified evaluation of the different terms in the

above equation is first given individually.

3.5.1 Determination of Energy Integral I

Assuming a continuous profile of density, velocity and pressure

behind the shock front, the energy integral I given by Eq. 4.5 can be

written as

$$I = \int_0^1 \left(\frac{f}{\gamma-1} + \frac{\psi\phi^2}{2} \right) \xi^j d\xi \qquad 5.4$$

and again re-written in the following form

$$I = \frac{1}{j+1} \left[\frac{\int_0^{R_s} (\frac{u^2}{2} + e)\rho k_j r^j dr}{\frac{k_j}{j+1} \rho_0 R_s^{j+1} \mathring{R}_s^2} \right] \qquad 5.5$$

The numerator in Eq. 5.5 denotes the kinetic and internal energies of the shocked gases, whilst the term $\frac{k_j}{j+1} \rho_0 R_s^{j+1} \mathring{R}_s^2$ in the denominator represents the kinetic energy if the entire mass of shocked gases were to move at the shock velocity $\mathring{R}_s$. For the shock strengths of interest in detonation initiation ($M_s \gtrsim 4$), the square of the particle velocity (u^2) and the internal energy (e) (proportional to temperature) just behind the shock front, are directly proportional to the square of the Mach number and hence to $\mathring{R}_s^2$. The density ratio across the shock front for $M_s \gtrsim 4$ is fairly high $\left[\frac{\rho_s}{\rho_0} = \frac{\gamma+1}{\gamma-1+2/M_s^2} \right.$, $\gamma \sim 1.35 \left. \right]$, so that most of the shocked mass will be concentrated in a region very close to the shock front. A detailed distribution of pressure, density and velocity should therefore not significantly influence the numerator in expression 5.5 since the major contribution comes from the close neighbourhood of the shock front wherein most of the mass is located. Further, since for the shock strengths of interest, the values of u^2 and e are proportional to $\mathring{R}_s^2$, the value of the numerator will also be proportional to $\frac{\rho_0 k_j}{j+1} R_s^{j+1} \mathring{R}_s^2$. As the denominator of the expression in square brackets in Eq. 5.5 is given precisely by the above expression, the value I should therefore be a relatively invariant parameter for a particular geometry. In fact, Rogers (60) and Dabora (61) find the value of I for the case of an energy release of the form $E_s = E_o t^\beta$ (E_o and β are constants) to remain fairly constant for values of β between 1 and 5.

It is possible to determine the value of I for a constant

velocity detonation for which the flow field can be exactly determined

since a similarity solution exists for the governing differential

Equations 5.1 to 5.3.   It is also possible to calculate the value of

I in the asymptotic limit from Eq. 4.11.   The value as determined by

the two methods are almost identical.   As an example, the value I

calculated for a 100 torr stoichiometric acetylene oxygen mixture in

case of cylindrical geometry (j=1) is 0.402 from the similarity solution

and is 0.410 from the asymptotic method.   The close agreement results

from the relative insensitivity of I to the details of the hydrodynamic

flow structure as expected on the basis of the arguments in the previous

paragraph.   In our analysis, we shall take the value of I as a

constant, and in order to achieve the appropriate limit of $M_s \rightarrow M_{CJ}$

when $R_s \rightarrow \infty$, we shall use the asymptotic value of I given by Eq. 4.11.

Appendix V gives the details of evaluating I using the

similarity solution for a constant velocity detonation.

3.5.2 Evaluation of Mass Integral $\int_0^{1-d(R_s^*)/R_s^*} \psi \xi^j d\xi$

In order to determine the mass integral we require a knowledge

of the density distribution behind the shock front.   It has been

demonstrated earlier (13) that a density distribution given by a power law

adequately describes the shock motion so long as the global conservation of mass and energy are satisfied. Following Lee (12), we shall assume the density distribution to be given by

$$\psi(\xi, M_s) = \psi(1, M_s)\ \xi^{q(M_s)} \qquad\qquad 5.6$$

The exponent $q(M_s)$ can be determined from the global conservation of mass, *viz.*, Eq. 4.7 giving

$$q(M_s) = (j+1)[\psi(1, M_s)-1] \qquad\qquad 5.7$$

The mass integral, therefore reduces to

$$\int_0^{1-d(R_s^*)/R_s^*} \psi\xi^j d\xi = \frac{(\ 1-d(R_s^*)/R_s^*\ )^{q+j+1}}{j+1} \qquad\qquad 5.8$$

In section 3.6, an alternate method of evaluating this mass integral is presented, and the validity of the assumption of a power law density profile is independently ascertained.

3.5.3 Value of Heat Release Q

Q is the heat release of the combustion per unit mass of the mixture.   It is to be expected that the value of Q should depend on the amount of dissociation of the product gases and therefore seemingly warrants equilibrium composition computations for each individual set of conditions.

Guirao (62) computed the heat release for several modes of combustion such as a C.J. detonation, a constant volume   combustion, a constant pressure combustion, and a C.J. deflagration for a wide range of explosive gas mixtures.   She found that the heat release does not differ markedly in the different combustion processes.   The table below shows the heat release obtained from the combustion of a stoichiometric hydrogen-oxygen mixture at an initial pressure of half-atmosphere in the different combustion processes.

Combustion process	Q kcal/gm	Q/C_o^2
C.J. Detonation	1.5002	21.54
Constant volume combustion	1.6176	23.23
Constant pressure combustion	1.7287	24.83
C.J. deflagration	1.8413	26.44

Based on the above, we shall take the value of Q to be a constant and determine its value using the C.J. criterion, viz.

$$\left(\frac{\gamma_0}{\gamma_1} - \eta \right)^2 = k\eta \qquad\qquad 5.9$$

where

$$k = 2 \left\{ \frac{\gamma_0 \,(\gamma_1 - \gamma_0)\,(\gamma_1 + 1)}{\gamma_1^2 \,(\gamma_0 - 1)} + \frac{\gamma_0^2 \,(\gamma_1^2 - 1)}{\gamma_1^2} \, \frac{Q}{C_0^2} \right\}$$

giving

$$\frac{Q}{C_0^2} = \frac{\dfrac{1}{2\eta} \left(\dfrac{\gamma_0}{\gamma_1} - \eta \right)^2 - \dfrac{\gamma_0 \,(\gamma_1 - \gamma_0)\,(1 + \gamma_1)}{\gamma_1^2 \,(\gamma_0 - 1)}}{\dfrac{\gamma_0^2 \,(\gamma_1^2 - 1)}{\gamma_1^2}} \qquad\qquad 5.10$$

3.5.4 Determination of $d(R_s^*)$

In Eq. 4.13, $d(R_s^*)$ denotes the separation between the shock front and the reaction zone when the shock is at R_s^*. Strictly speaking, the evaluation of $d(R_s^*)$ requires a complete knowledge of the shock hydrodynamic flow structure for $R_s < R_s^*$. This is because the fluid particle which burns when the shock travel is R_s^* has actually crossed

the shock much earlier in time when $M_s > M_s^*$ and has been subjected
to the transient gas dynamic processes during its induction time
prior to explosion.   However, the experiments of section 2.4 have
conclusively revealed to us the quasi-steady propagation of the shock
reaction complex when its Mach number is around M_s^* just prior to the
formation of the local explosion centres and the sudden transition to
a highly asymmetric multiheaded detonation front.   The numerical
solutions of Kyong (19) and Feay and Bowen (20) also show a relatively
constant pressure and density profiles adjacent the shock front in this
region.   Figures 10, 11 and 12 show the numerical results for
pressure, velocity and density profiles as obtained by Kyong for the
propagation of a spherical detonation wave with critical initiation
energy in a 100 torr stoichiometric oxyacetylene mixture. R_o denotes
the characteristic explosion length of the source energy which was
defined by him to be $(E_o/k_j \rho_o C_o^2)^{1/j+1}$.   A zone of constant properties
behind the shock front is clearly evident before the onset of severe
instabilities associated with the strong coupling in the detonative
mode of combustion.

We shall therefore assume that near R_s^* the fluid particles,
under critical conditions of initiation, enter the shock when $M_s = M_s^*$
and since the shock is quasi-steady and the properties behind it are
relatively invariant, we shall also assume the fluid particle states
to remain constant during its induction process.   Thus we can write
$d(M_s^*)$ for $d(R_s^*)$ and evaluate the local induction distance based on the
local critical shock Mach number M_s^*.

The induction time is calculated using the empirical shock
tube correlations of the form

$$\ln \{ (fuel)^m (oxygen)^{1-m} \tau \} = A + B/T. \qquad 5.11$$

The temperature T of the shocked gases is determined by assuming the
shocked particles of the gas to reach a state of rotational and
vibrational equilibrium immediately after being shocked.   The
induction distance $d(M_s^*)$ is evaluated directly from the induction
time τ using the condition of the quasi-steady propagation of shock
around $M_s \neq M_s^*$ viz.,

$$d(M_s^*) = \frac{M_s^* C_o \tau (M_s^*)}{\psi(1, M_s^*)} \qquad 5.12$$

3.5.5 Value of R_s^*

On the basis of the simplifications discussed in sections
3.5.1 to 3.5.4 and using the perfect gas equation

$$e = \frac{P}{\rho(\gamma-1)} \qquad 5.13$$

the critical size of the detonation kernel can be explicitly evaluated to be

$$R_s^* = \sqrt{\dfrac{d(M_s^*)}{\left\langle 1 - \left\{ \dfrac{j+1}{2} \dfrac{C_0^2}{Q} \left[M_s^{*2} I - \dfrac{1}{(j+1)\gamma(\gamma-1)} \right] \right\}^{\frac{1}{q+j+1}} \right\rangle}} \qquad 5.14$$

3.6 An Alternate Determination of the Mass Integral in Eq. 4.13

Consistent with the assumption of quasi-steady conditions near R_s^*, it is possible to estimate the burnt mass and hence the combustion energy without the assumption of a power law density profile as was done in section 3.5.2.

Sketch 2 shows the shock trajectory and the path of a fluid particle (shown by the dotted line) which burns off at E when the shock radius is R_s^*.   This particle would have entered the shock at a time τ earlier (*viz*, at D) where τ is the induction time corresponding to the quasi-steady Mach number of the shock during this period.   The mass of the gas burnt when the shock is at C (radius R_s^*) corresponds to the mass enclosed by the shock front when it is at point D.

$$\delta = \overset{\circ}{R_s^*} \; \tau(M_s^*)$$

PARTICLE PATH

BLAST WAVE

R_s^*

t

r

d

E

C

D

τ

δ
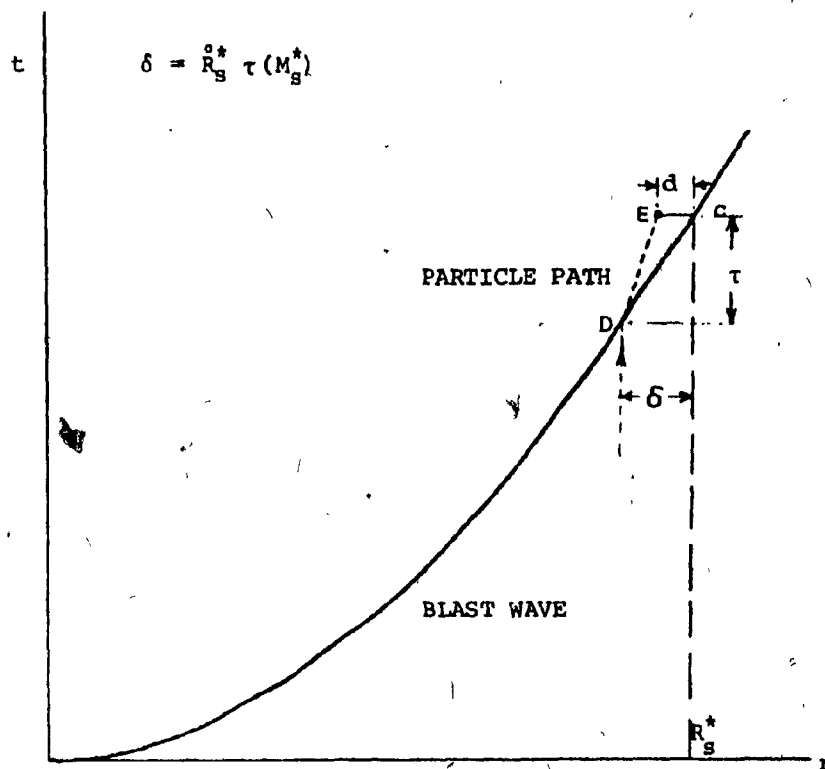
SKETCH 2: ESTIMATE OF BURNT MASS, m_b

The burnt mass corresponding to R_s^* can therefore be written as

$$m_b = \frac{k_j\,\rho_o}{j+1}\left[R_s^* - \overset{\circ}{R}_s^*\ \tau\,(M_s^*)\right]^{j+1}$$ 6.1

The chemical energy release corresponding to R_s^* is $m_b Q$. Substituting this value in Eq. 4.1 and simplifying, we get

$$M_s^{*2} = \frac{1}{I}\left[\frac{E_s}{\rho_0 k_j R_s^{*\,j+1} C_0{}^2} + \frac{Q}{(j+1)C_0{}^2}\left(1 - \frac{\overset{\circ}{R}_s^*\tau(M_s^*)}{R_s^*}\right)^{j+1} + \frac{e_o}{(j+1)C_0{}^2}\right]$$ 6.2

giving

$$R_s^* = \frac{M_s^* C_0\,\tau(M_s^*)}{1 - \left\{\dfrac{j+1}{2}\dfrac{C_0^2}{Q}\left[M_s^{*\,2}I - \dfrac{e_o}{(j+1)C_0^2}\right]\right\}^{\frac{1}{j+1}}}$$ 6.3

The value of R_s^* corresponding to several values of M_s^* based on the density profile method (Eq. 5.14) and the above method (Eq. 6.3) are calculated for a 100 torr stoichiometric acetylene-oxygen mixture. The results, shown in Figure 13, are almost identical, indicating the insensitivity of the results to the assumption of a density profile.

3.7 Choice of M_s^*

We have seen in sections 2.3 and 2.4 of Chapter 2 that the lower limiting Mach number (M_s^*) corresponded to about the autoignition limit, *viz.*, the limit for spontaneous chemical reactions to occur. It is, however, difficult to quantitatively specify a unique value for the autoignition condition since it is very much "system and definition dependent"(63). Thus, *e.g.*, the dimensions of the experimental apparatus such as the shock tube diameter and its characteristics can influence its value. This is due to the fact that near the autoignition limit, the induction time increases exponentially and the transport effects become important.

The induction and autoignition characteristics of the oxyhydrogen mixtures have been studied rather extensively over the past several years, and on the basis of these investigations it is possible to derive some quantitative estimates for M_s^*. The dominant chemical reaction steps

during the induction period for the H_2-O_2 system are known to be (64)

1. **Initiation step** H_2, $O_2 \rightarrow O$, H, OH (A)

2. Chain branching step $H + O_2 \xrightarrow{k_1} OH + O$ (B)

                                            $O + H_2 \xrightarrow{k_2} OH + H$ (C)

                                            $OH + H_2 \xrightarrow{k_3} H_2O + H$ (D)

and 3.   Chain termination $H + O_2 + M \xrightarrow{k_4} HO_2 + M$ (E)

The chain branching reactions C and D are much faster than the reaction B so that the oxygen atom and hydroyl radicals are consumed as soon as they are produced. The principal chain carrier is therefore the hydrogen atom. From the classical explosion limit studies (46) it is also known that the HO_2 produced in the three-body recombination reaction diffuses to the walls where it is inactivated

$$HO_2 \xrightarrow{\text{wall}} \text{destruction} \qquad (F)$$
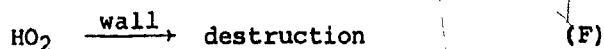
Thus, the rate at which the chain carriers can be generated depends on the competition between the chain branching step B and the chain termination step E, a consequence of which is the existence of the well-known classical second explosion limit (viz., at which $\frac{d[H]}{dt} = 0$ so that the second explosion limit criterion becomes $2k_1 = k_4[M]$).

In the case of detonations, a condition of steady diffusion of HO_2 radicals to the walls followed by their destruction through surface reactions is unacceptable. The HO_2 radicals will be expected to react in the gas phase and produce further free radicals. On the basis of matching the experimentally observed behaviour of induction times with the theoretical computations, Hirsch and Ryason (65) have shown the chain termination step to be unimportant in shock tube studies when the temperature of the shocked gases is in the range of 1200-1800°K. At lower temperatures typically of the order of 900-1100°K, however, Voevodsky and Soloukhin (66) demonstrate the profound influence of the chain termination reaction (E) in considerably increasing the induction times obtained from shock tube experiments. The large increase of induction time, in the above temperature range, also brought about a change in the character of the ignition of the shocked particles of the gas, *viz.*, from a "strong" spontaneous ignition mode to a weak "multispot" ignition mode. The temperatures calculated on the basis of the second explosion limit criterion ($2k_1 = k_4[M]$) was seen to predict the experimentally observed temperatures at which the nature of ignition changed from a strong detonative character to the weak multispot character.

Meyer and Oppenheim (67) conducted more refined experiments on the autoignition characteristics of H_2-O_2 mixtures behind reflected shocks. They showed that the change in ignition character from the spontaneous detonative mode to a weak multispot mode could be better

described by a constant value in the gradient of the induction time
with temperature.   For a shock tube of size 3.1 cm x 4.4 cm they
determine the gradient $\frac{\partial \tau}{\partial T}\Big|_p$ to be $- 2 \frac{\mu s}{{}^\circ k}$.

The shock Mach number M_s , corresponding to the extended
second explosion limit (*viz.*, [M] $= 2k_1/k_4$) using the recent chemical
kinetic data of Gardiner (68)[†] is shown in Figure 14 as a function of
the initial pressure of the gas for a stoichiometer hydrogen-oxygen
mixture.   In the same figure is also shown the Mach number obtained
using Oppenheim's criterion for the strong ignition limit (*viz.*,
$\frac{\partial \tau}{\partial T}\Big|_p = - 2 \frac{\mu s}{{}^\circ k}$).   The agreement is fairly good.   The value of M_s is
also about the same as the minimum Mach numbers observed towards the
end of the characteristic detonation cell wherein conditions are also
known to correspond to about the autoignition limit (39).   We shall
choose the value of M_s^* for hydrogen-oxygen mixtures to be given by the
criterion of the extended second explosion limit and the critical value
of the gradient of induction time as given by Oppenheim.

For other explosive gas mixtures, whose detailed kinetics are
not known, it is more difficult to independently estimate the value of
M_s^*.   In view of the rapid increase of the induction time near the
autoignition limit, we shall define M_s^* for these mixtures to be based

[†] $k_1 = 1.22 \times 10^{17} T^{-.907}$ exp ($\frac{16.62}{RT}$) $\frac{cm^3}{mol\ sec}$

$k_2 = 2 \times 10^5$ exp ($\frac{0.87}{RT}$) $\frac{cm^6}{mol^2 sec}$

R is in $\frac{kcal}{mol\ {}^\circ k}$ and T is in ${}^\circ k$

on the standard procedure for defining relaxation time in an
exponential growth or decay process (*i.e.*, 1/e of the limiting value).
Figure 15 illustrates this procedure for a 100 torr stoichiometric
oxyacetylene mixture.

The estimate of M_s^* on the basis of the large increase in
induction times and the consequent exponential cut-off procedure can
be justified by the following reasoning.   A particle entering a shock
burns after its induction reactions have taken place.   The pressure
pulse generated during the burning of the particle goes to reinforce
the strength of the shock wave.   This sequence of events is illustrated
in sketch 3.

OE) represents a decaying shock trajectory.   A particle enters
the shock at A and after an induction time τ explodes (*viz.*, at B).
The pressure pulse sent out during this explosion travels along a c^+
characteristic to catch up and strengthen the shock at D after a time t_+.
It is seen that the particle entering the shock at A is able to reinforce
the shock after a time $\tau + t_+$ during which the shock front has travelled
a distance X.   For the chemical energy to be effective in driving the
shock, it is necessary that X and $\tau + t_+$ should not be excessively long
so that the shock wave does not considerably decay before the pressure
pulse can strengthen it.   It is also possible that with large travel
(BD) the pressure pulse will get significantly attenuated before reaching
the shock.   Hence a large increase in induction time is likely to bring
about a decoupling of the shock and chemical reactions so that an expo-
nential cut-off procedure based on an exorbitant increase of induction
time is reasonable.
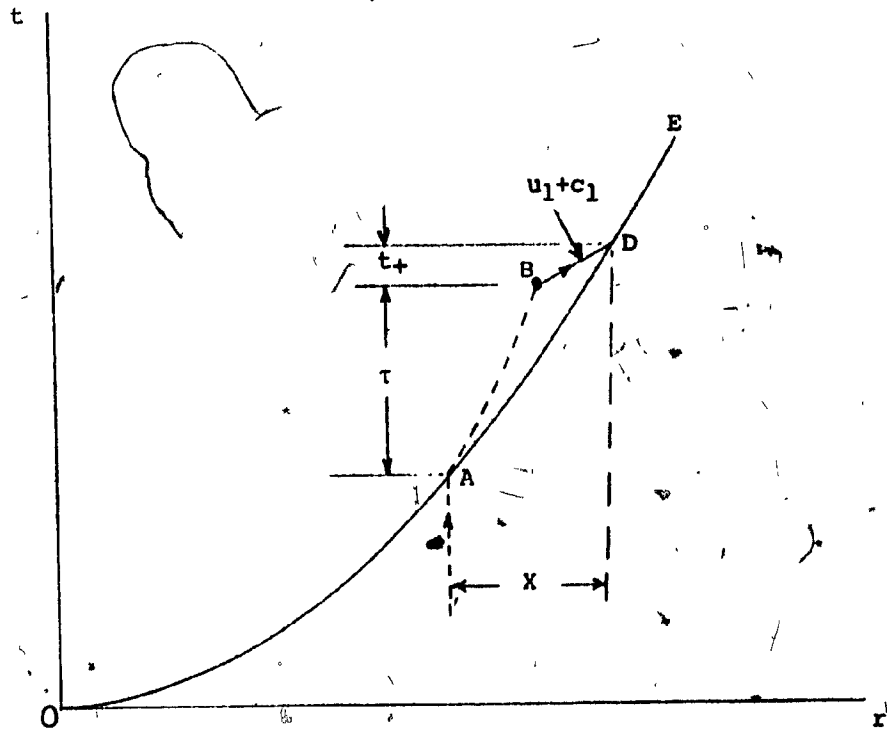
SKETCH 3: MECHANISM OF SHOCK-REACTION COUPLING

It is pertinent to note that the autoignition conditions established from experiments in rapid compression machines are much lower than those obtained on the basis of the shock tube experiments. This is partly due to the dominant role played by the walls in the former. Since the influence of walls on a detonation is fairly insignificant, it is necessary to derive the data on autoignition on the basis of the shock tube experiments.

3.8 Estimation of Initiation Energy

With the value of M_s^* known, the induction distance d is readily determined from Eq. 5.12 of section 3.5.4 and the critical detonation kernel R_s^* is obtained from Eq. 5.14. Using the value of

$$\frac{Q}{C_0^2} \int_0^{1-d(R_s^*)/R_s^*} \psi \xi^j d\xi$$

from Eq. 4.12 in Eq.4.13 and simplifying, the critical source energy required for direct initiation is determined to be

$$E_s = \frac{k_j \rho_0 C_0^2 R_s^{*j+1}}{2} \left(M_s^{*2} I - \frac{1}{(j+1)\gamma(\gamma-1)} \right) \qquad 8.1$$

Since R_s^* is proportional to the induction distance d (Eq.5.14) we note that the critical energy for blast initiation is proportional to d^{j+1} (e.g., for spherical $E_s \sim d^3$). This result is in agreement with the experimentally observed trend first demonstrated by Zel'dovich (29).

For most explosive gases of interest, the initial internal energy e_o will be very small compared to the exothermicity of the gas mixture Q, so that the Equations 8.1, 5.14 and 4.11 can be written as

$$E_s = \frac{k_j \rho_0 C_0^2 R_s^{*j+1} M_s^{*2} I}{2} \qquad 8.1(a)$$

$$R_s^* = \frac{d(M_s^*)}{1 - (\frac{j+1}{2} \frac{C_0^2}{Q} M_s^{*2} I)^{\frac{1}{q+j+1}}} \qquad 5.14(a)$$

and

$$I = \frac{Q}{(j+1) C_0^2 M_{CJ}^2} \qquad 4.11(a)$$

Substituting the value of R_s^* and I from Eqs. 5.14(a) and 4.11(a) in Eq. 8.1(a), and simplifying, we get

$$E_s = \frac{\frac{k_j \rho_0 C_0^2}{2(j+1)} d(M_s^*)^{j+1} M_s^{*2} \frac{Q}{C_0^2 M_{CJ}^2}}{\left\{ 1 - \left[\frac{1}{2} \left(\frac{M_s^*}{M_{CJ}} \right)^2 \right]^{\frac{1}{q+j+1}} \right\}^{j+1}} \qquad 8.2$$

Further, the value of Q/C_0^2 from Eq. 5.10 can be written as

$$\frac{Q}{C_0^2} \simeq \frac{M_{CJ}^2}{2(\gamma^2-1)} \qquad \qquad 5.10(a)$$

by assuming $\gamma_0 = \gamma_1 = \gamma$ and $\frac{1}{M_{CJ}^2} \ll 1$.

Also noting from Eq. 5.7 that $q+j+1 = (j+1)\psi_1$, we get E_s to be

$$E_s = \frac{\frac{k_j \rho_0 C_0^2}{4(j+1)(\gamma^2-1)} \; d \; (M_s^*)^{j+1} \; M_s^{*2}}{\left\{ 1 - \left[\frac{1}{2}\left(\frac{M_s^*}{M_{CJ}}\right)^2 \right]^{\frac{1}{(j+1)\psi_1}} \right\}^{j+1}} \qquad \qquad 8.3$$

In the above expression we note that ψ_1 is typically of the order of 6 ($\psi_1 \simeq \frac{\gamma+1}{\gamma-1}$; $\gamma \sim 1.35$) and $M_s^* < M_{CJ}$ so that the value of the denominator increases as M_{CJ} increases. Hence the equation predicts a decreasing trend in E_s with increasing M_{CJ}. This behaviour is also in agreement with the experimentally observed inverse dependence between the critical energy and CJ velocity discussed in Chapter 2.

3.9 Results and Discussion

Having recovered the experimentally observed trends by the theory, we proceed to make additional checks on the theory. The second check involves experiments conducted with an 80 torr stoichiometric oxyacetylene mixture in a cylindrical geometry in which an argon dilution of 46% was replaced by an equivalent helium dilution The detonation properties computed for these mixtures are shown in the following table.

Mixture	$2C_2H_2+5O_2+5.95$ Ar 80 torr	$2C_2H_2+5O_2+5.95$ He 80 torr
Initial density ρ_0	0.149 Kg/m^3	0.0784 Kg/m^3
Initial sound speed C_0	319 m/sec	441 m/sec
C.J. velocity	1943 m/sec	2683 m/sec
M_{CJ}	6.091	6.084
P_{CJ}/P_0	25.113	25.116
T_{CJ}	3492°K	3492°K
γ_0	1.43	1.43
γ_2	1.36	1.36
Q/C_0^2	21.26	21.25
Heat release/mass of mixture	2.16 x 10^6 J/kg	4.13 x 10^6 J/kg
Volumetric heat release	3.22 x 10^5 J/m^3	3.24 x 10^5 J/m^3

The mixture diluted with helium has a higher detonation velocity than the argon diluted mixture because of the higher sound velocity in the former.   The CJ Mach number, the pressure ratio across a detonation, the temperature of the CJ plane, the volumetric heat release rate, and the value of Q/C_0^2 are almost identical for the two mixtures.   The reaction kinetic behaviour, *viz.*, the induction time behaviour and the autoignition characteristics will also remain unchanged because both the diluent gases are equally inert (6). Hence the ratio of critical energies with argon and helium dilution using Eq. 8.3 is

$$\frac{E_{s_{Ar\ dil.}}}{E_{s_{He\ dil.}}} = \frac{\left(\rho_0 C_0^2 \ C_0^{j+1} \right)_{Ar\ dil.}}{\left(\rho_0 C_0^2 \ C_0^{j+1} \right)_{He\ dil.}} \qquad 9.1$$

which, for the cylindrical geometry (j=1), yields

$$\frac{E_{s_{Ar\ dil.}}}{E_{s_{He\ dil.}}} = 0.52 \qquad 9.2$$

Experiments give the initiation energy to be about 0.6 J/cm for the argon diluted mixture and about 1.8 J/cm for the helium diluted mixture so that the ratio of $E_{s_{Ar\ dil.}} \Big/ E_{s_{He\ dil.}}$ is about 0.33.

This value is lower than that predicted theoretically as given by
Eq. 9.2. **With the higher sound velocity and the higher thermal**
conductivity of the helium diluted mixture, the initial shock formation
process will not be as efficient as with the argon diluted mixtures.
Hence the slightly lower ratio of source energies obtained experi-
mentally for the argon and helium diluted mixture is apparently in
the right direction.

The third check on the theory is shown in Figure 16. Here
a comparison is made with the experiments in the lower range of sub-
atmospheric pressures (30 torr to 300 torr) in the cylindrical and
spherical geometries for stoichiometric oxyacetylene and oxyhydrogen
mixtures. The experimental data for the oxyacetylene mixture in the
spherical geometry is taken from the works of Bach *et al.* (39) with a
laser spark as the energy source. The results in the cylindrical
geometry for the oxyacetylene mixture are those obtained by Lee and
Matsui (28) using electric sparks. The experimental data for the
stoichiometric oxyhydrogen mixture were generated with electrical
sparks during the course of this investigation.

The shock tube induction time data of Strehlow and Cohen (69)
and White (70) was used to compute the induction distance $d(M_s^*)$ in
Eq. 5.14 for the oxyhydrogen and oxyacetylene mixtures respectively.
These induction time relations are given by the following:

$$\log_{10} \{ \tau [O_2] \} = -10.162 + \frac{16328}{4.58T} \qquad\qquad 9.3$$

$$\log_{10} \{ [O_2]^{1/3} [C_2H_2]^{2/3} \tau \} = -10.81 + \frac{17300}{4.58T} \qquad\qquad 9.4$$

The above induction time data have been obtained in highly diluted mixtures at low initial pressures for shocked gas temperatures in excess of 1200°K. There is some concern whether such data can be used near the autoignition conditions where the temperature of the shocked gases is somewhat lower. Steinberg and Kaskan (71) report data of ignition behind shocks in a 2 H_2+O_2 mixture in a shock tube 5 cm x 5 cm in the lower range of temperatures for an initial pressure of approximately 200 and 300 torr. Their data ($\tau = 3.4 \times 10^{-4}$ exp. ($\frac{11,000}{T}$)) agrees well with those given by Eq. 9.3 at the extended second explosion limit conditions for initial pressures less the half-atmosphere. Strehlow, Crooker and Cusey (72) also indicate that good agreement is obtainable with the experiments on detonation initiation behind accelerating shock waves through the use of the high temperature induction time data such as Eq. 9.3. Lee, Soloukhin and Oppenheim (1) also show that the induction times calculated behind shocks near the autoignition conditions in the experiments involving the transitional mode of initiation give very good agreement with the induction time data of Strehlow and Cohen (Eq. 9.3). Figure 17, reproduced from the work of Lee, Soloukhin and Oppenheim, demonstrates the better results obtained with Strehlow and Cohen's induction time data.

Unlike the case of the H_2-O_2 mixtures, it is not possible to ascertain the validity of the high temperature, low pressure induction time data for the conditions involved in the detonation experiments for the acetylene oxygen mixtures. We shall assume the induction data given by Eqs. 9.3 and 9.4 to be valid and compute the critical energy using Eqs. 5.14 and 8.1.

Fairly close agreement is observed between the theoretical predictions and experimental results for both the 2 H_2+O_2 and 2 C_2H_2+5O_2 mixtures over the given range of pressure (Fig. 16). From the results of the oxyhydrogen mixture, it is seen that the criterion of the extended second explosion limit for calculating M_s^* yields better agreement than the criterion $(\frac{\partial \tau}{\partial T})_p = -2 \frac{\mu s}{°k}$. The departure, in the case of the latter, is probably due to the fact that the critical value of $-2 \mu s/°k$ has been obtained in a particular shock tube of dimensions 3.1 cm x 4.4 cm and the autoignition limit is peculiar to this particular shock tube. We shall henceforth base our estimates of M_s^* for the H_2-O_2 mixtures on the basis of the extended second explosion limit.

In the theoretical model, the chemistry of the combustion process was modelled in terms of an induction zone followed by a spontaneous liberation of chemical energy Q. The variation in the induction time τ with pressure corresponding to the CJ Mach number and several other Mach numbers is shown in Figure 18 for the stoichiometric oxyacetylene mixture. The close similarity in the behaviour of the

experimentally determined critical energy curve and the induction time

curve,along with the close agreement of the theory with the experiments,

seemingly confirm the validity of modelling the chemical reactions in

terms of an induction zone followed by a spontaneous chemical energy

release.

3.10 Deviation in Initiation Behaviour at the

Higher Range of Pressure

The source energy required to initiate a cylindrical

detonation in stoichiometric oxyhydrogen mixtures begins to flatten

out when the initial pressure of the mixture is around half-atmosphere.

This tendency towards levelling off of the initiation energy with

pressure is shown in Figure 19.[†]   Knystautas (74) has also observed

---

[†]   It must be pointed out that the results reported with exploding
wires in Fig. 19 do not conform to the true source energies necessary
for direct initiation.   This is because the value of the stored
energies in the capacitors has been used in this case.   The large
changes in the resistance of the exploding wire during the electrical
discharge (73) makes the determination of the effective portion of the
stored energy causing a detonation rather difficult to estimate.
However, since the circuit elements and the length and diameter of the
wire remain the same in all the experiments, the qualitative trend
obtained with stored energy must be the same as with the true source
energy.   The results with exploding wire are included in order to be
certain that the energy deposition characteristics of the electrical
spark are not responsible for the observed pressure dependence.

the energy necessary to initiate a spherical detonation in a
propylene oxide-oxygen-nitrogen mixture (90% (2 C_3H_6O + $5O_2$) + 10% N_2)
to have a minimum at an initial pressure around 0.66 atmosphere.
Again, the experiments in planar geometry with 2 H_2+O_2 mixture reveal
that the critical energy begins to increase with pressure for the
larger values of initial pressure of the mixture.

The theoretical model predicts a continually decreasing trend
in the value of the critical energy with pressure. Our immediate
reaction is therefore to doubt the validity of the theoretical model
for the higher range of pressures. However, a closer scrutiny of
the parameters involved in the theory show that the induction time
behaviour as given by the conventional shock tube data of the form
such as Equation 5.11 gives a continually decreasing value of the
induction time with pressure ($\tau \sim 1/p_o$) so that a monotonic decrease of
the critical source energy with pressure is predicted.

Restricting our discussion to hydrogen-oxygen mixtures, we
realize that the conventional shock tube data have been derived at
relatively low pressures and high temepratures for which the three-body
recombination reactions are not influential during the induction period
(65). At the higher range of pressures, with the larger number
density of the molecules present, the probability of three-body collisions
is more likely. Hence there is an increased possibility that the
three-body recombination reactions such as given by reactions 1, 2 and 3
will occur during the build-up of chain carriers during the induction
process itself.

$$H + O_2 + M \longrightarrow HO_2 + M \qquad (1)$$

$$H + H + M \longrightarrow H_2 + M \qquad (2)$$

$$H + OH + M \longrightarrow H_2O + M \qquad (3)$$
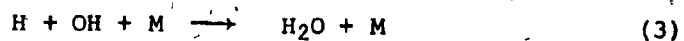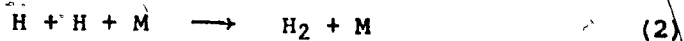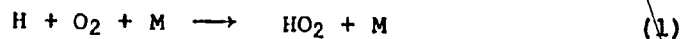
These recombination reactions will compete with the chain
initiation and chain branching reactions so that a longer period of
time will be necessary to generate an adequate number of chain carriers
for an explosive reaction to occur.   The higher the initial pressure,
the greater is the likelihood that these recombination reactions occur
earlier in the process so that the induction time can be expected to
increase at the higher range of pressures.

Oppenheim's data (67) on induction time derived in shock tubes
with the pressure of the shocked gases up to 1.96 atmospheres qualitatively
illustrates the tendency for the induction times to level off and also to
increase with pressure near the limits of autoignition.   Figure 20
shows the induction times, derived from Oppenheim's least square fit,
plotted as a function of pressure for shock Mach numbers of 5, 4.5 and 4.
Though an increasing trend with pressure is observed, no quantitative
estimates for energy are possible using these induction times.   This
is due to the large variations in induction times for relatively small
changes in pressure due to the double exponential nature of the curve
fit employed.   The absence of any reliable induction time data at
these higher range of pressures makes a theoretical prediction of
initiation energies in the high pressure region extremely difficult.

3.11 Comparison of the Present Theory with the Theories of Zel'dovich and Lee and Bach

The present phenomenological model, the Zel'dovich model (29) and the model of Lee and Bach (35) are all primarily derived by conserving the total energy enclosed by the shock front. In the following the basic similarities and differences in these different theories are briefly indicated.

In the Zel'dovich theory, the energy conservation relation is derived by neglecting the density changes behind the shock front. The total energy enclosed by the shock (viz., sum of the source and chemical energies) is given by

$$E = E_s + \frac{Q\rho_0 k_j (R_s - d)^{j+1}}{j+1} \tag{10.1}$$

From considerations that the pressure behind the shock is proportional to the energy density of the shocked volume of gas, the pressure in the wake of a detonation is written as

$$p = A \cdot \frac{E_s + \dfrac{Q\rho_0 k_j (R_s - d)^{j+1}}{j+1}}{\dfrac{k_j R_s^{\,j+1}}{j+1}} \tag{10.2}$$

where A is a proportionality constant.

By expressing the pressure, source energy and shock radius in the following dimensionless form

$$\alpha = \frac{p}{AQ\rho_0} \qquad\qquad 10.3$$

$$\beta = \frac{E_s}{\frac{k_j}{j+1} Q\rho_0 d^{j+1}} \qquad\qquad 10.4$$

and $\quad r = \frac{R_s}{d} \qquad\qquad 10.5$

Eq.10.2 can be written in the form

$$\alpha = (1 - \frac{1}{r})^{j+1} + \frac{\beta}{r^{j+1}} \qquad\qquad 10.6$$

A plot of the non-dimensional pressure α versus r for several values of the source energy parameter β is shown in Figure 21 for a spherical geometry ($j=2$).   It is observed that α passes through a minimum value and asymptotically approaches unity for $r \to \infty$.   For smaller values of the source energy parameter β, a lesser minimum pressure is obtained.   Zel'dovich postulated that the rapid drop in pressure for small values of β can quench a detonation.   He hypothesized that for the direct initiation of a detonation the decay rate must be such

that the pressure behind the shock front should not decay to a level below the Chapman-Jouguet pressure before the shock front travels a distance of the order of the reaction zone thickness d.   This statement is equivalent to saying that the time taken for the shock wave generated by the ignition source to decay to the CJ Mach number must exceed the time taken for chemical reactions to occur.

Sichel (75) recently used the Zel'dovich criterion at the radius where the source energy and chemical energy are equal.   His criterion reads

$$\frac{d(R_s^*)}{R_s^*} \leq k \qquad\qquad 10.7$$

where k is a parameter less than unity and depends on the particular gas mixture used.   The equality in Eq. 10.7 holds good at the critical conditions of initiation.   The determination of parameter k is rather difficult in Sichel's theory.   Sichel neatly avoided the evaluation of k by normalizing the initiation energy in terms of the initiation energy of a stoichiometric mixture.   The influence of finite time taken for chemical reactions to occur was not considered while determining R_s^* in this theory.   The shock behaviour at R_s^* was also approximated to be given by the ideal blast wave theory.

In the present phenomenological model, we also derived the expression for shock strength (Eq. 4.8) by conserving the total energy enclosed by the shock front. The variation of flow properties behind the shock was considered unlike that of Zel'dovich. By non-dimensionalizing the induction zone thickness d and the shock travel R_s in terms of the explosion length R_o ($R_o = (E_s/p_o)^{1/j+1}$), viz.,

$$\Delta = d/R_o \qquad\qquad 10.7$$

$$R = R_s/R_o \qquad\qquad 10.8$$

Eq. 4.8 can be written in the form

$$M_s^2 = \frac{a}{R^{j+1}} + b \ (1 - \frac{\Delta}{R})^{(j+1)\psi_1} + C \qquad\qquad 10.9$$

where a, b and C are given by

$$a = \frac{1}{k_j \gamma I} \qquad\qquad 10.10$$

$$b = \frac{Q}{(j+1)C_0^2 I} \qquad\qquad 10.11$$

and

$$C = \frac{e_o}{(j+1)C_0^2 I} \qquad\qquad 10.12$$

A plot of M_s versus R for several values of Δ is shown in Figure 22. The parameter Δ corresponds to the reciprocal of the energy parameter β in the Zel'dovich theory. The curves exhibit the tendency to pass through a minimum value in Mach number and to asymptotically approach M_{CJ} as $R \to \infty$. The initiation criterion is derived from considerations that the mimumum value of shock strength must not fall below the autoignition limit (M_s^*).

The model of Lee and Bach (35) likewise basically hinges on the conservation relation for the total energy enclosed by the shock. The effect of finite time taken for the chemical reactions to occur is modelled in terms of an equivalent heat release (Q_e) at the shock front, viz.,

$$\int_0^{R_S} \rho_0 Q_e k_j r^j dr = \int_0^{R_S-d} \rho Q k_j r^j dr \qquad 10.13$$

The flow distribution behind the shock front is presumed to be given by the reactive blast wave model with infinite chemical reaction rates. An arbitrary function for the reaction zone thickness d of the form

$$d = \delta \left[1 - e^{-E_C/E_B}\right] \qquad 10.14$$

where $\quad \delta = $ constant

$\qquad E_C = $ chemical energy enclosed by the blast wave

and $\quad E_B = $ blast energy

is chosen. A lower limit for the shock strength, *i.e.*, an auto-ignition limit M_s^* is assumed below which the chemical energy is supposed to decouple from the shock motion (a cut-off condition, *viz.* $Q_e = 0$ if $M_s < M_s^*$).

Using the functional dependence (10.14) and an equivalent heat release Q_e, the equation expressing the conservation of energy is integrated numerically for specified values of δ/R_0 to obtain the shock trajectory. Figure 23 shows the variation in Mach number with radius for a 100 torr stoichiometric $C_2H_2 + 2.5\ O_2$ mixture in the spherical geometry. The existence of steady state sub CJ velocities (corresponding to δ/R_0 of 0.004 and 0.02 in Fig. 23) is indicated unlike the acceleration to an asymptotic CJ state in the Zel'dovich model and the present theory. Mathematical instabilities are also observed to occur for certain values of δ/R_0.

The initiation energy in the Lee and Bach's theory is obtained by determining the value of δ/R_0 which yields a shock trajectory which does not decay below M_s^*. The value of δ is chosen on the basis of the experimental measurements of reaction zone thickness (hydro-dynamic thickness) in a CJ detonation.

In the present theory no functional form for the induction zone thickness is assumed, nor is an experimentally measured reaction zone thickness used. The induction distance is calculated on the basis of the experimentally observed quasi-steady propagation at Mach

numbers around M_s^* before a violent transition to a detonation.

• A simplified method is used to solve the energy conservation equation and the initiation energy is determined in terms of the chemical and physical properties of the explosive gas mixture itself.

CHAPTER 4

CHOICE OF EXPERIMENTAL PARAMETERS

4.1 Introduction

The theoretical model yields critical energies for direct
initiation in planar, cylindrical and spherical geometries.   In
order to compare the results of the theory with experiments, it is
necessary to generate reproducible results pertaining to these
geometries.   A considerable number of experiments have been conducted
over the last two decades using a variety of ignition sources (*viz.*,
electrical sparks, exploding wires, solid explosive detonators, planar
detonation from a tube, *etc.*) in spherical, cylindrical and tubular
geometries.   The magnitude of the initiation energies obtained by
the different investigators for the same explosive gas mixture at the
same initial conditions of temperature and pressure differ by orders
of magnitude.   It is therefore not possible, on the basis of these
experiments, to evolve unique values for the magnitude of the critical
energy.

The wide discrepancies in the experimental results can be
attributed mainly to the fact that the mechanisms involved in the
formation of a detonation have not been taken into account by these
researchers.   The motivation for the investigations of critical

energies for direct initiation evolved primarily from a desire to develop safety criterion in order to prevent accidental explosions in mines. There was no theoretical model to guide the experimental research and the absence of any systematic mode of investigation resulted in the haphazard collection of experimental data yielding little quantitative information other than to indicate the relative ease for a given igniter to form a detonation in a given explosive gas mixture.

For instance, much of the earlier work on direct initiation (32,76-79) using electrical sparks and exploding wires report the electrical energy stored in the capacitors ($1/2$ Cv^2) to represent the critical energy for direct initiation. It is to be expected that the stored energy is not a valid measure of the energy deposited in the gas by the spark or exploding wire discharge, since a substantial amount of ohmic losses is bound to occur in the circuit elements. Again, not all of the energy deposited in the gases is meaningful for direct initiation because a detonation may be formed fairly early in the process of energy deposition and once formed the detonation is sustained by chemical reactions. Consequently, only a fraction of the stored energy in the capacitors is meaningful for blast initiation and this fraction can be sensitive to the configurations of the electrical discharge circuit.' Since most of the reported experiments do not give details of the discharge, no quantitative information on critical energies can be deduced from these experiments.

It is also difficult to discern the geometry of initiation in many of the experiments reported in the literature. This is because we do not have, in practice, ideal point, line or planar energy sources which produce perfectly spherical cylindrical or planar blast waves. The following example best illustrates this aspect of the problem. Collins (25), in his experiments on direct initiation with MAPP[†] mixtures, employs the disc type of condensed explosive igniters (diameters ranging from 2.5 cm to 25 cm) at the centre of a container whose dimensions are 1.2 m x 1.2 m x 6 m. It is expected that the initial shock wave formed from such an igniter (especially with the larger diameters of the igniter) will be more planar than spherical. In the far field, however, the shock front will approach a spherical geometry due to the unconfined nature of the surroundings. The problem that now arises is how do we classify the geometry of initiation in these experiments. Apparently, if the mechanisms involved in the initiation process are operative very near the source itself, the initiation could be planar; if not, the geometry of initiation could as well be spherical. Collins arbitrarily presumes the initiation to be spherical.

The problem of identifying the geometry of initiation is not limited to the larger igniter sizes associated with condensed explosives. Detailed observations (22,80) of the shock waves formed during the very

---

[†] MAPP consists of a mixture of methyl acetylene, propane and propadiene.

early stages of energy release from a laser spark of submillimeter size ($\sim$ 100 μ diameter) in a spherical container show it to be highly elliptical (almost approaching a cylindrical geometry), with a large curvature in the direction of the focussing beam. It is, therefore, possible that even with the almost point source laser experiments the initiation could correspond to a cylindrical geometry rather than a spherical one. Similar problems also arise with electrical discharges. Thus it becomes difficult to recognize the geometry of initiation in the existing experiments.

We can therefore infer that the neglect of the nature of energy deposition by the ignition source and the subsequent shock dynamic phenomenon raise considerable ambiguities on the usefulness of the previous experimental investigations. For detonations in cylindrical diverging geometry and planar geometry, another factor, *viz.*, the confining walls, could influence the critical energy for direct initiation. No efforts have thus far been made to recognise the role of the confining walls on the initiation process in these geometries. The common practice has been to choose the dimensions of the explosion vessel (diameter of the tube or the width of the cylindrical chamber) to be greater than the characteristic size of the detonation structure (cell size) with the hope that the wall influences on initiation would then be small. But the experiments of Brossard and Niollet (81), and Matsui and Lee (27) show the influence of walls

on the initiation energy in the cylindrical geometry to be considerable.
An analysis of the early experimental results of Zel'dovich (29) in
tubes also demonstrates the wall influence to be considerable.

If the choice of the dimensions of the explosion chamber were
to be arbitrary, then the experiments in the different explosion
chambers could lead to varying results depending on the degree of
influence of the confinement, thus making the initiation experiment
unique for a particular configuration. Researchers, in general, have
not met with adequate success in solving the confinement effects on a
steady propagating detonation. Consequently, it cannot be predicted
off-hand how the walls of the explosion chamber could influence the
process of blast initiation.

This chapter deals essentially with the results of experiments
conducted to determine the influence of the igniter and explosion
chamber characteristics on the initiation process so as to help evolve
experimental conditions which would yield meaningful quantitative
results of a generalized nature for the direct initiation of detonations.
In view of the flexibility of control and the relative ease of monitoring
the energy deposited in the gaseous mixture, the electrical spark was
chosen for the igniter. Experiments were mainly conducted in cylin-
drical and spherical geometries and direct initiation of detonation was
inferred from velocity and pressure measurements. Details of the
experiments and methods employed to determine the critical energies are
discussed in Appendices I and II.

4.2 Minimum Explosion Area

The area of the detonation front in planar and cylindrical detonations depends on the dimensions of the detonation tube and the width of the cylindrical chamber respectively. If the source energy necessary for direct initiation were to be a unique property of the explosive gas mixture alone without being influenced by the confining walls, then the source energy per unit width of the cylindrical chamber in the cylindrical geometry and the energy per unit area of the tube in the planar geometry must be a constant for a particular gas mixture regardless of the width of the cylindrical chamber or the diameter of the tube.

To simulate the influence of confinement a series of experiments were performed in the cylindrical geometry with the height of the cylindrical chamber varying between 1/2 cm to 5 cm. Different gas mixtures ranging from the highly detonable acetylene oxygen mixture to the relatively less detonable H_2-O_2 mixture at substmospheric pressures were employed.

Figure 24 shows a plot of the energy per unit height of the cylindrical chamber (joules/cm) versus the height of the chamber (1) for the different explosive gas mixtures. The characteristic transverse wave spacing (S) for these particular mixtures is also shown in the figure. It is obvious that the value of $E_s/1$ is considerably influenced by the width of the chamber, the influence becoming aggravated as the cell size of detonation, S, increases. A tendency for $E_s/1$ to

approach a constant value is seen when the height of the chamber
contains about 7 to 14 detonation cells.

That the walls can exercise such a controlling influence
on the initiation process is rather surprising. The quenching
thickness for a detonation is known to be extremely small (10),(less
than a transverse wave spacing). In fact it is well documented that
steady detonations can be maintained in sub-millimeter size tubes (82)
and in a cylindrical-diverging geometry with an extremely small height
of the cylindrical chamber (13). Consequently some doubt is likely
to arise as to whether the observed dependence on gap length is a
reflection of the characteristics of the spark discharge itself.

In order to verify that the trend in the results is not due
to the energy transfer characteristics of the spark discharge itself,
the overpressure of an unreactive blast wave at fixed distances from
the spark was measured by monitoring the reflected shock pressure for
different heights of the chamber. It was observed that the measured
pressures at a fixed value of E/l for the different widths, l, were
about the same (Fig. 24a). It can therefore be inferred that the
energy deposition characteristics are not responsible for the observed
trend in the results.

Besides, the experiment of Brossard and Niollet (81) also
confirms the observed influence of confinement on initiation. Brossard
and Niollet conducted an investigation of the transfer of energy from
an exploding wire to a detonating gas in circular sectored discs of

height 2, 6, 14 and 25 mm.   The gas mixture used was stoichiometric

propane oxygen at a pressure of one atmosphere.   They reported the

energy for direct initiation in terms of the stored energy in the

capacitor for the different heights of the sectored disc.   As

mentioned in the introduction to this chapter, the stored energy is

not a meaningful quantitative parameter because it fails to take into

account the losses in the switch and circuit connections and also ignores

the fraction of the total energy deposited in the explosive gas that

actually contributes to the formation of a detonation.   Nevertheless,

the stored energy measurements of Brossard and Niollet can be expected

to indicate the trend in the critical energy for the different heights

of the chamber.   Their results are replotted in Figure 25 in terms of

stored energy per unit chamber height.   The tendency for E/1 to be

a constant is observed for 1 greater than about 7 mm.

The transverse wave spacing for the one atmosphere stoichio-

metric propane oxygen mixture has been deduced to be about 1/2 mm. by

Edwards (33) on the basis of spin frequency measurements.   We

therefore see that even in Brossard and Niollet's experiments E/1

reaches a constant value when the chamber width contains about 14 cells

of detonation.

The table, given below, compares the height of the chamber

at which E/1 tends to be a constant (we shall call this l) with the

transverse wave spacing, S, for the different gas mixtures.

Gas mixture	l^* (cm)	S (cm)	$n = \dfrac{l^*}{s}$
300 torr 2 C_2H_2 + 5 O_2	1	.07	14
100 torr 2 C_2H_2 + 5 O_2 (a)	1.5	.23	7
80 torr 2 C_2H_2 + 5 O_2 + 6 Ar	2.5	.45	6
80 torr 2 C_2H_2 + 5 O_2 + 6 He	3.5	.7	5
380 torr 2 H_2 + O_2	3	.25	12
1 atm C_3H_8 + 5 O_2 †	.7	.05	14

(a) Result of Matsui and Lee

†   Result from Brossard and Niollet

A few experiments conducted in the planar geometry in circular tubes also reveal that the source energy per unit cross-sectional area (E_s/A) tends to a constant value when the diameter of the tube contains about ten characteristic cells of detonations. Figure 26 shows the values of E_s/A plotted as a function of the tube diameter ϕ for a 100 torr 2 H_2 + O_2 and a 40 torr 2 C_2H_2 + 5 O_2 mixture. For the 40 torr oxyacetylene mixture, E_s/A reaches a constant value for a tube diameter around 6 cm.   The transverse wave spacing S is about 0.55 cm for this mixture so that the ratio of this limiting tube diameter to the transverse wave spacing is about 11.   For the 100 torr oxyhydrogen mixture, whose transverse wave spacing is about 1 cm, E_s/A tends to reach a constant value when the tube diameter is about 8 cm.

These experiments in cylindrical and planar geometries
indicate that E/1 and E/A reach unique values independent of the
dimensions of the explosion chamber when an adequate explosion area
containing about 7 to 14 characteristic cells of detonation across it
is formed.   If the dimensions of the explosion chamber allow the
formation of a smaller explosion front, the confinement begins to
influence the initiation process and larger magnitudes of source energy
are required.

On the basis of the detonation kernel theory a qualitative
analysis reveals that the source energy must be able to form an adequate
explosion area containing about 10 cells of detonation even in the
spherical unconfined geometry.   This is seen as follows: It has been
shown that the ignition source in blast initiation must be capable of
forming a kernel of size R_s^*.   It is also known that the propagation
of a detonation is through a series of periodic initiations at the
intersection of the transverse waves so that the length of the detonation
cell must approximately correspond to R_s^* (section 5.2.1).   The
characteristic cell size of a detonation, S, is about 0.6 times the cell
length (6).   Hence the number of cells of detonation associated with the
detonation kernel is

$$\frac{2\pi R_s^*}{S} \simeq \frac{2\pi}{.6} \simeq 10.$$

4.3   Role of a Minimum Explosion Area

4.3.1   Pressure and Detonation Cell Measurements

It is instructive to determine why a minimum explosion area
containing about 10 cells of detonation across it is necessary in
order to overcome the adverse effects of the confinement on the initiation
process.   In order to gain some understanding of the process it
seemed appropriate to examine the influence of different explosion
areas on the characteristics of a detonation.   Hence pressure profiles
behind a detonation front and the characteristic detonation cell sizes
were monitored for various heights of the cylindrical chamber.   The
energy released by the spark was adjusted to be equal to the critical
energy for the particular mixture at that particular chamber height
so as to avoid any possibility of an overdriven detonation. . The
pressure transducer, located in flush with the walls of the chamber,
was placed at a distance of 17.5 cm. from the ignition source.

Figure 27 shows the pressure profiles obtained for a
stoichiometric hydrogen-oxygen mixture at an initial pressure of half-
atmosphere with the height of the cylindrical chamber maintained at
6 mm, 19 mm and 30 mm.   For the smaller chamber width there is
observed to be a considerable overshoot in pressure in excess of the
CJ pressure at the detonation front.   The classical Jouguet, Taylor,
Zel'dovich (JTZ) theory is seen to predict the pressure profiles
fairly well though there is a clear tendency for the pressure downstream

of the detonation front to be lower with smaller heights of the

chamber.[†]   Edwards (83), on the basis of experiments in tubes of

diameters 1.6, 3.8, 5 and 10 cms., also found a decrease in pressure

far downstream of the detonation front for smaller diameters of the

tube.

Smoked pictures showing the characteristic detonation cells

for an 80 torr stoichiometric acetylene oxygen mixture diluted with 46%

helium are given in Figure 28 for the case of the cylindrical chamber

with different heights of the chamber.   The assortment of continually

varying sizes makes it difficult to specify a unique transverse wave

spacing from these records.   However, the trend for an increased

wave spacing with smaller chamber heights is clearly evident.   For

larger chamber heights the cell structure is seen to approach that

determined in a tube having a diameter of 25 mm.   Pressure profiles

behind a detonation front corresponding to these structures are also

included in the figure.

The tendency towards larger cell sizes with the corresponding

overshoot in frontal pressures (von Neumann spike) is suggestive of the

approach to a marginal detonation (84).   It is relevant to note that

increases in cell sizes have also been observed with steady detonations

in tubes and the common belief has been one that the tube will influence

---

[†]   The determination of pressure profile using the JTZ theory
      is given in Appendix V.

the cell size only if its diameter is less than the cell spacing (85).
However, a closer look at the already existing data obtained for cell
sizes in tubes of different diameters reveals that the cells begin
to grow even when the tube contains about 7 to 10 cells of detonation.
As an example, Figure 29 shows the dependence of cell size on tube
diameter for a stoichiometric H_2-O_2 mixture at a pressure of 130 torr.

We are therefore led to conclude that the cell size of a
detonation and the pressure profile behind a front are also affected
by the confinement. The pressure profile approaches that given the
JTZ theory and the cell size also approaches a constant value as the
initiation energy per unit length or area tends to a constant value.
The confinement then contains an adequate number of detonation cells.

4.3.2   Momentum and Heat Losses

Confinement is always associated with losses and the most
natural tendency is to try to explain the above experimental observations
in terms of friction and heat transfer to the walls of the chamber. A
considerable amount of work in the fifties has attempted to explain
the characteristics of a steadily propagating detonation in tubes in
terms of friction and heat transfer at the boundary layer. A critical
survey of these works should help us decide whether we should pursue in
this direction to interpret the observed experimental behaviour.

Kistiakowsky et al. (86), Peek and Thrap (87), and Guenoche
and Manson (88) have shown that the velocity of a detonation is reduced

due to the presence of walls of the tube and that the reduction in velocity depends on the tube diameter and the initial pressure of the explosive gas mixture.   Fay (89) in 1959 developed a phenomenological explanation in terms of the friction losses in the boundary layer.   He used the classical one-dimensional ZDN model of a detonation[†] and showed that the momentum loss at the boundary layer resulted in the divergence of the flow behind the shock front (negative displacement thickness).   He was able to obtain reasonable estimates of the velocity deficit and also recover the experimentally observed dependence of the deficit on tube diameter and initial pressure of the gas mixture. More recently Dove et al. (8) employed this one-dimensional friction loss model with the detailed kinetics of the chemical reactions to predict velocity deficits.   They also recover the experimentally observed trends though their numerical predictions are a gross underestimate.

The detonation velocity is proportional to the square-root of the negative slope of the Rayleigh line joining the initial state with the final state in the Hugoniot curve.   Hence relatively large changes in the location of the final state will only produce second order changes in detonation velocity making the latter a relatively in-sensitive parameter.   It is therefore rather dangerous to accept a theory on the basis that it recovers the experimentally observed trend

---

[†]   The ZDN model of a detonation, named after the originators of the model, viz., Zel'dovich, Döring and von Neumann, treats a detonation as an unreactive shock followed by a zone of chemical reactions culminating in a sonic CJ plane.

in the insensitive velocity parameter.   The effect on more sensitive

parameters such as pressure or density must be ascertained.   Edwards

(90), on the basis of pressure profile measurements in tubes, showed

that Fay's boundary layer friction model gives a gross overestimate

for the effect of tube diameters on the pressure profile.

The role of heat losses, on the other hand, has been considered

by Edwards et al. (91).   Using an experimentally determined skin

friction coefficient on the basis of Reynolds analogy, they demonstrated

that a one-dimensional theory based on heat loss to the walls in the

expansion region behind the detonation front gives reasonable agreement

with the observed pressure profile in a 1.6 cm diameter tube.   The

heat loss measurements were in agreement with the theoretical estimates

of Sichel and David (92).   Again, Strehlow (93) reported that the

heat loss theory gives good prediction for pressure profiles in a

marginal detonation when an arbitrary value of skin friction coefficient,

25% less than that of Edwards', is used.   The heat loss theory is,

however, unable to explain the relative ineffectiveness of the walls

in influencing the pressure profile for the larger diameters of the tube.

It is also well-known that the one-dimensional lossless

theories predict pressures and densities very well for overdriven

detonations but yield considerable errors for self-sustained detonations

(94).   A radical change in the loss mechanisms cannot be expected

to be operative between the self-sustained and overdriven regimes.   The

one-dimensional loss theories are obviously useful as engineering
models in that they yield some quantitative predictions.   But their
limited validity and the, by now, well-established three-dimensional
character of a detonation suggest that a more appropriate explanation
for the confinement effect should arise from the interaction of the
walls with the self-sustaining character of a detonation wave.

4.3.3 Influence of Wave Interactions

We shall attempt a qualitative explanation of the confinement
effect in terms of the self-sustaining character of the detonation wave.
It is well-understood that a detonation has a strong three-dimensional
character with transverse shock waves propagating laterally along the
detonation front.[+]   The transverse waves in a steady propagating
detonation derive their strength from the chemical reactions occurring
behind them (95,96).

A decrease in the rate of chemical reactions adjacent to the
walls due to the cooling of the gases or loss of chain carriers to the
walls would lead to a weakening of the strength of those transverse
waves immediately near the wall.   The strength of the Mach stem
shock generated from the intersection of such a weakened transverse
wave would be less than what it would have been in the absence of any
attenuation in the strength of the causal transverse shocks.

[+]   Details of the wave interaction process and the terminology used
to describe the different shock waves are given in section 5.2.1 of
Chapter 5.

Barthel (97), from his work with isolated Mach stems, has shown that the explosive release of energy behind the newly formed Mach stem shock could lead to either an augmentation in the strength of the transverse waves or a decrease in their strength depending on the induction time delay and the time taken for a pressure pulse associated with the explosive release of energy behind the initial Mach stem shock to catch up with the lead shock. He demonstrated that the strength of a transverse shock is increased if the interaction between the pressure pulse and the lead shock occurs when the latter is still a Mach stem shock while a decrease in the strength of the transverse wave takes place if the pressure pulse is so delayed that it meets the lead shock when it has already become an incident shock wave.

The reduction in the strength of the initial Mach stem shock, consequent to the wall effect, results in a longer induction time so that the pressure pulse generated from the explosive energy release behind the initial Mach stem shock is now generated later in the process. If the increase in the induction time is such that the pressure pulse reaches the lead shock wave when it has already become an incident shock, then in accord with Barthel's theory, the strength of the transverse shock further decreases. Such a process leads to the failure of the transverse wave and a cell of detonation, as such, near the wall. However, local ignition sites may be produced after the transverse wave has almost disappeared and the interaction of the waves from these ignition points could lead to the formation of new transverse waves later in the process (4).

The transverse pressure oscillations in the wake of the detonation caused by the transverse waves tend to couple with the acoustics of the explosion chamber. The acoustical vibrations, in turn, tend to even out the lateral distribution of the transverse waves. Consequently, if the detonation consists of a few number of cells and if one or two of these cells were to disappear, say due to the wall effect, the tendency to even out the transverse wave distribution would lead to a conspicuous increase in the average size of a cell. On the other hand, when the front consists of a large number of cells the influence would be minimal.

The cumulative decrease in the strength of the transverse shock waves will also cause chemical reactions to occur further down the tail of the transverse waves (since the induction time is now longer) so that the von Neumann spike now becomes more distinct. With the chemical energy released later in the process, the effective chemical energy available for driving the shock front decreases. It will, therefore, be necessary for the source energy to generate a larger detonation kernel before the chemical energy can sustain the shock. Hence the trend towards larger source energies for blast initiation associated with larger cell sizes and a marked increase in the pressure spike with a reduced number of cells in the detonation front can be explained.

The difficulties in mathematically describing the Barthel theory along with the complexities associated with the coupling of the

transverse waves with chemical reactions make a quantitative

estimation rather difficult.   Fujiwara recently reported some

experiments in tubes with catalytic wall surfaces (98) wherein gas

phase reactions adjacent to the wall are retarded in preference to

surface reactions at the walls.   The large decrease of the detonation

velocity in these experiments also point towards the likelihood of an

explanation for the confinement effects in terms of weakening of the

transverse waves adjacent to the wall.   Further work needs to be done

in this area to evolve a quantitative explanation.   It is interesting

to note that even in the detonation diffraction experiments, the failure

of the detonation occurs when the smaller tube contains about ten cells'

of detonation (99).   The hydrodynamic thickness of a detonation also

contains about the same number of cells of detonation (34,100).

4.4 Geometry of Initiation

In practice it is impossible to have ideal sources of energy,

e.g., a point, a line or a planar source.   Consequently it is not

likely that a perfectly spherical, cylindrical or planar shock wave

can originate from these ignition sources.   During the early phase

of shock travel, the shock motion is considerably influenced by the

characteristics of the energy source whilst with a longer distance of

travel the shock wave tends to adjust to the constraints imposed by the

confining chamber.   In this section, the results of experiments carried out to evolve a criterion for identifying the geometry of initiation is discussed.   These experiments essentially follow up the work of Matsui and Lee (27) to a wider range of conditions.

Matsui and Lee report on experiments conducted to determine the influence of different electrode configurations on the initiation of spherical detonations.   Linear electrical sparks with varying distance between the electrodes $\mathcal{L}$ were used in their experiments. On the basis of the results obtained by them for a stoichiometric oxy-acetylene mixture at an initial pressure of 100 torr, it is seen that the explosion length $R_o^\dagger$ $\left(R_o = (E_s/P_o)^{1/j+1}\right)$ can be used to identify whether the geometry of initiation is cylindrical or spherical for this particular mixture.   When R_o is less than the length of the electrical spark $\mathcal{L}$, the geometry of initiation is seen to be cylindrical whilst for $R_o > \mathcal{L}$ the geometry of initiation is spherical.

The experiments of Matsui and Lee were extended to stoichio-metric mixtures of acetylene and oxygen at pressure of 300 torr, 200 torr and 80 torr with 46% of argon.   Experiments were done in a spherical geometry with flat 1/8" brass electrodes at different electrode spacings (Appendix I).   Figures 30 and 31 show the critical energy in joules and joules/cm for the various electrode gaps $\mathcal{L}$.   Also included in the figures are the results of Matsui and Lee for the 100 torr oxy-acetylene mixture.

$\dagger$ This definition of explosion length is slightly different from that of Matsui and Lee in that the factor γk_j in the denominator, is deleted.

For the 200 torr mixture the critical energy E_s is seen to be constant around 0.05 joules for electrode spacing up to 1.4 cm indicating a spherical detonation. Thereafter for larger gaps, E_s is observed to increase with ℓ suggesting the approach to a cylindrical initiation with E_s/ℓ tending to be a constant. The value of R_o calculated on the basis of spherical initiation with $E_s = 0.05$ joule is 1.23 cm and is 1.3 cm on the basis of the asymptotic cylindrical value of 0.047 j/cm.

For the 80 torr acetylene oxygen mixture with argon dilution the initiation energy is observed to be steady up to a gap size of 4.5 cm. It was not possible to conduct experiments for larger electrode spacings because of the erratic nature of the spark discharge. The initiation is seen to conform to a spherical mode for the range of electrode spacings employed. The value of R_o is seen to be about 7 cm.

With the acetylene-oxygen mixture at a pressure of 300 torr the initiation energy monotonically increases with the electrode spacings indicating the difficulty of achieving a spherical initiation. The R_o calculated on the basis of cylindrical symmetry is 0.8 cm.

In view of the errors involved in evaluating the smaller resistances associated with spark gap lengths less than 1/2 cm, and the erratic nature of breakdown for gaps larger than 5 cm., it was not possible to extend the results to mixtures with R_o varying by orders of magnitude. The limited results of Figures 30 and 31, however, confirm

the hypothesis that with a linear electric spark of length $\mathcal{L}$ in an unconfined medium, initiation is spherical if $R_o > \mathcal{L}$ and cylindrical if $R_o < \mathcal{L}$.

The physical interpretation for the above experimental findings, *viz.*, that the geometry of initiation can be characterized by R_o, is as follows: For a given value of source energy the blast wave has a stronger force and a relatively longer travel when the initial pressure of the gas mixture is reduced. This is due to the reduced mass of the gas processed by the blast wave at the smaller pressures for the same distance of travel. The explosion length R_o, therefore, is a relative measure of how far away from the source a specified shock strength can be maintained – the larger the R_o, the greater is the distance at which the source can support a strong shock wave. The region of influence of the source configuration, on the other hand, depends on the size of the source. Hence it is to be expected that for large values of R_o compared to the characteristic source demension L, the igniter source configuration will exert a much lesser influence on shock motion than when $R_o < L$.

From the detonation kernel theory, the condition for direct initiation is seen to be the formation of a sufficiently strong shock wave (M_s^*) at a sufficient distance (R_s^*) from the ignition source. If the source energy in the critical energy experiments is such that $R_o > L$, then the influence of the source characteristics on the shock

configuration when the Mach number has decayed to about M_s^* will be much less than if $R_o < L$.   Hence the value of R_o in relation to characteristic source dimension L can be used to decide whether the geometry of initiation is characterized by either the source or the confinement.

In the experiments considered above, the source energy was a linear electrical spark approximating more or less to a line source of energy, and thus the observed trend was towards a cylindrical initiation with small values of R_o.   If an almost planar source of energy were used, such as the disc type of igniter used by Collins (25), then with R_o less than the characteristic dimension of this igniter (say, diameter of the disc D) the initiation should be expected to be planar.   For $R_o > D$, the geometry of initiation would be spherical.

We have so far restricted our discussions to an unconfined geometry for which the late time motion of the blast wave approaches a spherical geometry.   With tubular and cylindrical geometries, the far field motion of the blast wave will approach planar and cylindrical geometries respectively.   The initiation geometries in these confinements should be expected to conform to a planar and cylindrical geometry only if R_o is greater than characteristic dimensions of the ignition source used unless a planar or line source of energy is employed.

It was also seen in section 4.2   that a minimum explosion area containing about 10 cells of detonations is necessary to overcome

the adverse effects of confinement on the initiation process.   Hence
the criterion to achieve meaningful results for planar and cylindrical
initiations in tubes and cylindrical containers is

$$R_o > L_{ignition\ source}$$

$$\phi\ ,\ 1 \geq 10S$$

(ϕ denotes diameter of the tube, and 1 the width of the

cylindrical chamber).

An upper ceiling to the diameter of the tube and the width
of the cylindrical chamber is expected since with very large dimensions
the geometry of the chamber will conform to an unconfined spherical mode.

4.5   Effect of Igniter Characteristics

4.5.1   Duration of Energy Release

In section 2.2 of Chapter 2 we saw that the source energy for
blast initiation could change by orders of magnitude as the duration of
the energy release increased.   For example, in a cylindrical geometry
with 2 C_2H_2 + 5 O_2 at 100 torr, E_s increases from about 0.1 J/cm to
about 10 J/cm as the energy release time is increased from 1 μs to 10 μs
whilst for a mixture of 2 H_2 + O_2 at half-atmosphere E_s increases from
3 J/cm to 40 J/cm with an increase in time from 3 μs to 10 μs (Fig. 1).

For energy release periods less than a microsecond for the 100 torr oxyacetylene mixture and 3 μs for the half-atmosphere oxyhydrogen mixture, E_s is seen to have a constant value. These results were obtained with damped oscillatory electrical discharges for which the time history of energy release is given by (see Appendix II)

$$E_s = \frac{I_o^2 R_{sg} \omega}{4(\alpha^2+\omega^2)} \left[\frac{\omega}{\alpha} (1-e^{-2\alpha t}) - e^{-2\alpha t} \left(\frac{2\alpha}{\omega} \sin^2\omega t + \sin 2\omega t \right) \right] \quad 5.1$$

It is shown in Appendix II that the effective energy driving a detonation from a damped electrical discharge, is released during the early period of the discharge itself (energy released till about the first quarter cycle of discharge). For these small times the energy can be shown to have a cubic dependence on time, viz.

$$E_s \simeq \frac{I_o^2 R_{sg} \omega^2}{3} t^3 \quad 5.2$$

For other energy sources, such as laser sparks, solid explosive detonators, etc., the time history of the energy release is expected to be different and it is not certain whether the minimum energy requirement will also correspond to those values obtained by the electrical discharge. Experiments with laser spark show that

the minimum energy requirement agrees very well with the results obtained with the short duration electrical spark (e.g., with spherical symmetry, the energy obtained for the initiation of a detonation in a 100 torr oxyacetylene mixture is 0.3 joule with a laser spark (15) as well as with a linear electrical discharge (Fig. 30)). This indicates that the time history of energy release does not really influence the magnitude of the initiation energy provided that the duration of the energy release is sufficiently short. It is necessary that the initiation energies be determined under this limiting condition of rapid energy deposition so as to eliminate their dependence on the source energy release characteristics.

In certain other classes of problems such as the initiation of a flame or a dust explosion wherein the governing mechanism is one of directly igniting the mixture rather than production of a shock wave which subsequently ignites the mixture, a longer duration spark is more effective. This aspect of the problem has been demonstrated by Eckhoff and Enstad (101) and by Balal (102).

4.5.2 Igniter Configurations

On the basis of the discussions of section 4.4 it is noted that the configurations of the ignition source will influence the detonation initiation process only if the explosion length R_o is less than the characteristic dimensions of the igniter. In other words, the

energy for blast initiation should be independent of the configurations

of the energy source provided $R_o > L_{ignition\ source}$.

Some simple-minded experiments were conducted to test the

above reasoning with concentrated line type of electrical discharges

and diffused type of electrical discharges in a tube of diameter 1.25 cm

for large values of R_o. The results, shown in Table I, indicate the

insensitivity of the initiation energy to the configurations of the ignition

source. The experiments of Matsui and Lee (27) with pointed, blunt

and spherically capped electrodes also demonstrate the configurations

of the source to have little influence on initiation energies when the

explosion length R_o of the source is much larger than the characteristic

dimensions of the igniter.

4.6 Equivalence of R_o in Different Geometries in Blast Initiation

The duty of the energy source in the blast initiation of

detonations has been shown to involve the formation of a sufficiently

strong shock at a certain distance R_s^* from the ignition source. Since

the initial shock motion is dominated by the energy released from the

ignition source, and since "self similar" blast waves are generated at

identical scaled distances (distance scaled with respect to R_o), R_o

appears to be a pertinent parameter by which we could also characterize

the initiation process. As discussed in section 4.4 the diminished

influence of the source energy in forming a shock wave of a certain strength at some fixed distance from the energy source is also contained in the parameter R_o. In the following, therefore, we shall investigate the behaviour of the parameter R_o in direct initiation in the different geometries.

We first note that from Eq. 8.3 of Chapter 3 we can express the explosion length R_o corresponding to the critical source energy for direct initiation as

$$R_o = \frac{\left(\dfrac{\gamma \, k_j M_s^{*2}}{4(j+1)(\gamma^2-1)} \right)^{1/j+1}}{1 - \left\{ \dfrac{1}{2} \left(\dfrac{M_s^*}{M_{CJ}} \right)^2 \right\}^{\frac{1}{(j+1)\psi_1}}} \, d(M_s^*) \qquad 6.1$$

The value of M_s^* is typically around 4 for most explosive gas mixtures. The Chapman-Jouguet mach number M_{CJ} varies between 8 to 5, depending on the particular fuel-air or fuel-oxygen mixture used. Taking a mean value of γ of 1.35, the value of $R_o/d(M_s^*)$ for a an M_{CJ} of 8, 7, 6 and 5 in the spherical, cylindrical and planar geometries is given in the following table.

M_{CJ}	$R_o/d(M_s^*)$		
	Spherical	Cylindrical	Planar
8	23	22	19
7	26	24	21
6	31	29	25
5	40	38	32

From this table we note that the value of $R_o/d(M_s^*)$ is fairly constant in the different geometries for a given value of M_{CJ}. We had also seen that at $M_s \sim M_s^*$ the shock motion is quasi-steady and that the flow gradients behind the shock can be neglected under the critical conditions of initiation (Ch.3, sec. 3.5.4). Hence $d(M_s^*)$ for a given explosive mixture at certain initial conditions of temperature and pressure must be the same in the three geometries. We can therefore hypothesize that the value of R_o corresponding to the critical energy for direct initiation of a given explosive gas mixture must be the same in the planar, cylindrical and spherical geometries.

The value of R_o obtained from the experiments in cylindrical and spherical initiation (Fig. 24 and 30) when the confinement does not influence the initiation process is shown in the following table. The value of R_o is seen to have almost the same value in the cylindrical and spherical geometry for each of the explosive gas mixtures used.

Gas mixture	R_0 with spherical initiation	R_0 with cylindrical initiation
	cm	cm
100 torr $2C_2H_2 + 5O_2$	2.8	3
200 torr $2C_2H_2 + 5O_2$	1.23	1.3
300 torr $2C_2H_2 + 5O_2$	0.83	0.82
80 torr $2C_2H_2 + 5O_2 + 6$ Ar	7	7.4
380 torr $2H_2 + O_2$	6.4[†]	7.4
800 torr $2H_2 + O_2$	7.2 (Zel'dovich [29])	6.9 (extrapolated)

The initiation energy for the spherical detonation of the 380 torr stoichiometric hydrogen-oxygen mixture is inferred from the critical tube diameter necessary to re-establish detonations in the detonation diffraction experiments. It is assumed that the initiation energy in this case corresponds to the compression work done by the unattenuated portion of the detonation as it expands into the larger volume (28).

In the planar geometry we obtain from the results of Zel'dovich (29) an E_s/A of 0.8 J/cm^2 for the 800 torr $2H_2 + O_2$ mixture. This gives a R_0 of 7.5 cm. This value of R_0 agrees very well with the value of 7.2 cm obtained in spherical symmetry and a value of 6.9 cm in the cylindrical symmetry given in the above table. For a 40 torr

---

[†] Deduced on the basis of diffraction experiment of Matsui (103).

$2C_2H_2+5O_2$ mixture, we got for planar initiation an E_s/A of about 0.04 J/cm^2 (Fig. 26) which gives R_o to be 7.5 cm. This compares with the value of R_o of 7.2 cm calculated on the basis of cylindrical initiation (28) for which E_s/l is about 0.28 J/cm.

Nicholls (24) and Collins (25) report experiments on the initiation of MAPP-air mixtures in cylindrical and spherical geometries respectively. Nicholls obtained an initiation energy of 3100 J/cm for the stoichiometric MAPP-air mixture in the cylindrical geometry which corresponds to an R_o of 175 cm. Collins, from the bag tests, obtained an initiation energy of 19 Kcals which corresponds to an R_o of 92 cm. The difference in the value of R_o for these two geometries is understandable since in Nicholls' experiments the geometry is not purely cylindrical. He uses a sectored disc whose width is about 5 cm and whose height varies from 2.5 cm to about 28 cm over a distance of 70 cm. The characteristic transverse wave spacing for this mixture is expected to be comparable with the width of the chamber so that the experimentally measured value of E_s/l is bound to be much larger due to the effect of the confinement (section 4.2). Consequently, the higher value of R_o in Nicholls' experiments is to be anticipated. With experiments conducted under proper conditions so as to yield results independent of the confinement and source energy characteristics, the value of R_o will remain the same in the different geometries for a given explosive gas mixture.

PROPAGATION AND LIMIT BEHAVIOUR OF DETONATIONS

5.1 Introduction

The initiation, propagation and limit characteristics of a detonation are closely related. Experiments show that a detonation wave, which appears to be globally steady and to propagate at a velocity given by the classical one-dimensional Chapman-Jouguet theory, is actually highly nonsteady and three-dimensional. It seems that a detonation wave proceeds through a series of localized and periodic self-initiation processes. An inability of the explosive gas mixture to generate the necessary conditions for the formation of such localized points of initiation or driving is known to result in the incapability of the mixture to support a detonation wave, and thereby leads to the existence of the limits of detonability. In view of the basic similarities of the initiation, propagation and limit behaviour, it appears worthwhile to evolve a unified study of these three basic features of a detonation. Such an attempt is made in this chapter. Detailed mechanisms of the propagation and limit characteristics are discussed and their theoretical modelling in terms of the initiation problem is considered. Quantitative prediction of these characteristics using the phenomenological theory of initiation based on the detonation kernel concept is explored.

5.2 - Propagation Characteristics of a Detonation

5.2.1 Modelling of the Propagation in Terms of Local Periodic Initiations

Figure 32 shows a schematic 2-d representation of the system of interacting shock waves in a detonation front. M, I and T represent the Mach stem shock, the incident shock and the transverse (or reflected) shock respectively. The interaction pattern of these shock fronts corresponds to a Mach type of interaction or the triple point interaction. The Mach stem shock is much stronger than the incident and reflected shocks. The slipstream s, shown in the figure by the thin chain lines, separates the gases processed by the Mach shock from the gas processed by the incident and transverse shocks. The path of the triple point, O, is shown by the broken lines.

The triple points on the detonation front trace out a typical diamond-shaped pattern which is known as the characteristic cell of a detonation. This characteristic shape arises out of the lateral motion of the transverse shock waves in the wake of the incident and Mach stem shocks. The distance between the adjacent transverse shock waves of the same family (viz., those moving in the same direction, i.e. either upwards or downwards) is spoken of as the characteristic transverse wave spacing. It is denoted by S in Figure 32. This characteristic spacing has been shown to depend on the chemical and physical properties of the explosive gas mixture (104,105).

In general, the characteristic cells of a detonation are not identical to each other. Numerous experiments of Strehlow and his students with a variety of reactive gas mixtures have revealed that a regularly repeatable structure can only be obtained for certain gas mixtures - hydrogen, acetylene or ethylene, when diluted with argon or helium. Nevertheless, even when the cells in a detonation are not perfectly repeatable, there is a tendency for the majority of the cells in a self-sustained detonation to favour some average cell size.

In Figure 32 it was presumed that the system of interacting shock fronts are two-dimensional. However, in practice, the detonation front has a three-dimensional character and we have transverse shock waves propagating in a direction perpendicular to the transverse waves shown and perpendicular to the direction of propagation as a whole. For detonations propagating in rectangular tubes, this second set of transverse waves is usually called "slapping" waves. Strehlow (6) has shown that these two sets of orthogonal transverse waves are decoupled and do not interact with each other. (They "walk" relative to each other). The characteristic transverse wave spacing and the strength of the transverse waves have been observed to be the same both with and without the presence of slapping waves in rectangular tubes. Hence a study of the two-dimensional wave structure should suffice to describe the basic propagation characteristic of a detonation, and in view of the simplicity we shall illustrate the basic three-dimensional non-steady character of a detonation through the planar model.

The shock front within a cell of detonation is commonly termed the lead shock wave. Detailed experimental studies of the propagation of the lead shock within the detonation cell (106,14) show the lead shock to be initially overdriven at the beginning of the cell ($M_s \sim 1.8\ M_{CJ}$ to $1.2\ M_{CJ}$) and to decay monotonically to a shock Mach number corresponding to about the autoignition limit towards the end of the cell ($M_s \sim 0.6\ M_{CJ}$ to $0.8\ M_{CJ}$). The zone of chemical reactions behind the lead shock wave has also been shown to decouple from the shock towards the end of the cell.

The overall picture of a detonation that can be reconstituted on the basis of the above discussions is as follows: The detonation wave front consists of a number of wavelets which individually behave like decaying blast waves followed by progressively lagging reaction zones. These decaying wavelets are periodically "energized" to an overdriven state at the start of the detonation cell. The points of driving of the wavelets correspond to the intersection of the triple points and therefore to the intersection of the adjacent transverse waves.

The orientation of these wavelets (*i.e.*, the lead shock within the detonation cell) can be determined, as demonstrated by Strehlow (6), by sprinkling sand grains over a smoked foil and allowing a detonation to pass over it. The interaction of the detonation wavelets with the sand grain writes a "flag" whose axis denotes the direction

perpendicular to the orientation of the shock at that point.

Figure 33 shows the orientation of the lead shocks as obtained by such a method by Lee *et al.*(107).   The lead shock is observed to have a larger curvature near the intersection point where it is strongly over-driven.   The curvature decreases as it passes through the cell and the strength decays as qualitatively indicated at the bottom of Figure 33. Hence the wavelet within a detonation cell can be treated as a decaying cylindrical blast wave which is driven at the beginning of the cell during the intersection of the transverse waves.

Experiments in a diverging geometry, in which the area of the detonation front continually increases with time, show that for a self-sustained detonation an adequate number of the localized points of driving must be continuously generated so as to maintain their number density (number per unit area of the front).   An inability to form these points of driving of the detonation wavelets invariably results in the failure of the detonation wave.   Figure 34 is an open-shutter photograph of a cylindrical detonation which illustrates the self-sustenance of the detonation when there is a continuous regeneration of the points of driving and a failure of a detonation when the regeneration mechanism is absent.

On the basis of the above we can infer that the propagation of a detonation is through a series of local periodic "energization".

The precise reason as to why the propagation is through such a
manner of periodic "energization" is not understood at present.
Stability analysis reveals a plane shock followed by exothermic
chemical reactions to be inherently unstable and it is to be expected
that the unsteady nature of the wave should arise as a consequence
of this instability.

Though the basic mechanisms responsible for the propagation
behaviour are not known, it is clear that the propagation is through a
periodic energization of the decaying wavelets of a detonation at the
intersection of the transverse waves. This suggests that the propaga-
tion behaviour can be modelled as one involving continuous initiation,
the energy release associated with the intersection of the transverse
waves (during the re-energization of the wave) being considered as the
initial release of the source energy E_s in the initiation process. This
is because the decaying motion of the lead shock conforms to the source
dominated shock motion in the initiation process. The conditions
existing at the end of the detonation cell wherein the localized energy
release occurs is also very much akin to the conditions existing at the
formation of localized explosions just after the quasi-steady period of
propagation during the re-establishment of the detonation in the critical
energy regime discussed in Chapter 2. It was seen that the formation
of these localized explosions in the critical energy regime corresponds
to the situation when the chemical energy release just begins to
dominate the shock motion (i.e, at the critical detonation kernel radius R_s^*).

Consequently, we can postulate the events occurring within a cell of detonation to correspond to those taking place till the formation of a critical detonation kernel R_s^* in the initiation process.

It is instructive to compare the energy released during the intersection of the transverse waves (triple points) with the critical value of the initiation energy. The estimation of the energy released in the interaction process is rather complicated in view of the extended zones of chemical reactions in the tail of the transverse waves and the curvature of the Mach, incident and transverse shocks. In the following we shall assume the incident and transverse shocks to be straight lines and to move in a direction perpendicular to each other. The path of the triple points adjacent the interaction is also taken to be a straight line. Figure 35 shows a sketch of the interaction pattern of the triple points. The detonation cell exit angle and the cell entrance angle are denoted by ϕ and ψ respectively in the figure. The chemical reactions occur fairly fast behind the Mach stem shock and after an induction distance X_{ind} behind the relatively weaker incident shock. We can crudely estimate the energy released in the collison process by assuming it to be equal to the energy released in the constant volume combustion of the mass of gas contained in the induction zone behind the incident shock prior to the intersection.

Biller (108), and Strehlow and Biller (109) have shown that the angles ϕ and ψ are relatively constant around 70° and 28° respectively provided we are not considering the case of marginal detonation. We

had also said that the lead shock strength towards the end of the

cell corresponds to about the autoignition limit.   Since the

induction time increases rather rapidly in this range there will be a

sizeable volume of unburnt gases at the end of the cell (shown shaded

in Fig. 36).   Considering a unit depth of the cell we get the chemical

energy released due to the autoexplosion of this end volume of the gas

after being doubly processed by the transverse shocks before and after

their collison to be

$$E_T \;=\; \rho_0 Q \, X^2_{ind} \, \tan 35° \qquad joules/length \qquad\qquad 2.1$$

For a stoichiometric oxyacetylene mixture at an initial

pressure of 100 torr, we had seen in Chapter 3 that $M^*_s = 4.05$ so that

induction distance X_{ind} is about 1.3 mm.   Taking a value of Q for

the 100 torr mixture to be 4.14×10^6 Joules/Kg and the density ρ_0 to

be 0.163 Kg/m^3, we get E_T to be 0.008 Joules/cm.

In order to compare this value of energy with the critical

energy required to initiate a cylindrical detonation wave, we note that

the former in essence drives a wave in a sector of angle ψ (Fig. 35), so

that the equivalent energy associated with driving a complete cylindrical

wave will be 0.008 x 360/ψ = .008 x 360/28 $\simeq$ 0.1 Joules/cm.   This

value compares favourably with the critical initiation energy of about

0.12 Joules/cm obtained from theory and experiments.

5.2.2 Calculation of the Transverse Wave Spacing

We shall assume the lead shock wave, within the cell of detonation, to propagate in a cylindrical symmetry. On the basis of the discussions in the previous section, we shall consider the length of a detonation cell to correspond to the critical size of a detonation kernel R_s^*.

The characteristic transverse wave spacings (s) can be related to the length of a detonation cell (L) through an average angle made by the triple point trajectory with the direction of propagation of the detonation wave (6) (if θ be this average angle, then $S = L \tan \theta$). Biller (108) has experimentally determined the ratio S/L for the hydrogen-oxygen mixture with dilution by various levels of argon. The values of S/L obtained by him are shown in Table II.

It is seen from Table II that the ratio of S/L varies randomly about an average value by about ten percent for each stoichiometry. We shall choose this average value to be 0.58 which corresponds to an average writing angle θ of the triple point trajectory of about 30°. This value of θ has also been quoted by Strehlow (6). The transverse wave spacing is therefore related to the detonation kernel radius R_s^* by

$$S = 0.58 \ R_s^* \qquad\qquad 2.2$$

From the critical size of the detonation kernel R_s^* computed in section 3.9 of Chapter 3, the transverse wave spacing is obtained using Eq. 2.2. The results, over two orders of magnitude, are shown in Figure 36 for the 2 C_2H_2 + 5 O_2, 2 H_2 + O_2 and 2 H_2 + O_2 + 17 Ar mixtures over a range of pressures.

2.3 Discussion of Results

In Figure 36 the experimental values of the spacing S determined by Strehlow (105) and by Voitsekhovsky, Mitrofanov and Topchian (85), are also included. The calculated spacings show good parallelism with the experimental results. The magnitude of the calculated results are, however, always invariably greater than those obtained from experiments. The discrepancy in the magnitude is the smallest for the oxyhydrogen mixture diluted with 85% argon and is much greater for the undiluted mixtures (theoretical spacing is about twice the experimental values in the undiluted mixtures).

In the theory we had assumed the intersection of the triple points to produce an energy release corresponding to a line source. Strehlow (6) has attempted to determine the effective centre of the lead shock within the cell of detonation by modelling the propagation of this wavelet as an unreactive strong blast wave. He finds the effective centre of the blast to be located much before the start of a cell of detonation and a tendency for the distance between the effective centre and the start of the detonation cell to increase with the decreasing dilution of the mixture. Lundstrom and Oppenheim (14)

also try to fit an unreactive blast wave trajectory for the lead shock

decay in a cell.   They likewise find the effective centre of the blast

wave to be upstream of the intersection point of the transverse waves.

The geometry of propagation of the lead shock is also found by them to

correspond to an intermediate situation between a cylindrical and a

planar geometry.

     The over-prediction by the theory especially for the undiluted

mixture probably arises because of the shift in the effective centre due

to the non-ideal nature of the energy released during the interaction

process, and due to the assumed cylindrical geometry.   However, since

Strehlow and Lundstrom and Oppenheim treat the lead shock wave as an

unreactive blast wave while in practice it is a reacting blast wave, it

does not appear worthwhile to introduce corrections in the transverse

wave spacing for the effective centre of a lead shock and for the geo-

metrical effects derived on the basis of a non-reactive trajectory.

We shall, in the following, compare our results with the existing

theories on the transverse wave spacings, viz.,

    1.   The acoustic theory of Barthel and Strehlow (5)

    2.   Acoustic theory of Strehlow (6)

    3.   Barthel's theory based on formation of caustics (7)

    4.   Chiu and Lee's simplification of the above theory (110)

and 5.   The finite amplitude theory of Barthel (97).

    Theories 1 to 4 deal with the convolution of an acoustical

disturbance in the reaction zone of a detonation.   The acoustic

theory of Barthel and Strehlow (theory 1) assumes the transverse
wave spacing to be given by the distance between the contact points
formed on the shock front by the convoluting acoustic wave.   In
theory 2, viz., the acoustic theory of Strehlow, the spacing is
determined by demanding a balance between the amplification of an
acoustic wave due to chemical reactions and the decay in its amplitude
during its traverse through a cell of detonation.   Theories 3 and 4
(Barthel's acoustic theory and Chiu and Lee's simplification thereof)
consider the transverse wave spacing to be equal to twice the distance
between "hot spots" generated from the intersection of caustics.   The
caustics are formed from the convoluting acoustic waves trapped in the
reaction zone of a detonation.   All the above four theories assume a
ZDN model of a detonation.

The finite amplitude theory of Barthel (theory 5) gives the
upper bound for cell lengths by specifying that the pressure pulse
generated from the explosive chemical energy release behind the initial
Mach stem shock should catch up with the lead shock while it is still a
Mach stem shock.   This theory is more realistic of the physics involved
in the wave interaction process and does not assume a one-dimensional
idealized structure for a detonation.

Figures 37 to 40 compare the results obtained on the basis
of these five theories with the present calculations for the stoichio-
metric oxyhydrogen mixture with various levels of dilution by argon
(0%, 50%, 70% and 85% Ar in $2 H_2 + O_2 + XAr$).   The acoustic theory of

Barthel and Strehlow (theory 1) is seen to considerably underestimate the transverse wave spacing for all levels of dilution. Theory 2 (Strehlow's acoustic theory) is seen to give fair predictions for high dilutions with argon though the dependence on pressure is much steeper than the experiments. The spacing calculated on the basis of generation of hot spots (theories 3 and 4) is seen to have good parallelism with the experimental results and to be about the same order of magnitude as the experimentally observed spacings for the 0% dilution and 70% dilution with argon. The results of this theory are not com- pared for the 50% and 85% argon dilutions since their spacing values have not been reported for these dilutions. The transverse wave spacing obtained from the finite amplitude theory of Barthel (taken from Biller (108)) is seen to yield better predictions as the dilution with the argon gas is decreased. The present theory, on the other hand, yields good prediction with 85% Ar dilution but results in increased error with the lower levels of dilution. However, good parallelism with the experimental results is obtained in all cases with the present theory.

The errors incurred with theories 1 and 2 are obviously associated with the acoustic approximations and the assumption of a one- dimensional ZDN structure for a detonation. The transverse waves are of finite strength ($M_s \sim 1.25$ for a normal detonation and about 1.5 for a marginal detonation) so that in all fairness it is necessary to consider the convolution of finite amplitude waves. The coupling between these

waves and the chemical reactions also ought to be considered.   This is suggested by the close predictions of theory 2 for the highly diluted mixture (85% Ar) for which the heat release is expected to be small.

The acoustic theory of Barthel (theory 3) has all three limitations associated with theories 1 and 2 (*i.e.*, assumption of acoustic waves, a ZDN structure and no coupling).   However, it seems to give good predictions for the wave spacings.   Barthel showed that the predictions can be further improved by arbitrarily assigning certain degrees of overdrive to the detonation wave.   The ability of this theory to yield good predictions, in fact, led Chiu and Lee to re-examine the model and to evolve a simplified version thereof.   They also obtained reasonable agreement with the experiments though their results were much below those of Barthel.   In spite of the good predictive ability, the theory wrongly estimates certain physical aspects of the propagation behaviour.   For instance, the theory predicts an increased number of hot spot formation due to the presence of the walls, thus implying that the influence of the walls is to decrease the size of the transverse wave spacing.   This is contrary to experimental findings.

The finite amplitude theory of Barthel (theory 5) is a phenomenological theory since its formulation relies on the experimentally observed physics of the wave interaction process.   As in the present theory, the unsteady characteristics of the wave front is taken into account.   It is, however, difficult in Barthel's theory to estimate accurately the time taken for a pressure pulse emanating from the initial

Mach stem to catch up with the lead shock in view of the non-uniform flow properties behind it. Barthel assumes a uniform flow field behind the lead shock, an assumption which inherently kills the unsteadiness of the detonation wavelet during the initial phase of travel. The theory is also not a true cell theory and gives an upper limit to the size of the cell that can be formed. Nevertheless, the concepts of this theory contain the essential gist of the coupling and wave interaction behaviour and, as demonstrated in Chapter 3, qualitatively explains the growth of a detonation cell due to the effect of the confining walls.

The present theory overpredicts the cell size by about the same amount for the 0%,50% and 70% dilution cases as Barthel's finite amplitude theory underestimates the upper bound for the cell size. The results for the 85% argon dilution are predicted much better by the present theory. The errors in the present theory are a result of the non-ideality of the energy release associated with the interaction of the transverse waves as mentioned earlier in this section.

5.3 Limits of Detonability

It is not always possible to generate and maintain a detonation in a given explosive gas mixture. There are conditions of a minimum initial pressure, a maximum dilution with inert gases, and a range of

stoichiometries beyond which a self-sustained detonation cannot occur. These limit conditions in pressure, dilution and stoichiometry are spoken of as **the pressure**, dilution and **concentration limits** of detonability.

From experiments in tubes it is known that the approach to the limits of detonability is normally evidenced by the loss of the transverse wave structure of the detonation front.   Thus, for example, the mode number of a multiheaded detonation wave (*viz.*, the number of transverse waves associated with a detonation front) decreases as the explosive gas mixture becomes progressively weaker until near the limits a single transverse wave moves laterally across the shock (spin detonation in circular tubes).   Sometimes unsteady detonations with periodic spurts in their velocity of propagation (the galloping detonation of Duff (111)) and without any transverse structure are also observed near the limits of detonability.   In general, the inability to generate transverse waves seems to govern the detonability limits of the mixture.[†]

We had seen earlier in this chapter that a detonation propagates through a series of local periodic initiations at the intersection of the transverse waves.   The limits of detonability therefore imply a situation wherein the mechanism of such local periodic initiation fails.

[†]   There appear to be a few exceptions to this generally observed trend.   The experiments of Biller (108) in a rectangular tube (3.8 cm x 8.3 cm) show a mixture of stoichiometric hydrogen and oxygen at low levels of dilution with argon to be incapable of sustaining less than three to five transverse waves.   In other words, the mode number of the multiheaded front is about 3 to 5 near the limits of detonability.

We shall explore the relation between the initiation characteristics and the limits of detonability in this section and strive to predict the limit behaviour on the basis of the phenomenological theory of initiation.   Before doing so, however, we shall briefly pause to examine whether it is possible to define and determine uniquely the limits of detonability of an explosive gas mixture.

5.3.1 True Detonability Limits?

Detonability limits are obtained from the experiments on the initiation and propagation of detonations in tubular, cylindrical and spherical explosion chambers.   The limits are ascertained from the inability either to initiate a detonation in the mixture or to propagate a steady detonation wave in the mixture.

The limits of detonability obtained in the unconfined geometries are usually much narrower than those obtained in tubes (38).   Manson and Ferrie postulated that the narrower limits are a consequence of the steep hydrodynamic gradients behind the cylindrical and spherical detonation waves as given by the Jouguet-Taylor-Zel'dovich (JTZ) theory. It is now well-established that the detonation front in cylindrical and spherical geometries comprises a transverse wave structure with a characteristic shock wave interaction system that is exactly similar to that in planar geometry.   Also, far from the ignition source the curvature of the wave front will be small, resembling more or less a planar detonation front.   Hence on the basis of wave structure and propagation behaviour one should not expect detonations in the unconfined mode to be

possible over a narrower range of compositions than for detonations

in tubes.

One major difference between the planar and diverging

geometries is the role played by the confining walls.   The confining

walls can influence the detonation wave in two ways.   Firstly, they

provide a means for energy and momentum to be lost by transport

processes from the zone of chemical reactions.   Secondly, the confining

walls play a stabilizing role by providing a surface for the reflection

of the transverse waves.   Strehlow (3) has shown that the interaction

of a transverse wave with the wall is exactly analogous to the intersection

of the adjacent transverse waves on a detonation front.   Therefore

the stabilizing role of the wall in planar geometry cannot be expected

to be greater than the effect produced by the interaction of adjacent

transverse waves in the unconfined geometry.   Consequently, there

does not appear to be any reason whereby the detonability limits should

be wider for detonation waves in tubes.   On the contrary the "loss"

effects due to the walls should cause them to be narrower.[†]

A closer examination of the problem reveals that the experiments

in cylindrical and spherical geometries have necessarily been conducted

---

[†]   Brossard et al.(112) reported some experiments on the propagation
of cylindrical detonations in a propane-oxygen-nitrogen mixture for
several widths of the cylindrical chamber.   They observed a tendency
for the dilution limits to increase with decreasing width of the chamber
and attributed this effect to the stabilizing influence of the wall. It
is difficult to see how the wall could possibly energize the system. The
results are probably due to the failure of the detonation at higher mode
numbers with the smaller dilutions, as observed by Biller.

in chambers whose dimensions are very much smaller than the length
of tubes used in planar experiments. This has been due mainly to
the difficulty in handling large volumes of the explosive gas in the
unconfined experiments and the associated hazards involved.
Consequently, the results are derived on the basis of being able to
initiate detonations in spherical and cylindrical containers of a
certain limited size (few cm to a few meters) using some available energy
sources (e.g., electrical sparks, exploding wires, detonators, etc.).
As an example, Figure 41 shows the variation in the critical energy
for direct initiation with the percentage of hydrogen in a hydrogen-
oxygen mixture at an initial pressure of one atmosphere in a 14 litre
spherical bomb (77). The ignition source corresponds to exploding
wires and electrical sparks and the electrical energy stored in the
capacitor is reported for the critical energy. A tendency towards a
large increase in the initiation energies is observed in the hydrogen-
rich and hydrogen-lean regions of the mixture so that a characteristic
U-shaped curve is obtained for the initiation energies. The lean
and rich limits of detonability are established in such experiments
through the two vertical assymptotes of the U-shaped curve of critical
energy obtained over a wide range of mixture compositions.

When the conditions of limits are discerned from experiments
of the above nature, the results depend on the maximum energy levels
of the igniter used and the scale on which the results are plotted.
Larger chambers are also necessary in order to determine whether a

self-sustained detonation can be formed after a sufficient distance
of travel.   It is relevant to note that Cassutt (113) did some
experiments with H_2-O_2 and H_2-air mixtures in huge latex balloons of
1.83 meters diameter and about 2830 liter capacity and ignited them
with condensed explosive charges of about 100 grams.   He crudely
estimated the limits of detonability on the basis of overpressure
measurements at a certain distance from the balloon.   His results
show very close agreement with the detonability limits obtained in
tubes.   Hence we are lead to believe that the narrower range of
detonability limits obtained by several investigators in the unconfined
mode is due to the limited size of the experimental apparatus and the
limited energy of the ignition device used.   With sufficiently large
experimental apparatus and powerful igniters, the limits of detonability
should be basically the same in the different geometries.

In the classical works of Sokolik (114) and Zel'dovich (115),
a clear distinction is made between the limits determined from the
ability to propagate a detonation in a tube from the ability to initiate
a detonation in a tube through the transition mode.   The latter is
spoken of as the limits of explosion in order to distinguish them from
the former which are called the limits of detonability.   The following
table shows these limits for the hydrogen-oxygen, hydrogen-air and
acetylene-air mixtures.   The so-called limits of explosion are always
seen to lie within the limits of detonability.

Mixture (1 atm. initial pressure)	Explosion limit (% fuel)		Detonability limits (% fuel)	
	lower	upper	lower	upper
H_2-O_2	23	85	20	90
H_2-air	27	35.5	18.2	58.9
C_2H_2-air	6.6	15.3	4.2	50

There is no reason why the limits obtained from the initiation and propagation experiments should be different.   If a mixture can support a stable detonation then it should be possible to initiate a detonation in the mixture.   The narrower limits obtained from the initiation experiments are likely due to the limited length of the tubes employed (40 m length of bent tube).

On the basis of the above discussions we are led to think that the limits determined in the different geometries and by different methods should be basically the same, provided appropriate experimental apparatus is used.   This common value should correspond to the true limits of detonability.   In tubes, however, an additional influence due to the boundary layer affects the detonability limits.   The concentration limits become narrower as the diameter of the tube is decreased.   For example, with the hydrogen-air mixture the fuel-lean limit of detonability is increased from 15% H_2 in a 30.5 cm diameter tube to 19.6% H_2 in a 2 cm diameter tube, whilst the fuel-rich limit decreases

from 63.5% H$_2$ to 58.8% H$_2$ (115). For the larger range of diameters, the influence of diameter on the concentration limits of detonation is known to be insignificant and the concentration limits can be established independent of the confinement effects.

The pressure and dilution limits of detonability have not been extensively studied like the concentration limits. We shall, therefore, restrict our discussions on theoretical predictions mainly to concentration limits of detonability.

5.3.2   Prediction of Limits by the Detonation Kernel Theory

In the phenomenological theory of initiation discussed in Chapter 3 we saw that for blast initiation the chemical energy released behind the shock front must be capable of overriding the decaying characteristics of the source-dominated shock motion by the time the shock strength decayed to a value corresponding to the limit of spontaneous chemical energy release (M_s^*). As the explosive gas mixture is progressively weakened, such as by dilution with an excess of fuel or oxidizer or an inert gas, the contribution of the chemical energy in driving the shock front progressively decreases due to (i) a decrease in the chemical energy per unit mass of the mixture and (ii) an increase in the chemical induction zone thickness d.   Consequently, a much larger detonation kernel is required in order that the chemical energy liberated by the shocked gases can arrest the decaying source-dominated shock motion and thereby form a self-sustained detonation. If a

situation arises such that the chemical energy can never really dominate the shock motion, the conditions for the limits of detonability are reached.

At large distances from the ignition source ($R_s \rightarrow \infty$) the shock motion is essentially governed by the chemical energy release as given by Eq. 4.11 in Chapter 3, provided the chemical reactions are coupled to the shock front.

$$M_s^2 = M_{CJ}^2 = \frac{1}{(j+1)\, C_0^2 I} (Q + e_0)$$

This is because the source energy density term $E_s / k_j R_s^{j+1} C_0^2$ becomes negligibly small for large values of R_s. The shock Mach number corresponds to the CJ value, i.e., the globally constant stable propagating velocity of a detonation when the chemical reactions are strongly coupled to the shock front. When the heat release is not all that effective in driving the shock, the Mach number of the shock front will be much less. The CJ value, as such, represents the upper bound of the shock velocities which can be maintained by the heat release at large distances from the ignition source.

We had seen in Chapter 3 that a decoupling of the shock and chemical reactions will occur if the shock strength falls below the critical autoignition limit ($M_s < M_s^*$). Since M_{CJ} represents the theoretically calculated upper bound of velocity which can be maintained

by the chemical heat release on the assumption of a strong coupling between heat release and the shock motion, and since for $M_s < M_s^*$ the heat release cannot effectively influence the shock motion, we can postulate that an adequate kernel of heat release can effectively drive the shock front at large distances from the ignition source only when $M_{CJ} > M_s^*$. In other words, the limits of detonability should correspond to a situation when $M_{CJ} = M_s^*$.

It was also seen in Chapter 3 that the critical shock strength (M_s^*) corresponds to a rapid increase in the time taken for the induction reactions to occur and that for the oxyhydrogen mixture the value of M_s^* can be explicitly stated in terms of the strong shock limit. This limit was also seen to be brought about by the inhibiting influence of the chain termination reaction on the chain branching reactions. More specifically, M_s^* was identified by the extended second explosion limit for the oxyhydrogen mixtures. Figure 42 shows a plot of M_{CJ} and M_s^* over a range of compositions for the H_2-O_2 and H_2-Air mixtures at an initial pressure of one atmosphere. Since the ratio of specific heats, γ_0, is almost constant around 1.4 for the whole range of compositions, M_s^* is a constant. The limits of detonability determined from this figure using the criterion $M_{CJ} \geq M_s^*$ are compared with the experimental data of Zel'dovich in the following table.

Mixture	% of H_2 in H_2-O_2 and H_2-Air mixtures			
	lower limit		upper limit	
	Theory	Experiments*	Theory	Experiments*
H_2-O_2	17	20	92	90
H_2-Air	16	18.2	64	58.9

* Zel'dovich (115)

The criterion $M_{CJ} \geq M_s^*$ for the prediction of detonability
limits is not new and has been postulated by Belles (116) for mixtures
of hydrogen with oxygen and air.   Belles derived the criterion on
the basis that a planar shock must propagate at a Mach number exceeding
a "critical Mach number for autoignition at the wave front" in order
that the chemical reactions can support a detonation wave.   The critical
Mach number for autoignition at the wave front was taken to correspond
to the classically determined second explosion limit.

It must be pointed out that in a later paper Belles and Ehlers
(117) criticized the calculation of limits using the classical explosion
limit criterion and labelled the predictive ability of the theory as
"fortuitous".   They argued that the classical explosion limit criterion,
as given by Lewis and von Elbe (46), assumes a steady state diffusion
of the radicals to the walls and that reactions such as the destruction
of HO_2 radicals at the walls are not likely to occur under conditions
of detonation.   Patch (118) also disagreed with the use of the second
explosion limit criterion for determining detonability limits and
demonstrated that an arbitrarily assigned constant value of temperature

behind the shock front (*viz.*, a rotationally equilibrated and vibrationally unrelaxed temperature of 1314° K) is better capable of predicting the detonability limits.

The more recent experiments (66,67) on the autoignition characteristics behind the shock in H_2-O_2 mixtures show that the conditions governing the classical second explosion limit (chain branching reactions arrested by the chain termination reaction) also decide whether ignition will occur spontaneously in a "strong ignition" mode or in a relatively "weak" mode without the generation of relatively strong gas dynamic effects. The experiments of Libouton, Dormal and van Tigglen (119) show that the addition of small traces of an inhibitor such as CH_3Cl, CH_3Br, CF_3Br or CF_3Cl to a CO-O_2-H_2 mixture leads to a significant inhibiting influence on the propagation of a detonation. The inhibitors do not markedly influence the heat release characteristics of the system but do severely restrict the formation of effective chain carriers (such as H atoms) in the chain branching steps through reactions of the type $RX + H \rightarrow R + XH$, RX denoting the inhibiting compound.

The key role of the chain branching and chain termination steps in the formation of a detonation is also beautifully illustrated in the experiments of Gordon *et al.* (120) wherein an increase in the moisture content from 50 parts per million to about 500 parts per million was seen to result in the failure of a detonation wave in a lean H_2-Air mixture. The third body effectiveness of the water molecule in the chain

termination step $H+O_2+M \rightarrow HO_2+M$ is about 30 times that of the other atoms and molecules.[†] Hence with water vapour the chain termination reaction is more rapid and competes more effectively with the main chain branching step $O_2+H \rightarrow OH+O$. Away from the lean hydrogen limit, where a sufficient concentration of the chain carrier H can be generated, the inhibiting influence of the water vapour on the formation of a detonation has been shown to be weak by Macek (121). The influence of the small amounts of water vapour in the lean mixtures also suggests that the reactions during the initial phase of the combustion essentially control the limits since considerable H_2O molecules are generated in the chemical reaction between hydrogen and oxygen.

The above considerations indicate that the ability to generate chain carriers basically governs the detonability limits and therefore the choice of M_s^* on the basis of the extended second explosion limit should be reasonable. We do not explicitly invoke the data derived from the classical second explosion limit in a constant volume bomb experiment but only realize that the processes governing autoignition behind shocks and hence the detonability limits arise from a competition between the chain branching and chain termination reactions. Hence the criticisms of Belles and Ehlers and of Patch are unjustified.

[†] The relative effectiveness of the various atoms and molecules in the reaction $H+O_2+M \rightarrow HO_2+M$ according to the kinetic data of Gardiner (68) is $H_2 = 1$, $O_2 = 1$, $H = 1$, $O = 1$, $OH = 1$, $HO_2 = 1$, $Ar = 1$ and $H_2O = 30$.

129

For mixtures whose autoignition characteristics are not
known it becomes somewhat difficult to determine the detonability
limits.   For certain mixtures like the $CO-O_2-H_2$ system whose chain
branching and chain termination steps are very similar to the H_2-O_2
system, the detonability limits calculated from the extended second
explosion limit criterion also agree well with the experiments (117).
For the acetylene oxygen mixture, if we take a value of M_s^* to correspond
to about 4.05 (based on the value determined in Chapter 3), we get the
lean limit to be about 3% acetylene in the oxyacetylene mixture (Fig. 43).
This compares well with the lean limit values of 3.5 - 3.6% C_2H_2 quoted
by Wagner (122).

CHAPTER 6

CONCLUSIONS AND RECOMMENDATIONS FOR FUTURE STUDIES

6.1 Concluding Remarks

A theoretical and experimental study of the blast initiation phenomenon is reported in this thesis. The theoretical phase of the investigation has been mainly concerned with the development of a simple phenomenological theory for the blast initiation of gaseous detonations. The experimental work is devoted to the determination of experimental data on initiation of a generalized nature independent of the configurations of the apparatus used. Some of the important results of this investigation are summarized below.

1. In analogy to the concept of a flame kernel used in the flame ignition theory, the concept of a detonation kernel is developed from phenomenological considerations to describe theoretically the blast initiation of detonations. The critical size of a detonation kernel is specified by the balance condition between the source energy density and the chemical energy density of the gas enclosed by the shock wave generated by the initiation source. The size of the detonation kernel is insensitive to the details of the shock hydrodynamic flow structure and depends mainly on the physical and chemical properties of the explosive gas mixture.

The results are quite general and are not restricted to any particular type of igniter used.

The source energies predicted by the **detonation kernel** theory recover the experimentally observed dependence on the various parameters. Quantitative estimation of the critical energy in good agreement with the experiments is also obtained in the lower range of sub-atmospheric pressures for which shock tube induction time data exist.

2. The propagation and limit behaviour of a detonation are closely related to the initiation behaviour. It is argued that the propagation of a detonation is through a series of periodic initiations so that the length of a cell of detonation corresponds to the critical size of a detonation kernel. Based on this reasoning good agreement is obtained with the experimental values of transverse-wave spacings determined in tubes. The predictions are, in general, much better than those obtained from the several existing theories on transverse wave spacings. The closer agreement obtained with experiments appears to confirm the mechanism of propagation as one involving a sequence of continuous periodic initiations.

The limits of detonability of a reactive gas mixture correspond to a situation when the critical size of the detonation kernel

approaches infinity.   It is seen that this condition implies

that $M_{CJ} > M_s^*$ for a gas mixture to be detonable.   This

criterion predicts well the concentration limits of detonability

of those mixtures whose M_s^* is known.

3. The magnitude of the explosion length (R_o) in relation to the

characteristic dimensions of the ignition source (L) can be used

to discern the geometry of initiation in the different experiments.

For R_o > L the geometry of initiation is characterized by the

confinement, whilst for R_o < L the initiation geometry is

characterized by the geometry of energy source itself.

4. For a given explosive gas mixture at certain initial conditions

of temperature and pressure, the explosion length R_o is the same

in each of the three geometries of initiation even though the

initiation energies may differ by several orders of magnitude.

The result is of immense practical significance as it provides

a method for estimating source energies required to cause detonations

in the unconfined geometry without having to do actual experiments

in the unconfined geometry.   It must be pointed out that experi-

ments in the unconfined geometry are difficult to conduct in view

of the relatively large quantities of gas involved and the

relatively larger magnitudes of the source energies required as com-

pared with the experiments in the planar and cylindrical geometries.

5. The confinement has a strong adverse influence on the initiation

of detonations.   In order to eliminate the effect of the con-

finement on the initiation process and to characterize the

initiation in terms of the physical and chemical properties of

the explosive gas mixture alone, the detonation front must contain

a minimum of about ten characteristic cells of detonation across

it.   This corresponds to the critical tube diameter necessary

to re-establish detonations in the detonation diffraction experi-

ments and to the hydrodynamic thickness of a detonation.

6.2   Suggestions for Improvements and Future Development

1.   In the present theoretical model, the chemistry of the

combustion processes has been depicted in terms of thermoneutral chain

branching reactions (an induction zone) followed by the spontaneous

liberation of chemical energy.   On the basis of the good agreement

obtained between the results of the theory and the experiments, this

simple modelling of the combustion processes seems to be adequate over

the range of conditions in which the experimental data exist.   Normally

the zone of actual heat release, i.e., the recombination zone, is about

an order of magnitude smaller than the induction zone so that the

neglect of the recombination zone thickness does not influence the

results.   The time taken for recombination reactions to occur is

inversely proportional to the square of the initial pressure
($\tau_R \sim 1/p_o^2$) so that at extremely low pressures the influence of the
recombination reactions may be substantial.   It will be instructive
to incorporate the finite time taken for recombination reactions to
occur in the present theory.   In order to keep the analysis simple
and tractable, gross modelling of the recombination reactions in terms
of an overall inverse exponential rate of heat release such as used by
Feay and Bowen (20), or in terms of a single overall parameter as given
by Getzinger and Schott (123), could be employed.

2.   The choice of the autoignition conditions in the detonation
kernel theory sometimes poses considerable difficulties.   For the
hydrogen-oxygen-diluent mixtures the problem does not arise since their
autoignition characteristics have been widely studied.   The method of
estimating the autoignition conditions on the basis of a large exponential
increase in induction times, such as was done for the 100 torr
stoichiometric oxyacetylene mixture, is not entirely satisfactory.   This
is because a change in the scale of plotting the induction times can
influence the results even though the range of the autoignition conditions
can be guessed on the basis of a minimum power requirement for direct
initiation, or on the basis of the quasisteady propagation conditions
prior to the formation of a detonation.   It is necessary to extend
the studies on autoignition of gases behind shock waves to different
explosive gas mixtures.   The work of Vermeer et al. (124) with hydro-
carbon fuels such as isooctane and n-heptane represents a step in this
direction.

3.   The behaviour of the chemical reactions during the induction period at the higher range of pressures also necessitates further investigation.   Such an enquiry should help us to understand the increasing trend towards larger initiation energies with increasing pressures at the higher range of sub-atmospheric pressure levels. The conventional shock tube method of studying induction kinetics may pose a problem in view of the transverse wave structure invariably associated with the reactive shocks at these higher pressures.   Special methods, such as the laminar detonation technique of White (125), should yield interesting results.

7. STATEMENT OF ORIGINALITY
AND CONTRIBUTION TO KNOWLEDGE

The author believes that the detonation kernel theory
introduced in this thesis is a distinct contribution to knowledge in
the field of detonative combustion.   This theory provides not only
a simple method for determining the initiation behaviour of gaseous
detonations but also links together the other aspects of a detonation
such as the transverse wave structure and the limits of detonability.

The experiments reported in this thesis reveal the profound
influence of confinement on the initiation of gaseous detonations. It
is shown for the first time how to determine meaningful experimental
results on detonation initiation in terms of the physical and chemical
properties of the explosive gas mixture alone, independent of the
characteristics of the ignition source and confinement,   The
importance of the explosion length parameter in the direct initiation
of detonations is also demonstrated for the first time.

REFERENCES

1. Lee, J.H., Soloukhin, R.I. and Oppenheim, A.K. Current views on gaseous detonations. Astronautica Acta., 14, 565 (1969).

2. Oppenheim, A.K. and Soloukhin, R.I. Experiments in gasdynamics of explosions. P.31 in Annual Review of Fluid Mechanics, Vol.5 (1973).

3. Strehlow, R.A. Gas phase detonations: Recent developments. Combustion and Flame, 12, 81 (1968).

4. Urtiew, P.A. From cellular structure to failure waves in liquid detonations. Combustion and Flame, 25, 241 (1975).

5. Barthel, H.O. and Strehlow, R.A. Wave propagation in one-dimensional reactive flows. Phys. Fluids, 9, 1896 (1966).

6. Strehlow, R.A. Multi-dimensional detonation wave structure. Astronautica Acta, 15, 345 (1970).

7. Barthel, H.O. Predicted spacings in hydrogen-oxygen-argon detonations. Phys. Fluids, 17, 1547 (1974).

8. Dove, J.E., Scroggie, B.J. and Semerjian, H. Velocity deficits and detonability limits of hydrogen-oxygen gas detonations. Acta Astronautica, 1, 345 (1974).

9. Tsuge, S. The effect of boundaries on the velocity deficit and the limit of gaseous detonations. Combustion Science and Technology, 3, 195 (1971).

10. Williams, F.A. Quenching thickness for detonations. Combustion and Flame, 26, 403 (1976).

11. Taylor, G.I. The dynamics of the combustion products behind
        plane and spherical detonation fronts in explosives.
        Proc. Roy. Soc., 222(A), 235 (1950).

12. Lee, J.H. Gasdynamics of detonations. Astronautica Acta, 17,
        455 (1972).

13. Lee, J.H. The propagation of shocks and blast waves in a
        detonating gas. Report 65-1, McGill University, Montreal (1965).

14. Lundstrom, E.A. and Oppenheim, A.K. On the influence of nonsteadyness
        on the thickness of the detonation wave. Proc. Roy. Soc. A310,
        463 (1969).

15. Bach, G.G., Lee, J.H. and Knystautas, R. Direct initiation of
        spherical detonations in gaseous explosives. Twelfth Symposium
        (International) on Combustion, p.853, The Combustion Institute,
        Pittsburgh (1969).

16. Korobeinikov, V.P. The problem of point explosion in a detonating
        gas. Astronautica Acta, 14, 411 (1969).

17. Bishimov, E., Korobeinikov, V.P. and Levin, V.A. Strong explosion
        in combustible gaseous mixture. Astronautica Acta, 15, 267 (1970).

18. Rajan, S. On the interaction between chemical kinetics and
        gasdynamics behind a cylindrical detonation front. University
        of Illinois, Urbana, Illinois. Tech. Rept., AAE 70-1 (1970).

19. Kyong, W.H. A theoretical study of spherical gaseous detonation
        waves. Ph.D. Thesis, McGill University, Montreal (1972).

20. Feay, B.A. and Bowen, J.R. A model of the ignition of cylindrically-
        confined explosive gas mixtures. Combustion and Flame, 20,
        111 (1973).

21. Levin, V.A. and Markov, V.V. Detonation with concentrated underwater
        energy. Fluid Dynamics, 9, 754 (1976).

22. Bach, G.G., Guirao, C.M., Knystautas, R., Lee, J.H. and Alcock, A.J.
        The laser spark for gas kinetic studies. Paper #34, Proceedings
        Eighth International Shock Tube Symposium, London (1971).

23. Fry, R.S. and Nicholls, J.A. Blast wave initiation of gaseous
     and heterogeneous cylindrical detonation waves. Fifteenth
     Symposium (International) on Combustion, p. 43. The
     Combustion Institute, Pittsburgh (1975).

24. Fry, R.S. and Nicholls, J.A. Blast initiation and propagation of
     cylindrical detonations in MAPP-air mixtures. AIAA J., 12,
     1703 (1974).

25. Collins, P.M. Direct initiation in unconfined fuel-air mixtures.
     Acta Astronautica, 1, 259 (1974).

26. Knystautas, R. and Lee, J.H. On the effective energy for direct
     initiation of gaseous detonations. Combustion and Flame,
     27, 221 (1976).

27. Matsui, H. and Lee, J.H. Influence of electrode geometry and
     spacing on the critical energy for direct initiation of
     spherical gaseous detonations. Combustion and Flame, 27,
     217 (1976).

28. Lee, J.H. and Matsui, H. A comparison of the critical energies
     for direct initiation of spherical detonations in acetylene-
     oxygen mixtures.
     (To appear in Combustion and Flame, December 1976).

29. Zel'dovich, Ia.B., Kogarko, S.M. and Simonov, N.N. An experimental
     investigation of the direct initiation of spherical detonation
     of gases. Soviet Physics Technical Physics 1, 1689 (1956).

30. Knystautas, R. An experimental study of spherical gaseous
     detonation waves. MERL Rept. 69-2, McGill University (1969).

31. Soloukhin, R.I. and Ragaland, K.W. Ignition processes in expanding
     detonations. Combustion and Flame, 13, 295 (1969).

32. Lee, J.H., Lee, B.H.K. and Knystautas, R. Direct initiation of
    cylindrical gaseous detonations. Phys. Fluids, 9, 221 (1966).

33. Edwards, D.H., Hooper, G. and Morgan, J.M. An experimental investi-
    gation of the direct initiation of spherical detonations.
    Acta Astronautica, 3, 117 (1976).

34. Vasiliev, A.A., Gavrilenko, T.P. and Topchian, M.E. On the Chapman-
    Jouguet surface in multiheaded gaseous detonations.
    Astronautica Acta, 17, 499 (1972).

35. Lee, J.H. and Bach, G.G. On the propagation of spherical detonation
    waves. MERL Rept. 72-9, McGill University, Montreal (1972).

36. Soloukhin, R.I. Nonstationary phenomenon in gaseous detonations.
    Twelfth Symposium (International) on Combustion, p. 799.
    The Combustion Institute, Pittsburgh (1969).

37. Laffitte, P. L'onde explosive spherique. Ann. de Phys., 10e
    serie 4, p. 645 (1925).

38. Manson, N. and Ferrie, F. Contribution to the study of spherical
    detonation waves. Fourth Symposium (International) on
    Combustion, p. 486. Williams and Wilkins Company, Baltimore (1953).

39. Bach, G.G., Knystautas, R. and Lee, J.H. Initiation criteria for
    diverging gaseous detonations. Thirteenth Symposium (Inter-
    national) on Combustion, p. 1097. The Combustion Institute,
    Pittsburgh (1971).

40. Lee, J.H., Knystautas, R., Guirao, C. and Lam, E. Direct initiation
    of explosions in flammable mixtures. Paper presented at the
    Fourth International Symposium on Transport of Hazardous Cargoes
    by Sea and Inland Waterways. New Orleans, Louisiana. April 1975.

41. Guirao, C.M., Lee, J.H. and Bach, G.G. The propagation of nonideal
    blast waves. MERL Rept. 74-1, McGill University, Montreal (1974).

42. Urtiew, P.A. and Oppenheim, A.K.   Transverse flame-shock interactions in an explosive gas.   Proc. Roy. Soc., A304, 379 (1968).

43. Lee, J.H., Knystautas, R., Guirao C., Bekesy, A. and Sabbagh, S. On the instability of H_2-Cl_2 gaseous detonations.   Combustion and Flame, 18, 321 (1972).

44. Lee, J.H. and Ramamurthi, K.   On the concept of the critical size of a detonation kernel. (To appear in Combustion and Flame, December 1976).

45. Strehlow, R.A.   Fundamentals of Combustion.   International Textbook Company, Pennsylvania (1968).

46. Lewis, B. and von Elbe, G.   Combustion, Flames and Explosions of gases.   Academic Press Inc., New York and London (1961).

47. Swett, C.C.   Spark ignition of flowing gases.   NACA Rept. 1287 (1956).

48. Williams, F.A.   Combustion Theory.   Addison-Wesley Publishing Company Inc., Massachusetts (1965).

49. de Soete, G.G.   The influence of isotropic turbulence on the critical initiation energy.   Thirteenth Symposium (International) on Combustion, p. 735.   The Combustion Institute, Pittsburgh (1971).

50. Ballal, D.R. and Lefebvre, A.H.   The influence of flow parameters on minimum ignition energy and quenching distance.   Fifteenth Symposium (International) on Combustion, p. 1473.   The Combustion Institute, Pittsburgh (1974).

51. Yang, C.H.   Theory of ignition and autoignition.   Combustion and Flame, 6, 215 (1962).

52. Nicholls, J.A., Sichel, M., Fry, R. and Glass, D.R.   Theoretical and experimental study of cylindrical shock and heterogeneous detonation waves.   Acta Astronautica, 1, 385 (1974).

142

53. Lee, J.H., Knystautas, R. and Guirao, C.M. Critical power density for direct initiation of unconfined gaseous detonations. Fifteenth Symposium (International) on Combustion, p. 53. The Combustion Institute, Pittsburgh (1974).

54. Taylor, G.I. The formation of a blast wave by a very intense explosion. 1. Theoretical discussion. Proc. Roy. Soc., 201A, 159 (1950).

55. Sedov, L.I. Similarity and dimensional methods in mechanics. Academic Press (1959). p.235.

56. von Neumann, J. The point source solution. P.219 in Vol. VI of 'John von Neumann Collected Works'. General Editor, A.H. Taub. Pergamon Press (1963).

57. Taki, S. and Fujiwara, T. One-dimensional nonsteady processes accompanied by the establishment of self-sustained detonations. Thirteenth Symposium (International) on Combustion, p. 1119. The Combustion Institute, Pittsburgh (1971).

58. Strehlow, R.A. and Hartung, W. On the early relaxation of an overdriven detonation wave. Combustion and Flame 9, 423 (1965).

59. Fickett, W. and Wood, W.W. Flow calculations for pulsating one-dimensional detonations. Phys. Fluids, 9, 903 (1966).

60. Rogers, M.H. Similarity flows behind strong shock waves. Quart. J. Mech. and Applied Math., 11, 411 (1958).

61. Dabora, E.K. Variable Energy Blast Waves. AIAA J., 10, 1384 (1972).

62. Guirao, C.M. Private communication.

63. Hermance, C.E. What do we know about ignition? Paper presented at the 25th Canadian Chemical Engineering Congress, Montreal, November 2-5, 1975.

64. Schott, G.L. and Kinsey, J.L. Kinetic studies of hydroxyl radicals in shock waves. II. Induction times in the hydrogen-oxygen reaction. J. Chem. Phys., 29, 1177 (1958).

65. Hirsch, E. and Ryason, P.R. Combustion delay surfaces in the oxidation of hydrogen. J. Chem. Phys., 40, 2050 (1964).

66. Voevodsky, V.V. and Soloukhin, R.I. On the mechanism of explosion limits of hydrogen-oxygen chain self-ignition in shock waves. Tenth Symposium (International) on Combustion, p. 279. The Combustion Institute, Pittsburgh (1965).

67. Meyer, J.W. and Oppenheim, A.K. On the shock-induced ignition of explosive gases. Thirteenth Symposium (International) on Combustion, p. 1153. The Combustion Institute, Pittsburgh (1971).

68. Gardiner, W.C. Communication to Prof. J.H. Lee. June 1974.

69. Strehlow, R.A. and Cohen, A. Initiation of detonation. Phys. Fluids, 5, 97 (1962).

70. White, D.R. Density induction times in very lean mixtures of D_2, H_2, C_2H_2 and C_2H_4 with O_2. Eleventh Symposium (International) on Combustion, p. 147. The Combustion Institute, Pittsburgh (1971).

71. Steinberg, M. and Kaskan, W.E. The ignition of combustible mixtures by shock waves. Fifth Symposium (International) on Combustion, p. 664. Reinhold Publishing Corp., New York (1955).

72. Strehlow, R.A., Crooker, A.J. and Cusey, R.E. Detonation initiation behind an accelerating shock wave. Combustion and Flame, 11, 339 (1967).

73. David, E. Exploding wires, calculation of heating. p. 271 in "Exploding Wires". Edited by Chace, W.G. and Moore, H.K. Plenum Press Inc., New York (1959).

74. Knystautas, R. Private communication.

75. Sichel, M. A simplified analysis of the blast initiation of detonations. Presented at the 1975 AFOSR combined Contractors' Meeting on Fuel-Air Explosion Research, August 20-22, Eglin AFB, Florida.

76. Litchfield, E.L., Hay, M.H. and Cohen, D.J. Initiation of spherical detonation in acetylene-oxygen mixtures. Report # 7061. United States Department of the Interior, Bureau of Mines.

77. Litchfield, E.L., Hay, M.H. and Forshey, D.R. Direct electrical initiation of freely expanding gaseous detonation waves. Ninth Symposium (International) on Combustion, p. 282. Academic Press, New York and London (1963).

78. Freiwald, H. and Koch, H.W. Spherical detonations of acetylene-oxygen-nitrogen mixtures as a function of nature and strength of initiation. Ninth Symposium (International) on Combustion, p. 275. Academic Press, New York and London (1963).

79. Litchfield, E.L. Freely expanding gaseous detonation waves initiated by electrical discharges. Phys. Fluids, $\underline{5}$, 114 (1962).

80. Klimkin, V.F., Soloukhin, R.I. and Wolansky, P. Initial stages of a spherical detonation directly initiated by a laser spark. Combustion and Flame, $\underline{21}$, 111 (1973).

81. Brossard, J. and Niollet, M. Transfer of energy from an exploding wire to a detonating gas. Astronautica Acta, $\underline{14}$, 513 (1969).

82. Getzinger, R.W., Bowen, J.R., Oppenheim, A.K. and Boudart, M. Steady detonations in gaseous ozone. Tenth Symposium (International) on Combustion, p. 779. The Combustion Institute, Pittsburgh (1965).

83. Edwards, D.H. and Williams, G.T. Effect of tube diameter on the pressure in gaseous detonation waves. Nature, #4595, Nov. 23, 1957. p. 1117.

84. Crooker, A.J.   Phenomenological investigation of low mode marginal planar detonations.   University of Illinois, Urbana, Illinois. Tech. Rept. AAE 69-2 (1969);   also references (6) and (93).

85. Voitsekhovskii, B.V., Mitrofanov, V.V. and Topchian, M.E.   The structure of a detonation front in gases.   Rept. # FTD MT 64-527 (AD 633 821),   Wright Patterson AFB, Ohio (1966).

86. Berets, D.J., Greene, E.F. and Kistiakowsky, G.B.   Gaseous detonations I. Stationary wave in hydrogen oxygen mixtures.   J. Am. Chem. Soc., $\underline{72}$, 1080 (1950).

87. Peek, H.M. and Thrap, R.G.   Gaseous detonations in mixtures of cyanogen and oxygen.   J. Chem. Phys., $\underline{26}$, 740 (1957).

88. Manson, N. and Guenoche, H.   Effect of charge diameter on the velocity of detonation waves in gas mixtures.   Sixth Symposium (International) on Combustion, p. 631.   Reinhold Publishing Corpn., New York (1957).

89. Fay, J.A.   Two-dimensional gaseous detonation: Velocity deficit. Phys. Fluids, $\underline{2}$, 283 (1959).

90. Edwards, D.H., Jones, T.G. and Price, B.   Observations on oblique shock waves in gaseous detonations.   J. Fluid Mechanics, $\underline{17}$, 21 (1963).

91. Edwards, D.H., Brown, D.R., Hooper, G. and Jones, A.T.   The influence of wall heat transfer on the expansion following a CJ detonation wave.   J. of Physics. D:Applied Physics, $\underline{3}$, 365 (1970).

92. Sichel, M. and David, T.S.   Theoretical estimates of wall heat transfer behind CJ detonations in H_2-O_2 mixtures.   AIAA J., $\underline{4}$, 1089 (1966).

93. Strehlow, R.A. and Salm, R.J.   The failure of marginal detonations in expanding channels.   (To be published).

146

94. White, D.R.   Turbulent structure of gaseous detonations.
    Phys. Fluids, 4, 465 (1961).

95. Schott, G.L.   Observations of the structure of spinning detonations.
    Phys. Fluids, 8, 850 (1965).

96. Edwards, D.H., Hooper, G., Job, E.M. and Parry, D.J.   The behaviour
    of frontal and transverse shocks is gaseous detonation waves.
    Astronautica Acta, 15, 323 (1970).

97. Barthel, H.O.   Reaction zone - shock front coupling in detonations.
    Phys. Fluids, 15, 43 (1972).

98. Fujiwara, T.   Slowdown of oxyhydrogen detonations by surface
    catalysis.   Presented at the Sixteenth International Symposium
    on Combustion at Massachusetts (1976).

99. Mitrofanov, V.V. and Soloukhin, R.I.   On diffraction of multiheaded
    detonation waves in gases.   Dokl. Akad. Nauk. 159(5), 1003 (1964).

100. Edwards, D.H., Jones, A.T. and Phillips, D.E.   The location of the
     CJ surface in a multiheaded detonation wave.   J. Physics
     D:Applied Physics 9, 1331 (1976).

101. Eckhoff, R.K. and Enstad, G.   Why are long electric sparks more
     effective as dust explosion initiators than short ones?
     Combustion and Flame, 27, 129 (1976).

102. Ballal, D.R. and Lefebvre, A.H.   The influence of spark discharge
     characteristics on minimum ignition energy in flowing gases.
     Combustion and Flame, 24, 99 (1975).

103. Matsui, H.   Decaying of gaseous detonation by expansion.
     Research Report of the Research Institute of Industrial Safety
     (Japan), RIIS-RR-22-2 (1973).

104. Strehlow, R.A., Maurer, R.E. and Rajan, S.   Transverse waves in
     detonations: I.Spacing in the hydrogen-oxygen system.
     AIAA J., 7, 323 (1969).

105. Strehlow, R.A. and Engel, C.D.   Transverse waves in detonations. II. Structure and spacing in H_2-O_2, $C_2H_2-O_2$, $C_2H_4-O_2$ and CH_4-O_2 systems.   AIAA J., $\underline{7}$, 492 (1969).

106. Strehlow, R.A. and Crooker, A.J.   The structure of marginal detonation waves.   Acta Astronautica, $\underline{1}$, 303 (1974).

107. Lee, J.H., Knystautas, R. and Bach, G.G.   Theory of explosions. MERL Rept. 69-10, McGill University, Montreal (1969).

108. Biller, J.R.   An investigation of hydrogen-oxygen-argon detonations. University of Illinois, Urbana, Illinois.   Tech. Rept. AAE 73-5, (1973).

109. Strehlow, R.A. and Biller, J.R.   On the strength of transverse waves in gaseous detonations.   Combustion and Flame, $\underline{13}$, 577 (1969).

110. Chiu, K.W. and Lee, J.H.   A simplified version of the Barthel model for transverse wave spacings in gaseous detonations. Combustion and Flame, $\underline{26}$, 353 (1976).

111. Duff, R.E., in discussion on p. 469 of the Proceedings of the Ninth Symposium (International) on Combustion, Academic Press, New York and London (1963).

112. Brossard, J., Manson, N. and Niollet, M.   Propagation and vibratory phenomenon of cylindrical and expanding detonation waves in gases.   Eleventh Symposium (International) on Combustion, p. 623.   The Combustion Institute, Pittsburgh (1967).

113. Cassutt, L.H.   Experimental investigation of detonation in unconfined gaseous hydrogen-oxygen-nitrogen mixtures. ARS. J. $\underline{31}$, 1122 (1961).

114. Sokolik, A.S.   Self-ignition, flame and detonations in gases. Israel Program for Scientific Translation, Jerusalem (1963).

115. Zel'dovich, Ia.B. and Kompaneets, A.S.   Theory of Detonations. Academic Press, New York and London (1960).

116. Belles, F.E.   Detonability and chemical kinetics: Prediction of limits of detonability of hydrogen.   Seventh Symposium (International) on Combustion, p. 745.   Butterworths (1959).

117. Belles, F.E. and Ehlers, J.G.   Shock wave ignition of hydrogen-oxygen-diluent mixtures near detonation limits.   ARS J., 32, 215 (1962).

118. Patch, R.W.   Prediction of composition limits for detonations of hydrogen-oxygen-diluent mixtures.   ARS J., 31, 46 (1961).

119. Libouton, J.C., Dormal, M. and van Tigglen, P.J.   The role of chemical kinetics on structure of detonation waves. Fifteenth Symposium (International) on Combustion, p. 79. The Combustion Institute, Pittsburgh (1974).

120. Gordon, W.E., Mooradian, A.J. and Harper, S.A.   Limits and spin effects in hydrogen-oxygen detonations.   Seventh Symposium (International) on Combustion, p. 752.   Butterworths (1959).

121. Macek, A.   Effect of additives on formation of spherical detonation waves in hydrogen-oxygen mixtures.   AIAA J., 1, 1915 (1963).

122. Wagner, H. Gg.   Gaseous detonations and the structure of a detonation wave. In, "Fundamental data obtained from shock tube experiments". AGARDOGRAPH # 41, p. 320. Pergamon Press. New York (1961).

123. Getzinger, R.W. and Schott, G.L.   Kinetic studies of hydroxyl radicals in shock waves. V.Recombination via the $H+O_2+M \rightarrow HO_2^{\bullet}+M$ reaction in lean hydrogen-oxygen mixtures.   J. Chem. Phys., 43, 3237 (1965).

124. Vermeer, D.J., Meyer, J.W. and Oppenheim, A.K.   Autoignition of hydrocarbons behind reflected shock waves.   Combustion and Flame, 18, 327 (1972).

125. White, D.R. and Cary, K.H.   Structure of gaseous detonation. Phys. Fluids, 6, 749 (1963).

126. Shchelkin, K.I. and Troshin Ya.K.   Gasdynamics of Combustion.
     Mono Book Corp., Baltimore (1965).

127. Urtiew, P.A. and Oppenheim, A.K.   Detonative ignition induced by
     shock merging.   Eleventh Symposium (International) on
     Combustion, p. 665.   The Combustion Institute, Pittsburgh (1967).

128. Moses, K.G. and Korneff, T.   Voltage measurements in the presence
     of strong fields.   Rev. Sci. Instruments., 34, 849 (1963).

129. Rose, H.E. and Priede T.   An investigation of the characteristics
     of spark discharges as employed in ignition experiments.
     Seventh Symposium (International) on Combustion, p. 454.
     Butterworths (1959).

130. Frungel, F.   High Speed Pulse Technology. Vol.II.   Academic Press,
     New York and London (1965).   P. 99.

131. Laumbach, D.D. and Probstein, R.F.   A point explosion in a cold
     exponential atmosphere.   J. Fluid Mechanics, 35, 53 (1969).

132. Chernyi, G.G.   The problem of a point explosion.   Dokl. Akad.
     Nauk., 112(2), 213 (1957).

133. Bach, G.G. and Lee, J.H.   Higher order perturbation solution for
     blast waves.   AIAA J., 7, 742 (1969).

134. Yang, C.H.   Burning velocity and the structure of flames near
     extinction limits.   Combustion and Flame, 5, 163 (1961).

DETAILS OF EXPERIMENTS

1. Explosion Chamber

1.1 Planar Case

For planar initiation, circular tubes (pyrex glass and plexi-glass) having inner diameters ranging from 6 mm to 76 mm and lengths between 10 cm and 30 cm, were used.   The ends of the tube were closed with delrin plugs through an 'O' ring assembly.   One of the delrin plugs was provided with a nipple for evacuating the tube and filling it with the test gas.   Two brass electrodes (6 mm diameter) were also radially screwed into the plug and glued with epoxy.   Provision was also made for mounting a pressure transducer in the delrin plug for reflected shock measurements.   Figure 44 shows a cross-section of the detonation tube with the end fittings.

In the case of the 76 mm diameter tube, the end plugs were directly glued to the plexiglass tube.   For measurement of the cell structure, longer tubes were employed.

1.2 Cylindrical Case

Two 600 mm diameter steel plates (25 mm thick) with spacer rings of ID 500 mm, OD 550 mm, and heights ranging from 2.5 cm to 10 cm, constituted the explosion chamber.   'O' ring seals were provided

between the spacer rings and the steel plates to form a vacuum tight joint. The steel plates had centrally threaded holes 7.5 cm and 10 cm in diameter for the location of the igniter. A number of $\frac{1}{4}$" NF 20 size holes were tapped at several radial and circumferential locations. One of these served for the gas inlet whilst others corresponded to different locations for the pressure transducer. A plan and sectional view of the cylindrical chamber is shown in Figure 45.

During the course of the experiments, it was found necessary to work with chamber widths less than 2.5 cm. Plexiglass plates, 6 mm thick and about 500 mm in diameter, were inserted in the chamber to reduce its height. A small hole was made at the centre of these plates so that the electrode could pass through this hole and be in flush with the surface of the plexiglass plate.

In some instances a totally different configuration was adopted. A cylindrical steel chamber 12 cm ID and 12 cm long was used for the explosion chamber. The ends were closed with 2.5 cm thick plexiglass windows. 'O' ring seals were provided between the windows and the body of the explosion chamber. At the top of the chamber a nipple was provided for the evacuation and filling of the gas mixture. A pressure transducer was also housed at the centre of a plexiglass window.

On the diametrically opposite ends of the chamber along the central diameter, provision was made to house the igniter assembly. Flanged electrodes were used to give the required cylindrical symmetry.

152

Plexiglass plates, 2 cm thick, were used for the flanges. The flanges extended right across the length of the chamber and it was possible to vary the distance between them from ¼ cm to 3½ cm.

1.3 Spherical Case

The 12 cm diameter by 12 cm long steel chamber was also used to study spherical initiation. The flanges, which constrained the wave to move in a cylindrical fashion, were removed to provide an unconfined surrounding.

2. Ignition Methods

2.1 Electrode Configurations

In experiments with spark discharge in circular tubes, the electrical spark was struck across two brass electrodes 6 mm in diameter. The electrodes were mounted radially near the end wall with their tips being almost in flush with the inner surface of the tube. In the case of the 39 mm and 76 mm diameter tubes, the electrodes were mounted in the longitudinal direction jutting about 3 mm inside the tube and spaced at a distance of 30 mm and 55 mm respectively.

With the large cylindrical chamber brass and stainless steel electrodes (3 mm diameter) were centrally located in plexiglass and delrin plugs (7.5 cm and 10 cm in diameter). The tip of the electrode

was kept in flush with the surface of the plug or with the surface
of a plexiglass plate when such plates were incorporated to reduce the
height of the cylindrical chamber.   For exploding wire ignition,
however, a somewhat different arrangement as shown in Figure 46 was
used.   A copper bridge was firmly screwed in the steel bushing and
the exploding wire was connected between this bridge and the brass
electrode housed centrally in the plexiglass plug as seen in Figure 46.
The height of the copper bridge was about equal to the height of the
cylindrical chamber.

Secondary discharges between the electrodes and the body of
the steel chamber presented a problem with the 12 cm x 12 cm cylindrical
chamber.   It was found necessary to insulate the electrodes.
Insulation was provided by 1/16" thick glass tubing surrounding the 3 mm
brass electrodes.   A typical configuration for the insulated electrodes
is shown in Figure 47.   With such an insulation, it was found possible
to vary the gap between the electrodes from $\frac{1}{2}$ cm to 4 cm without any
secondary discharges whatsoever.

2.2   Electrical Discharge System

A schematic diagram of the electrical circuit is shown in
Figure 48.   A high voltage DC power supply (0-60 KVDC, Hipotronix)
was used to charge the condenser bank to a voltage between 8 and 55 kv.
The condenser bank consisted of low inductance capacitors connected in
parallel in a compact coaxial geometry (Maxwell, ECM and Deutschmann).

The range of the capacitances employed was between 0.005 μF and 8 μF. The choice of the operating voltage and the capacitance of the condenser bank was dictated by the energy requirement for direct initiation.

The electrical energy stored in the condenser bank was discharged across the electrodes of a detonation chamber by triggered spark gap switches. A high voltage 30 KV pulse from an EG and G Trigger module (TM 11-A) was used to fire these switches. The electrical connections were made with 1" wide copper strips (gauge 21) in order to minimize the inductance of the electrical circuit.

During the early phase of the work with stoichiometric H_2-O_2 mixtures, commercially obtainable triggered spark gap switches, viz., EG and G model GP 12 B and GP 41 B, were employed. Considerable fluctuations in the results were observed and the inconsistency was initially blamed to the bad mixing of the gases. Attempts were made to improve the mixing by a centrifuging effect and also by invoking convective mixing by heating the bottom of the bottle containing the gas mixture with copper coils conveying hot water. Even with this the inconsistency in the results persisted. Visual observations of the discharge in 12 cm x 12 cm cylindrical chamber later revealed that the voltage pulse from the trigger module often caused a feeble discharge across the electrodes before the main discharge from the condenser bank and this tendency was seen to be aggravated at higher operating pressures. Apparently the feeble discharge across

the electrodes had brought about the preignition of the combustible

gases resulting in the formation of a deflagration wave before a shock

wave was formed by the rapid discharge of the energy stored in the

condenser bank.   The subsequent interaction of the shock and

deflagration could have resulted in a detonation, but then the mode

of initiation does not conform to one of blast initiation with which

we are concerned.

To eliminate this problem of a feeble discharge forerunning

the main discharge, a "home-made" switch which had a provision to vary

the distance between the electrodes and also vary the pressure of the gas

in the switch, was employed.   The electrodes, in the switch, were of

polished stainless steel 2 cm in diameter with a flat face.   One of

the electrodes had a central hole to accommodate the triggering pin for

firing the switch.   It was possible to maintain the pressure of gas

in the switch from low sub-atmospheric levels to around five atmospheres

by hooking it to a vacuum pump and to a cylinder of pressurized

nitrogen gas.

For every experiment the distance between the electrodes in

the switch (i.e., the switching gap) and the pressure of the nitrogen

gas in the switch were so adjusted that a small reduction in either the

gap or the pressure would result in a spontaneous discharge of the

condenser bank even in the absence of the high voltage pulse from the

triggering source.   With the switch operating under these threshold

conditions, it was possible to eliminate the initial weak discharge across the electrodes of the detonation chamber.

At operating voltages in excess of 25 kv corona discharges posed a serious problem. The body of the switch would accumulate sufficient static charge which often resulted in an inherent spontaneous breakdown across the electrodes of the detonation chamber. This problem was eliminated by grounding the body of the switch through a resistance of 10 MΩ and thus bleeding off the surface electrostatic charge.

In some experiments which required longer discharge times (*i.e.*, smaller discharge frequency) the inductance of the discharge circuit was increased by connecting induction coils in series. These induction coils typically consisted of 5 to 30 turns of insulated copper wire (gage 16) wound on a 4 cm diameter plexiglass tube.

3. Diagnostic Techniques

3.1 Energy from the Electrical Discharge

The energy dissipated by an electric spark is given by

$$E_s = \int_0^\tau i(t)\, v(t)\, dt \qquad\qquad A.1.1$$

$$= \int_0^\tau i(t)^2\, R(t)\, dt \qquad\qquad A.1.2$$

where τ is the total discharge period and $v(t)$, $i(t)$ and $R(t)$ denote the resistive voltage drop across the spark, the discharge current and the resistance of the spark respectively. The quantities i, v and R are expected to be functions of time with the damped oscillatory discharges.

The time history of the spark discharge current $(i(t))$ was monitored with calibrated wide band current transformers (model 1025, 0.025 volts/amp; and model 301, 0.01 volts/amp., Pearson Electronics). The current signal was displayed on the screen of a high frequency dual beam oscilloscope (Types 555 and 556 Tektronix) through a high-gain, fast-rise calibrated preamplifier (Types H and 1A1 plug in unit, Tektronix) and was recorded on a polaroid film (Types 47 and 410).

The determination of the resistive voltage drop across the spark [$v(t)$] is rather cumbersome. This is because the high frequencies of discharge encountered in the present experiments (~ 0 [.5 MHz]) cause the inductive voltage drop across the spark to be of the same order of magnitude as the resistive voltage drop. Though it is possible to eliminate the inductive component by use of two identical voltage probes with a compensating coil and a differential amplifier as demonstrated by Moses and Korneff (128), the relative ease of evaluating the resistance of the electric spark makes the determination of energy using Eq. A.1.2 (viz., the current and resistance histories) more attractive. In this investigation no attempt has been made at measuring voltages and all energy determinations are made on the basis of current measurements and resistance evaluation. The method of finding resistances is given in Appendix II.

3.2   Detonation Wave Parameters

3.2.1   Pressure Measurements

Two different types of pressure transducers were used: a hand-made barium titanate pressure transducer and a miniature quartz pressure transducer (model 113A; PCB, Piezotronics).

The barium titanate pressure transducer was a crude version of that designed by Khystautas (30). The positive end of a 6 mm diameter by a 6 mm length barium titanate piezoelectric crystal was joined to a 4 cm long zinc rod of the same diameter with silver epoxy. The barium titanate-zinc rod combination was encased in a brass housing but insulated from the brass body with epoxy glue. The negative face of the barium titanate crystal was earthed by soldering bare copper wire (20 gage) between the crystal face and the brass housing. A sketch of the transducer is shown in Figure 49. The output from the transducer was directly fed to the plug-in preamplifier of the oscilloscope without any emitter follower circuit.

The barium titanate pressure transducers were used for the determination of the time of arrival of the detonation wave and for qualitative appraisal of the pressure. For quantitative measurements of pressure and detailed pressure profiles behind the detonation front a high frequency, 1 μs response PCB quartz pressure transducer was employed. The transducer had a built-in amplifier and was powered by a battery power unit (model 480 A PCB).

3.2.2 Determination of Cell Structure

The smoked film technique was used to determine the cell structure. Thin mylar films (~ .25 mm thick) were coated with a thin layer of soot from a kerosine oil lamp and placed on the walls of the cylindrical bomb or along the walls of the tube. There was a tendency for the mylar film to warp when placed in the cylindrical bomb and this tendency was corrected by employing thicker mylar sheets bonded firmly to the wall by scotch tape.

The imprint of the detonation wave on the sooted mylar films was fixed with clear lacquer.

4. Identification of Direct Initiation

Following Litchfield, Hay and Forshey (77), the direct initiation of a detonation was inferred from the time of arrival of the pressure wave and the magnitude and profile of the pressure trace. The principle behind the method is given below.

When the initiation energy is much below the threshold value for direct initiation, a relatively small and smooth pressure rise associated with a deflagration is observed. Weak shock waves sometimes precede the deflagration wave. The mean velocity of the pressure wave is very much less than the CJ velocity. Figure 50(a) shows such a pressure trace. For critical value of source energy needed for direct initiation, there is a distinct jump in the magnitude of the peak pressure.

The mean velocity of the wave also suddenly increases to about the CJ value (Fig. 50(b)). For the source energies larger than this value the pressure profile does not significantly change and the mean velocity increases only slightly. This is made clear in Figure 51 where the velocity calculated from the time of arrival is plotted against the operating voltage (the energy deposited by a given electrical spark is approximately proportional to the square of the voltage, the capacitance and the inductance of the current remaining the same) in one of the experiments. Apparently the source energy corresponding to V_c^* denotes the critical energy for direct initiation.

In certain cases, especially with planar and cylindrical geometries, the pressure trace had the sharp profile of a detonation but the time of arrival disproved the likelihood of direct initiation. Obviously the transitional mode of initiation has taken place. For mixtures near the limits of detonability, wherein large magnitudes of the source energy were required, it became difficult to employ the mean velocity criterion to identify a detonation. This situation was particularly conspicuous in mixtures for which the sound speed was high (e.g., high dilution with helium and stoichiometric hydrogen-oxygen mixtures) and for the spherical geometry for which the blast wave decay with distance is less than for the planar and cylindrical geometries. Larger explosion chambers are then necessary to clearly determine if direct initiation of detonation has occurred.

5. Experimental Procedure

5.1 Preparation of Gas Mixture

The gases used were of commercial purity (Matheson grade).
The gas mixture was prepared in 100 litre capacity high pressure steel
tanks by the method of partial pressures. Mixing of the gases was
achieved by allowing the gases to diffuse for 24 hours before use.

With mixtures containing very light gases such as helium or
hydrogen, the lighter gas tends to rise to the top of the steel tank
so that mixing by diffusion becomes rather difficult.   In such cases
the steel tanks were placed on the ground along their length rather
than on their base to prevent the stratification of the lighter and
denser gases.   Some experiments were also conducted with such lighter
gases, viz., $H_2 + \frac{1}{2}O_2$ in which mixing was promoted by a centrifugal action
and also by natural convection (heating the steel tank with copper coils
containing hot water) as mentioned in section 2.2 of this appendix.
The consistency of the results obtained with diffusional mixing and with
the above two methods confirmed that adequate mixing is achieved by
allowing the gases to diffuse for about a day before use.

5.2 Test Procedure

The explosion chamber and the various lines connecting the
explosion chamber with the mixture tank were first evacuated to a pressure
around 0.01 mm of mercury. The evacuated system was then flushed with

the test gas and evacuated again.   The gas mixture was then filled
to a pressure about 100 torr greater than the desired initial pressure
and then slowly evacuated till the necessary pressure level was
achieved.   Thereafter the lines connecting the explosion chamber and
the mixture tank were evacuated again to guard against any likelihood
of a detonation feedback.

    The pressure and the distance between the electrodes in the
switch were adjusted to be just above the threshold values for the
spontaneous breakdown across the electrodes of the detonation chamber
corresponding to the desired operating voltage of the experiment. The
condenser banks were charged to this operating voltage and the breakdown
achieved by the manual triggering of the trigger module.   For
experiments at lower pressures, wherein the electrical discharge across
the electrodes in a detonation chamber posed no problem, the breakdown
was achieved by rapid suction of the nitrogen gas in the switch.

    The operating voltage and/or the capacitances were progressively
changed in the subsequent experiments until the condition for direct
initiation was obtained as evidenced by the pressure trace. , A few
experiments were conducted with energies somewhat above and below the
critical value to make sure of the results.

RESISTANCE OF THE SPARK AND THE

EFFECTIVE ENERGY OF DISCHARGE

1. Resistance of the Electrical Spark

The method of evaluating the resistance of the spark discussed in this section follows from the work of Rose and Priede (129).

The discharge circuit, as discussed in section 2.2 of Appendix I, consists of a capacitance C, an inductance L, and a resistance R.   The basic differential equation governing the discharge current is given by

$$L \frac{d^2 i}{dt^2} + R \frac{di}{dt} + \frac{i}{C} = 0 \qquad\qquad A.2.1$$

In all the experiments conducted, the parameters C, L and R were such that we get a damped oscillatory discharge. The solution to Eq. A.2.1 for the case of a damped oscillatory discharge is

$$i(t) = I_o e^{-\alpha t} \sin (\omega t + \theta), \qquad\qquad A.2.2$$

where

I_o and θ are constants of integration,

α is the damping factor $= \frac{R}{2L}$

and ω is the angular frequency $= \sqrt{\frac{1}{LC} + \frac{R^2}{4L^2}}$

In practice, with the range of capacitances used (0.005 μF to 8 μF) and the associated small values in resistance, $\frac{1}{LC} \gg \frac{R^2}{4L^2}$ so that $\omega \simeq \frac{1}{\sqrt{LC}}$. Further, from the experimental discharge current trace, it is seen that the relation

$$i(t) = I_o e^{-\alpha t} \sin \omega t \qquad\qquad A.2.3$$

adequately models the time history of the current.

The magnitude of the peak values in current (i_p) is given by

$$|i_p| = I_o e^{-\alpha t_p} \qquad\qquad A.2.4$$

t_p denoting the time of occurrence of the peak values in the current.

Taking natural logarithm of both sides of Eq.A.2.4 and simplifying we get

$$\alpha = \frac{\ln|i_{p_1}| - \ln|i_{p_2}|}{t_{p_2} - t_{p_1}} \qquad\qquad A.2.5$$

where i_{p_1} and i_{p_2} denote the values of peak currents at times t_{p_1} and t_{p_2} respectively. It is therefore possible to determine the damping factor α from a semilogarithmic plot of peak currents with time.

165

The angular frequency of the discharge can be readily monitored from the experimental current trace ($\omega = 2\pi/T$, T being the periodic time). Assuming the capacitance of the leads, connections, and spark gap to be negligibly small in comparison to the capacitance of the condenser bank, the circuit inductance can be readily determined from the value of $\omega(L = 1/\omega^2 C)$. With α determined from the semilogarithmic plot of i_p versus t_p, and L known from the angular frequency of discharge, the resistance of the discharge circuit is found from the relation $R = 2\alpha L$.

This value of resistance is the total resistance of the discharge circuit. In order to determine the resistance of the spark gap alone (R_{sg}) it becomes necessary to determine the resistance of the remaining circuit, viz., the resistance of the leads, connections, electrodes, switch and the internal resistance of the capacitors. This is done by shorting the gap between the electrodes with an extremely well-conducting material and obtaining an oscillatory current discharge with the capacitors charged to the same voltage as before. From this discharge current trace the resistance of the remaining circuit R_c is determined in the same manner as with the main discharge across the electrodes of the detonation chamber.

The resistance of the spark is then given by

$$R_{sg} = R - R_c \qquad\qquad A.2.6$$

It is important to realize that the act of shorting the electrodes to determine the resistance of the remaining circuit must not change the inductance of the circuit. In all experiments the electrodes were shorted with a brass or copper rod 6 mm in diameter.

Figure 52 shows a typical plot of the natural logarithm of the peak currents versus time for the experimental discharge current trace. Curve A refers to the peak currents with discharge across the electrodes of the detonation chamber, whilst the Curve B pertains to these peak currents obtained with the gap between the electrodes shorted. It is seen that the plot is remarkably linear over the first few cycles of the discharge indicating that the decay factor α (and therefore the resistance) is constant over this period.[**] Towards the tail of the discharge, however, the value of α is seen to increase indicating an increase in the resistance of the spark. This growth in the value of resistance is to be expected since towards the end of the discharge the spark channel expands and cools in the process resulting in a decrease in the density of electrons and therefore of electrical conductivity.

We shall see in the next section that the effective portion of the discharge that actually contributes to form a detonation corresponds to the energy released in less than the first half cycle of discharge.

[**] This is in agreement with the results of Rose and Priede who also observed the values of α and R to be constant over a considerable portion of the discharge with damped oscillatory discharges obtained from condensers in the micro-microfarad range.

On the basis of the resistance remaining constant over the first few cycles of discharge, we shall assume, in our calculations, the spark resistance to be a constant and to be given by the constant value determined from the first few cycles of the discharge.

Toepler and Binder (130) have given an empirical law for the resistance of an electrical spark in terms of the length of the spark l, the pressure of the gas p, the capacitance of the discharging condenser C, and the charging voltage of the condensers V_o. Their relation is given by

$$R_{sg} = \frac{Klp}{CV_o} \qquad A.2.7$$

The resistances evaluated on the basis of the discharge current records by determining the decay coefficients, as given in this section, exhibited the direct dependence on length and pressure and the inverse dependences on capacitance and charging voltages as postulated by Toepler and Binder for charging voltages up to about 35 kv. For charging voltages exceeding 35 kv, however, the value of the spark resistance tended to be relatively unaffected by a change in the charging voltage V_o.

2. Effective Energy of a Spark Discharge in Direct Initiation

In the first exploratory studies on the initiation of detonations, the critical energy for direct initiation was based on the total electrical energy stored in the capacitors. The stored energy can approximate the energy deposited in the gases only if the resistance of the discharge circuit is dominated by the resistance of the spark gap. In practice, however, the resistance of the switch and the circuit leads is of the same order of magnitude as the resistance of the spark so that ohmic dissipation in the switches and the connecting leads must also be considered. Hence the energy deposited by a spark discharge in the detonating gas must be evaluated on the basis of

$$\int_0^{\tau_D} i(t)v(t)dt \quad \text{or} \quad \int_0^{\tau_D} i^2(t)R(t)dt \quad \text{where} \quad \tau_D \text{ is the total duration of the}$$

discharge and i,v and R denote the current, the resistive voltage drop across the spark and the resistance of the spark respectively.

A closer examination of the initiation process reveals that not all of the above energy deposited in the gases need to contribute to the initiation of detonation. Using a "crowbar" technique to truncate the electrical discharge at different times, and working with different frequencies of discharge, Knystautas and Lee (26) recently demonstrated that the effective energy for direct initiation with electrical sparks corresponds to the energy delivered up to a time corresponding to the attainment of the peak average power.

Denoting the time for the attainment of the peak averaged power as τ_p and the resistance of the spark to be R_{sg}, the effective energy release for initiation of detonation with damped oscillatory electrical discharge $(i(t) = I_o e^{-\alpha t} \sin \omega t)$ can be evaluated to be

$$E_s = \int_0^\tau i(t)^2 R_{sg} \, dt$$

$$= \frac{I_o^2 R_{sg} \, \omega}{4(\alpha^2+\omega^2)} \left[\frac{\omega}{\alpha} (1-e^{-2\alpha\tau_p}) - e^{-2\alpha\tau_p} \left(\frac{2\alpha}{\omega} \sin^2\omega\tau_p + \sin 2\omega\tau_p\right) \right] \qquad \text{A.2.8}$$

The value of I_o here is determined from the intercept on the $\ln|i_p|$ axis in the plot of $\ln|i_p|$ versus t_p (Fig. 52).

3. Theoretical Considerations for the Choice of the Effective Energy

That the effective energy for direct initiation does indeed conform to the energy released up to the time of the peak averaged power can be seen from the following theoretical model. The early time behaviour of the shock driven by the energy released from the electrical spark is considered. Since the shock wave is fairly strong and the core of the gases, heated by the energy release from the spark, is extremely hot, most of the shocked mass is concentrated in the near

vicinity of the shock front.   Consequently, the 'Snowplow' approximation of Laumbach and Probstein(131) and Chernyi (132) is used to model the shock motion.

3.1 Formulation of the 'Snowplow" Model[†]

The basic equations for continuity, momentum and energy in Lagrangian coordinates are

Continuity: $\quad \rho_0 k_j R^j dR = \rho k_j r^j dr$ $\qquad$ A.2.9

Momentum: $\quad \dfrac{\partial^2 r(R,t)}{\partial t^2} + \left(\dfrac{r}{R}\right)^j \dfrac{1}{\rho_0} \dfrac{\partial p}{\partial R} = 0$ $\qquad$ A.2.10

Energy: $\quad \dfrac{p(R,t)}{\rho^\gamma(R,t)} = \dfrac{p_s(R)}{\rho_s^\gamma(R)}$ $\qquad$ A.2.11

Here R and r denote the Lagrangian and Eulerian coordinates respectively, while $j = 0$, 1 and 2 denote the planar, cylindrical and spherical geometries respectively.   The energy Eq. A.2.11 assumes isotropic expansion of the gases after being shocked.   In other words, the energy addition due to the chemical reaction is neglected.   The justification for such an assumption stems from the fact that the chemical energy released during the initial phase of shock motion is negligible.

[†]   The author is thankful to Dr. K.W. Chiu for helping in the formulation of this theory — in particular, with the mathematical simplification of the internal energy term given by Eq. A.2.24.

The jump conditions at the shock are given by the Rankine Hugoniot relations. For strong shocks they are

$$\frac{\rho_s}{\rho_0} = \frac{\gamma+1}{\gamma-1} \qquad\qquad\qquad\qquad A.2.12$$

and

$$p_s = \frac{2}{\gamma+1}\,\rho_0 R_s^{02} \qquad\qquad\qquad A.2.13$$

From the snowplow approximation, *viz.*, that the gas particles follow the shock front closely, we may write

$$r = R_s - \epsilon\,(R_s - R) \qquad\qquad\qquad A.2.14$$

where ϵ is a small quantity.

Differentiating Eq. A.2.14 with respect to R, we get at the shock front

$$\left.\frac{\partial r}{\partial R}\right|_{R_s} = \epsilon$$

Further, from Eq. A.2.9 we have at the shock front

$$\left.\frac{\partial r}{\partial R}\right|_{R_s} = \frac{\rho_0}{\rho_s}$$

so that

$$\epsilon = \frac{\gamma-1}{\gamma+1} \qquad\qquad\qquad\qquad A.2.15$$

giving $r = R_s - \frac{\gamma-1}{\gamma+1}(R_s - R)$ 　　　　　　A.2.16

The energy deposited by the electrical spark in the gases goes to increase the kinetic and internal energies of the gas. If the shock at time t is at a distance R_s from the source, the global conservation of energy yields

$$E_s(t) = \int_0^{R_s} \frac{1}{2}\left(\frac{\partial r}{\partial t}\right)^2 \rho k_j r^j dr + \int_0^{R_s} \frac{p}{\gamma-1} k_j r^j dr$$ 　　A.2.17

Here the initial internal energy of the shocked gases is neglected since it is expected to be small.

From Eq. A.2.16 we get

$$\frac{\partial r}{\partial t} = \frac{2}{\gamma+1} \overset{\circ}{R}_s$$ 　　　　　　A.2.18

Using Eq. A.2.18, we can write the kinetic energy term in Eq. A.2.17 as

$$\frac{2 \rho_0 k_j \overset{\circ}{R}_s{}^2 R_s{}^{j+1}}{(\gamma+1)^2 (j+1)}$$ 　　　　　　A.2.19

The evaluation of the internal energy term in Eq. A.2.17 is slightly more complicated. To determine p(R) we use the momentum Eq. A.2.10 to obtain

$$\frac{\partial p}{\partial R} = - \rho_0 \frac{R^j}{r^j} \frac{\partial^2 r(R,t)}{\partial t^2}$$

Using the above in Eq. A.2.18, we get

$$\frac{\partial p}{\partial R} = - \frac{2}{\gamma+1} \overset{\circ\circ}{R}_s \frac{\rho_0 R^j}{r^j} \qquad\qquad A.2.20$$

The value of p(R) near the shock front is therefore given by

$$p(R,t) - p_s = - \frac{2}{\gamma+1} \overset{\circ\circ}{R}_s \frac{\rho_0}{R_s^{\,j}} \int_{R_s}^{R} R^j \, dR \qquad\qquad A.2.21$$

so that

$$p(R,t) = \frac{2}{\gamma+1} \rho_0 \overset{\circ}{R}_s^{\,2} \left[1 + \frac{R_s \overset{\circ\circ}{R}_s}{\overset{\circ}{R}_s^{\,2}(j+1)} \left\{ 1 - \left(\frac{R}{R_s} \right)^{j+1} \right\} \right] \qquad A.2.22$$

174

The above equation can also be written as

$$p(R,t) = \frac{2}{\gamma+1} \rho_0 \overset{\circ}{R}_s^2 \left[1 + \frac{\theta}{j+1} \left\{ 1 - \left(\frac{R}{R_s} \right)^{j+1} \right\} \right] \qquad \text{A.2.22a}$$

where the decay coefficient θ is given by

$$\theta = \frac{R_s \overset{\circ\circ}{R}_s}{\overset{\circ}{R}_s^2} \qquad \text{A.2.23}$$

The internal energy term can be re-written using Eq. A.2.9 as

$$\int_0^{R_s} \frac{p}{\gamma-1} k_j r^j dr = \int_0^{R_s} \frac{p(R,t)-p(0,t)}{\gamma-1} \frac{\rho_0}{\rho} k_j R^j dR + \int_0^{R_s} \frac{p(0,t)}{\gamma-1} k_j r^j dr \qquad \text{A.2.24}$$

From Eq. A.2.9 and A. 2.16 we also get

$$\frac{\rho}{\rho_0} = \frac{\gamma+1}{\gamma-1} \left(\frac{R}{R_s} \right)^j$$

and using the value of p from Eq. A.2.22a we get

$$\int_0^{R_S} \frac{p}{\gamma-1} k_j r^j dr = -\frac{2 \rho_0 \mathring{R}_s^2 \theta k_j}{(\gamma+1)^2 (j+1) R_s} \int_0^{R_s} R^{j+1} dR + \frac{2}{\gamma+1} \rho_0 \mathring{R}_s^2 \left(1+\frac{\theta}{j+1}\right) \frac{k_j}{\gamma-1} \int_0^{R_s} r^j dr$$

giving

$$\int_0^{R_S} \frac{p}{\gamma-1} k_j r^j dr = \frac{2 k_j \rho_0 \mathring{R}_s^2 R_s^{j+1}}{(j+1)(\gamma+1)(\gamma-1)} \left[1 + \frac{\gamma+2j+3}{(j+1)(\gamma+1)(j+2)} \theta\right] \qquad A.2\ 25$$

Substituting Eq. A.2.19 and A.2.25 in Eq. A.2.17 and simplifying
we get

$$\frac{(\gamma+1)(\gamma-1)(j+1)E_s(t)}{2 k_j \rho_0 \mathring{R}_s^2 R_s^{j+1}} = \frac{2\gamma}{\gamma+1} + \frac{(\gamma+2j+3)}{(j+1)(\gamma+1)(j+2)} \theta \qquad A.2.26$$

Using the value of θ from Eq. A.2.23 and re-arranging the terms we
get the following differential equation

$$\overset{\circ}{R}_s + A \frac{\overset{\circ}{R}_s^2}{R_s} - \frac{B}{R_s^{j+2}} = 0 \qquad\qquad \text{A.2.27}$$

$$\text{where} \quad A = \frac{2\gamma(j+1)(j+2)}{\gamma+2j+3} \qquad\qquad \text{A.2.28}$$

$$\text{and} \quad B = \frac{E_s(t)(j+1)^2(j+2)(\gamma+1)^2(\gamma-1)}{(\gamma+2j+3)\ 2k_j\ \rho_0} \qquad\qquad \text{A.2.29}$$

This ordinary differential equation can be readily integrated for any energy time history $E_s(t)$ by the Runge-Kutta method once the initial conditions are known. It is interesting to note that the solution obtained with this model agrees very well with the strong blast similarity solution when the time dependent energy source is replaced by the ideal energy source, viz., $E_s = E_o$ = a constant. This is seen as follows:

With $E_s(t) = E_o$ = constant and $\chi = \overset{\circ}{R}_s^2/2$, Eq. A.2.27 reduces to

$$\frac{d}{dR_s}\left[\chi R_s^c\right] = B\ R_s^{c-j-2} \qquad\qquad \text{A.2.30}$$

where $c = 2A$.

Integrating Eq. A.2.30 and setting the constant of integration equal to zero to recover the point blast solution, we get

$$\overset{o}{R}_s = \left(\frac{2B}{c-j-1}\right)^{\frac{1}{2}} \quad R_s^{\frac{-(j+1)}{2}} \qquad \qquad \text{A.2.21}$$

On integrating Eq. A.2.21 we get the shock trajectory to be

$$R_s = \left[\left(\frac{E_o}{\rho_0}\right)^{1/j+3} \left(\frac{j+3}{2}\right)^{2/j+3} \left\{\frac{(j+1)(j+2)(\gamma+1)^2(\gamma-1)}{k_j(7\gamma+4\gamma j-2j-3)}\right\}^{\frac{1}{j+3}} \right] t^{2/j+3} \qquad \text{A.2.22}$$

Based on the self similar solution for an ideal blast wave the shock trajectory is obtained to be (107)

$$R_s = \left(\frac{(j+3)^2 E_o}{4k_j I \rho_0}\right)^{1/j+3} t^{2/j+3} \qquad \qquad \text{A.2.23}$$

Using the values of I given by Bach and Lee (133) and by Rogers (60), the shock trajectory using Eq.A.2.22 and A.2.23 is compared

below for γ of 1.4 or 1.2 respectively.

Geometry	Eq. A.2.22	Eq. A.2.23
$\gamma = 1.4$		
Planar	$1.151 \ (E_o/\rho_0)^{1/3} \ t^{2/3}$	$1.229 \ (E_o/\rho_0)^{1/3} \ t^{2/3}$
Cylindrical	$0.959 \ (E_o/\rho_0)^{1/4} \ t^{1/2}$	$1.008 \ (E_o/\rho_0)^{1/4} \ t^{1/2}$
Spherical	$0.996 \ (E_o/\rho_0)^{1/5} \ t^{2/5}$	$1.067 \ (E_o/\rho_0)^{1/5} \ t^{2/5}$
$\gamma = 1.2$		
Planar	$0.931 \ (E_o/\rho_0)^{1/3} \ t^{2/3}$	$0.963 \ (E_o/\rho_0)^{1/3} \ t^{2/3}$
Cylindrical	$0.820 \ (E_o/\rho_0)^{1/4} \ t^{1/2}$	$0.838 \ (E_o/\rho_0)^{1/4} \ t^{1/2}$
Spherical	$0.879 \ (E_o/\rho_0)^{1/5} \ t^{2/5}$	$0.804 \ (E_o/\rho_0)^{1/5} \ t^{2/5}$

3.2 Discussion of Results

Two different types of initial conditions were used to
integrate Eq. A.2.27.   One assumed an acoustic wave to be generated
at the initial spark kernel radius immediately on striking the discharge
[i.e., $\overset{o}{R}_S = C_O$ and $R_S = R_{S_O}$ at $t = 0$; R_{S_O} denoting the initial
spark radius].   The other initial condition was that the early energy
release caused a pressure wave to originate from the source, the
magnitude of the pressure being given by a constant volume energy
addition, viz., $p = (\gamma-1)E(t_O)/v_O$ (v_O denotes the initial volume, viz.,

$\dfrac{k_j R_{S_O}^{\,j+1}}{j+1}$ and $R_S = R_{S_O}$ at $t = t_O$).

Figure 53 shows the results obtained in the cylindrical
geometry ($j = 1$) for spark discharge parameters given by the following:

Spark gap resistance $R_{sg} = 0.1\Omega$

Total circuit resistance $R = 0.18\Omega$

Capacitance $C = 0.049$ μF

I_O = 8360 Amp

Discharge frequency $f = 0.905$ MHz

Charging voltage = 30 kv

The dotted line and solid line show the variation of Mach
number of the shock with time for the acoustic starting condition and

a constant volume starting condition respectively. The results are shown for an initial spark kernel radius R_{s_o} of 1 mm and 2 mm. It is seen that the nature of the starting condition (viz., an acoustic start or a constant volume start) does not influence the shock trajectory. The value of the initial radius R_{s_o}, however, is seen to significantly influence the magnitude of the shock Mach number. In Figure 53 is also shown the variation of the energy released by the spark and the average power of the energy release as a function of time.

The initial radius of the spark kernel with a line source of energy can at the utmost vary between 1/2 mm to about 2 mm. Figures 54 and 55 show the Mach number of the shock obtained by successively truncating the energy release at various times with an initial radius of spark kernel of 1/2 mm and 2 mm. The circled figures on the curves denote the number of cycles of discharge after which the energy release is terminated. For instance, 0.1, 1/4, 1, PAP etc. denote that the energy release from the spark is stopped after the first 1/10th cycle of discharge, after a 1/4 cycle of discharge, after one complete cycle of discharge, or after the attainment of the peak average power. It is seen from the figure that truncating the discharge at times earlier than the time corresponding to the attainment of the peak average power (t_{pap}) produces a significant decrease in the peak values of the shock Mach number generated by the source. But the truncation of the discharge at times greater than t_{pap} does not produce any noticeable change in the region around the peak Mach number and only reinforces

the shock strength much later in the process.   In direct initiation

of detonations, the detonation is formed fairly early in the process

so that the strengthening of the shock at later periods when a

detonation is already formed cannot affect the phenomenon.   Since the

capacity to form a strong shock is seen to be impaired if the energy

release is stopped before t_{pap} and is relatively unaffected if the

discharge is terminated after t_{pap}, it is not surprising that the

effective energy for direct initiation with a spark discharge corresponds

to the energy released up to the attainment of the peak average power.

ESTIMATION OF A MINIMUM SHOCK MACH NUMBER

FROM THE MINIMUM POWER REQUIREMENT

An estimate of the Mach number corresponding to the experimentally observed minimum power requirement in the initiation of a detonation is made in this appendix. The energy release pertaining to the minimum power requirement is modelled in terms of a constant velocity piston driving a shock wave. The simplified analytical method of Guirao, Lee and Bach (41) for a piston-driven shock is used for this purpose. Their analytical solution is first reviewed in this appendix and then applied for the calculation of the shock strength corresponding to the minimum power requirement.

Consider a shock wave driven by a piston at constant velocity. Let us assume a one-dimensional radial motion of the gas enclosed between the piston and the shock front. The one-dimensional conservation equations for mass, momentum and energy are given by

$$\frac{\partial \rho}{\partial t} + \rho \frac{\partial u}{\partial r} + u \frac{\partial \rho}{\partial r} + \frac{j\rho u}{r} = 0 \qquad \text{A.3.1}$$

$$\frac{Du}{Dt} + \frac{1}{\rho} \frac{\partial p}{\partial r} = 0 \qquad \text{A.3.2}$$

$$\frac{D}{Dt} e + p \frac{D}{Dt} \left(\frac{1}{\rho}\right) = 0 \qquad \text{A.3.3}$$

Here $j = 0$, 1 and 2 denote the planar, cylindrical and spherical geometries respectively.

In the blast wave coordinates the above conservation equations become

$$(\phi-\xi)\frac{\partial\psi}{\partial\xi} + \psi\frac{\partial\phi}{\partial\xi} + j\frac{\phi\psi}{\xi} = 2\theta\eta\frac{\partial\psi}{\partial\eta} \qquad\qquad \text{A.3.4}$$

$$(\phi-\xi)\frac{\partial\phi}{\partial\xi} + \theta\phi + \frac{1}{\psi}\frac{\partial f}{\partial\xi} = 2\theta\eta\frac{\partial\phi}{\partial\eta} \qquad\qquad \text{A.3.5}$$

$$(\phi-\xi)\frac{\partial f}{\partial\xi} + \gamma f\frac{\partial\phi}{\partial\xi} + \frac{\gamma j f\theta}{\xi} + 2\theta f = 2\theta\eta\frac{\partial f}{\partial\eta} \qquad\qquad \text{A.3.6}$$

where θ is the decay coefficient given by $R_s\overset{\circ\circ}{R}_s/\overset{\circ}{R}_s{}^2$.

While deriving the above equations an equation of state of the following form $\left(e = \frac{p}{\rho(\gamma-1)}\right)$ is assumed.

For a constant velocity shock front driven by a piston ($\overset{\circ}{R}_s$ = constant) the decay coefficient $\theta = 0$. Further, the flow bounded between the piston and the shock front is isentropic.

Introducing the local sound speed as a dependent variable, viz.,

$$\beta^2 = C^2/\overset{\circ}{R}_s{}^2 = \frac{\gamma p}{\rho} \cdot \frac{1}{R_s^2} = \frac{\gamma f}{\psi} \qquad\qquad \text{A.3.7}$$

and noting that $\theta = 0$ for the constant velocity shock which is driven by a piston, the conservation equations A.3.4-A.3.6 can be reduced to the following two:

$$\frac{2}{\gamma-1} (\phi-\xi) \frac{\partial \beta}{\partial \xi} + \beta \frac{\partial \phi}{\partial \xi} + \frac{j\phi\beta}{\xi} = 0 \qquad\qquad A.3.8$$

$$\frac{2}{\gamma-1} \beta \frac{\partial \beta}{\partial \xi} + (\phi-\xi) \frac{\partial \phi}{\partial \xi} = 0 \qquad\qquad A.3.9$$

Solving for $\frac{\partial \phi}{\partial \xi}$ and $\frac{\partial \beta}{\partial \xi}$ from Eq. A.3.8 and A.3.9 we get

$$\frac{\partial \phi}{\partial \xi} = \frac{j\phi\beta^2}{\xi} \frac{1}{(\phi-\xi)^2-\beta^2} \qquad\qquad A.3.10$$

$$\frac{\partial \beta}{\partial \xi} = -\left(\frac{\gamma-1}{2}\right) \frac{j\phi\beta (\phi-\xi)}{\xi[(\phi-\xi)^2-\beta^2]} \qquad\qquad A.3.11$$

The boundary conditions at the shock front ($\xi = 1$) are given by the Rankine-Hugoniot relations.

$$\phi(1) = \frac{2}{\gamma+1} (1-\eta) \qquad\qquad A.3.12$$

$$\beta(1) = \left[\frac{2\gamma}{\gamma+1} (1-\frac{\gamma-1}{2\gamma} \eta) \left(\frac{\gamma-1+2\eta}{\gamma+1}\right)\right]^{\frac{1}{2}} \qquad\qquad A.3.13$$

Once a desired shock Mach number is specified $\phi(1)$ and $\beta(1)$ are known so that it is possible to integrate Eq. A.3.10 and A.3.11 numerically to determine the hydrodynamic flow structure between the shock front and the piston.

Guirao, Lee and Bach (41) observed that for moderately strong shock waves (e.g., $M_s \geq 2$) the solution for the velocity is remarkably linear of the form

$$\phi(\xi) = A + B\xi \qquad \text{A.3.14}$$

where A and B are constants for a given geometry j, shock strength η and specific heat ratio γ. By formally assuming the velocity profile to be linear and to be given by Eq. A.3.14, they solved Eq. A.3.10 and A.3.11 and obtained

$$\beta(\xi) = \left\{ \beta^2(1) + \frac{\gamma-1}{2} B \left[A + \frac{B-1}{2} - (A + \frac{B-1}{2} \xi) \xi \right] \right\}^{\frac{1}{2}} \qquad \text{A.3.15}$$

Using the boundary conditions at the shock front ($\xi = 1$), viz., Eq. A.3.12 and A.3.13, the equations A.3.14 and A.3.15 can be solved to give values of constants A and B as below.

$$A = \frac{2}{(\gamma+1)^2} \left[\gamma(2j+1) + 1 - \eta \ (\gamma(j+1) + 1-j) \right] \qquad \text{A.3.16}$$

$$B = \frac{2j}{(\gamma+1)^2} \left[\eta(\gamma-1) - 2\gamma \right] \qquad \text{A.3.17}$$

At the piston surface $\phi(\xi_p) = \xi_p$. From Eq. A.3.14

we get

$$\xi_p = \phi(\xi_p) = \frac{A}{1-B} \qquad\qquad\qquad \text{A.3.18}$$

and substituting the values of A and B from Eq. A.3.16 and A.3.17 in Eq. A.3.18 we get

$$\xi_p = \phi(\xi_p) = 2\left[\frac{\gamma(2j+1) + 1 - \eta(\gamma(j+1) + 1 - j)}{(\gamma+1)^2 + 2j(2\gamma - \eta(\gamma-1))}\right] \qquad \text{A.3.19}$$

With A and B known from Eq. A.3.16 and A.3.17, and the position of the piston determined from the above, the particle velocity (ϕ) and sound speed (β) variation between the shock front and the piston surface are readily determined from Eq. A.3.14 and A.3.15.

In order to get the pressure and density variation between the shock and piston surface we invoke the fact that the flow is isentropic in this region. Hence, for $\xi_p < \xi < 1$ we can write

$$\frac{p(r)}{\rho(r)^\gamma} = \frac{p(R_s)}{\rho(R_s)^\gamma} \qquad\qquad\qquad \text{A.3.20}$$

which gives

$$\frac{f(\xi)}{\psi(\xi)^\gamma} = \frac{f(1)}{\psi(1)^\gamma} \qquad\qquad\qquad \text{A.3.21}$$

Using the definition of β from Eq. A.3.8, *viz.*,

$$\beta(\xi) = \left(\frac{\gamma f(\xi)}{\psi(\xi)} \right)^{\frac{1}{2}} \qquad\qquad \text{A.3.22}$$

we get

$$f(\xi) = \frac{\beta(\xi)}{\gamma}^{\frac{2\gamma}{\gamma-1}} \left(\frac{\psi^{\gamma}(1)}{\gamma f(1)} \right)^{\frac{1}{\gamma-1}} \qquad\qquad \text{A.3.23}$$

and $\quad \psi(\xi) = \beta(\xi)^{\frac{2}{\gamma-1}} \left(\frac{\psi^{\gamma}(1)}{\gamma f(1)} \right)^{\frac{1}{\gamma-1}} \qquad\qquad \text{A.3.24}$

The values of $\psi(1)$ and $f(1)$ are the density ratio and the non-dimensional pressure at the shock front $\xi = 1$. These are given by the Rankine-Hugoniot relations, *viz.*,

$$\psi(1) = \frac{\gamma+1}{\gamma-1 + 2\eta} \qquad\qquad \text{A.3.25}$$

$$f(1) = \frac{2}{\gamma+1} \left[1 - \frac{(\gamma-1)\eta}{2\gamma} \right] \qquad\qquad \text{A.3.26}$$

Thus, from Eq. A.3.14, 15, 23 and 24 the velocity, pressure and density distribution can be analytically determined.

The energy supplied by the constant velocity expanding piston to the surrounding gas is *via* the compression work. This can be written as

$$E = \int_0^{V_p} p_p \, dv \qquad \text{A.3.27}$$

where p_p is the pressure at the piston surface and V_p is the volume swept by the piston.

Eq. A.3.27 can be written as

$$E = \int_0^{R_p} p_p \, k_j \, r^j \, dr = \frac{k_j}{j+1} \, p_p \, R_p^{j+1} \qquad \text{A.3.28}$$

For a constant velocity piston $R_p = \dot{R}_p t = \phi_p \dot{R}_s t$, where t is the duration of travel of the constant velocity piston. Hence the energy delivered to the adjoining gas by the constant velocity piston becomes

$$E = \frac{k_j}{j+1} \, p_p \, (M_s C_o \phi_p t)^{j+1} \qquad \text{A.3.29}$$

Expressing p_p in terms of the dimensionless pressure and simplifying we get

$$E = \frac{k_j \, \gamma \, P_o \, f_p \, M_s^{j+3} \, (C_o t \phi_p)^{j+1}}{(j+1)} \qquad\qquad A.3.30$$

In the above equation, ϕ_p and f_p are determined from Eq. A.3.23, A.3.14, and A.3.19 once the shock Mach number M_s is specified.

A plot of the energy released by a constant velocity cylindrical piston ($j = 1$) driving a shock wave of M_s between 3 and 7 is shown for various durations of the piston motion in Figures 56 and 57. In Figure 56 the properties of the gas mixture correspond to a 100 torr stoichiometric oxyacetylene mixture whilst in Figure 57 the properties correspond to a 380 torr stoichiometric oxyhydrogen mixture. By assuming the minimum power requirement for the initiation of a cylindrical detonation to correspond to the energy released by a constant velocity cylindrical piston delivering the initiation energy over the effective duration of energy release, the shock Mach number M_s pertaining to the experimentally measured minimum power requirement is read off from the figures (Power $= \frac{E_s}{t}$). These are shown by the triangular points in Figures 56 and 57 for the oxyacetylene and oxyhydrogen mixtures. The value of M_s is seen to be about 5 in either case.

YANG'S ANALYSIS OF THE FLAME IGNITION PROBLEM

Yang (51) considers the ignition of a gas by a plane, line and point energy source. He considers the energy source to be located at the origin of the particular coordinate system. He formulates the ignition problem in a frame of reference with the flame front stationary. The unburnt gases are assumed to flow towards the ignition source at some rate G and the burnt gases are assumed to be exhausted by a mass sink located at the source. Considering an elemental volume of thickness, δr, at a spatial coordinate r from the origin, the basic differential equations governing energy and diffusion are written as

$$ K \left[\frac{\partial^2 T}{\partial r^2} + \frac{j}{r} \frac{\partial T}{\partial r} \right] - \frac{GC}{k_j r^j} \frac{\partial T}{\partial r} + R(\alpha, T) - L(\alpha, T) = \rho C \frac{\partial T}{\partial t} \qquad \text{A.4.1} $$

and

$$ D_f \rho \left[\frac{\partial^2 \alpha}{\partial r^2} + \frac{j}{r} \frac{\partial \alpha}{\partial r} \right] - \frac{G}{k_j r^j} \frac{\partial \alpha}{\partial r} - \frac{R(\alpha, T)}{Q} = \rho \frac{\partial \alpha}{\partial t} \qquad \text{A.4.2} $$

where K is the thermal conductivity

α is the fuel concentration

C is the specific heat

R is the volumetric heat generation rate

L is the volumetric heat loss rate

Q is the gravimetric heat generation rate

D_f is the diffusion coefficient

and k_j = 1, 2π and 4π for j = 0, 1 and 2 corresponding to the
planar, cylindrical and spherical geometries.

Equations A.4.1 and A.4.2 can be integrated for any instant
of time (say at t = t_1) between the energy source (r = 0) and the
undisturbed medium (r → ∞) to yield

$$- CG \ (T_m - T_u) + \int_0^\infty k_j \ r^j \ R(\alpha, T) \ dr - \int_0^\infty k_j \ r^j \ L(\alpha, t) \ dr = \int_0^\infty \rho C (\frac{\partial T}{\partial t})_{t=t_1} dr \qquad A.4.3$$

$$- G \ (\alpha_0 - 1) - \frac{1}{Q} \int_0^\infty k_j \ r^j \ R \ (\alpha, T) \ dr = \int_0^\infty \rho \ (\frac{\partial \alpha}{\partial t})_{t=t_1} dr \qquad A.4.4$$

Here α_0 , T_m and T_u denote the fuel concentration at the origin,
the temperature at the origin and the temperature at r → ∞ respectively.

The right hand sides of Eq. A.4.3 and A.4.4 denote the net rate of increase of heat release and fuel concentration respectively at time $t = t_1$. For ignition to be successful, the net heat release rate within the system must be positive at all times (heat generation rate $>$ rate of heat loss; i.e., $\int_0^\infty \rho C \left(\frac{\partial T}{\partial t}\right)_{t=t_1} > 0$) and the reaction should also progress with time $\left[$ i.e., fuel should be consumed or $\int_0^\infty \rho \left(\frac{\partial \alpha}{\partial t}\right)_{t=t_1} dr < 0 \right]$. The critical conditions are therefore seen to be

$$\int_0^\infty \rho C \left(\frac{\partial T}{\partial t}\right)_{t=t_1} dr = 0 \qquad \text{A.4.5}$$

$$\int_0^\infty \rho \left(\frac{\partial \alpha}{\partial t}\right)_{t=t_1} dr = 0 \qquad \text{A.4.6}$$

On the basis of the above, Yang asserts that the steady state portion of the governing differential equations A.4.1 and A.4.2 will adequately represent the energy and diffusion equations under the critical conditions of ignition since the generation and dissipation terms then balance each other. If G^* represents the mass flow rate G under these conditions, the governing differential equations for the critical ignition behaviour become

$$K \left[\frac{\partial^2 T}{\partial r^2} + \frac{j}{r} \frac{\partial T}{\partial r} \right] - \frac{G^* C}{k_j r^j} \frac{\partial T}{\partial r} + R(\alpha, T) - L(\alpha, T) = 0 \qquad \text{A.4.1a}$$

$$D_f \left[\frac{\partial^2 \alpha}{\partial r^2} + \frac{j}{r} \frac{\partial \alpha}{\partial r} \right] - \frac{G^*}{k_j r^j} \frac{\partial \alpha}{\partial r} - \frac{R(\alpha, T)}{Q} = 0 \qquad \text{A.4.2a}$$

In one of the earlier papers (134), Yang demonstrates a method of solution for the Eq. A.4.1a and A.4.2a in order to determine G^* and the α and T distributions. Knowing G^*, it is possible to calculate the net heat generation rate corresponding to the critical conditions from Eq. A.4.4

$$\int_0^\infty k_j \, r^j \, R(\alpha, T) \, dr = Q \, G^* \, (1 - \alpha_o) \qquad \text{A.4.7}$$

For successful ignition, therefore, the energy release from the igniter must be capable of causing chemical reactions in an adequate volume (corresponding to a critical mass flow rate G^*) so as to lead to a heat generation rate greater than or equal to the value specified by Eq. A.4.7. On this basis the source energy is determined in Yang's analysis of the ignition problem.

The critical ignition problem is therefore seen to identify a critical mass flow rate G^* (or equivalently, a certain minimum volume of burning gases - flame kernel) so as to override the losses due to the transport phenomenon.

DETERMINATION OF THE ENERGY INTEGRAL I

AND THE JTZ PRESSURE PROFILE FOR A CJ DETONATION*

We need to know the hydrodynamic flow structure behind a

detonation wave in order to determine the energy integral I and the

pressure profile.   For a steady CJ detonation, the decay coefficient

$\theta = 0$ and the flow behind the wave is isentropic.   The basic equations

governing the flow are the same as those derived for a constant

velocity piston-driven shock (Eq. A.3.10 and A.3.11 of Appendix III)

$$\frac{\partial \phi}{\partial \xi} = \frac{j\phi\beta^2}{\xi} \cdot \frac{1}{(\phi-\xi)^2-\beta^2} \qquad\qquad A.5.1$$

and

$$\frac{\partial \beta}{\partial \xi} = -\frac{\gamma-1}{2} \frac{j\phi\beta(\phi-\xi)}{\xi[(\phi-\xi)^2-\beta^2]} \qquad\qquad A.5.2$$

The boundary conditions, however, are different and correspond

to the non-dimensional values of velocity, pressure and density

---

* ·The subject matter of this appendix is the classical Jouguet-Taylor-
Zel'dovich theory and is essentially a summary of the treatment discussed
by Lee, Knystautas and Bach (107) and by Lee (12).

immediately behind the detonation front. For a CJ detonation these values are

$$\phi(1) = \frac{\gamma_0 - \gamma_1 \eta}{\gamma_0 (\gamma_1 + 1)} \qquad\qquad\qquad A.5.3$$

$$f(1) = \frac{\gamma_0 + \eta}{\gamma_0 (\gamma_1 + 1)} \qquad\qquad\qquad A.5.4$$

and $\qquad \psi(1) = \frac{\gamma_0 (\gamma_1 + 1)}{\gamma_1 (\gamma_0 + \eta)} \qquad\qquad\qquad A.5.5$

β is given by $\sqrt{\dfrac{\gamma_1 f}{\psi}}$. γ_0 and γ_1 refer to the specific heat ratios

of the gases before and after being processed by the detonation wave.

According to the Chapman-Jouguet condition, the flow relative to the detonation wave is sonic, i.e.,

$$u_1 + c_1 = \overset{\circ}{R}_s \qquad\qquad\qquad A.5.6$$

or $\qquad \phi + \beta = 1$

so that $\qquad (\phi - 1)^2 - \beta^2 = 0 \qquad\qquad\qquad A.5.7$

Hence the denominator of Eq. A.5.1 and A.5.2 becomes zero at $\xi = 1$, and evaluation of the flow field poses a problem unlike the case of a constant velocity shock driven by a piston.

For the planar case $(j = 0)$, the numerator is zero as well. Hence two solutions are possible. One is $\frac{\partial \phi}{\partial \xi} = 0$ and $\frac{\partial \beta}{\partial \xi} = 0$, implying

uniform properties behind the detonation front. The other solution is that $(\phi-\xi)^2 - \beta^2$ is zero throughout giving finite values of $\frac{\partial \phi}{\partial \xi}$ and $\frac{\partial \beta}{\partial \xi}$. This latter solution represents a simple rarefaction wave behind a CJ detonation wave viz.,

$$\phi = \frac{2}{\gamma+1} \; (\xi-1) \; + \; \phi(1) \qquad\qquad\qquad \text{A.5.8}$$

and

$$\beta = \frac{\gamma-1}{\gamma+1} \; (\xi-1) \; + \; \beta(1) \qquad\qquad\qquad \text{A.5.9}$$

The value of ϕ in Eq. A.5.8 becomes zero at $\xi_0 = 1 - \frac{\gamma+1}{2} \phi(1)$. The flow field therefore consists of an expansion region from the detonation front ($\xi = 1$) to ξ_0 followed by a zone of constant properties for $0 < \xi < \xi_0$.

The former solution obtained with $\frac{\partial \phi}{\partial \xi} = \frac{\partial \beta}{\partial \xi} = 0$ (viz., constant properties behind the detonation front) pertains to a piston driven detonation whilst the latter solution represents a self-propagating detonation.

In the case of cylindrical and spherical geometries ($j \neq 0$) the numerator is not equal to zero so that $\frac{\partial \phi}{\partial \xi}$ and $\frac{\partial \beta}{\partial \xi}$ tend to infinity as $\xi \to 1$. This singularity poses a problem in starting a numerical integration of Eq. A.5.1 and A.5.2. It becomes necessary to seek a

solution near the CJ front. This is done by assuming a perturbation series of the form

$$\phi(\xi) = a_0 + a_1 (1-\xi)^x + \ldots \qquad A.5.10$$

and

$$\beta(\xi) = b_0 + b_1 (1-\xi)^y + \ldots \qquad A.5.11$$

and solving for the constants a_0, a_1, b_0, b_1, x and y. The solution near the CJ detonation front $(1-\xi) < <1$ is obtained to be

$$\phi(\xi) = \phi(1) \pm \left[\frac{2j\phi(1)\beta(1)}{\gamma+1} (1-\xi) \right]^{\frac{1}{2}} \pm \ldots \qquad A.5.12$$

and

$$\beta(\xi) = \beta(1) \pm \frac{\gamma-1}{2} \left[\frac{2j\phi(1)\beta(1)}{\gamma+1} (1-\xi) \right]^{\frac{1}{2}} \pm \ldots \qquad A.5.13$$

The above equations suggest two possible solutions corresponding to the positive or negative signs. The plus sign indicates a compression solution (piston driven detonation) whilst the negative sign denotes a free expansion solution. We are interested in the free expansion solution.

In order to determine the flow field for the cylindrical and spherical detonations, we numerically integrate the Eq. A.5.1 and A.5.2 by the fourth order Runge-Kutta method with the starting values given by Eq. A.5.12 and A. 5.13. We start the integration at $\xi = 0.999$ and choose a step size of 0.001. The velocity ϕ drops to zero at a certain distance $(1 - \xi_0)$ behind the front after which there is a zone of constant properties as in the planar case. The values of pressure $f(\xi)$ and density $\psi(\xi)$ are determined from $\beta(\xi)$ using the condition of isentropic flow behind the detonation front (similar to Eq. A.3.23 and A.3.24 of Appendix III).

Knowing the distribution of ψ, ϕ and f, the value of energy integral is readily determined from the expression

$$I = \int_0^1 \left(\frac{f}{\gamma-1} + \frac{\psi\phi^2}{2} \right) \xi^j \, d\xi \qquad\qquad A.5.14$$

whilst the pressure profile is determined from the relation

$$p = \rho_0 \, \mathring{R}_s{}^2 f(\xi) \qquad\qquad A.5.15$$

TABLE I.   INFLUENCE OF IGNITER CONFIGURATION ON THE INITIATION ENERGY
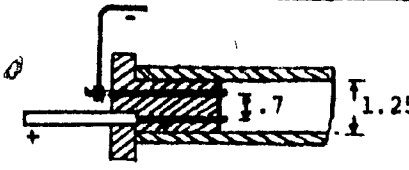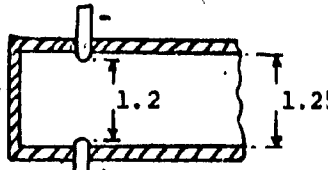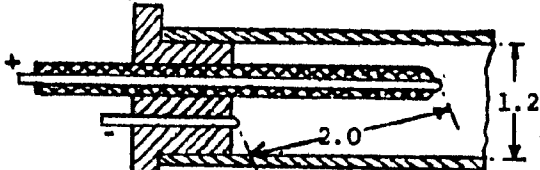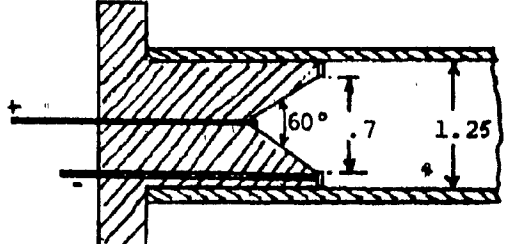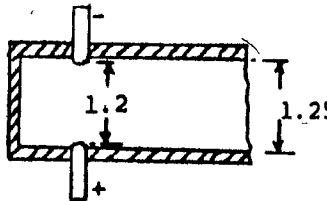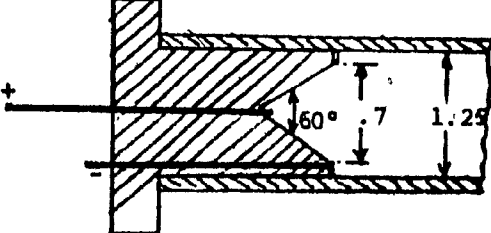
GAS MIXTURE	SKETCH OF THE IGNITER CONFIGURATION (dimensions are in cm)	E_s JOULES
$2 H_2 + O_2$ AT 100 TORR		0.40
		0.45
		0.49
		0.52
$2 C_2H_2 + 5 O_2$ AT 40 TORR		.048
		.051

TABLE II.   S/L RATIOS FOR H_2-O_2-Ar SYSTEM OBTAINED BY BILLER (108)

% Ar dilution	S/L		
	$\phi = 0.4$	$\phi = 1.0$	$\phi = 2.5$
0	0.528	0.474	0.575
20	0.555	0.581	0.516
40	0.575	0.533	0.612
50	0.560	0.497	0.642
60	0.587	0.546	0.577
70	0.582	0.607	0.617
75	No data	No data	0.657
77.5	No data	0.591	No data
80	0.619	No data	0.560
85	0.642	0.596	No data
Case Average	0.595	0.553	0.595

(ϕ denotes the stoichiometry on fuel/oxygen basis)
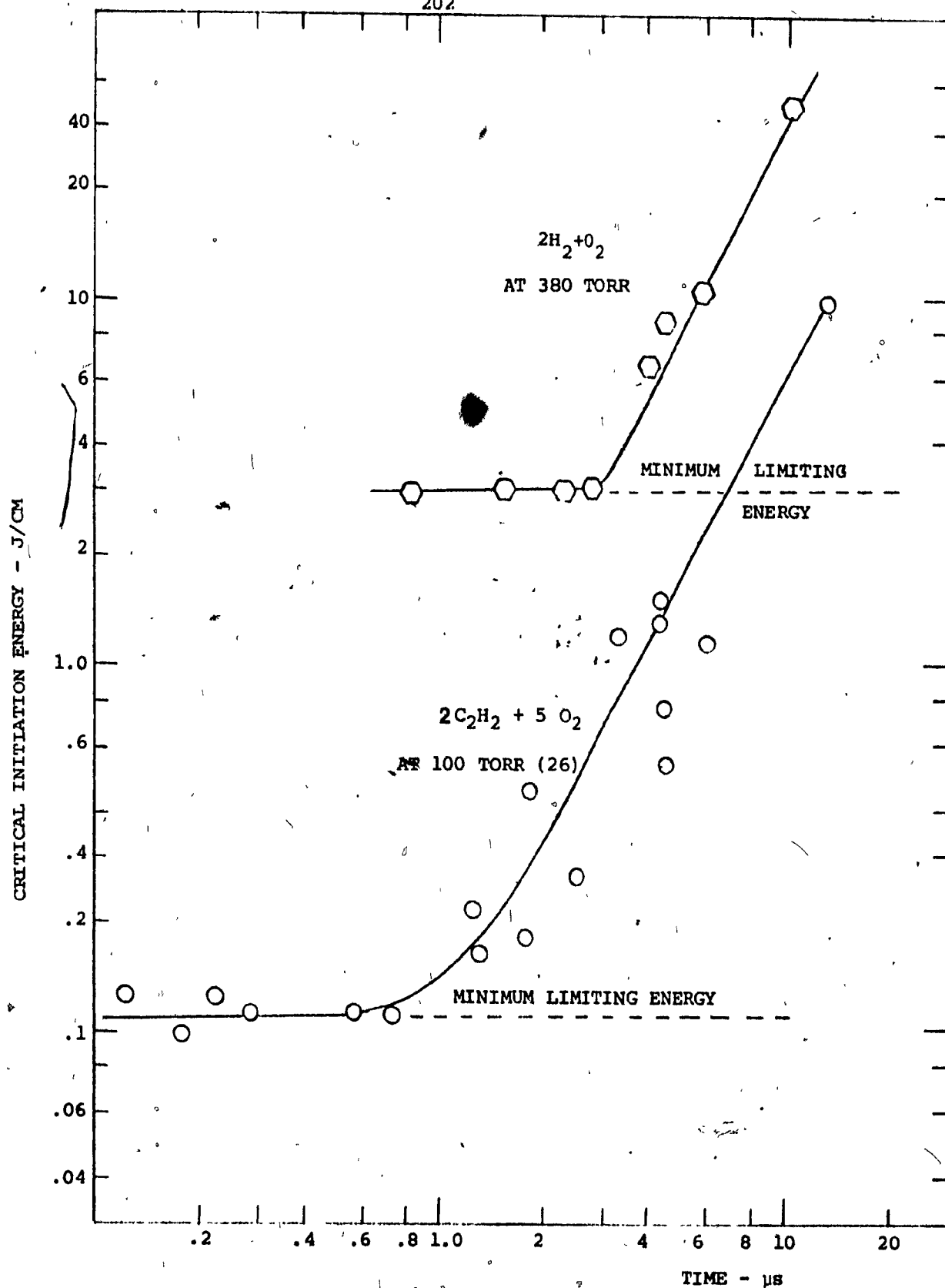
FIG. 1. VARIATION OF CRITICAL ENERGY WITH THE DURATION OF ENERGY RELEASE
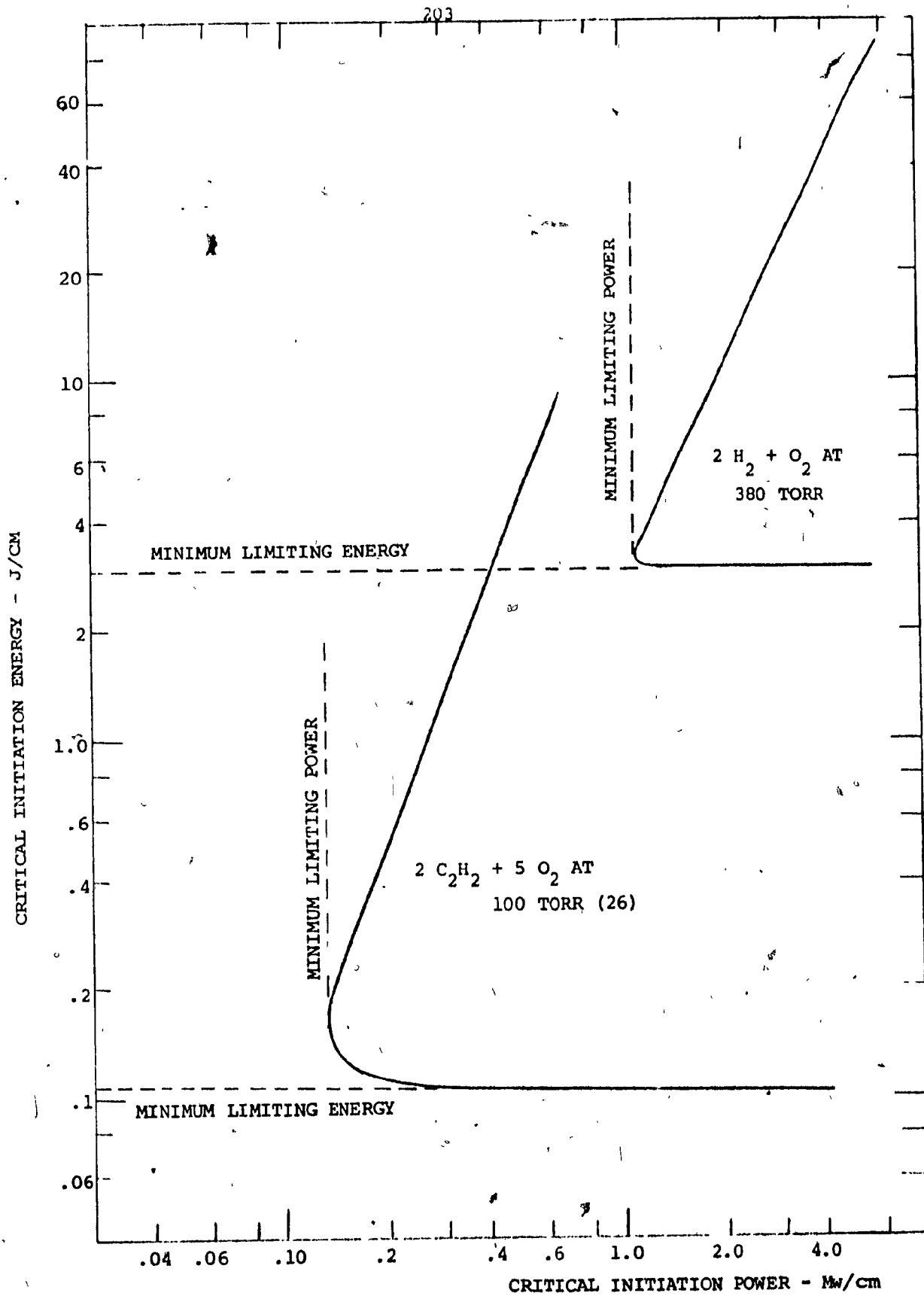
FIG.2.   DEPENDENCE OF CRITICAL INITIATION ENERGY ON THE PEAK
AVERAGE POWER OF THE IGNITION SOURCE

a. Supercritical   b. Subcritical   c. Critical
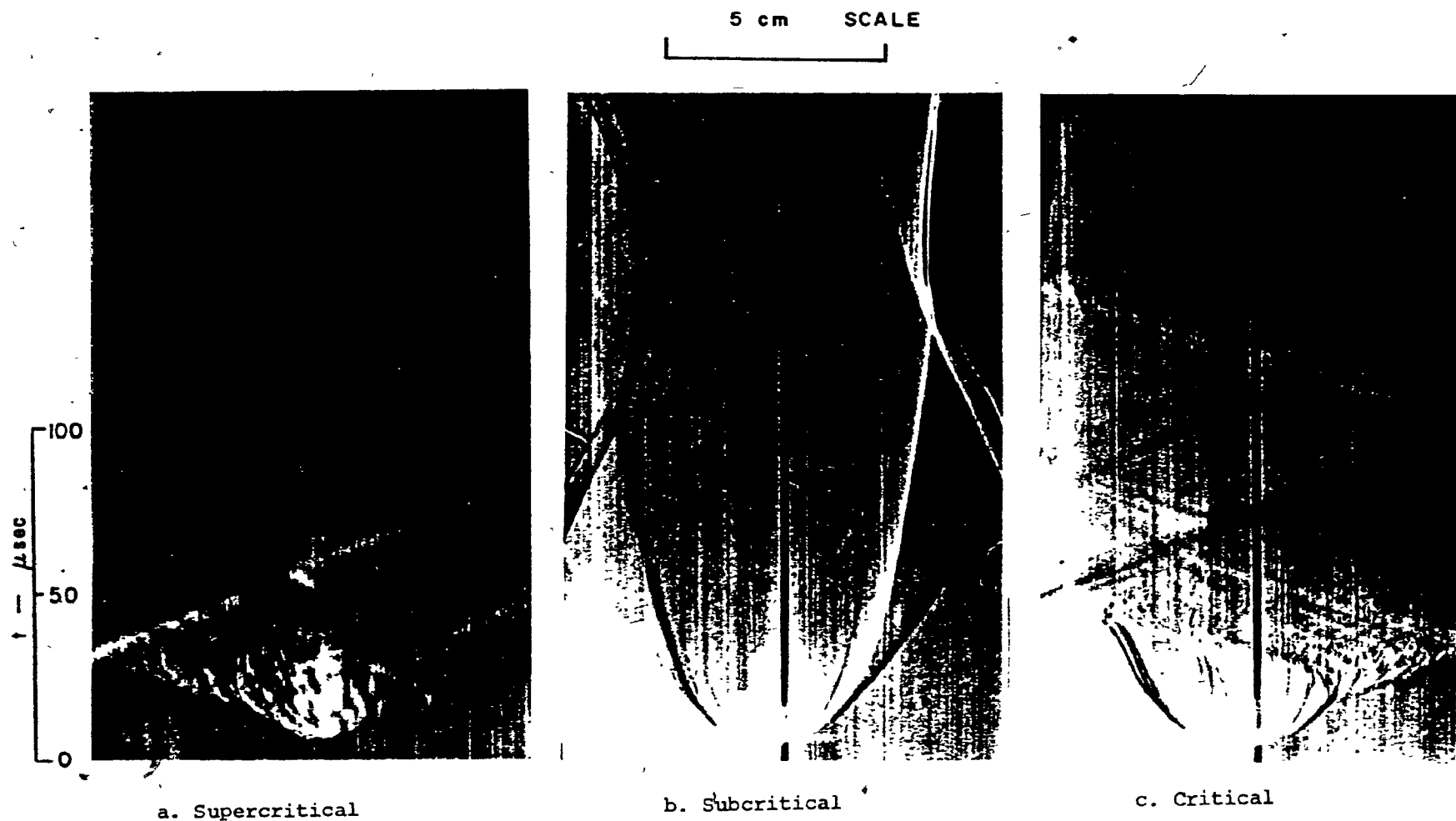
FIG. 3.   STREAK SCHLIEREN PICTURES SHOWING THE SUPERCRITICAL, SUBCRITICAL AND CRITICAL REGIMES
         OF PROPAGATION.   (MIXTURE: STOICHIOMETRIC OXYACETYLENE AT 100 TORR; IGNITION: LASER SPARK)
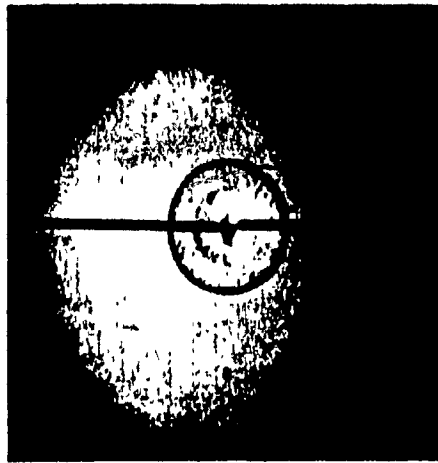
a

b

c

FIG. 4.   SCHLIEREN PHOTOGRAPHS OF A SPHERICAL DETONATION WAVE
IN THE SUPERCRITICAL REGIME
(MIXTURE: STOICHIOMETRIC OXYACETYLENE AT 100 TORR;
IGNITION: EXPLODING WIRE)

1·6 μsec   4·8 μsec   8·0 μsec
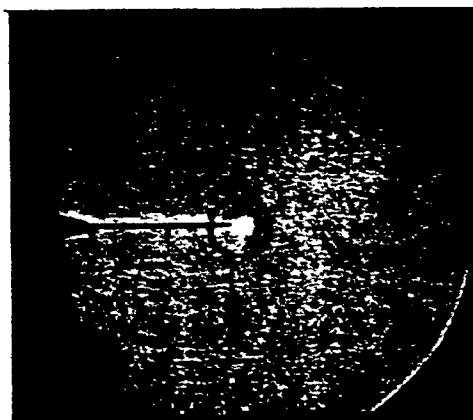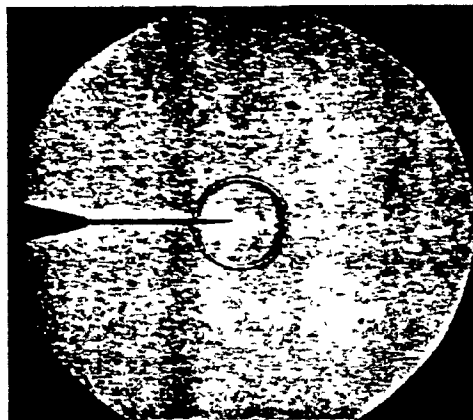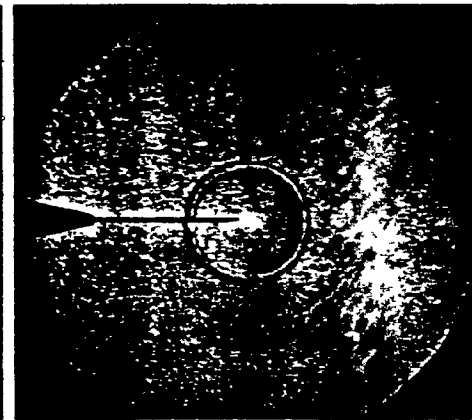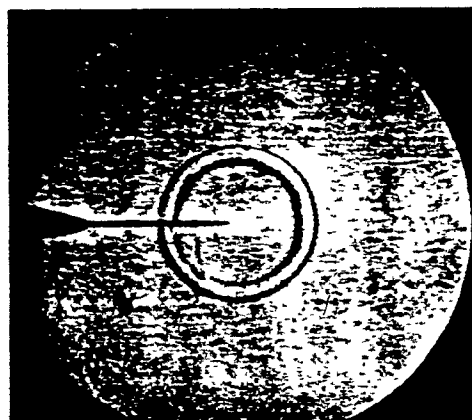
13·0 μsec   22·5 μsec   - 32·3 μsec

FIG. 5.   SCHLIEREN PHOTOGRAPHS OF A SPHERICAL DETONATION WAVE IN THE SUB-CRITICAL REGIME
(MIXTURE: STOICHIOMETRIC OXYACETYLENE AT 80 TORR;   IGNITION: LASER SPARK)

SCALE 2 cm

t = 6.5 μsec   t = 9.0 μsec   t = 11.5 μsec
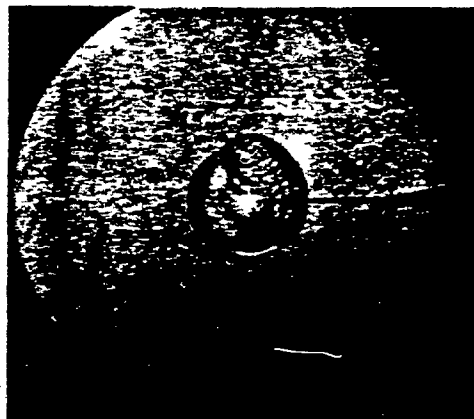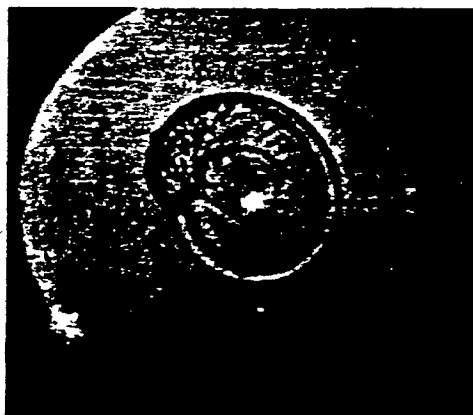
t = 14.4 μsec   t = 16.6 μsec   t = 20.3 μsec

FIG. 6. SCHLIEREN PHOTOGRAPHS OF A SPHERICAL DETONATION WAVE IN THE CRITICAL REGIME OF INITIATION
(MIXTURE: STOICHIOMETRIC OXYACETYLENE AT 100 TORR; IGNITION: LASER SPARK)
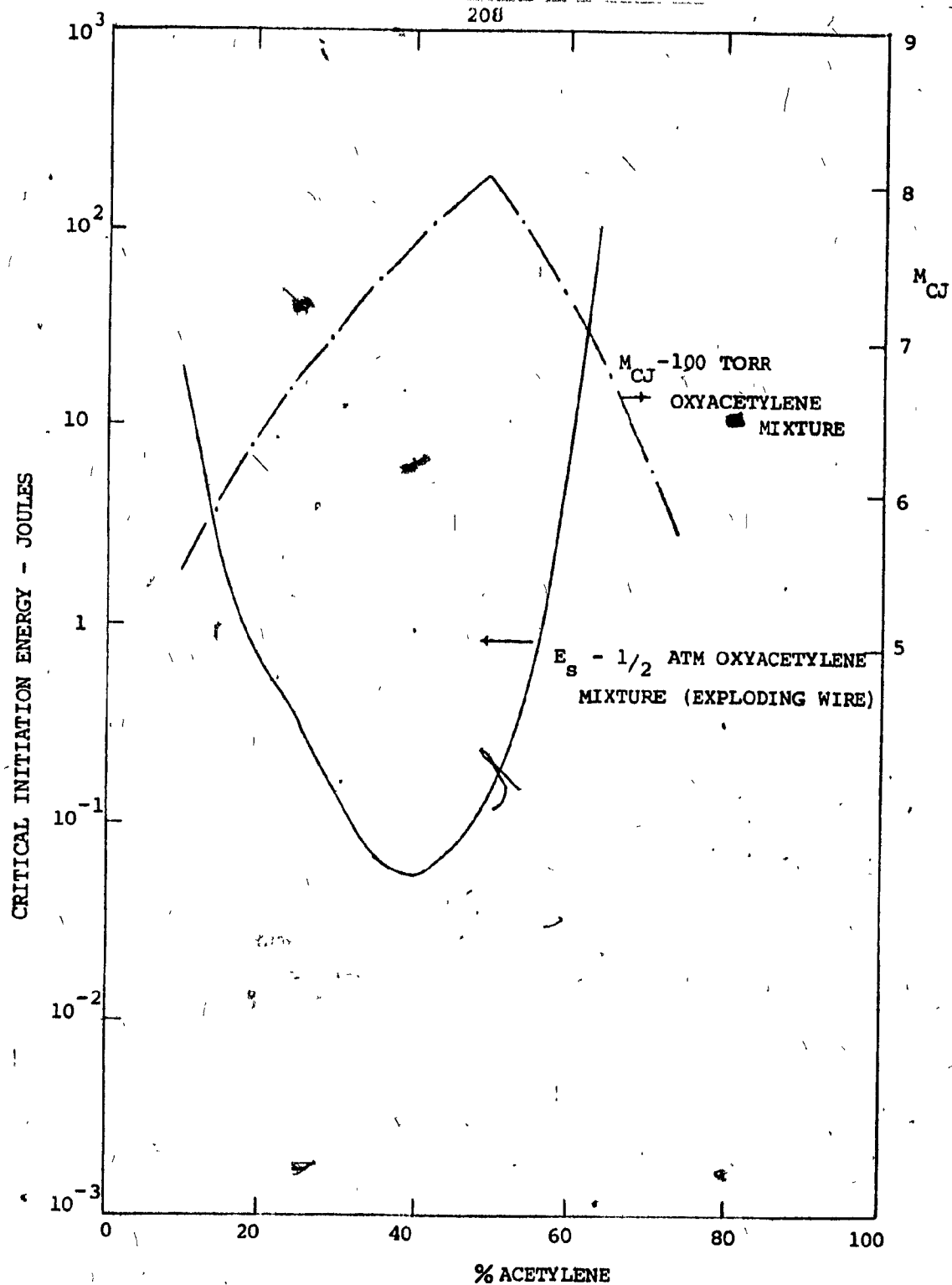
FIG.7. VARIATION OF CRITICAL INITIATION ENERGY AND M_{CJ} WITH COMPOSITION
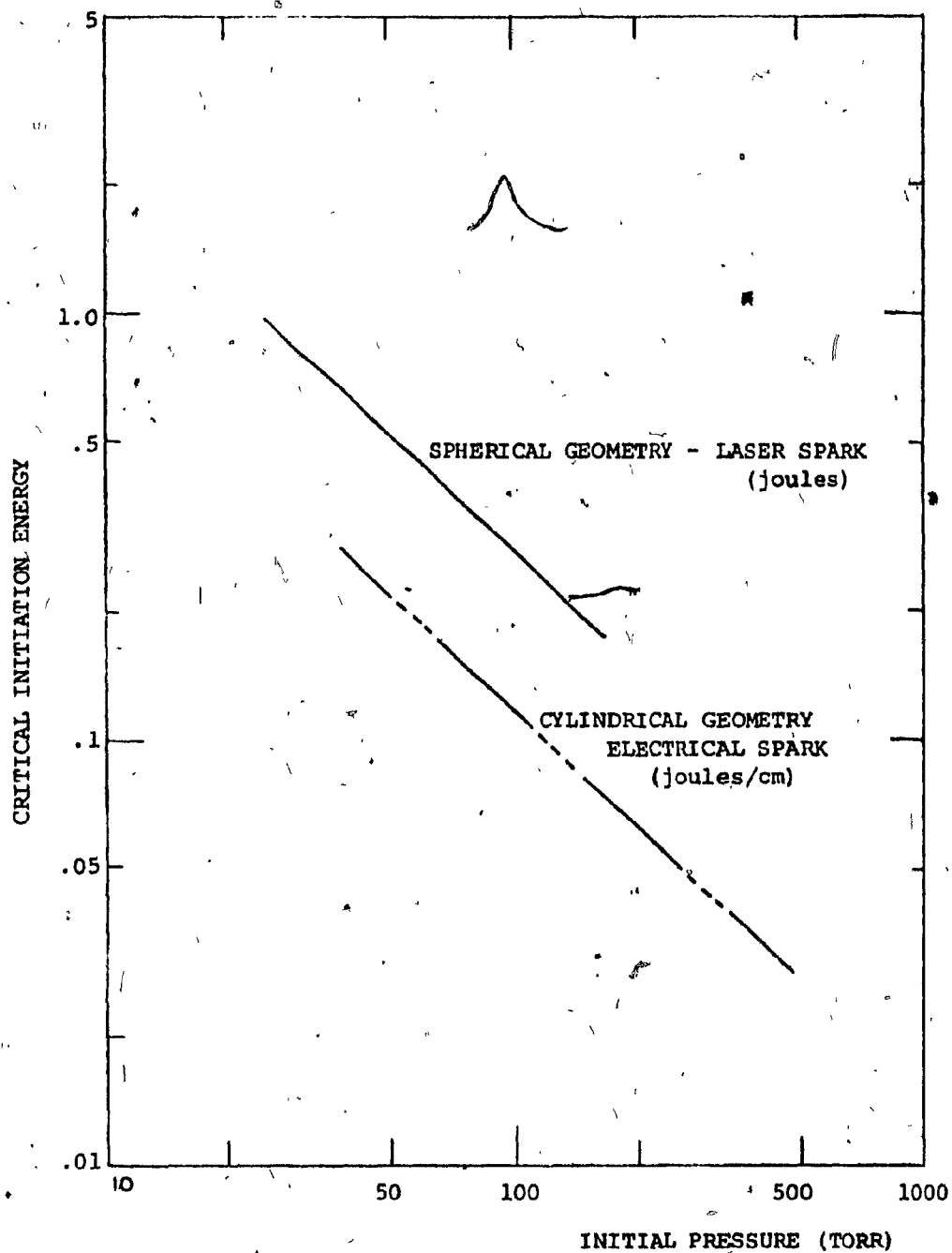
FIG. 8. DEPENDENCE OF CRITICAL INITIATION ENERGY ON INITIAL
PRESSURE FOR A 2 C_2H_2 + 5 O_2 MIXTURE (from ref. 28)

a. Sequence of events following the release of source
   energy in an unreactive gas mixture
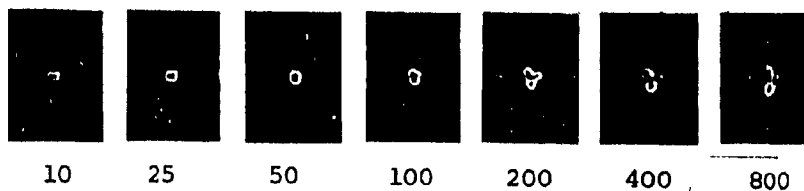
b. Sequence of events following the release of source
   energy less than the threshold value necessary for
   successful ignition in a reactive mixture of propane-air
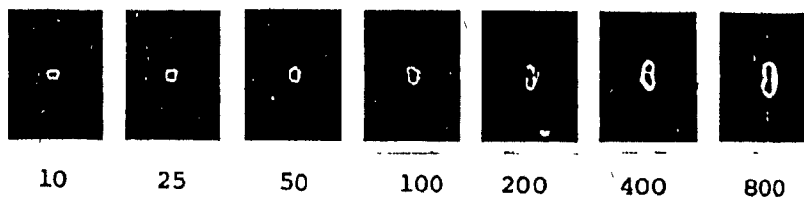
c. Sequence of events following the release of source
   energy greater than the threshold value necessary for
   successful ignition in a mixture of propane-air

FIG. 9.   SCHLIEREN PICTURES TAKEN FROM STREHLOW (45) ILLUSTRATING THE
          NECESSITY FOR THE FORMATION OF AN ADEQUATE FLAME KERNEL FOR
          THE INITIATION OF A SELF-SUSTAINED FLAME.
          (The numerals denote time in μs after the release of
          source energy)

$$R_o = \left(\frac{E_s}{k_j \rho_0 C_o{}^2} \right)^{1/3}$$

Mixture: $2\ C_2H_2 + 5\ O_2$
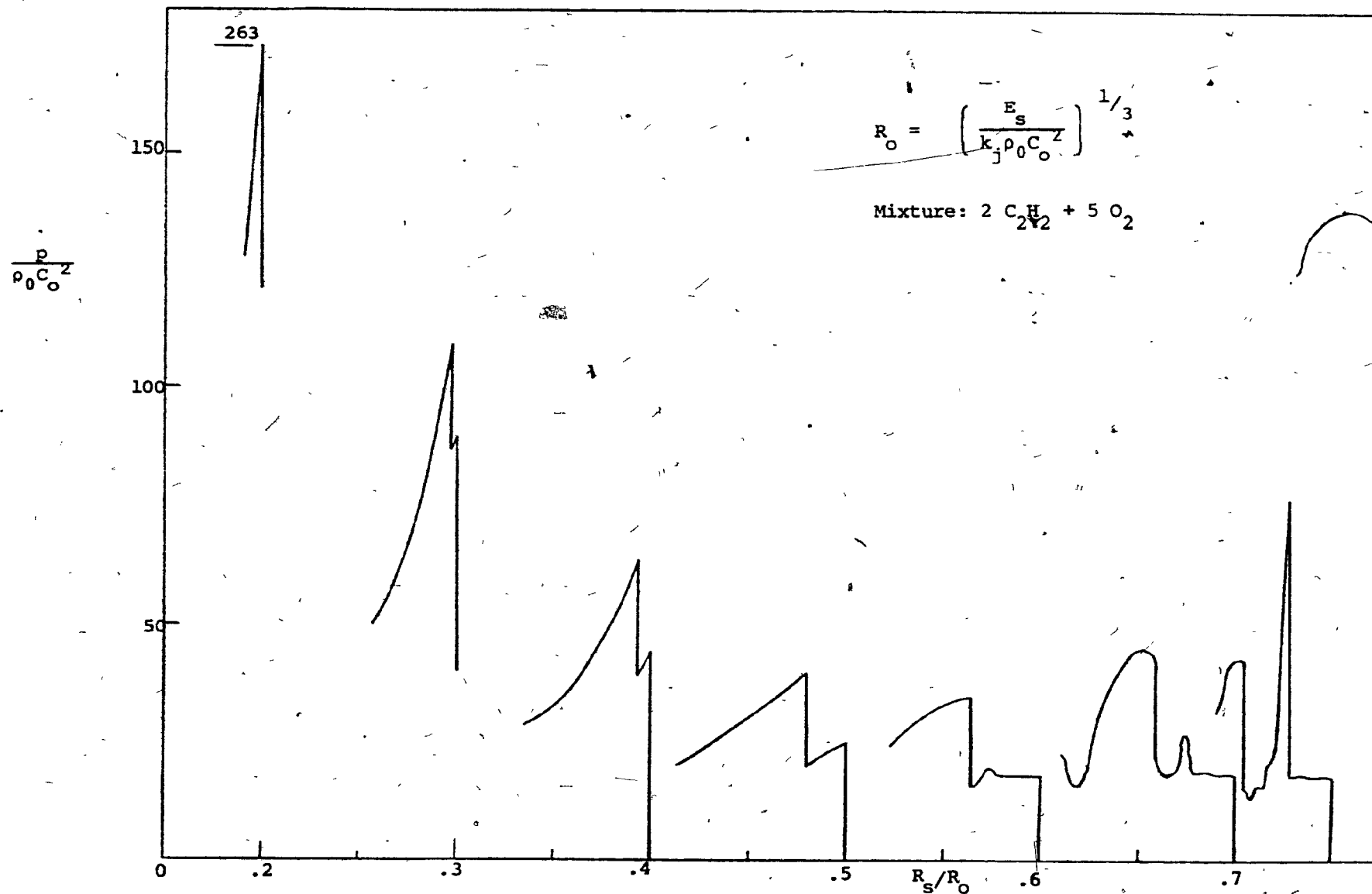
FIG. 10. NUMERICAL SOLUTION OF KYONG (19) FOR PRESSURE PROFILES FOR A SPHERICAL DETONATION WITH CRITICAL INITIATION ENERGY

$$R_o = \left(\frac{E_s}{k_j \rho_0 C_o^2} \right)^{1/3}$$

Mixture: 2 C_2H_2 + 5 O_2
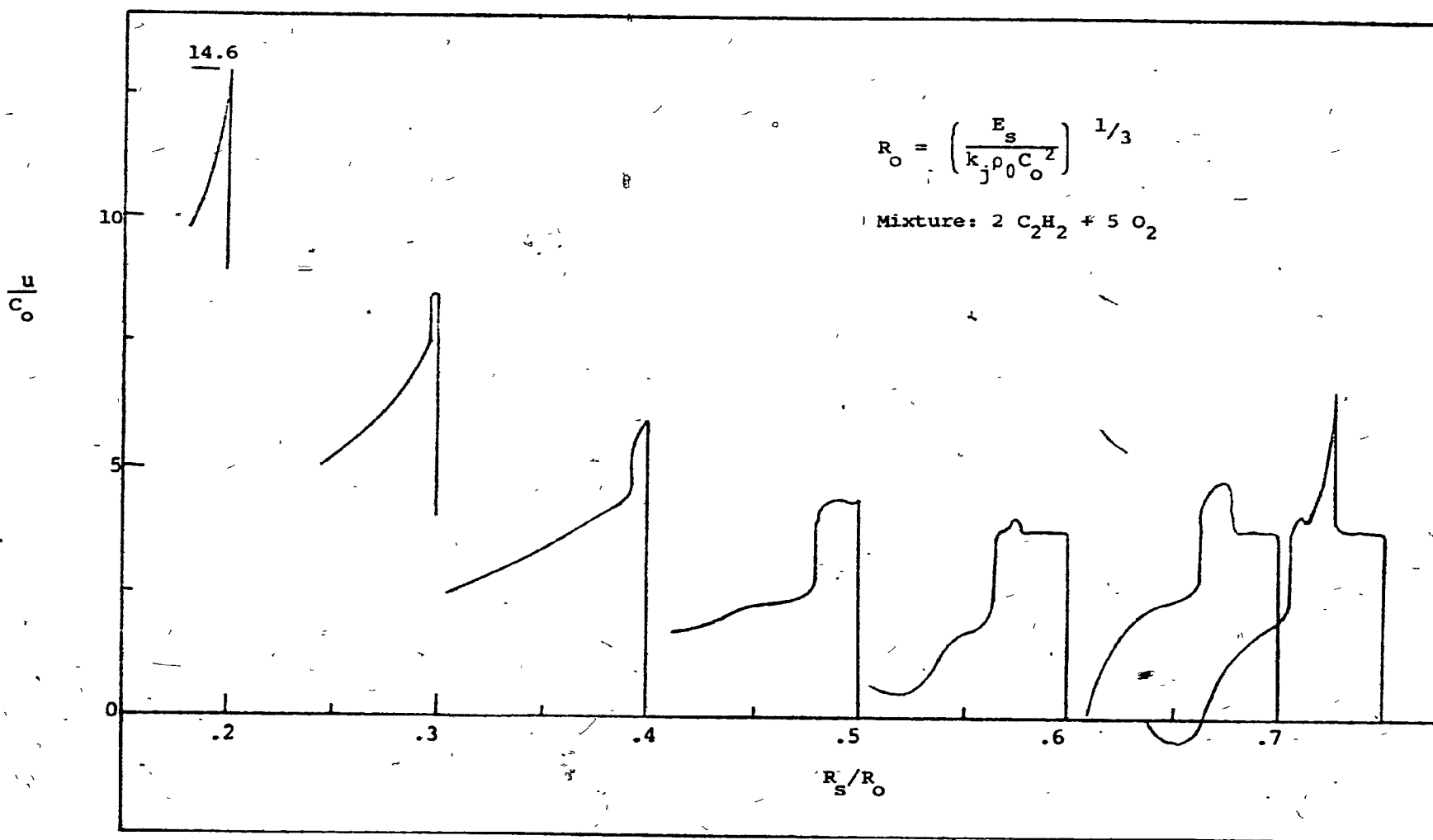
FIG. 11. NUMERICAL SOLUTION OF KYONG (19) FOR PARTICLE VELOCITY PROFILES FOR A SPHERICAL DETONATION WITH CRITICAL INITIATION ENERGY

$$R_o = \left(\frac{E_s}{k_j \rho_0 C_o^2} \right)^{1/3}$$

Mixture: $2\ C_2H_2 + 5\ O_2$

$\frac{\rho}{\rho_0}$

R_s/R_o

213
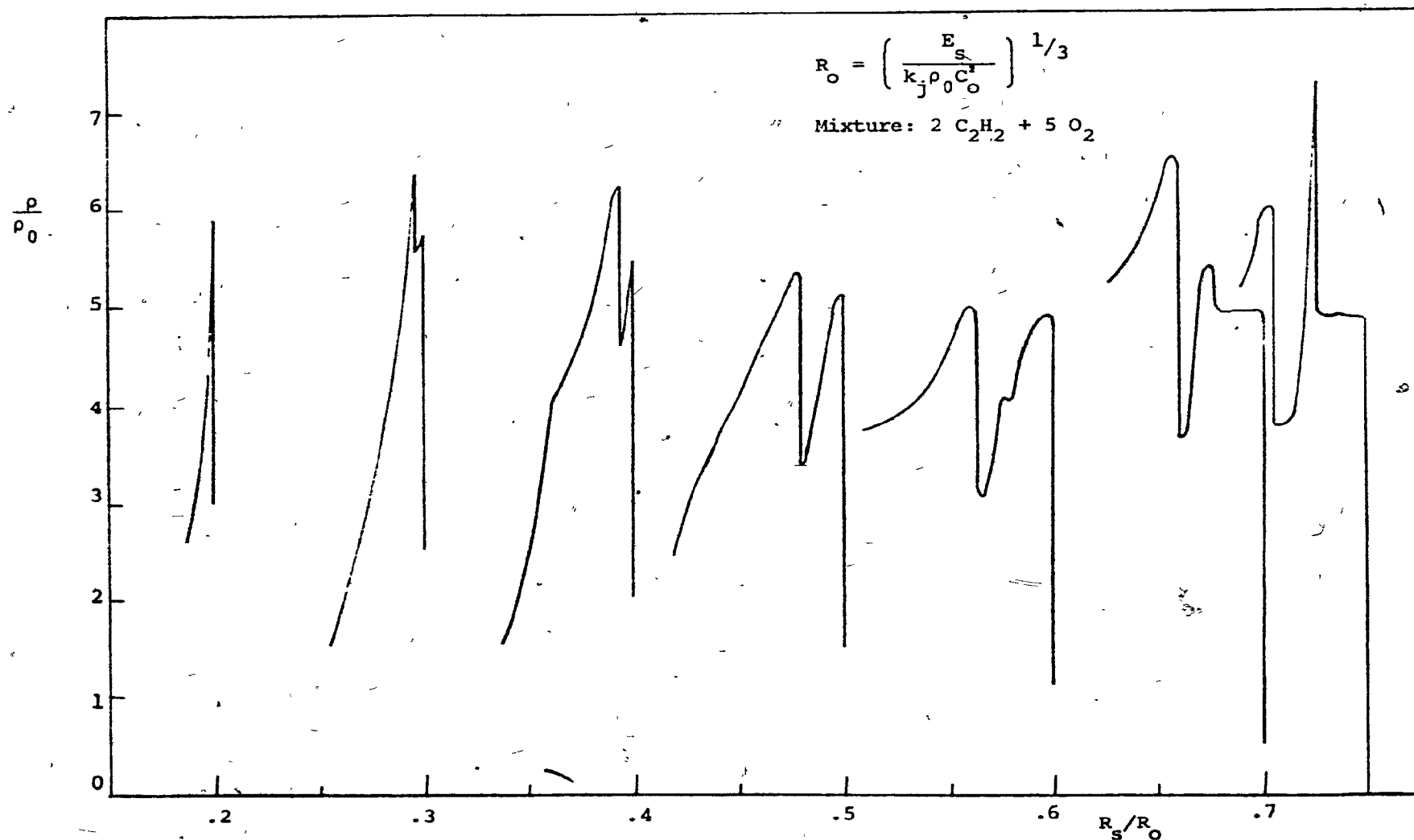
FIG. 12. NUMERICAL SOLUTION OF KYONG (19) FOR DENSITY PROFILES FOR A SPHERICAL DETONATION WITH CRITICAL INITIATION ENERGY

CYLINDRICAL GEOMETRY

Mixture: $2 C_2H_2 + 5 O_2$ AT 100 TORR

M_S^*

POWER LAW DENSITY
PROFILE (EQ. 5.14)

QUASI-STEADY ASSUMPTION (EQ. 6.3)

$R_S^* - mm$

$1/M_S$
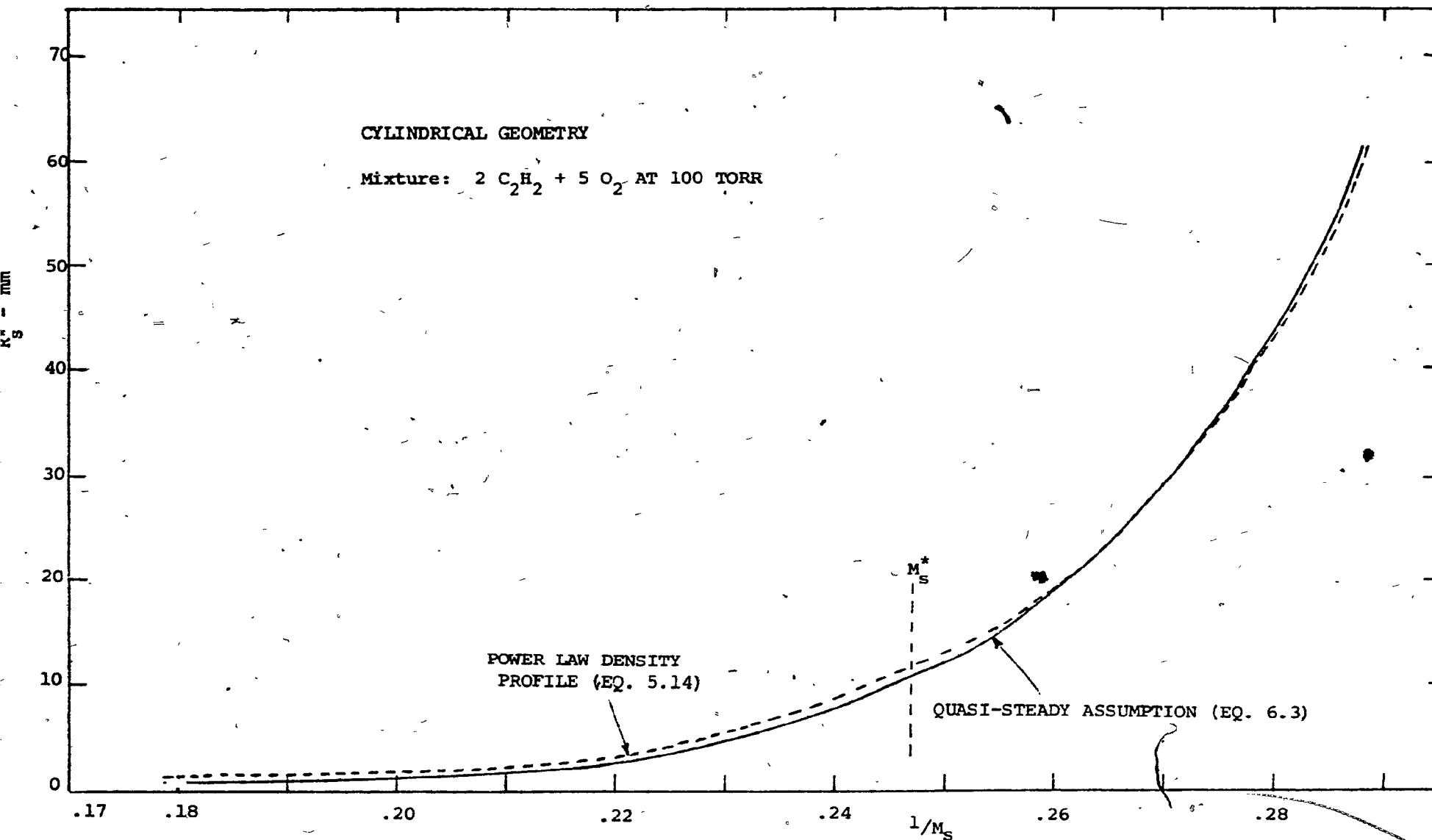
FIG. 13.   INSENSITIVITY OF THE DETONATION KERNEL RADIUS TO THE DETAILS OF HYDRODYNAMIC FLOW STRUCTURE
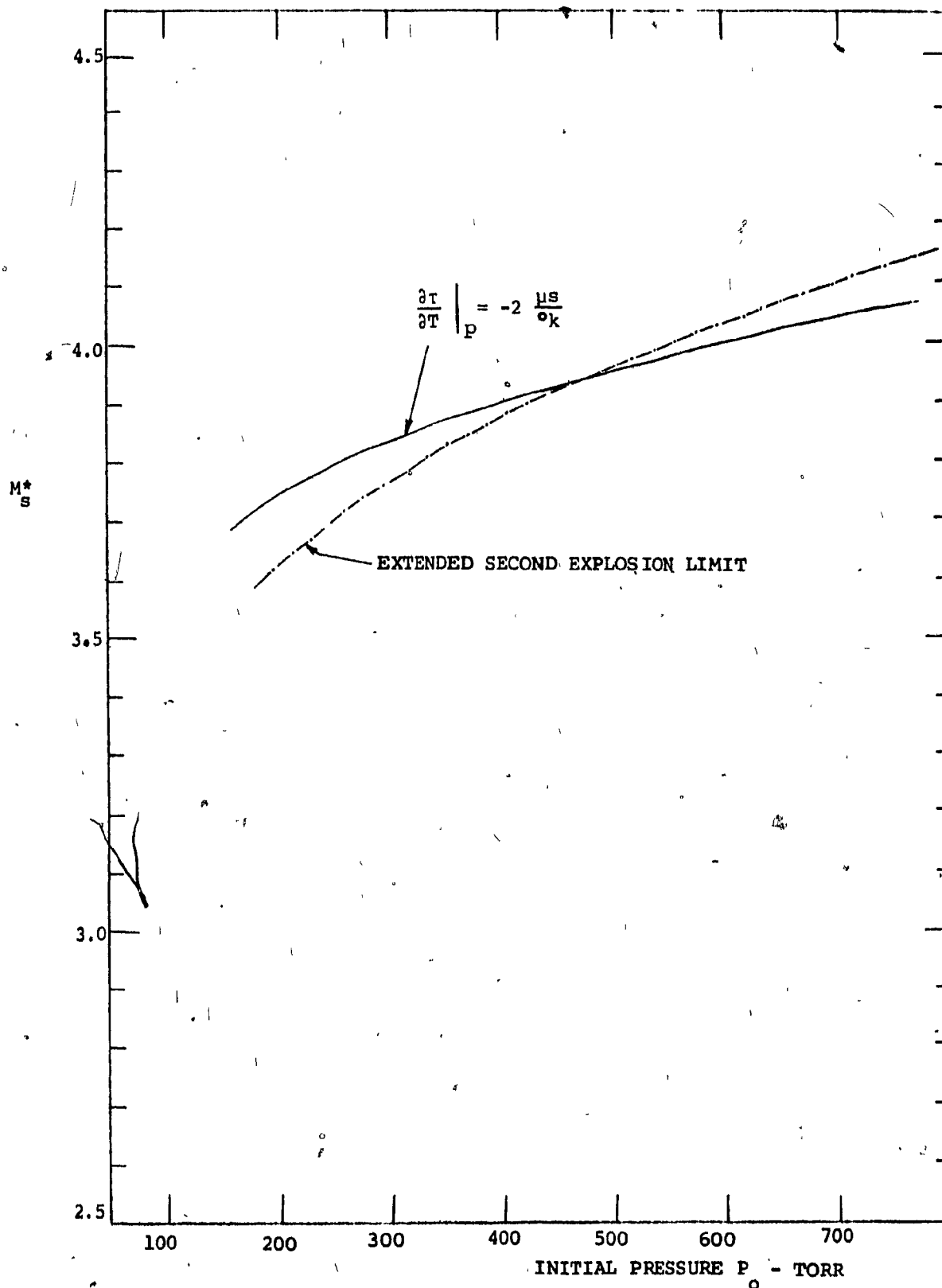
FIG. 14. VALUE OF M_s^* OBTAINED FROM THE EXTENDED SECOND EXPLOSION LIMIT CRITERION AND FROM MEYER AND OPPENHEIM'S CRITERION (67) FOR THE 2 $H_2 + O_2$ MIXTURE AT SEVERAL VALUES OF INITIAL PRESSURE

100 TORR $2 C_2H_2 + 5 O_2$

$$M_s^* = \frac{5-3.5}{e} + 3.5 = 4.05$$
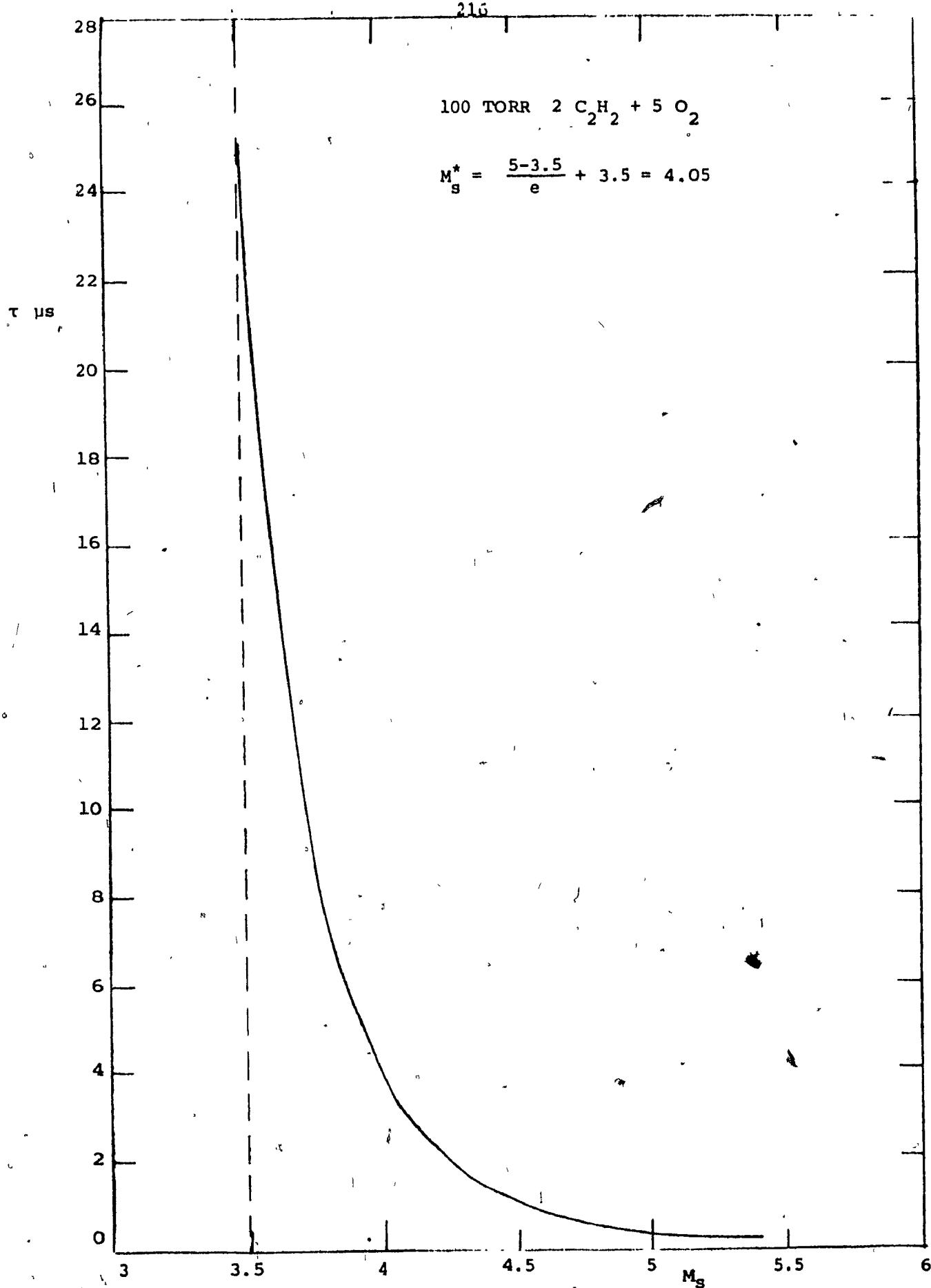
FIG. 15. ESTIMATION OF M_s^* ON THE BASIS OF LARGE INCREASE IN INDUCTION TIME

400

100

40

10

4

1.0

.4

.1

.04

.01

CRITICAL INITIATION ENERGY

EXTENDED 2nd EXPLOSION LIMIT

$$\frac{\partial \tau}{\partial T}\bigg|_p = -2 \; \frac{\mu s}{\delta k}$$

EXPERIMENTS

CYLINDRICAL 2 H_2 + O_2
(joules/cm)

SPHERICAL 2 C_2H_2 + 5 O_2 (joules)

THEORY

CYLINDRICAL
2 C_2H_2 + 5 O_2
(joules/cm)

.04   .10   .2   .4   .7   1.0

INITIAL PRESSURE - ATMOSPHERES
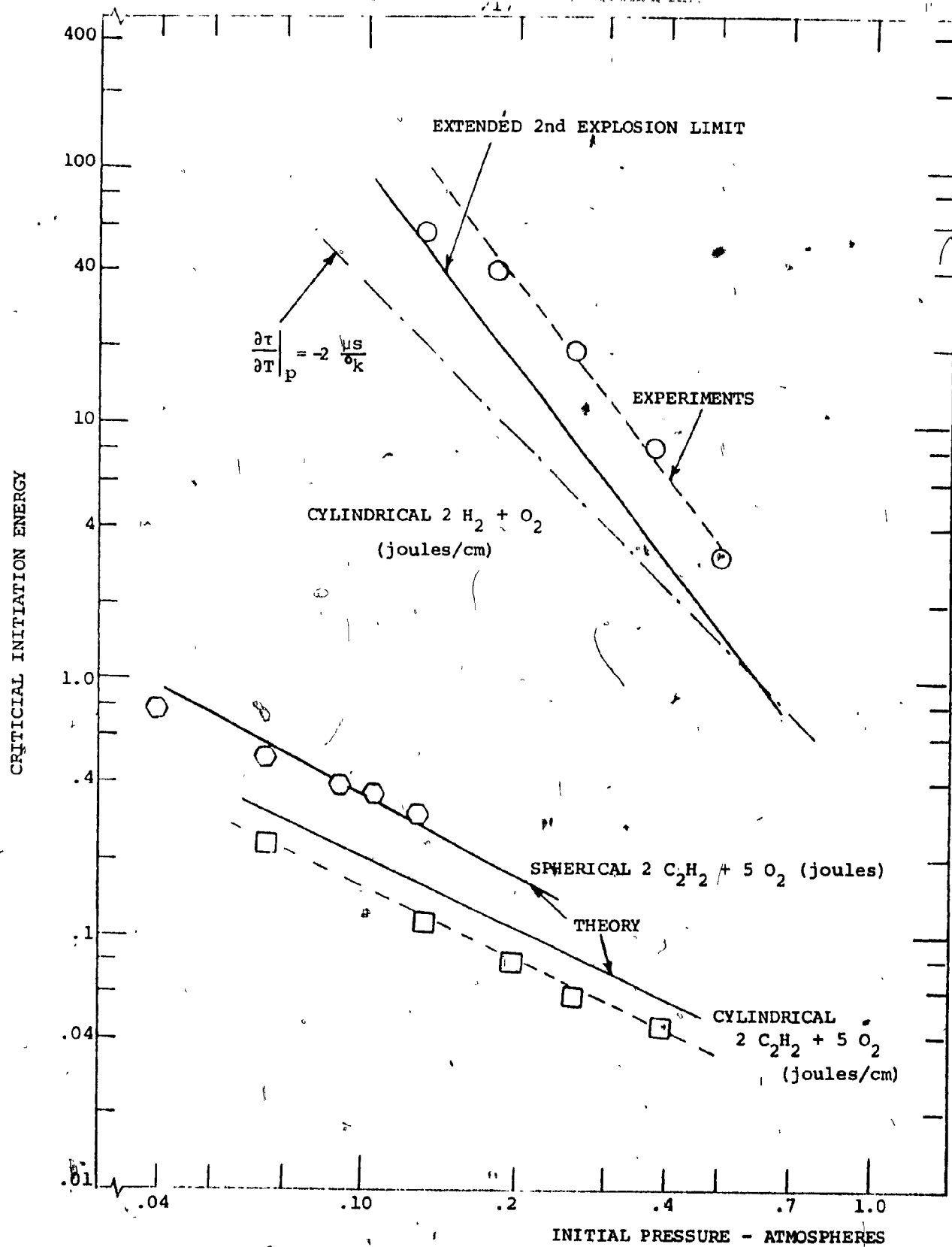
FIG. 16.   COMPARISON OF THEORETICALLY CALCULATED VALUES OF INITIATION
ENERGY WITH EXPERIMENTS AT LOWER VALUES OF SUB-ATMOSPHERIC
PRESSURE
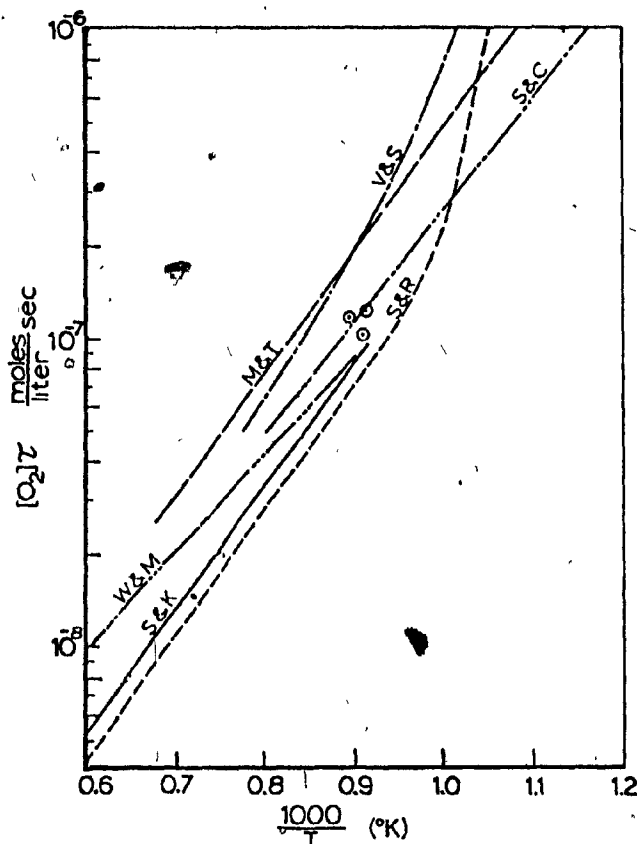
FIG. 17. INDUCTION TIME DIAGRAM FOR HYDROGEN-OXYGEN SYSTEM REPRODUCED FROM REFERENCE (1).

(V & S refer to data of Voevodsky and Soloukhin; S & R to Skinner and Ringrose; M & T to Miyama and Takeyama; S & C to Strehlow and Cohen; W and M to White and Moore; and S & K to Schott and Kinsey. For references, see (127). Circles denote points obtained from experiments on detonative ignition due to shock merging in the transitional mode of initiation).

MIXTURE: $2 C_2H_2 + 5 O_2$

$LOG_{10} \{[O_2]^{1/3}[C_2H_2]^{2/3}\tau\} =$

$-10.81 + 17300/4.58 \, T$ (70)
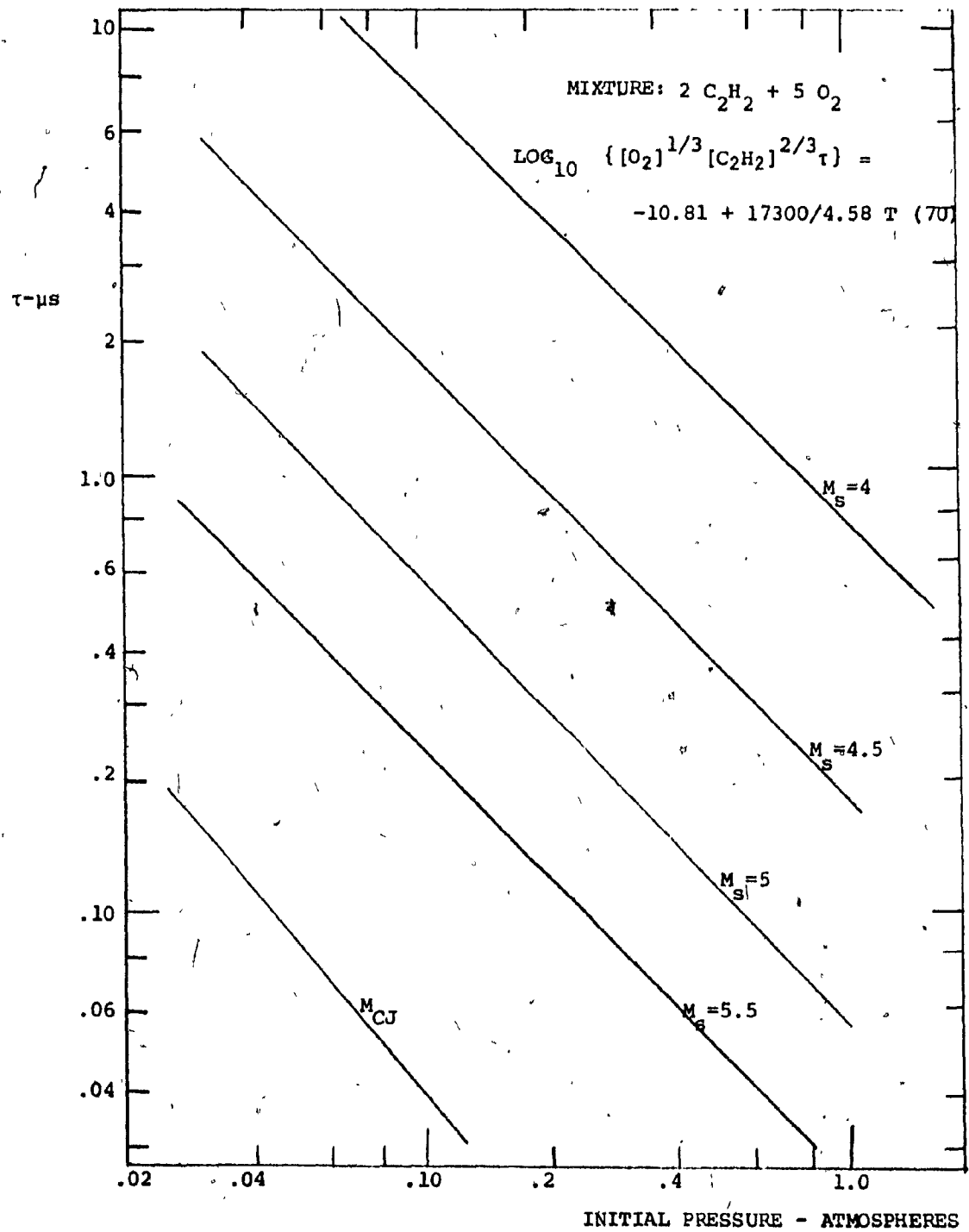
FIG.18. VALUE OF INDUCTION TIME CALCULATED ON THE BASIS OF
CONSTANT THERMODYNAMIC PROPERTIES BEHIND SHOCK WAVES
OF DIFFERENT MACH NUMBERS

CRITICAL INITIATION ENERGY

CYLINDRICAL SPARK $2 H_2+O_2$
(J/cm)

CYLINDRICAL
EXPLODING WIRE $\frac{1}{2}$ CV^2 ENERGY
$2 H_2+O_2$ (J/cm)

SPHERICAL $PO-O_2-N_2$
joules (74)

PLANAR $2 H_2+O_2$ (1.25 CM TUBE)
(joules)

INITIAL PRESSURE - ATMOSPHERES
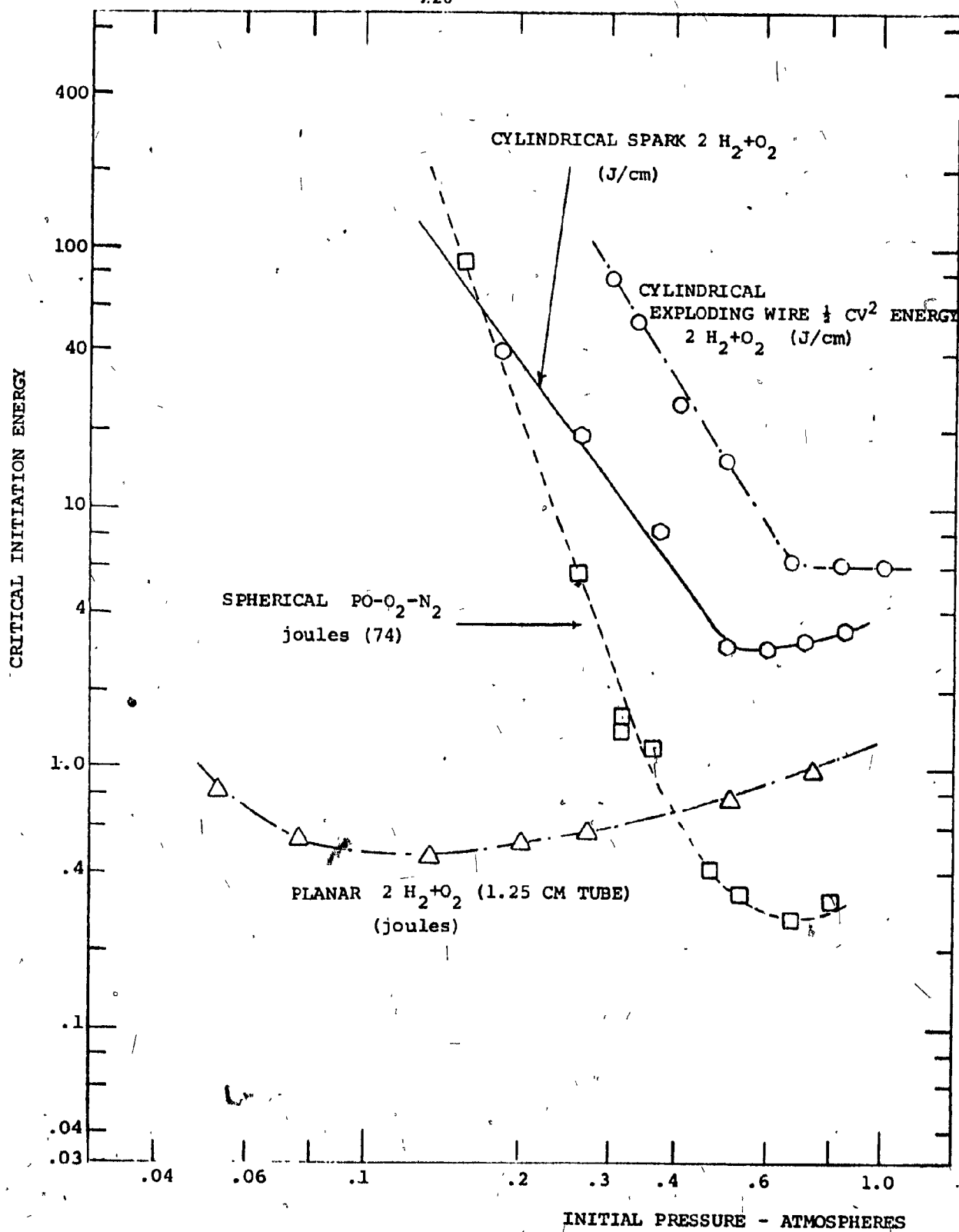
FIG. 19. PRESSURE DEPENDENCE OF INITIATION ENERGY

$$\ln\left(\tau\left[o_2\right]\right) = A+B/T+C\ P^n \exp\left(\frac{D}{T}\right) \quad (67)$$

where A = -10.7 ln (μs-mole/liter)

B = 9130 (°K) ln (μs-mole/liter)

n = 2

C = 3 x 10^{-9} (atm)^{-2} ln (μs-mole/liter)

D = 19000 (°K)

P is in atmospheres and τ is in microseconds

INITIAL PRESSURE - ATMOSPHERES
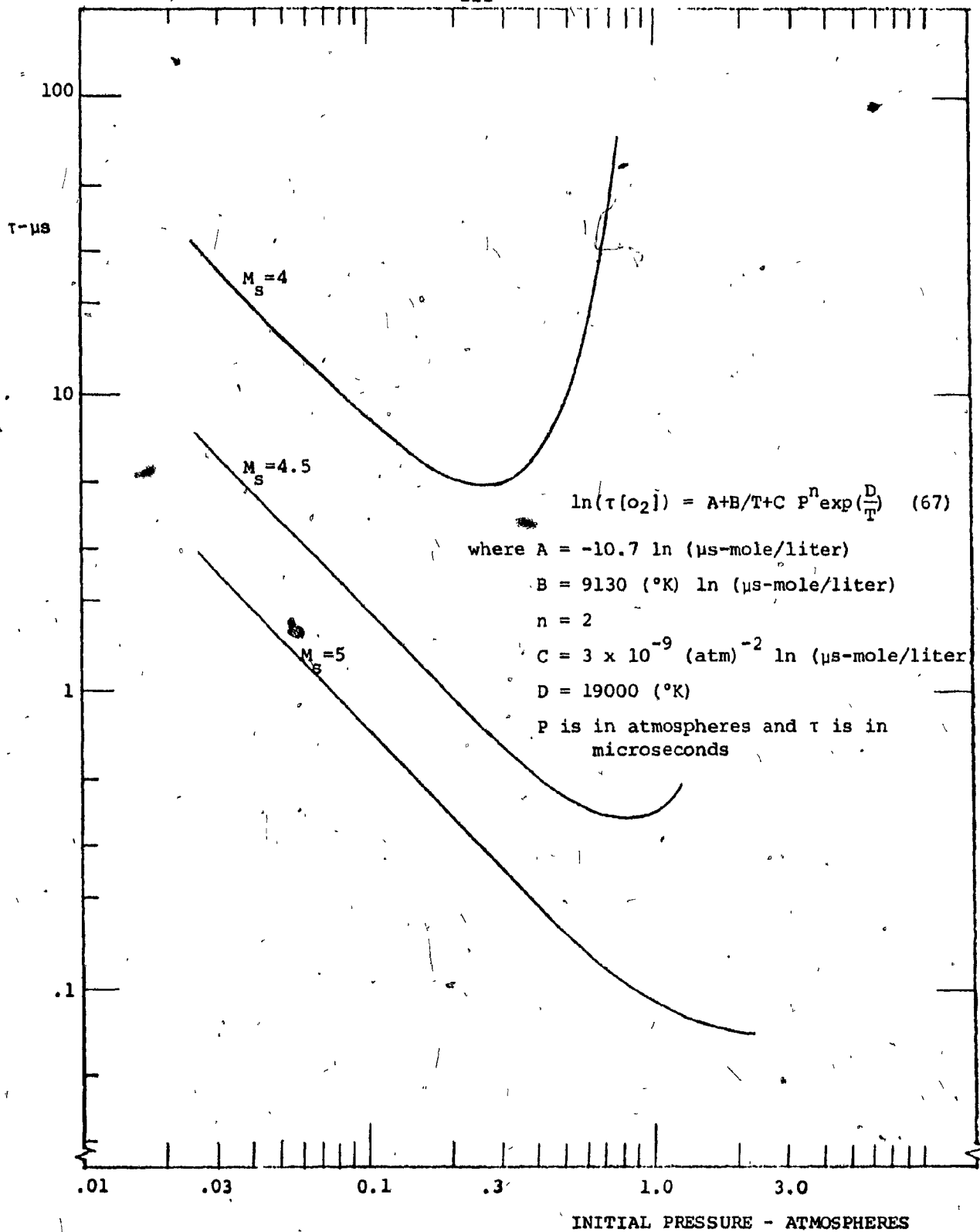
FIG.20.   INCREASING VALUES OF INDUCTION TIME WITH INITIAL PRESSURE
AS INDICATED BY THE DATA OF VERMEER AND OPPENHEIM (67)
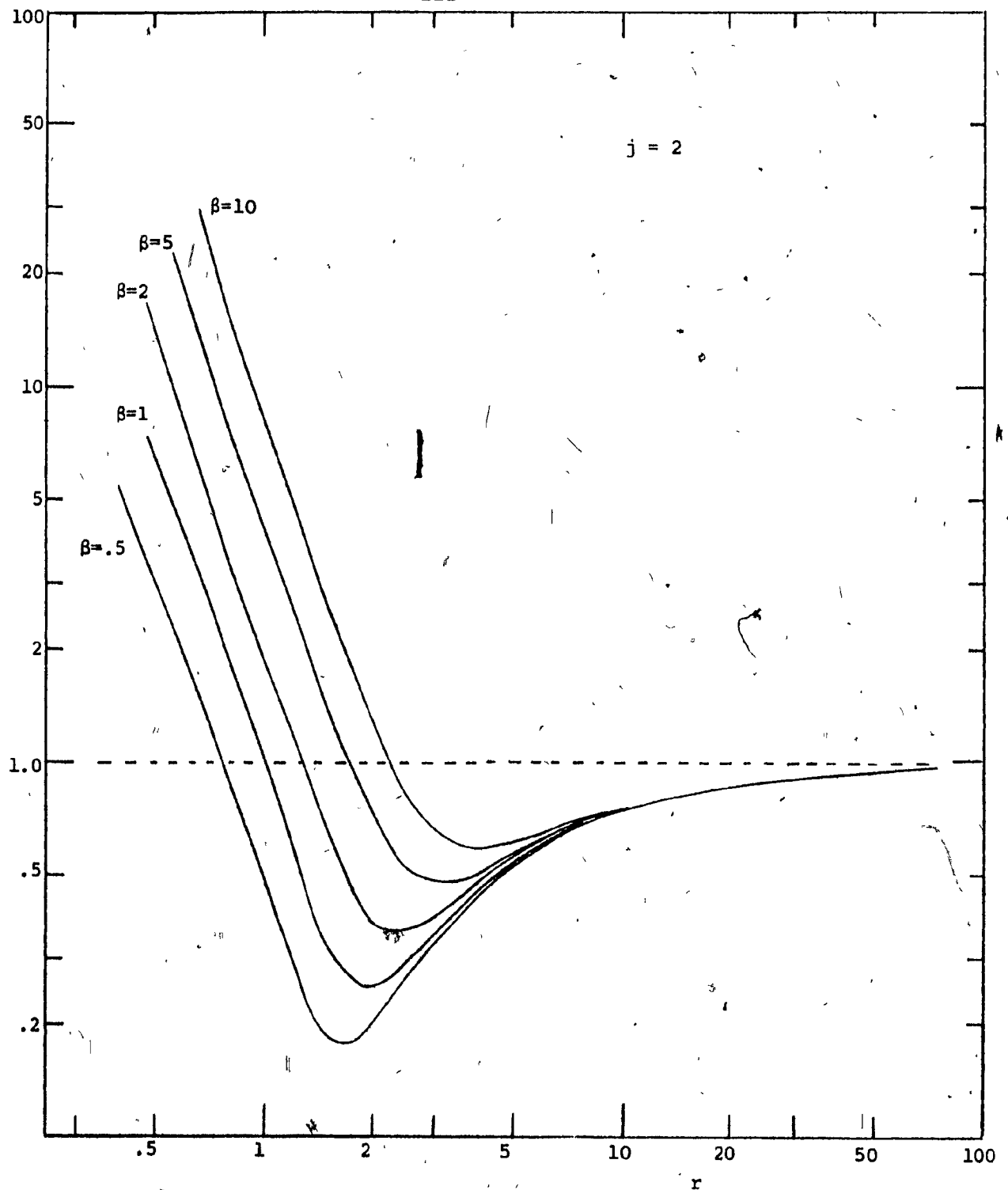
FIG. 21. VARIATION OF NON-DIMENSIONAL PRESSURE α WITH NON-DIMENSIONAL RADIUS r IN ZEL'DOVICH's THEORY FOR SEVERAL VALUES OF SOURCE ENERGY PARAMETER β
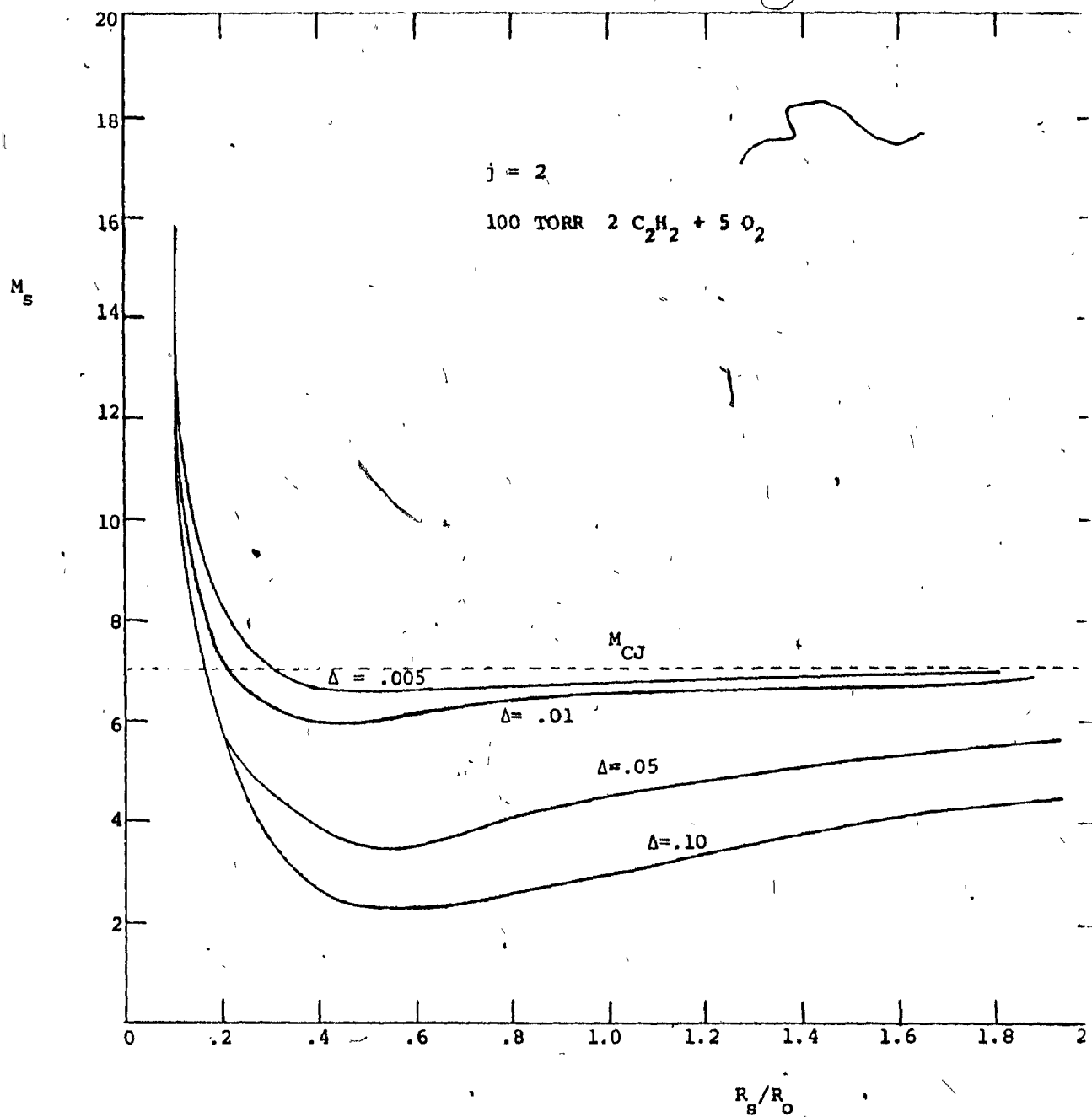
FIG. 22. VARIATION OF SHOCK MACH NUMBER WITH NON-DIMENSIONAL RADIUS
FOR SEVERAL VALUES OF SOURCE ENERGY PARAMETER Δ.
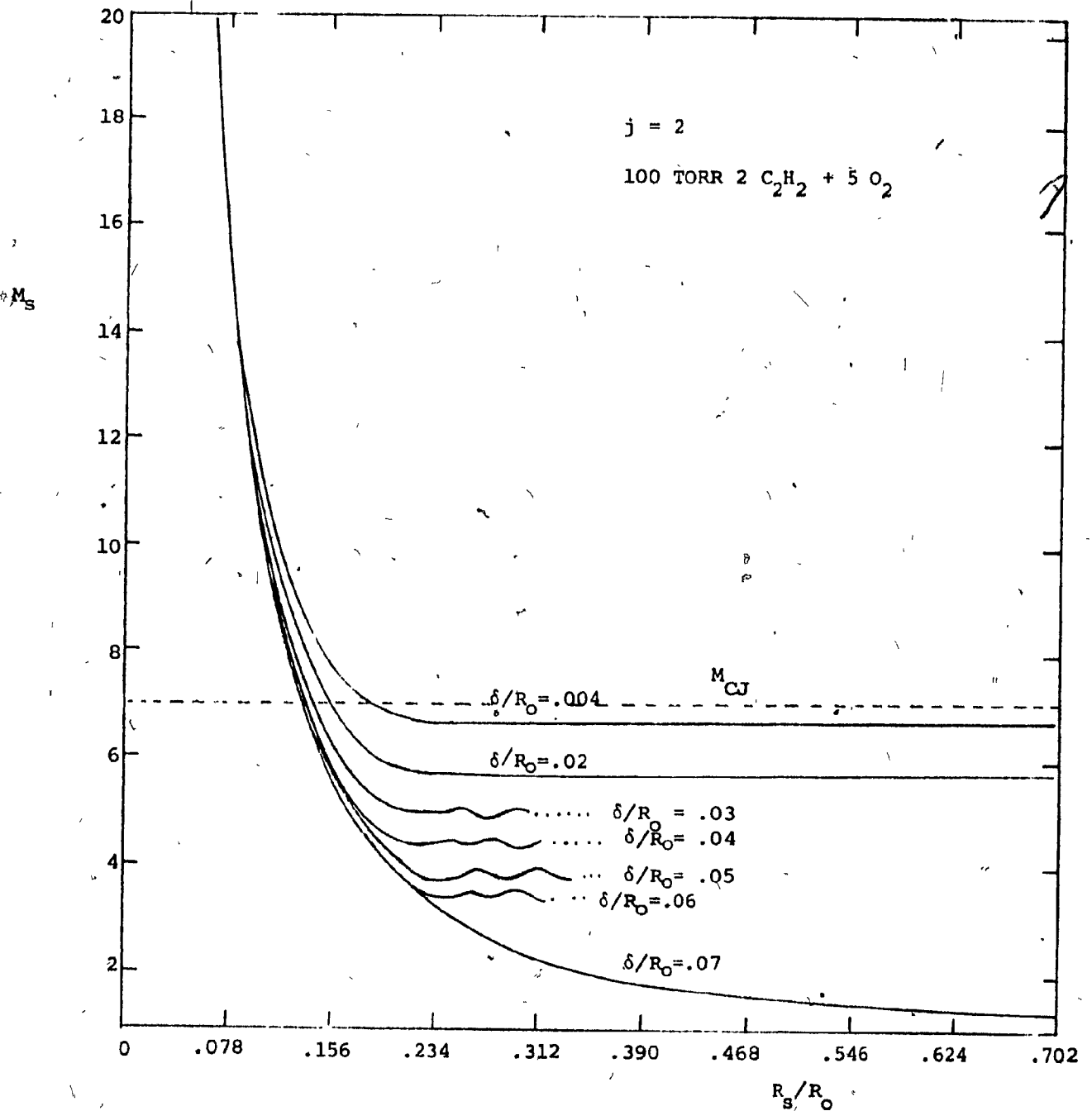
FIG. 23. VARIATION OF SHOCK STRENGTH WITH RADIUS IN LEE AND BACH's
PHENOMENOLOGICAL MODEL

FIG. 24. DEPENDENCE OF CRITICAL INITIATION ENERGY ON THE HEIGHT OF THE CHAMBER IN THE CYLINDRICAL GEOMETRY

CRITICAL INITIATION ENERGY - Joules/cm

10

6

4

2

1.0

0.1

.06

.04

.03

380 TORR $2H_2 + O_2$

S = 0.25 cm

80 TORR $2 C_2H_2 + 5O_2 + 6He$

S = 0.7 cm

80 TORR $2 C_2H_2 + 5 O_2 + 6 Ar$

S = 0.45 cm

100 TORR $2 C_2H_2 + 5 O_2$

S = 0.23 cm

300 TORR $2 C_2H_2 + 5 O_2$

S ≃ .07 cm

0   1.0   2.0   3.0   4.0

1 cm
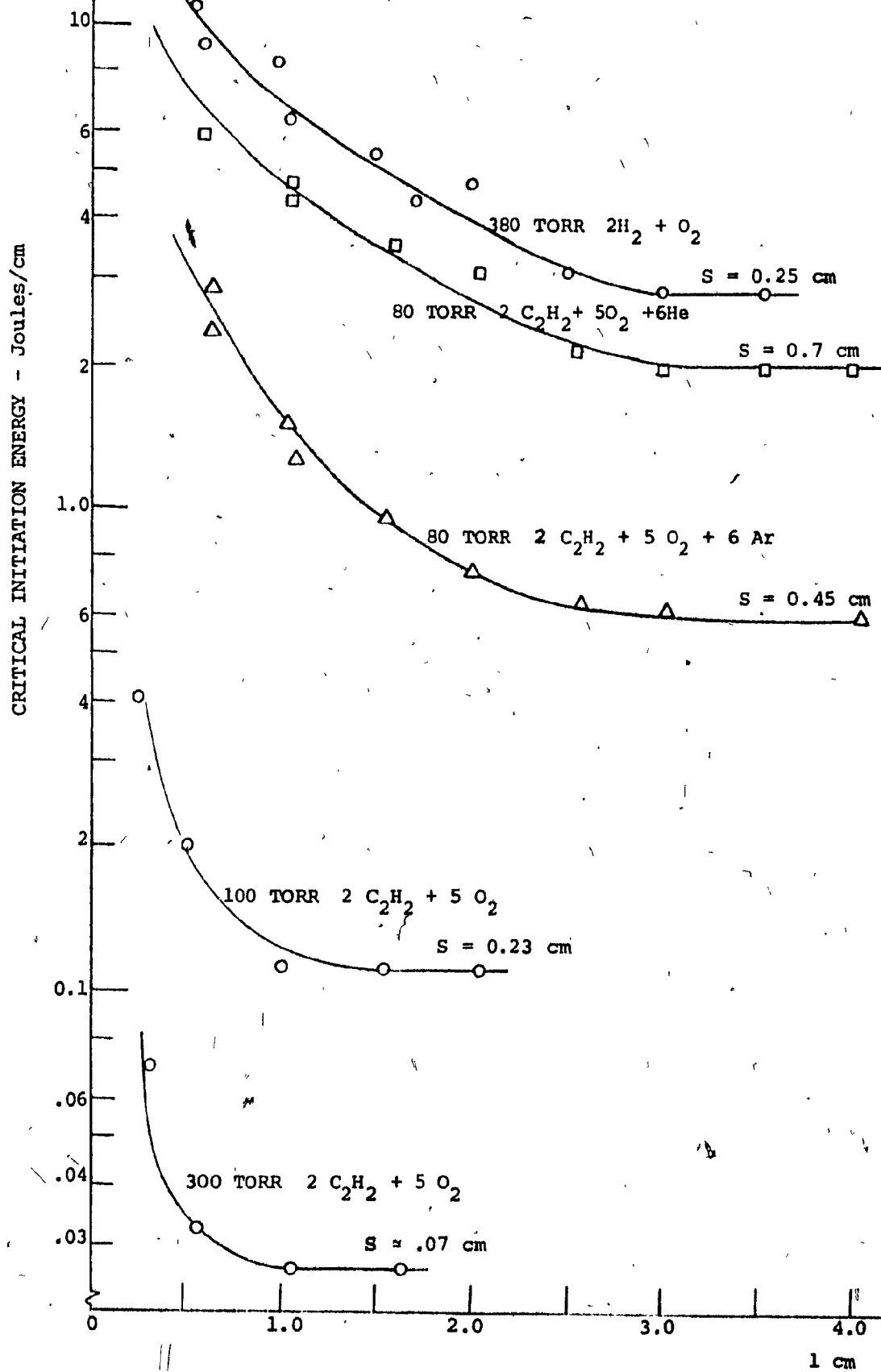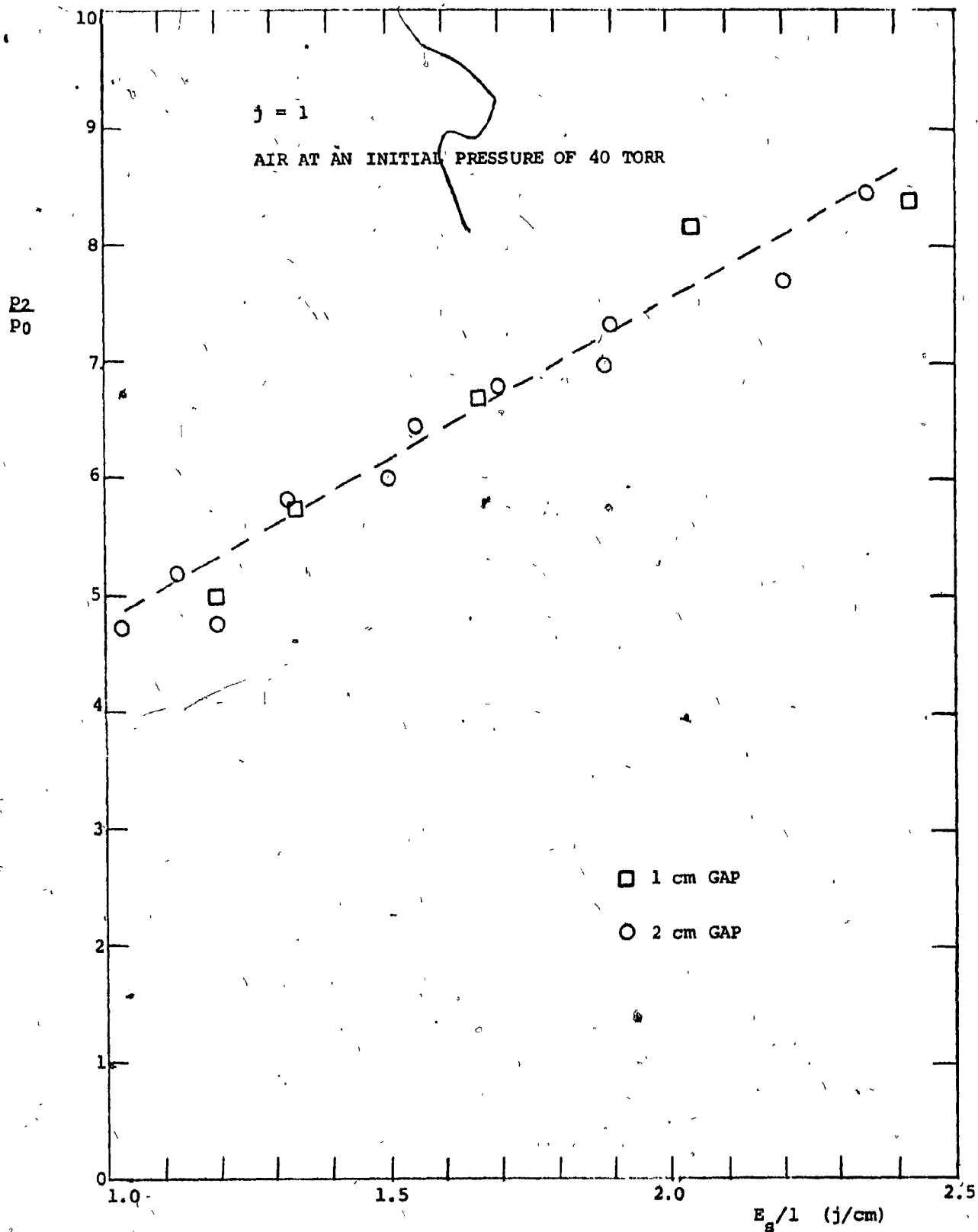
FIG. 24a. PRESSURE RATIO ACROSS AN UNREACTIVE BLAST WAVE AT A DISTANCE OF 5 cm FROM THE ENERGY SOURCE FOR TWO DIFFERENT HEIGHTS OF THE CYLINDRICAL CHAMBER
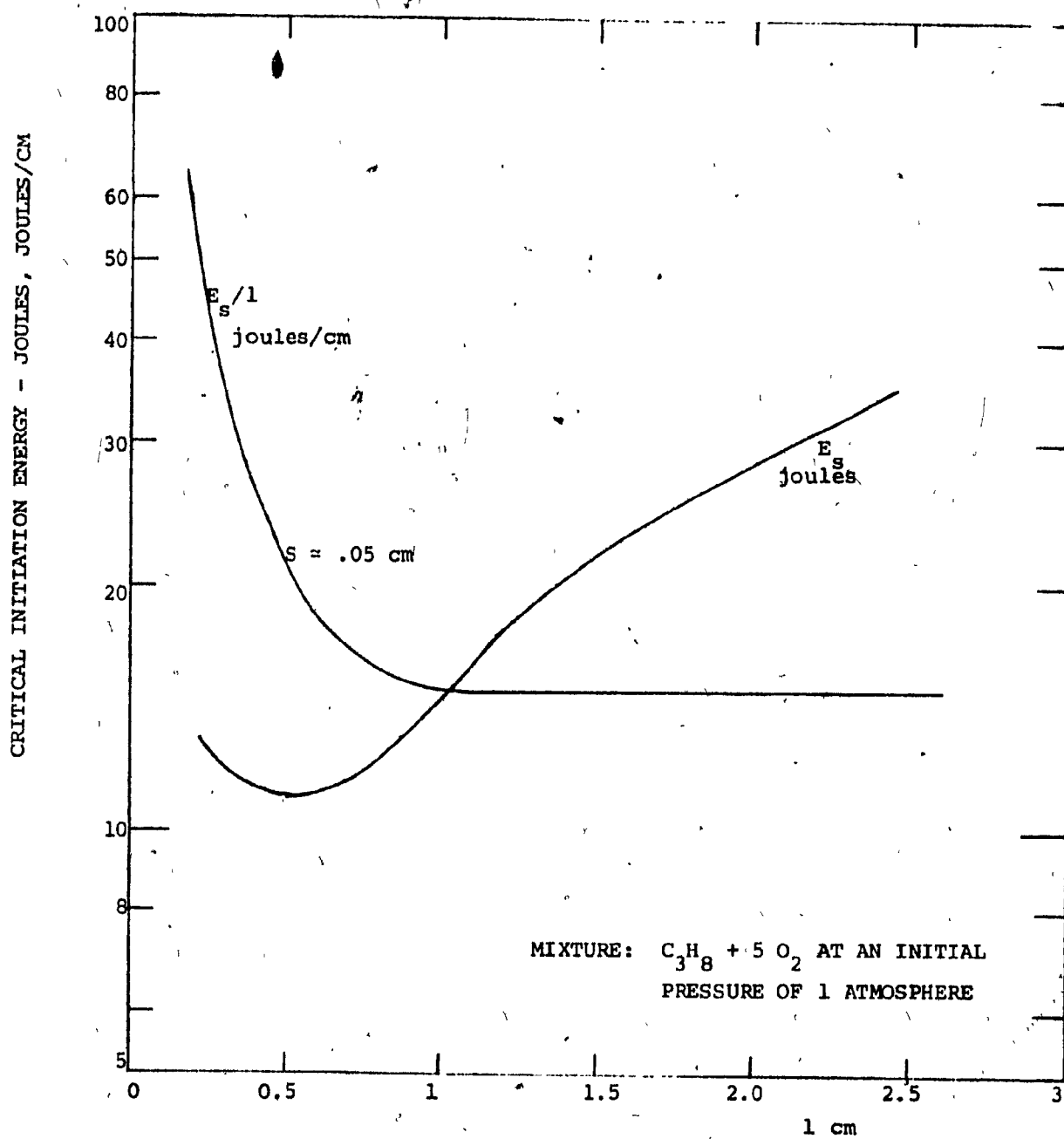
FIG. 25.   VARIATION OF INITIATION ENERGY WITH THE HEIGHT OF THE
CHAMBER IN THE EXPERIMENTS OF BROSSARD *ET AL.* (81)
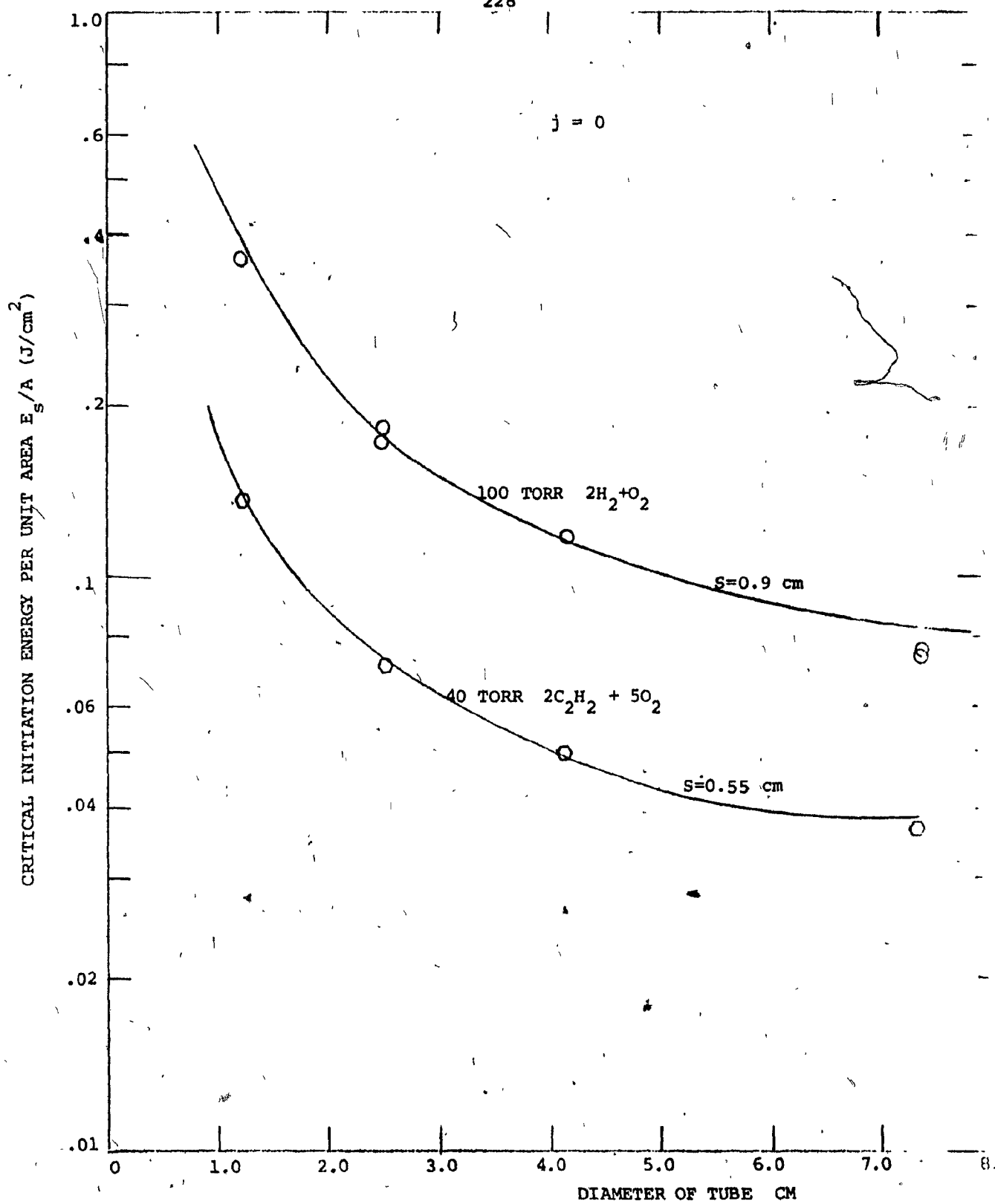
FIG. 26. VARIATION OF INITIATION ENERGY PER UNIT CROSS-SECTIONAL AREA
OF THE TUBE WITH THE DIAMETER OF THE TUBE

2 $H_2 + O_2$ AT HALF ATMOSPHERE

j = 1

$\dfrac{p}{p_o}$

1 = 29 mm

JTZ theory

1 = 19 mm

1 = 6 mm

TIME   µs
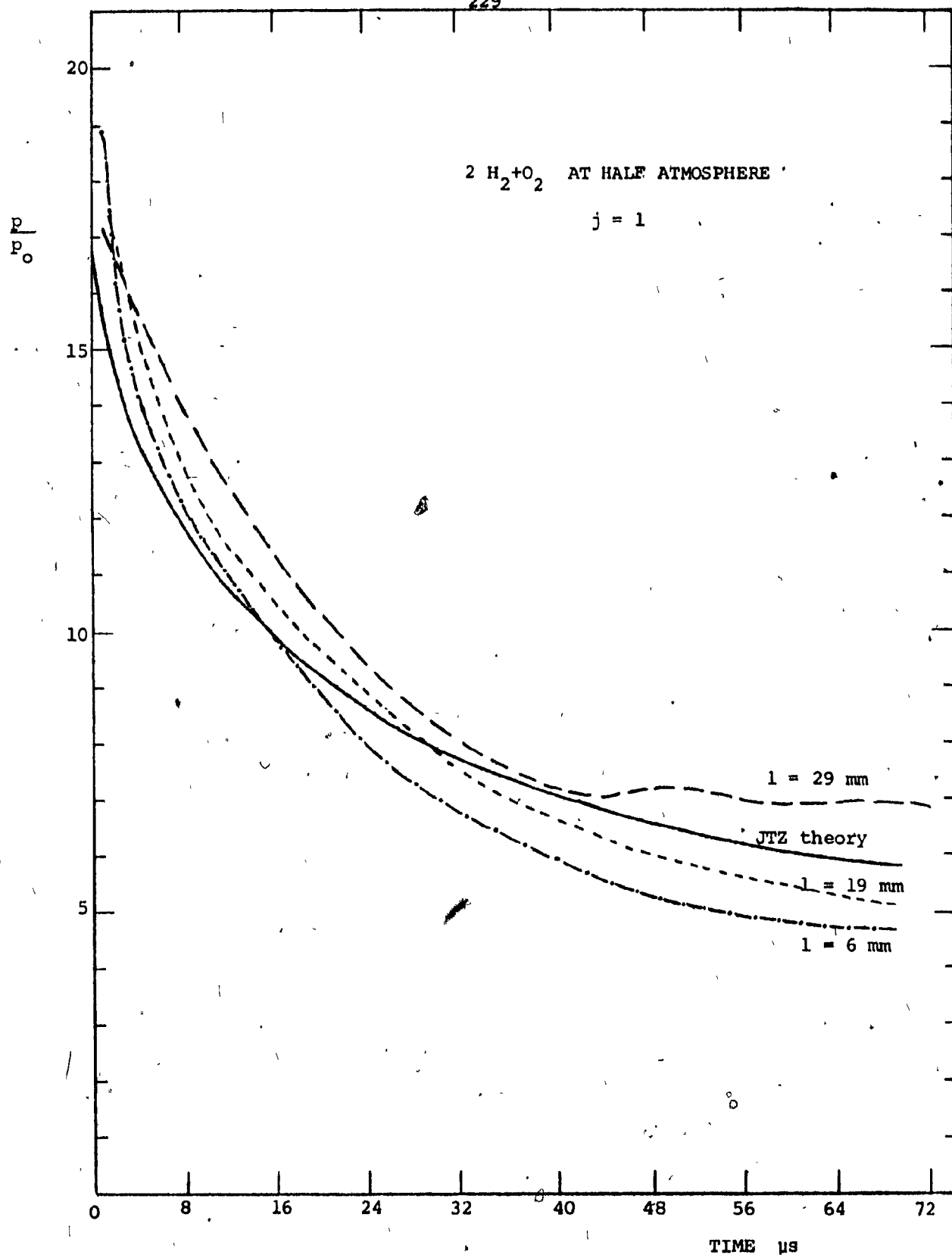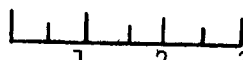
FIG. 27. PRESSURE PROFILE BEHIND A DETONATION AT A DISTANCE OF 17.5 cm
          FROM THE IGNITION SOURCE FOR DIFFERENT HEIGHTS OF THE
          CYLINDRICAL CHAMBER

230

1 = 29 mm

1 = 29 mm

1 = 19 mm

1 = 19 mm

1 = 6 mm
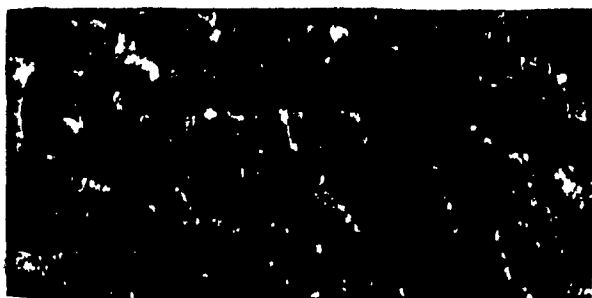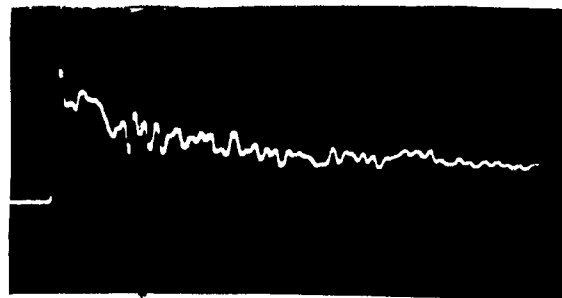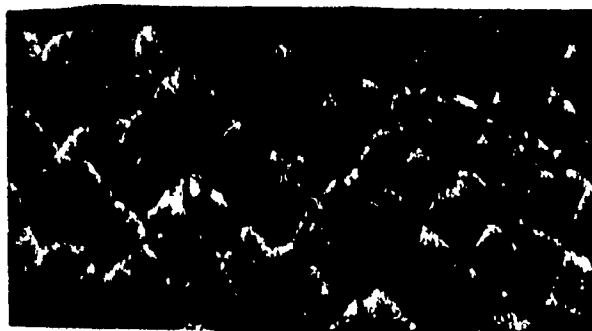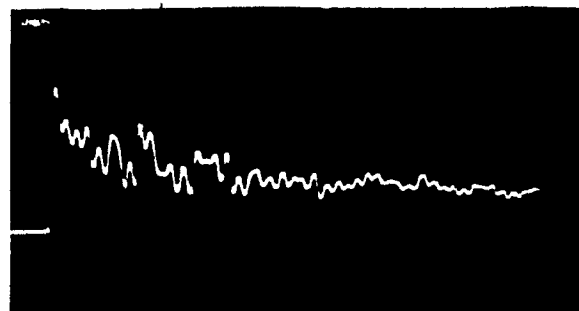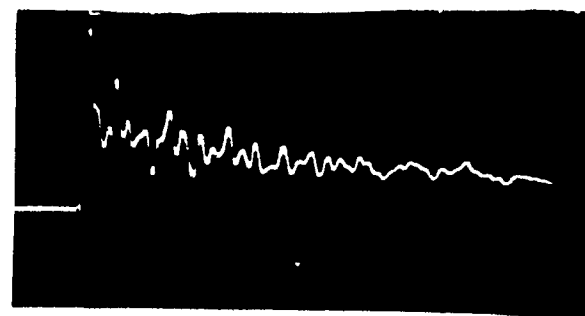
1 = 6 mm

tube of diameter 24 mm

FIG. 28.   CELL STRUCTURE AND PRESSURE PROFILES BEHIND A CYLINDRICAL
DETONATION WAVE WITH DIFFERENT HEIGHTS (1) OF THE CHAMBER
IN A MIXTURE OF 80 TORR 2 C_2H_2+ 5 O_2 + 6 He.
(The pressure profiles are at 10 µs/cm sweep and

2.76 x 10^5 $\frac{N}{m^2}$/cm)
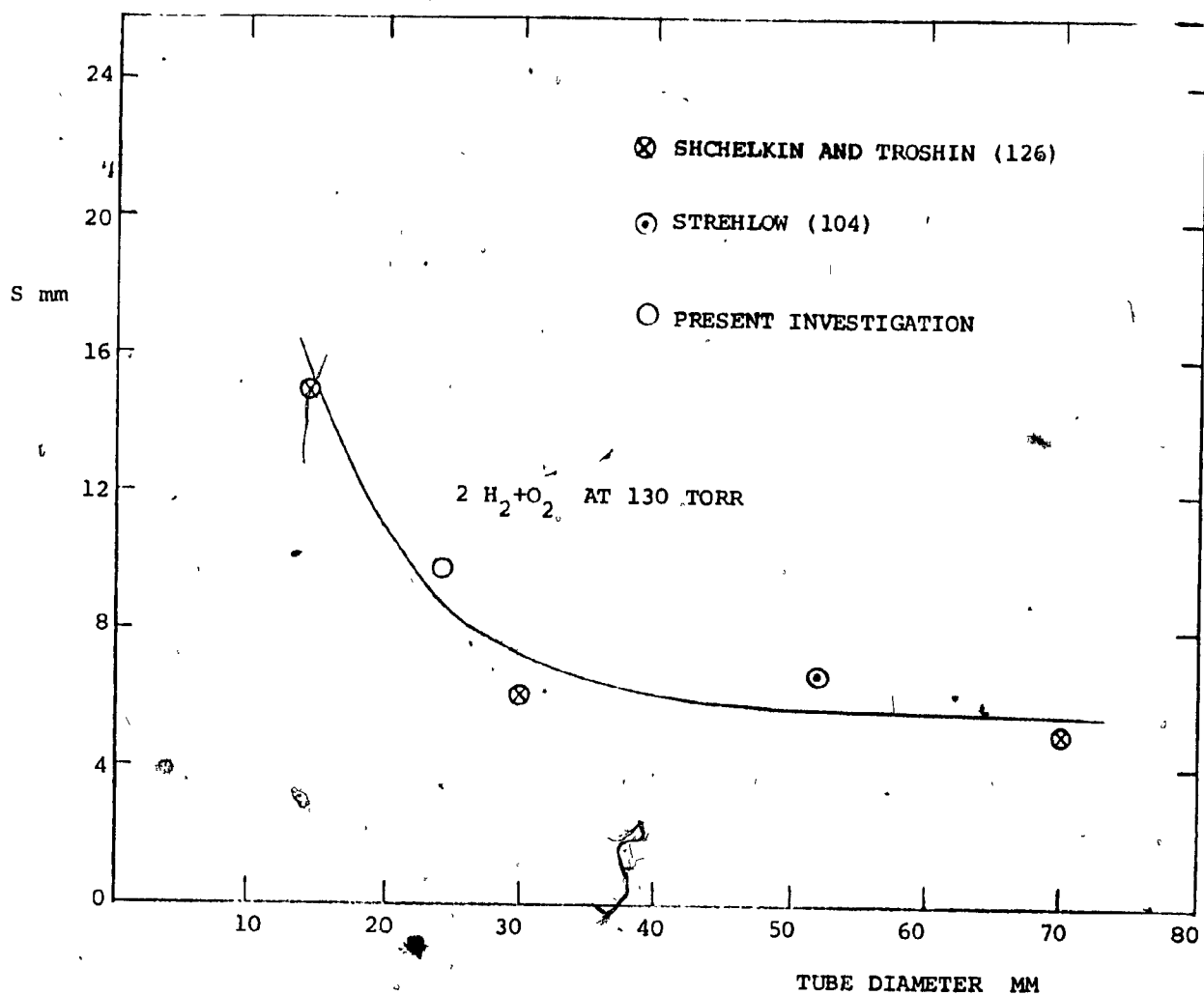
FIG. 29.   DEPENDENCE OF CELL SIZE ON DIAMETER OF THE TUBE
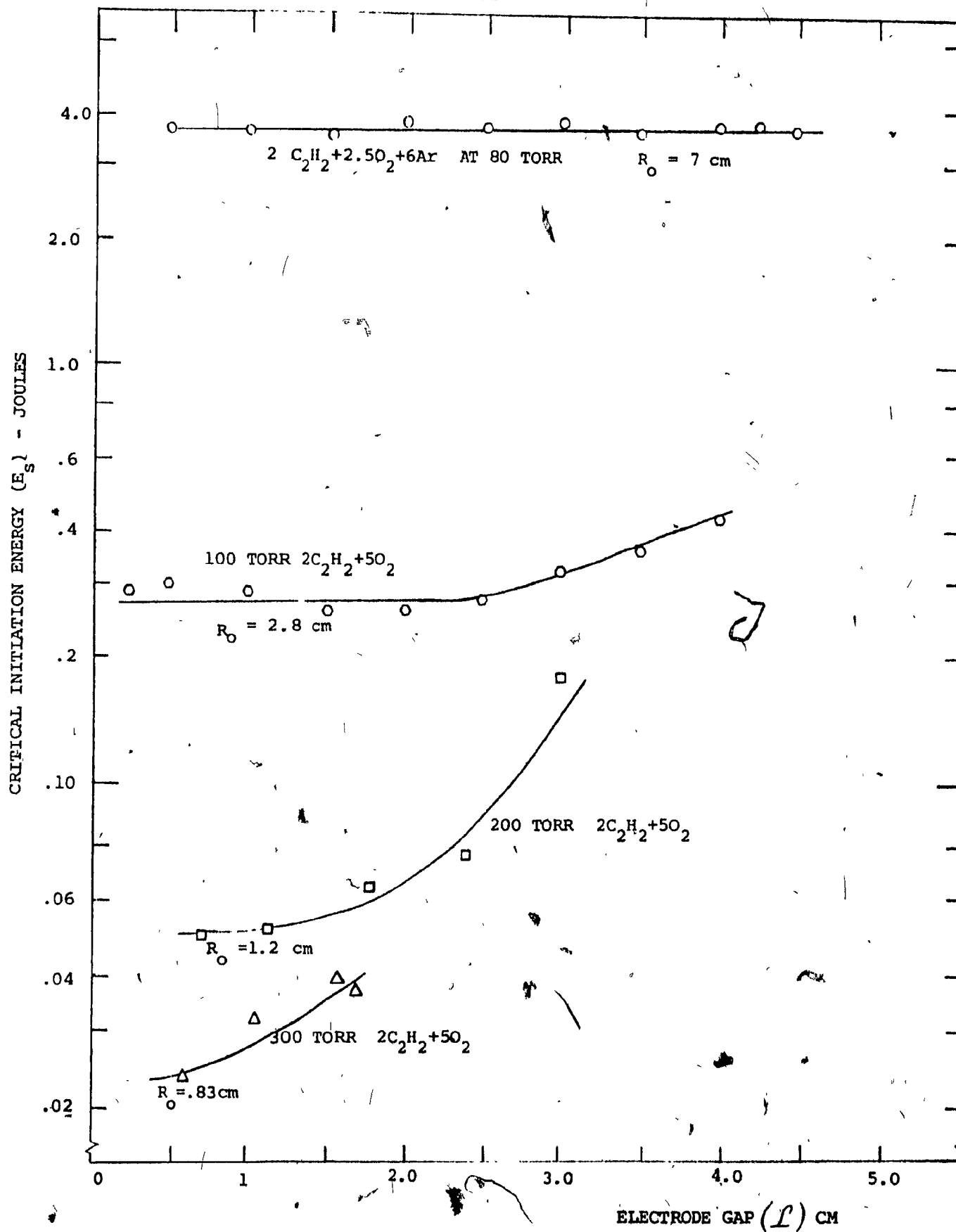
FIG. 30. VARIATION OF CRITICAL INITIATION ENERGY WITH ELECTRODE GAP
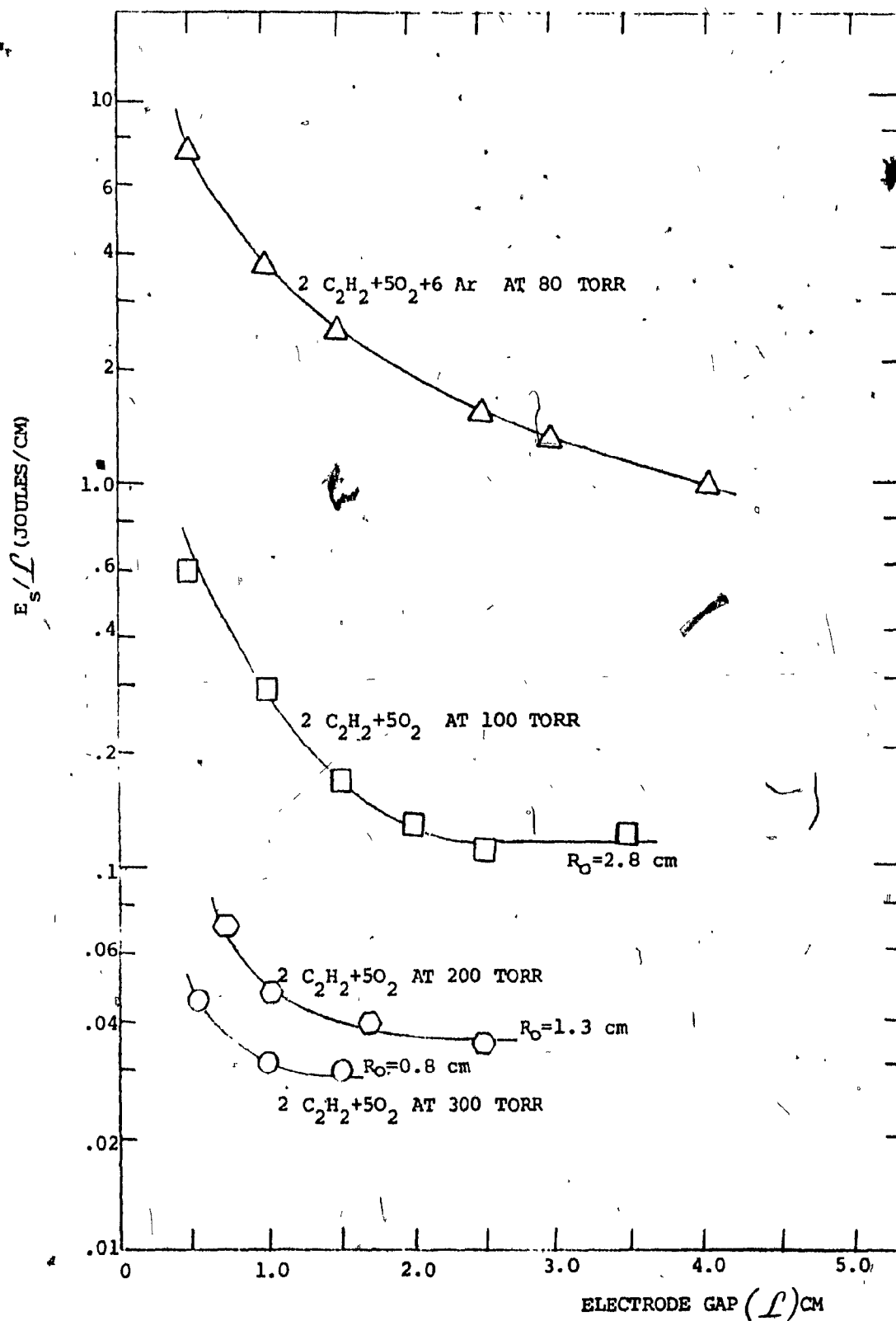
FIG. 31. VARIATION OF CRITICAL INITIATION ENERGY PER UNIT
GAP LENGTH WITH THE LENGTH OF THE ELECTRODE GAP
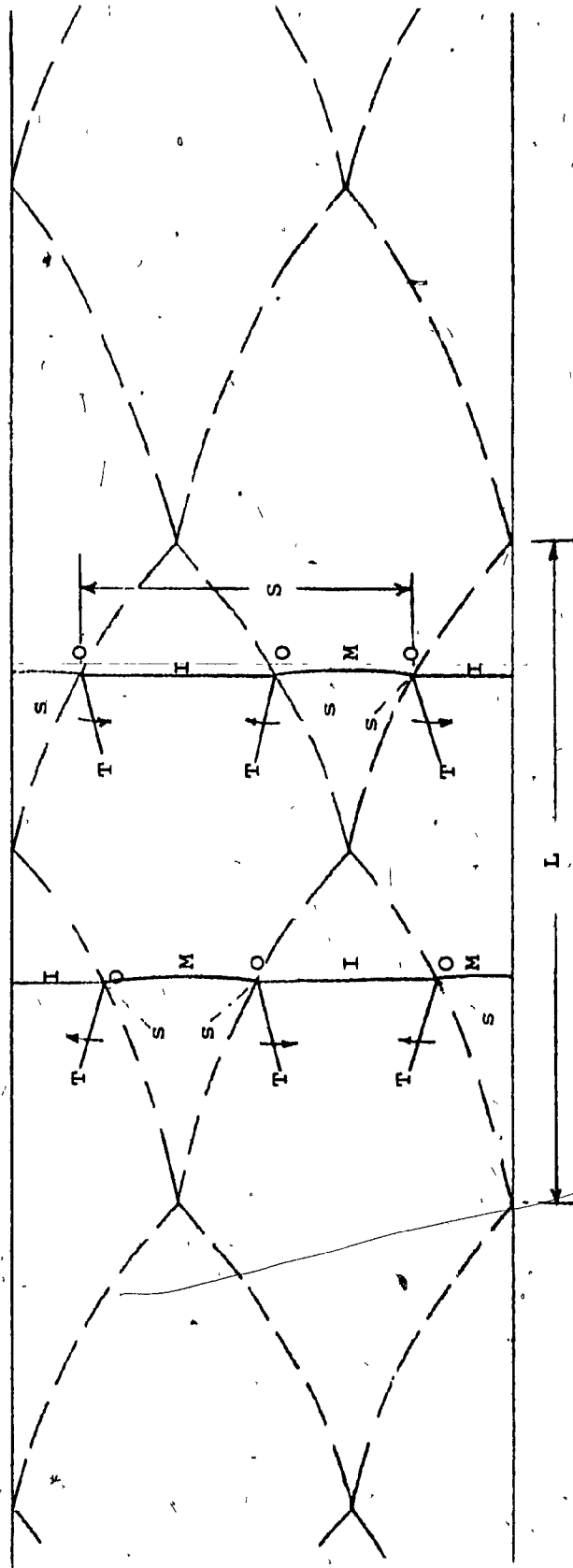
FIG. 32. TWO-DIMENSIONAL REPRESENTATION OF THE TRANSVERSE WAVE STRUCTURE
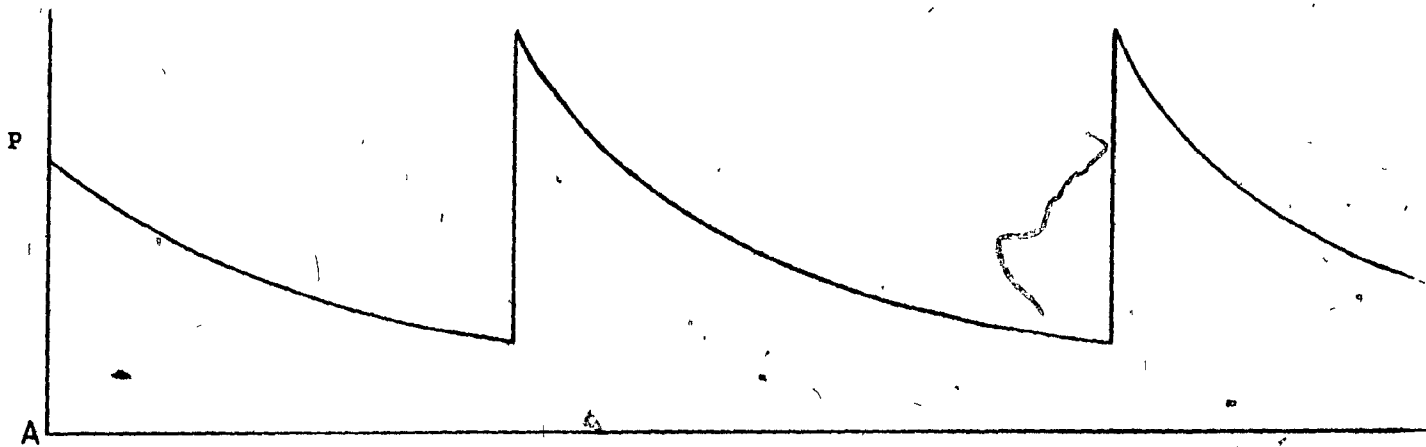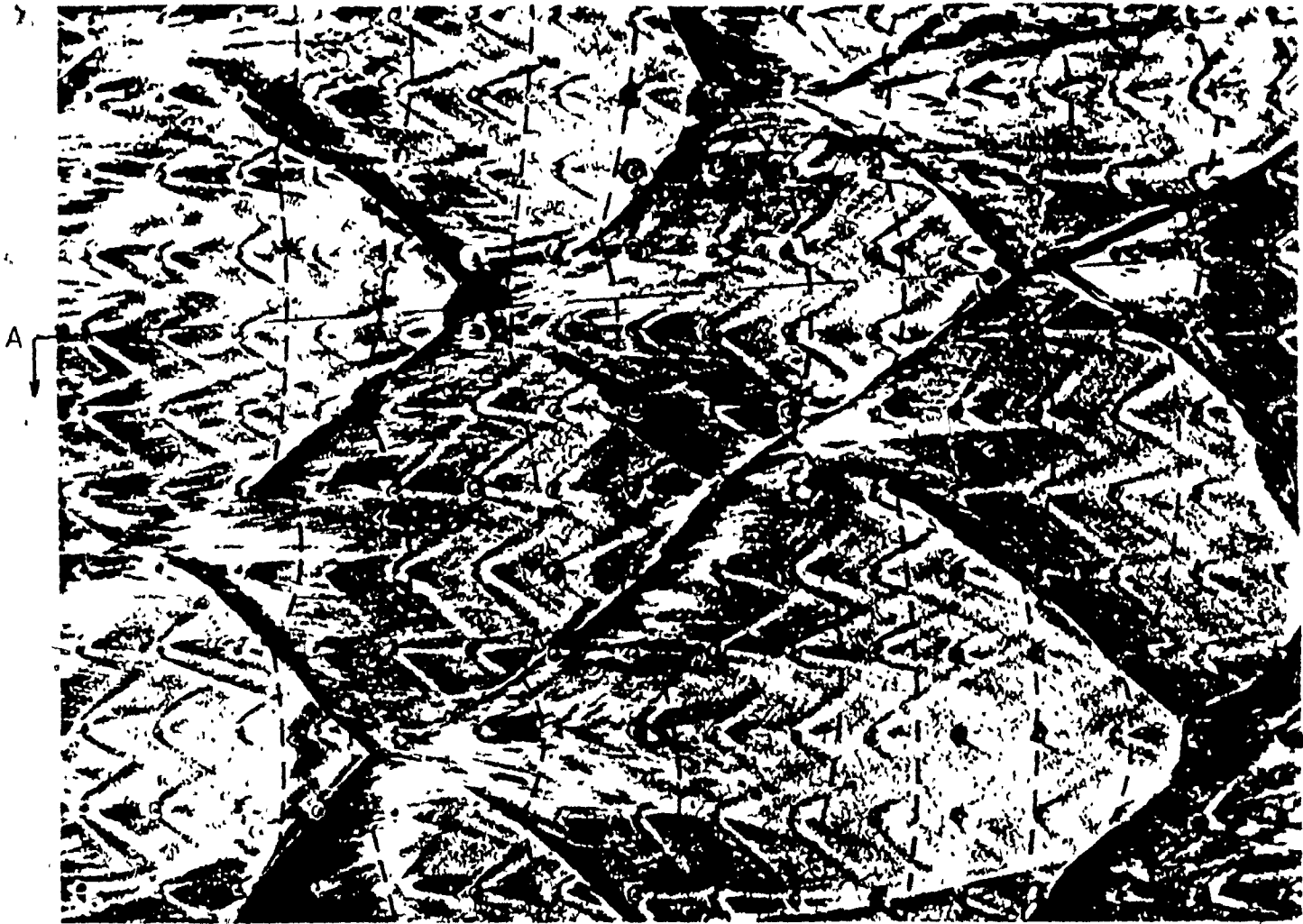
FIG. 33. ORIENTATION OF THE LEAD SHOCK WAVE AND THE DECAYING NATURE OF LEAD SHOCK BETWEEN COLLISIONS OF THE TRIPLE POINTS
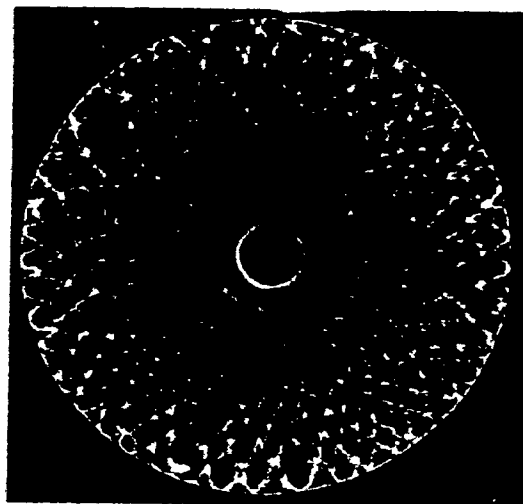
a. Failure of detonation wave
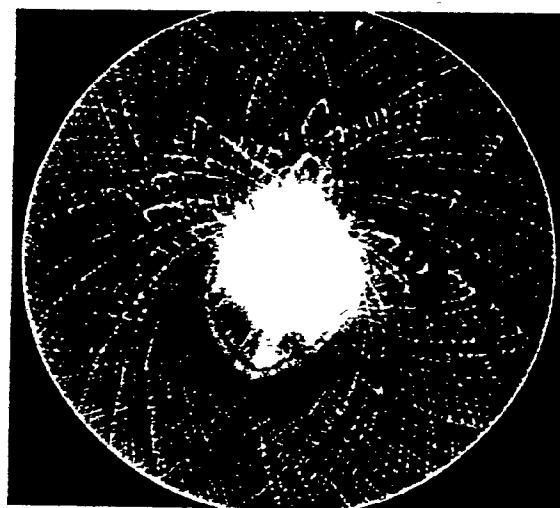
b. Self-sustenance of the
    detonation wave

FIG. 34.   OPEN SHUTTER PHOTOGRAPH OF A CYLINDRICAL DETONATION WAVE
            ILLUSTRATING THE REGENERATION OF TRANSVERSE WAVES IN A
            SELF-SUSTAINED DETONATION
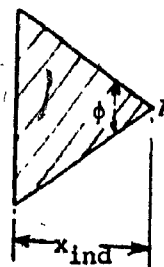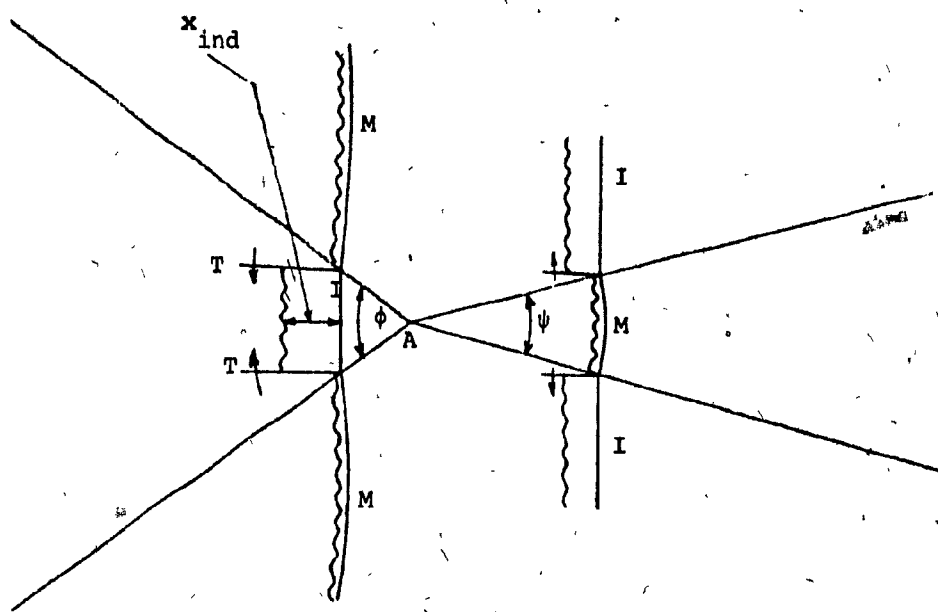
FIG.35.   SCHEMATIC DIAGRAM OF THE INTERACTION OF THE TRIPLE POINTS
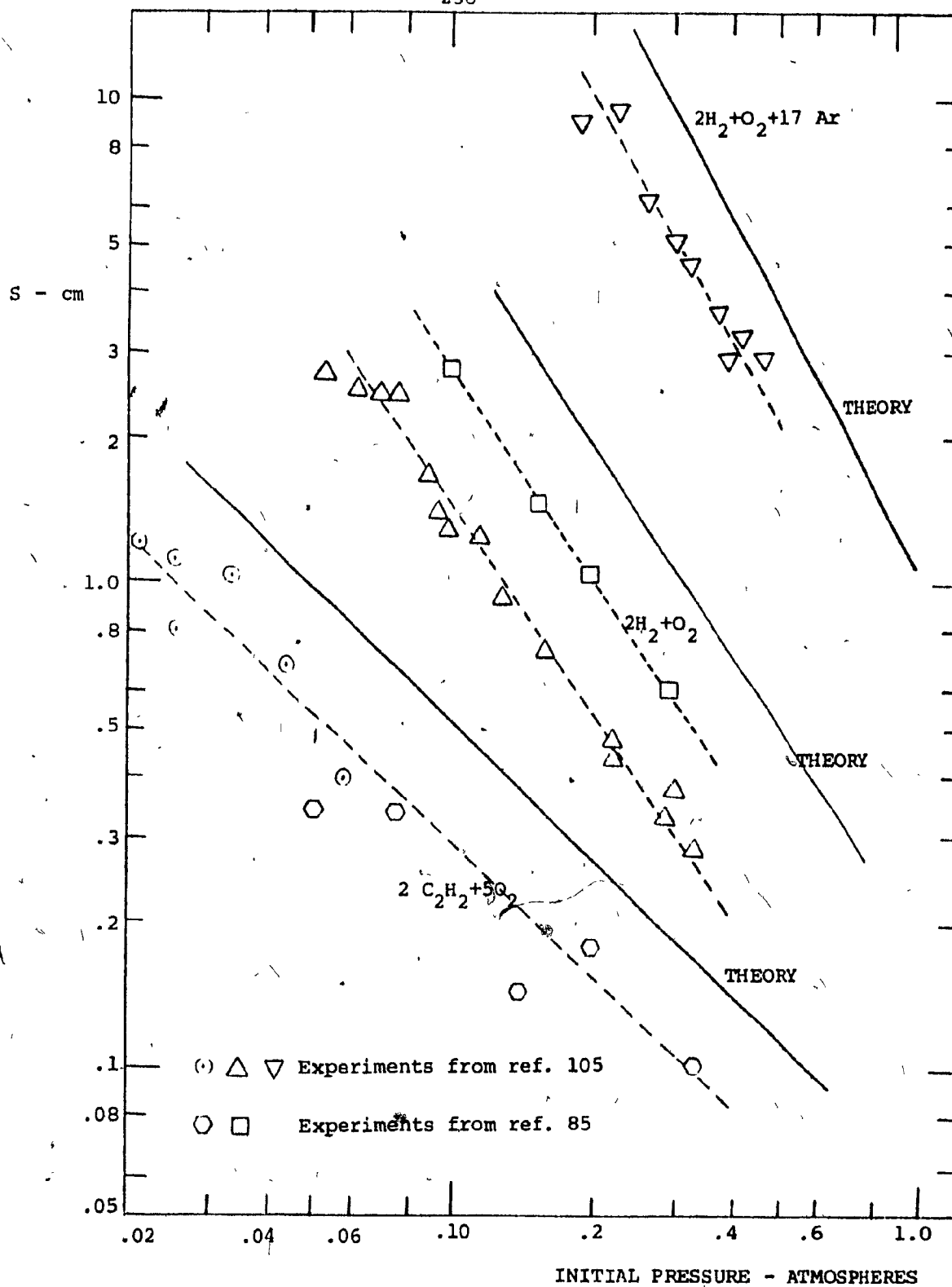
FIG. 36. COMPARISON OF THE THEORETICALLY CALCULATED TRANSVERSE
WAVE SPACING WITH EXPERIMENTS
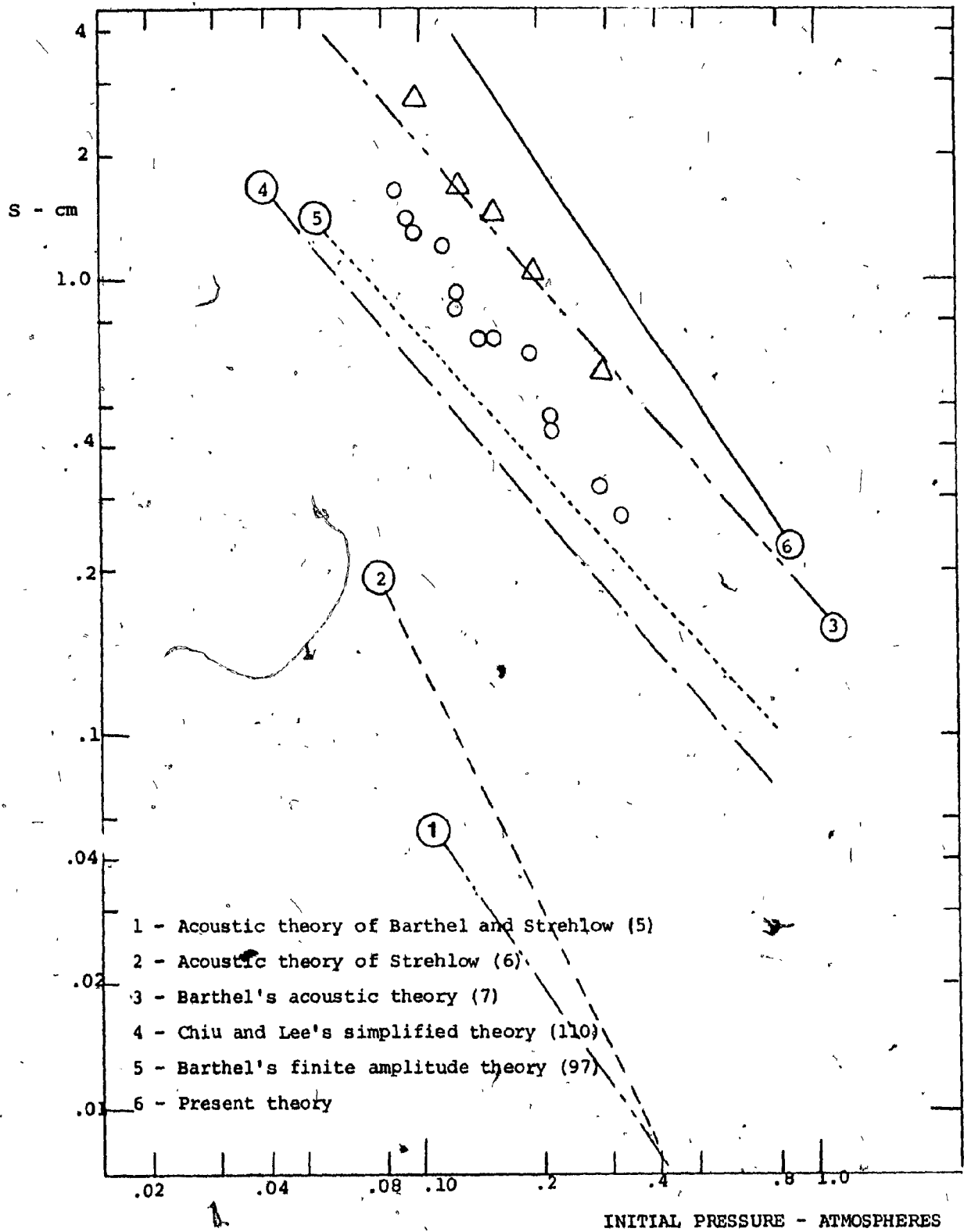
FIG. 37. COMPARISON OF TRANSVERSE WAVE SPACINGS OBTAINED FROM
DIFFERENT THEORIES FOR A 2 H_2+O_2 MIXTURE

Legend (within figure):

1 - Acoustic theory of Barthel and Strehlow (5)
2 - Acoustic theory of Strehlow (6)
3 - Barthel's acoustic theory (7)
4 - Chiu and Lee's simplified theory (110)
5 - Barthel's finite amplitude theory (97)
6 - Present theory

Axis labels: S - cm (vertical), INITIAL PRESSURE - ATMOSPHERES (horizontal)
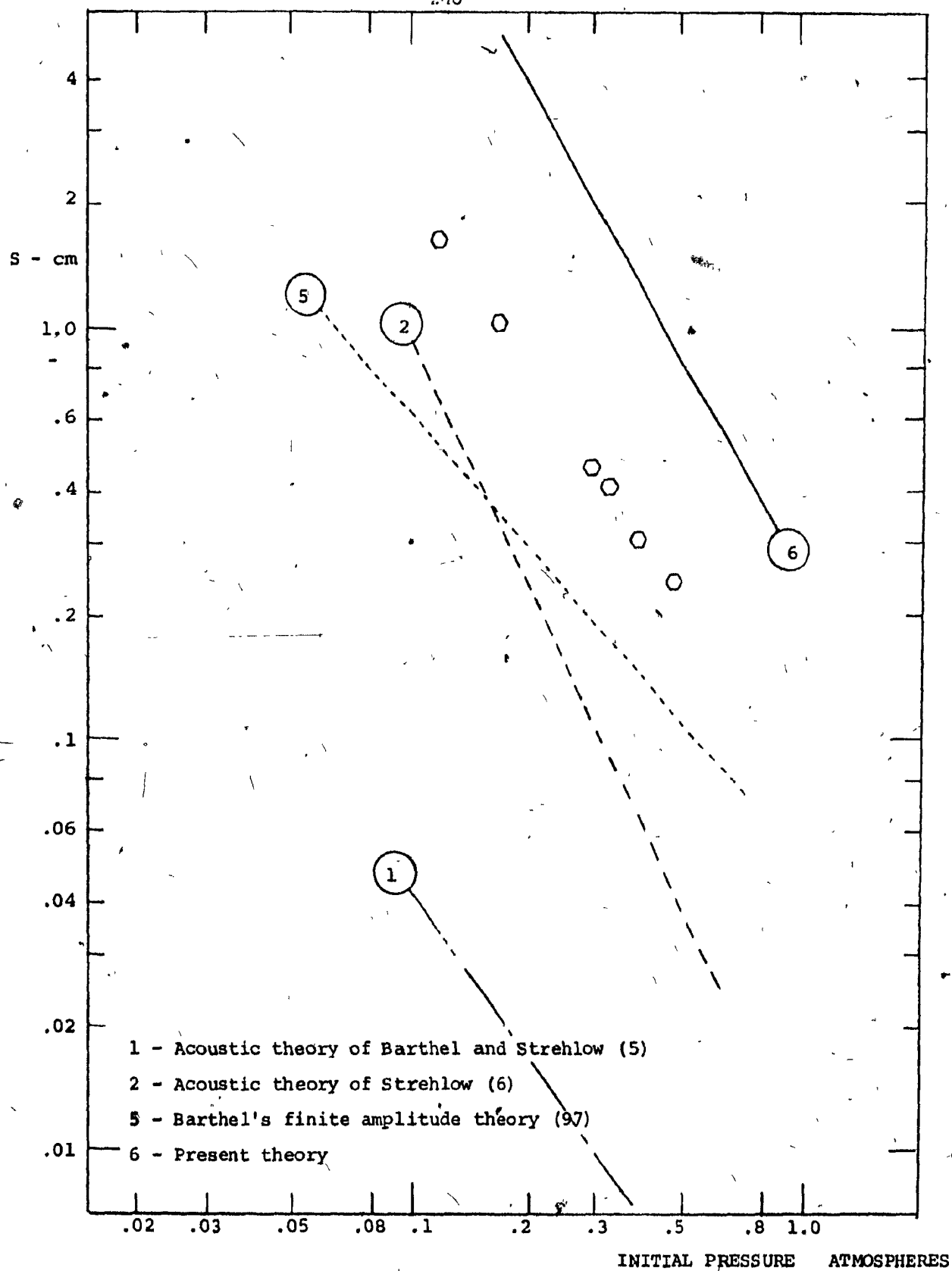
FIG. 38. COMPARISON OF TRANSVERSE WAVE SPACINGS OBTAINED FROM DIFFERENT
THEORIES FOR A 2 H_2+O_2 MIXTURE WITH 50% ARGON DILUTION

1 - Acoustic theory of Barthlet and Strehlow (5)

2 - Acoustic theory of Strehlow (6)

3 - Barthel's acoustic theory (7)

4 - Chiu and Lee's simplified theory (110)

5 - Finite amplitude theory of Barthel (97)

6 - Present theory

S - cm

INITIAL PRESSURE - ATMOSPHERES
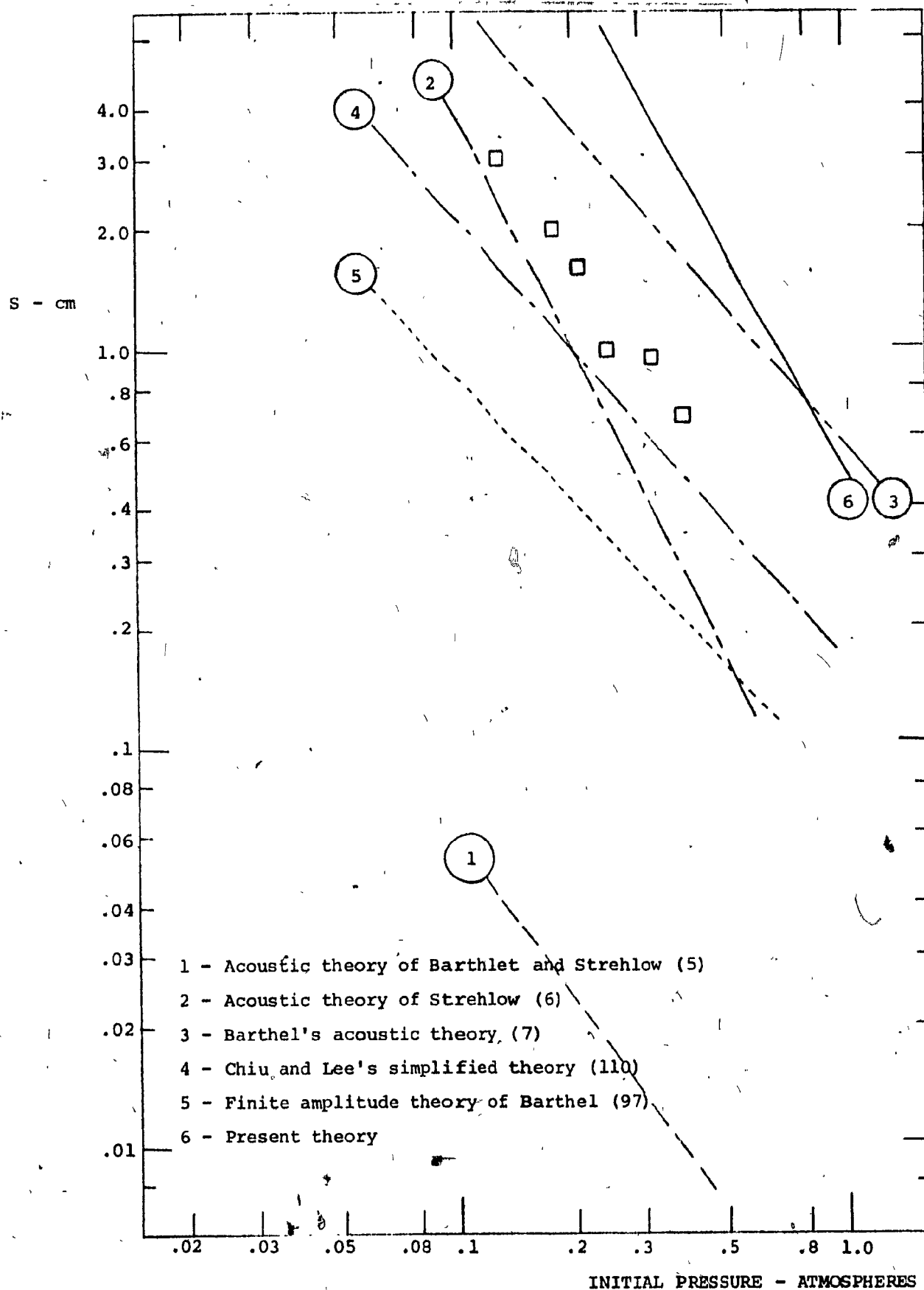
FIG. 39.   COMPARISON OF THE TRANSVERSE WAVE SPACING OBTAINED FROM
DIFFERENT THEORIES FOR A 2 H_2+O_2 MIXTURE WITH 70% ARGON
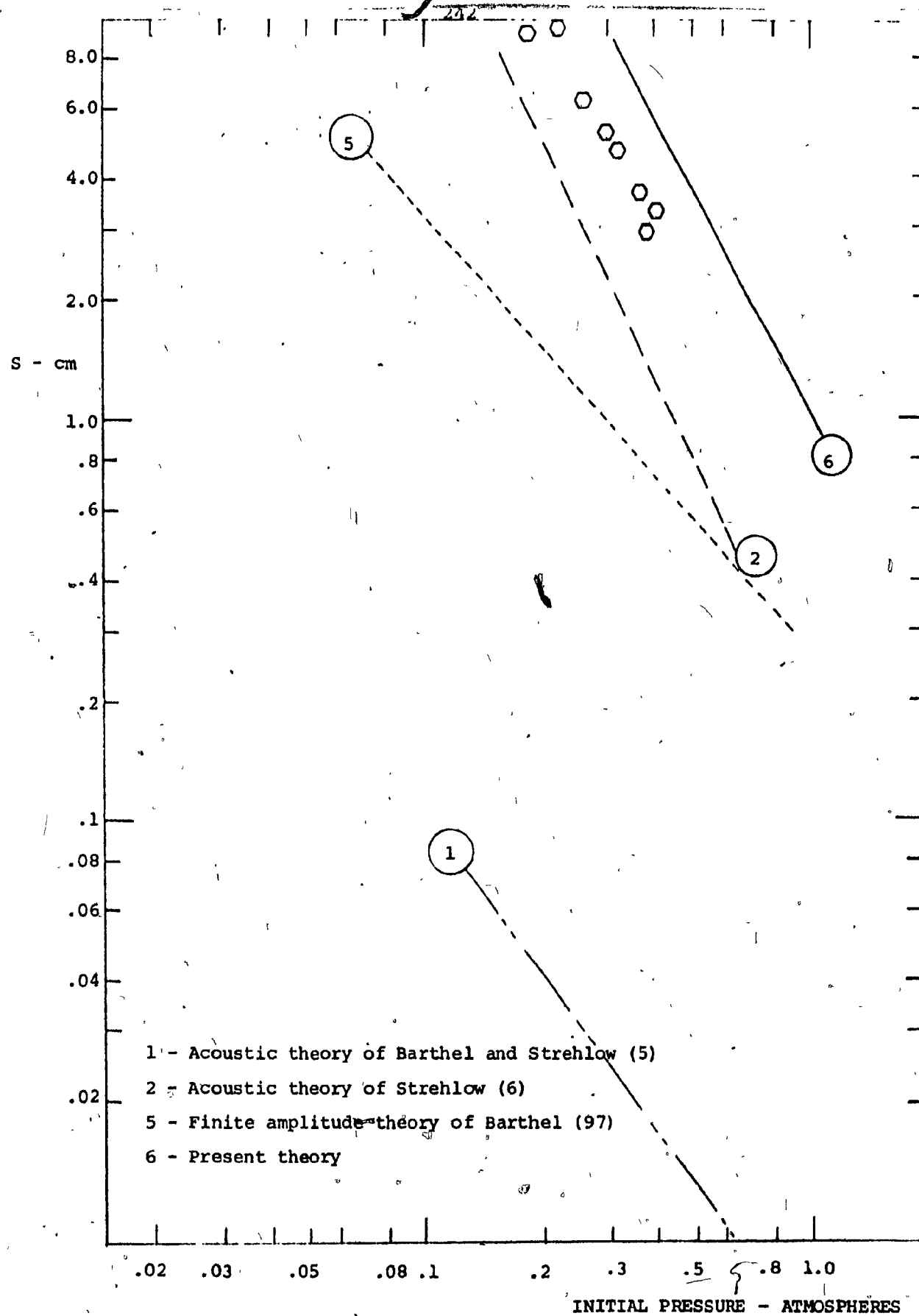
FIG. 40. COMPARISON OF THE TRANSVERSE WAVE SPACING OBTAINED FROM DIFFERENT THEORIES FOR A 2 H_2+O_2 MIXTURE WITH 85% ARGON

Legend within figure:

1 - Acoustic theory of Barthel and Strehlow (5)
2 - Acoustic theory of Strehlow (6)
5 - Finite amplitude theory of Barthel (97)
6 - Present theory

Axis labels:
S - cm (vertical)
INITIAL PRESSURE - ATMOSPHERES (horizontal)
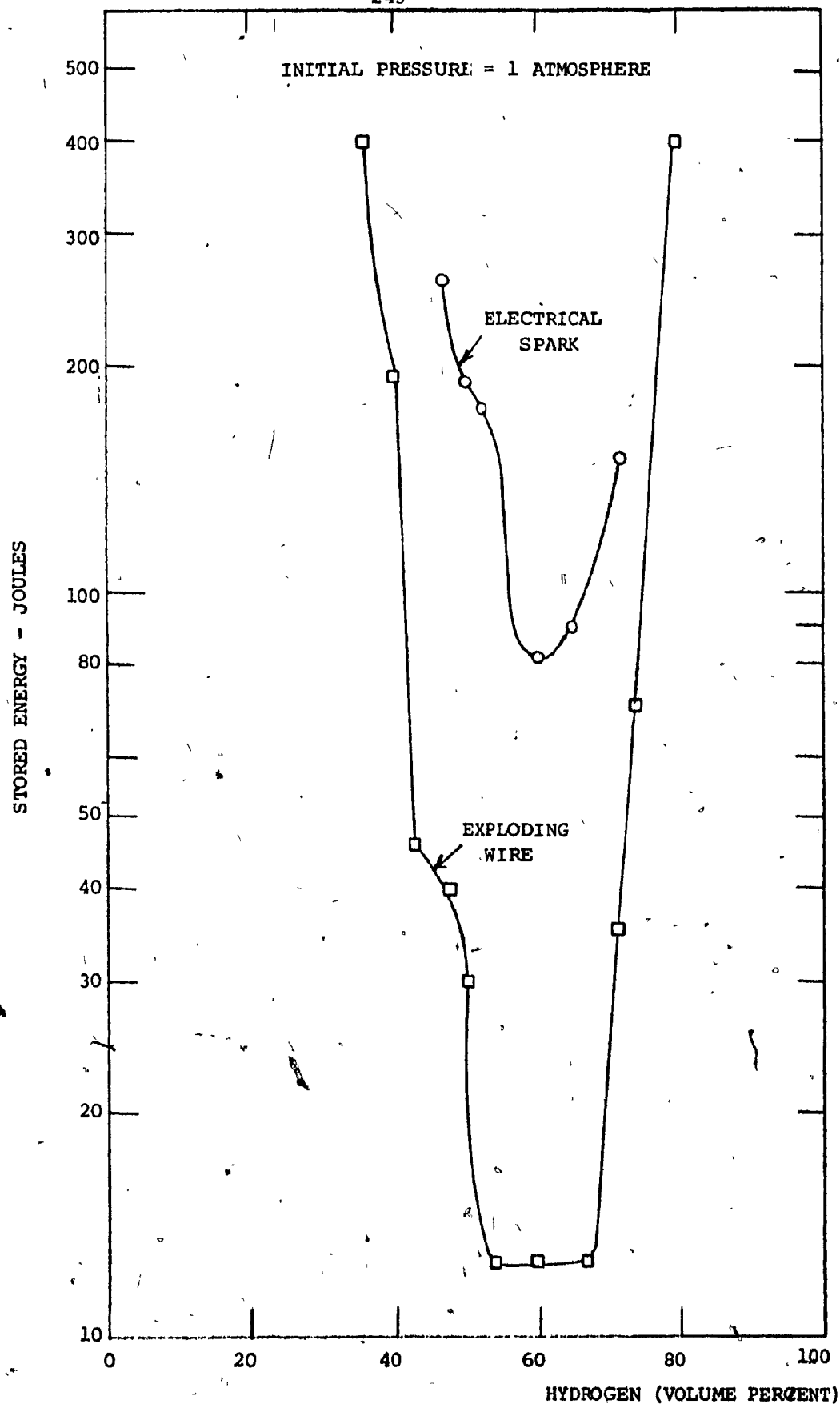
FIG. 41. STORED ENERGY REQUIRED FOR INITIATION OF
DETONATION IN OXYHYDROGEN MIXTURES (77)
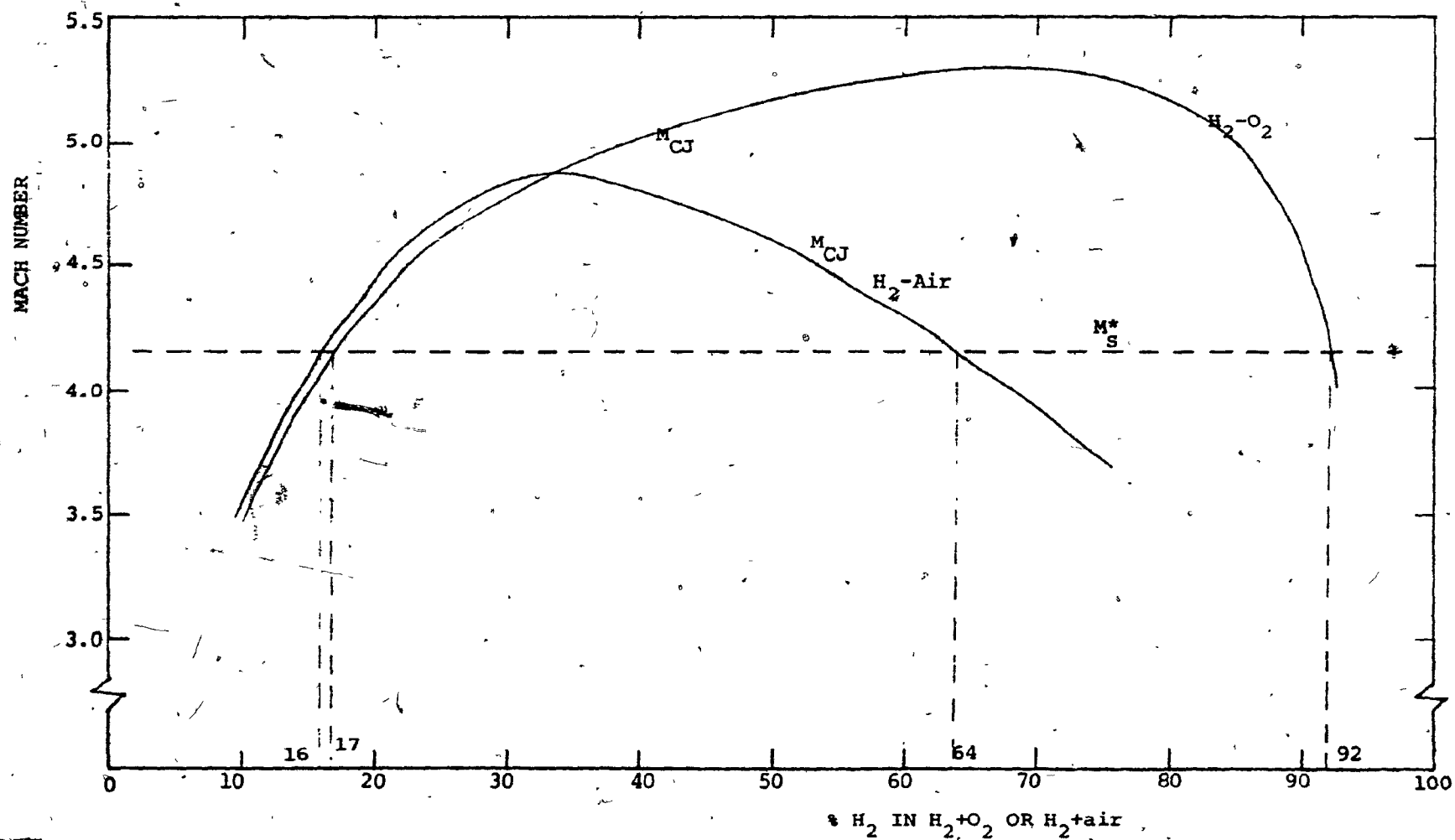
FIG. 42. PLOT OF M_{CJ} AND M_S^* VERSUS COMPOSITION FOR A MIXTURE OF HYDROGEN AND OXYGEN

244
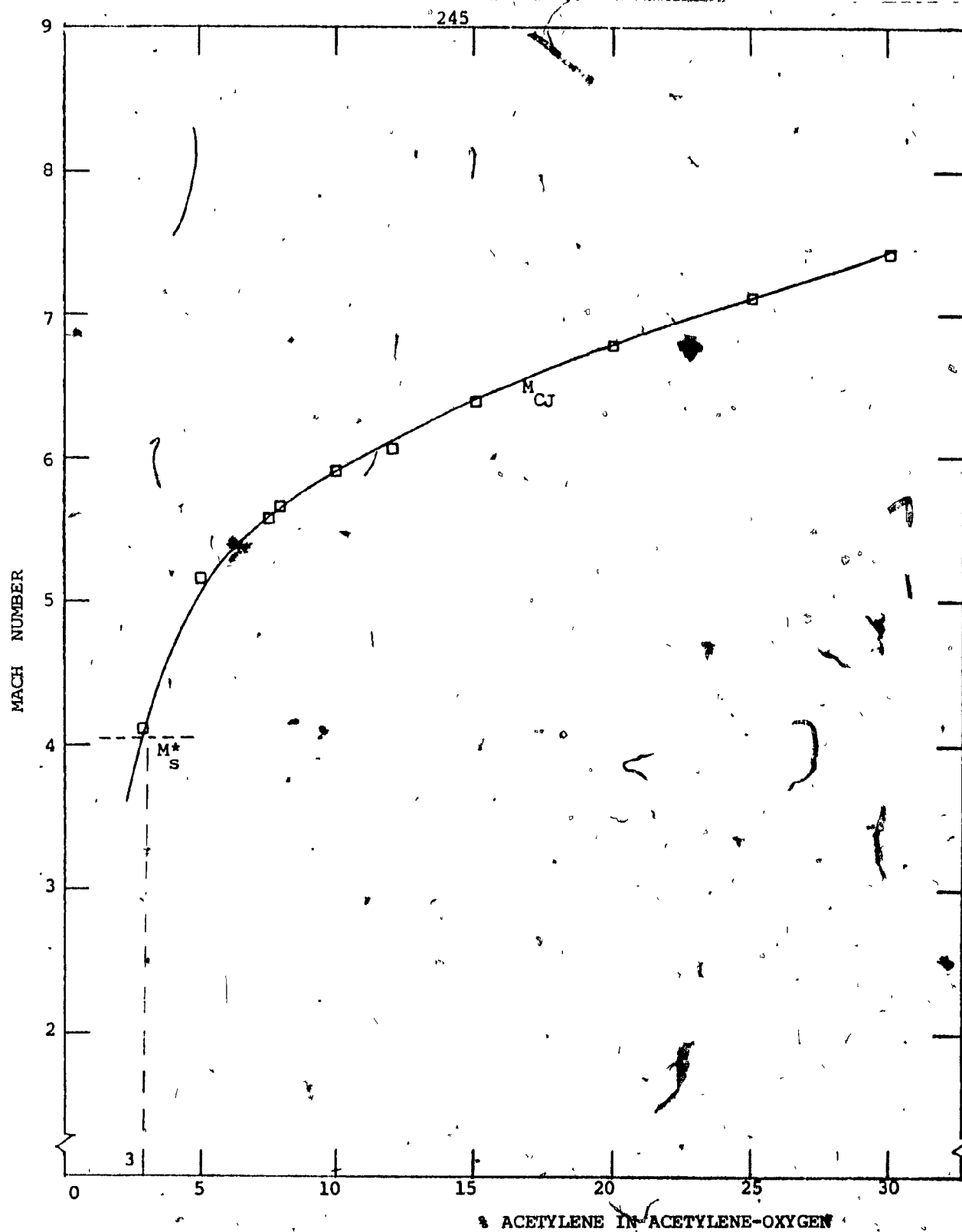
FIG. 43. DETERMINATION OF THE FUEL-LEAN LIMIT OF DETONABILITY
IN THE ACETYLENE-OXYGEN MIXTURE
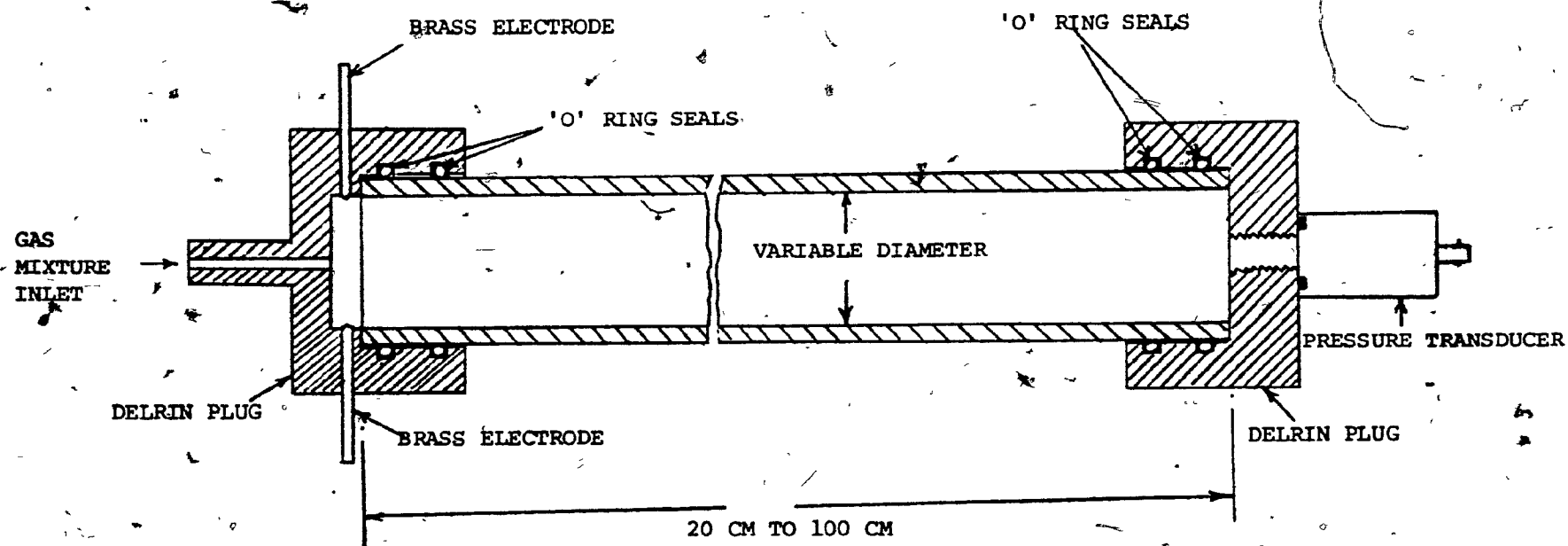
FIG. 44. SKETCH OF THE DETONATION CHAMBER IN THE EXPERIMENTS IN PLANAR GEOMETRY
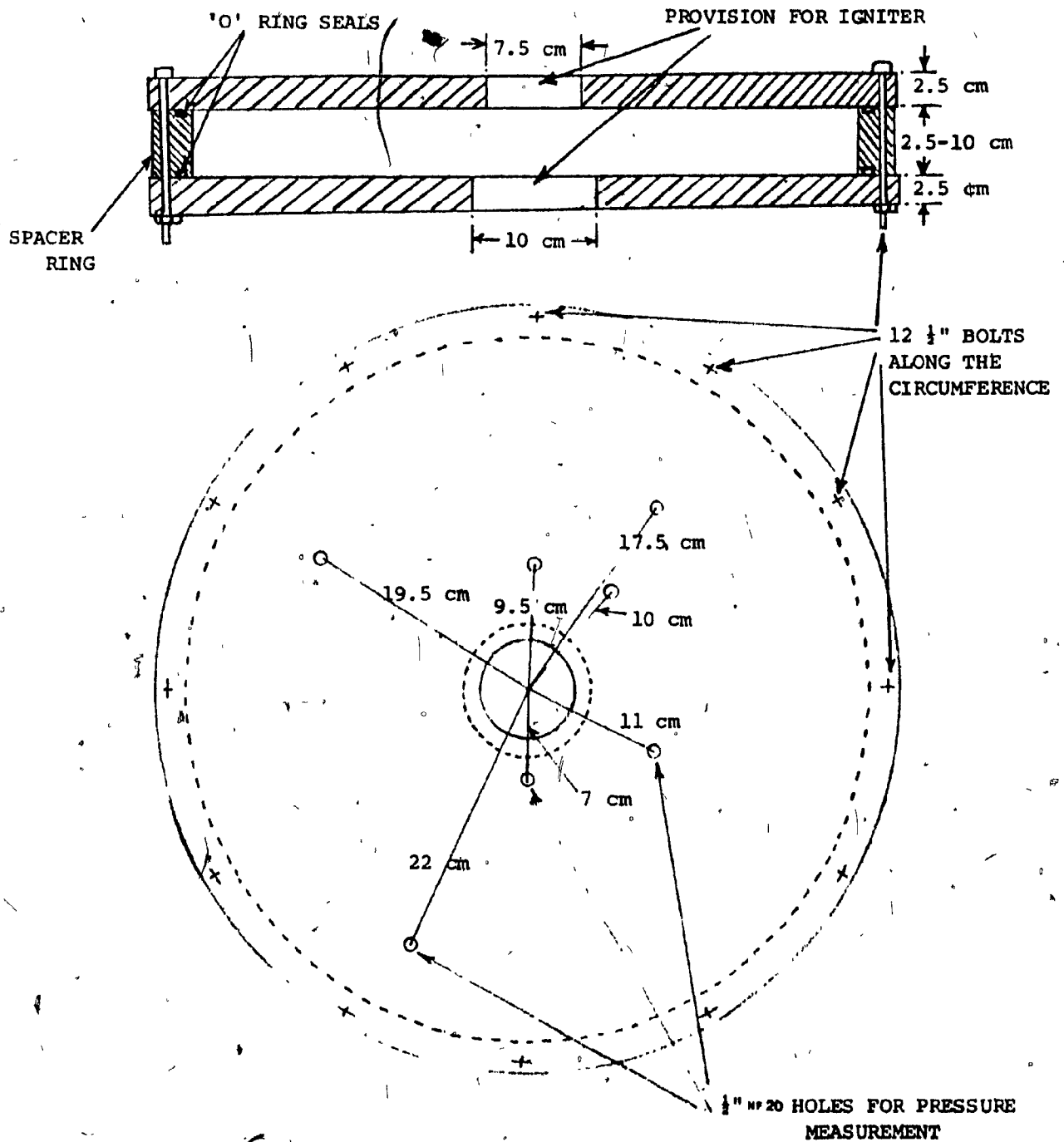
FIG. 45. SKETCH OF THE CYLINDRICAL CHAMBER

STEEL
HOUSING

PLEXIGLASS

EXPLODING
WIRE

COPPER BRIDGE

BRASS ELECTRODE
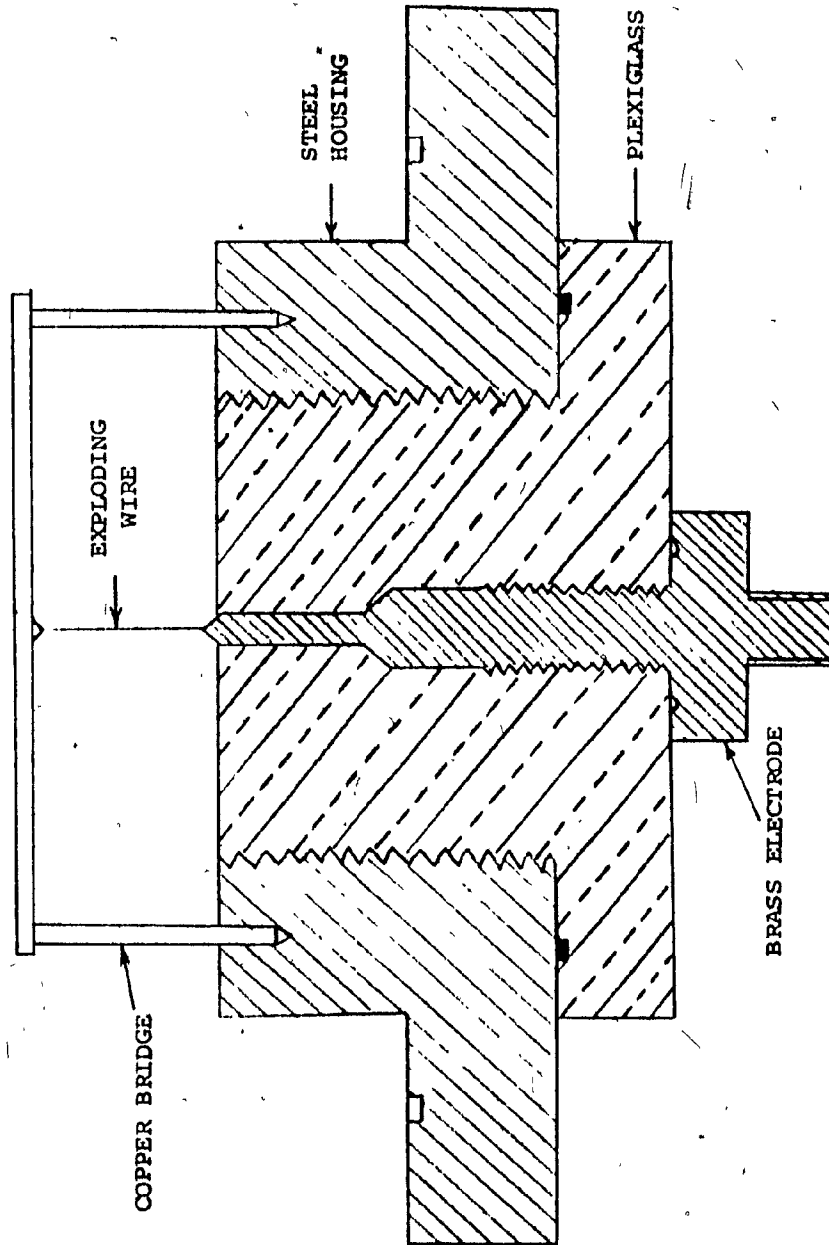
FIG. 46. SKETCH OF THE EXPLODING-WIRE ATTACHMENT

'O' RING SEALS

PYREX GLASS INSULATION

BRASS ELECTRODE

DELRIN INSULATION

DELRIN PLUG
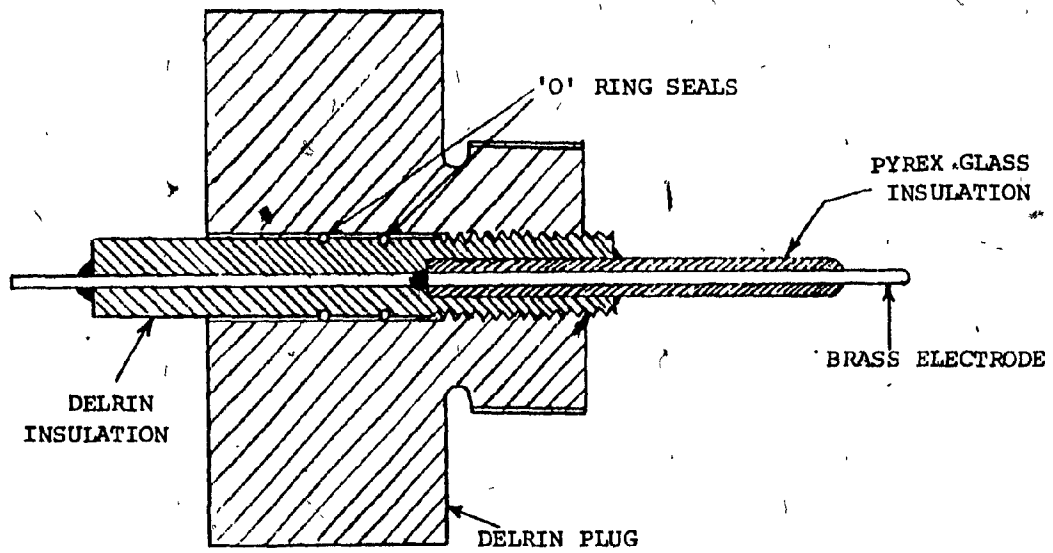
FIG. 47.   SKETCH OF THE INSULATED ELECTRODES
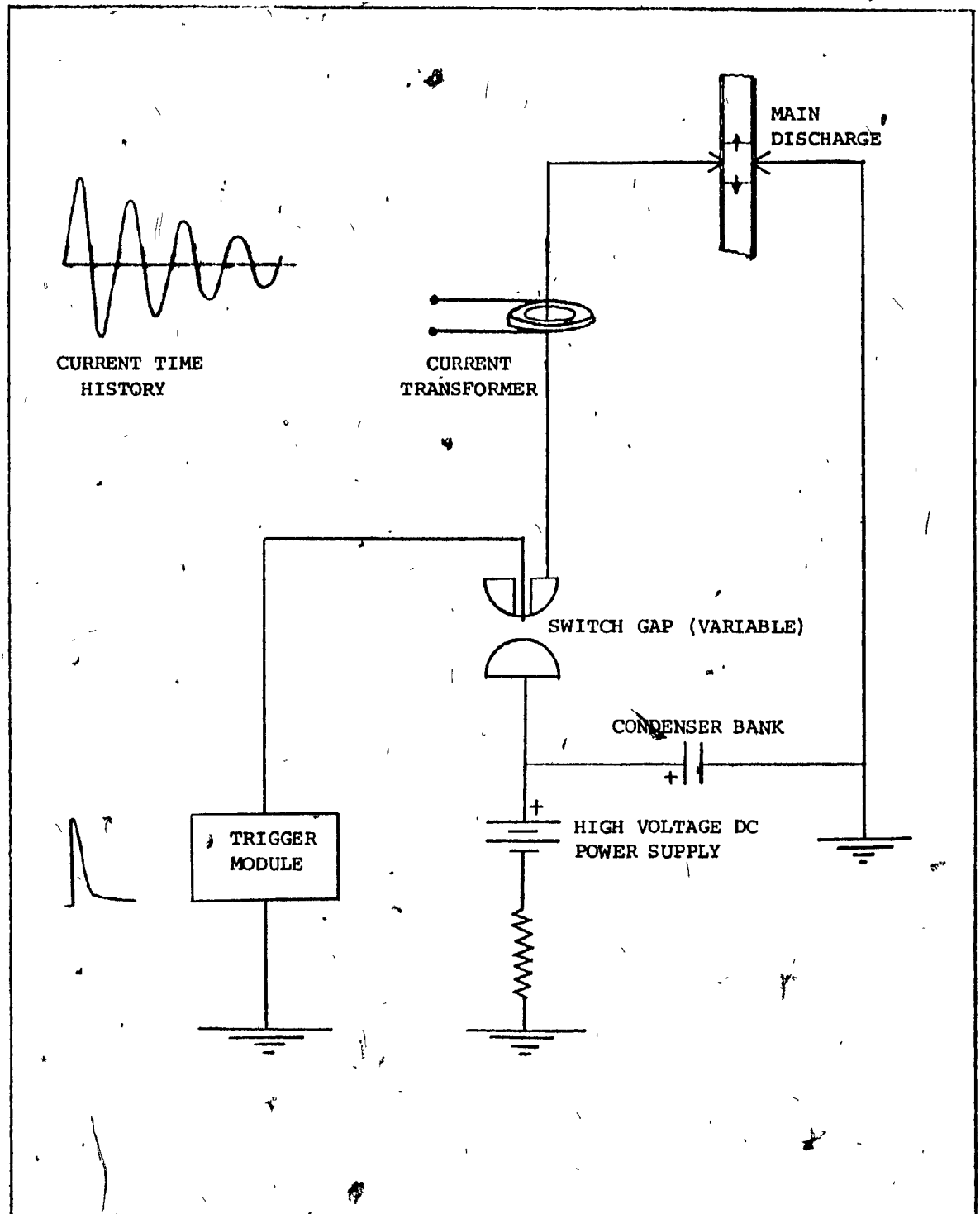
FIG. 48.   SKETCH OF THE ELECTRICAL DISCHARGE CIRCUIT
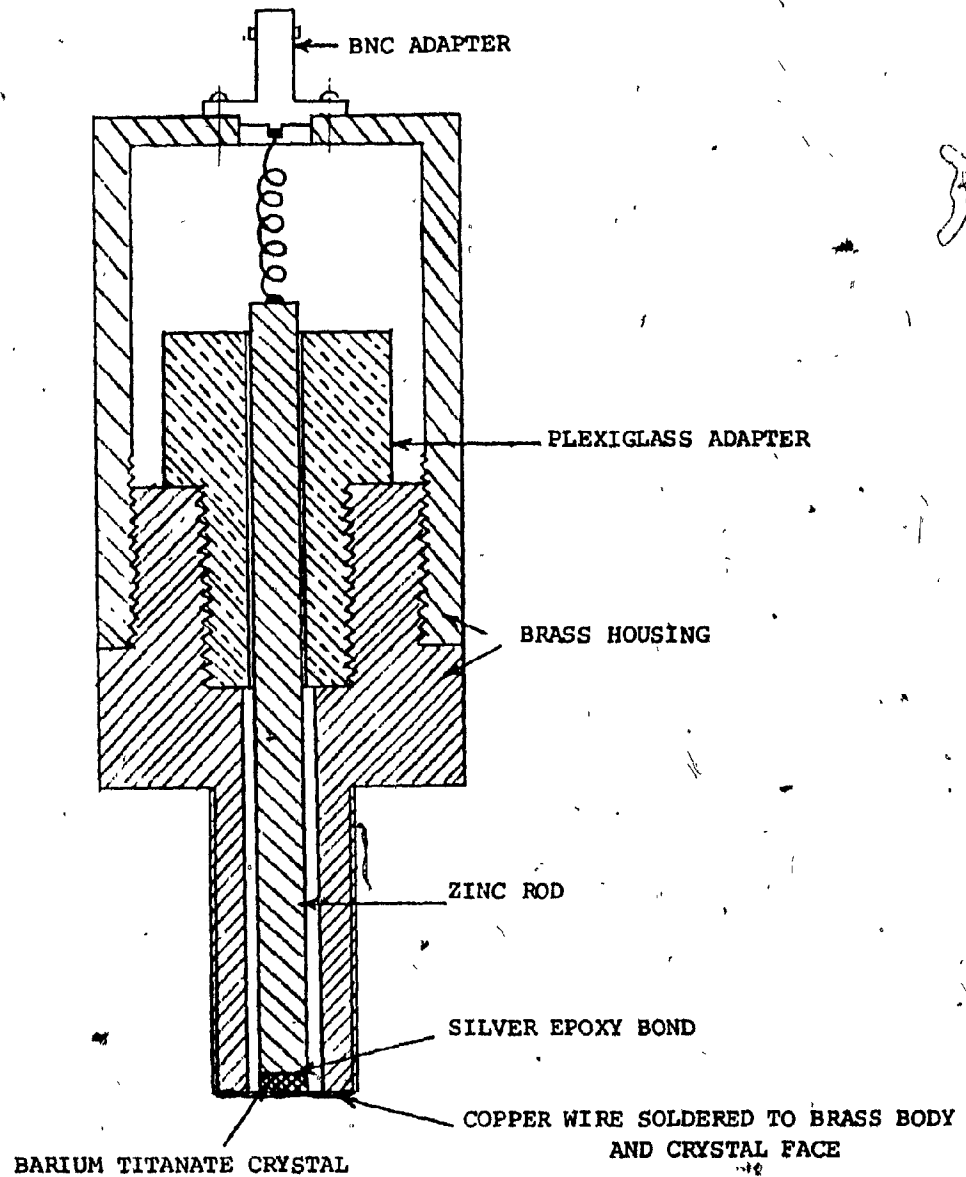
FIG. 49. SKETCH SHOWING THE CONSTRUCTION OF THE
          BARIUM TITANATE PRESSURE TRANSDUCER
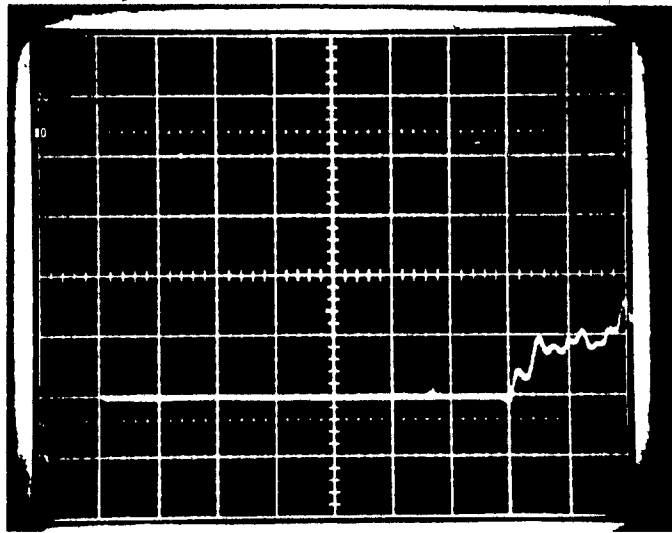
a. SMALL INCREASE IN PRESSURE ASSOCIATED WITH A DEFLAGRATION
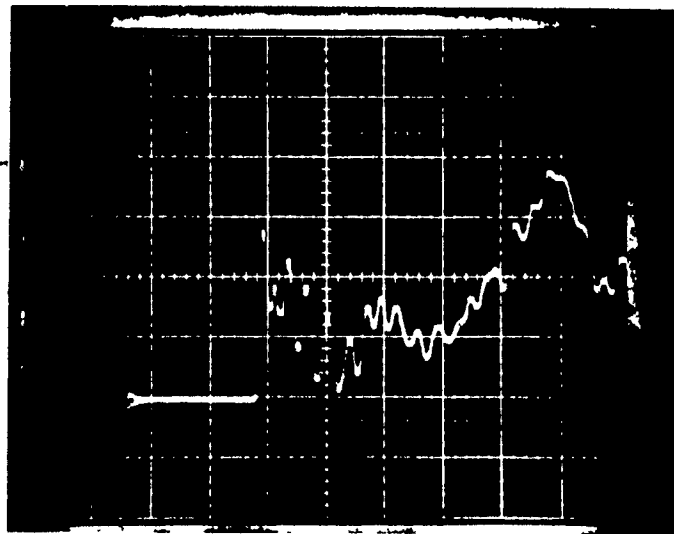
b. SPONTANEOUS AND RAPID INCREASE IN PRESSURE WITH
   A DETONATION

FIG. 50. IDENTIFICATION OF DETONATION ON THE BASIS OF TIME OF ARRIVAL
         AND PRESSURE PROFILE
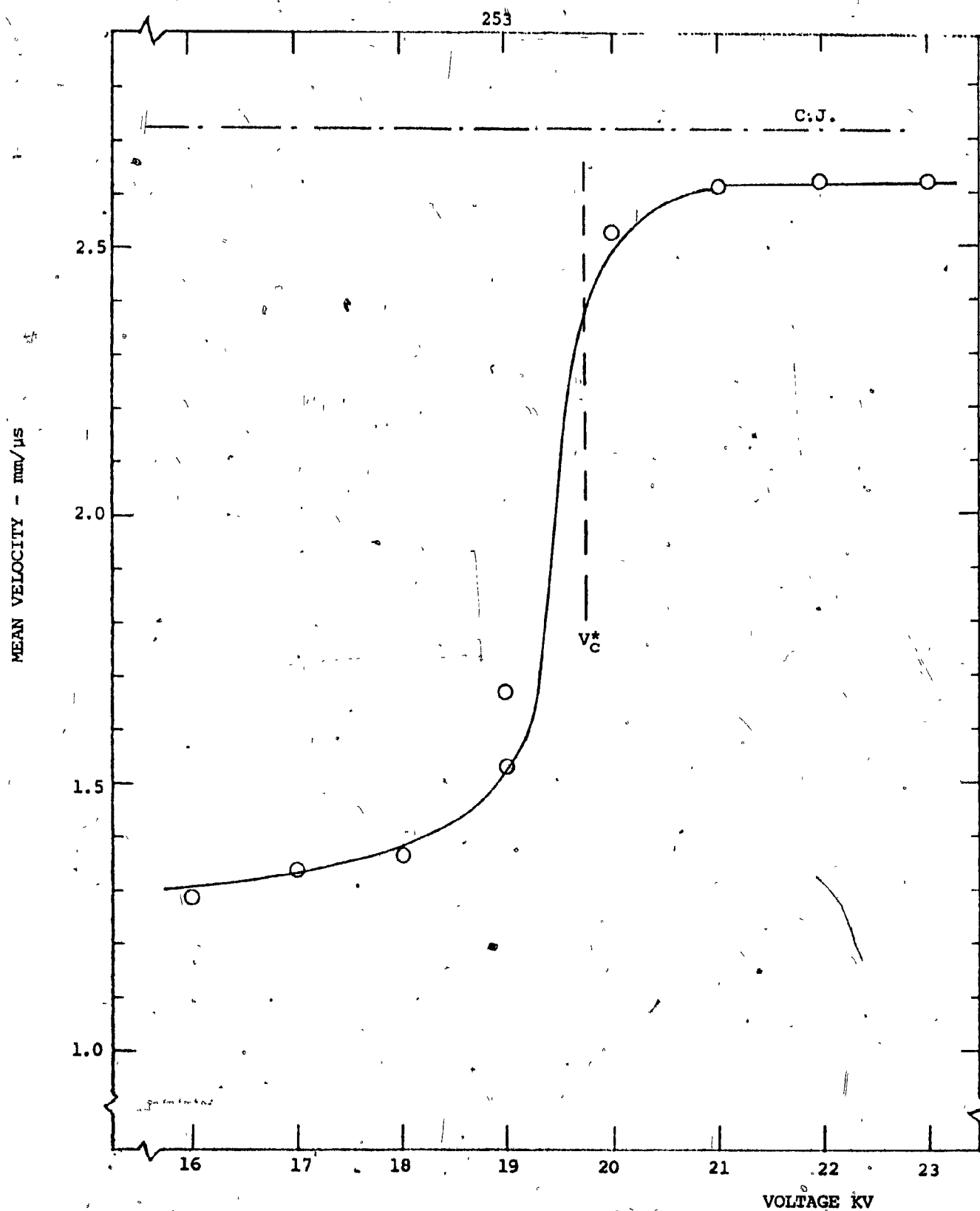
FIG. 51.   IDENTIFICATION OF DETONATION FROM THE MEAN VELOCITY OF THE WAVE
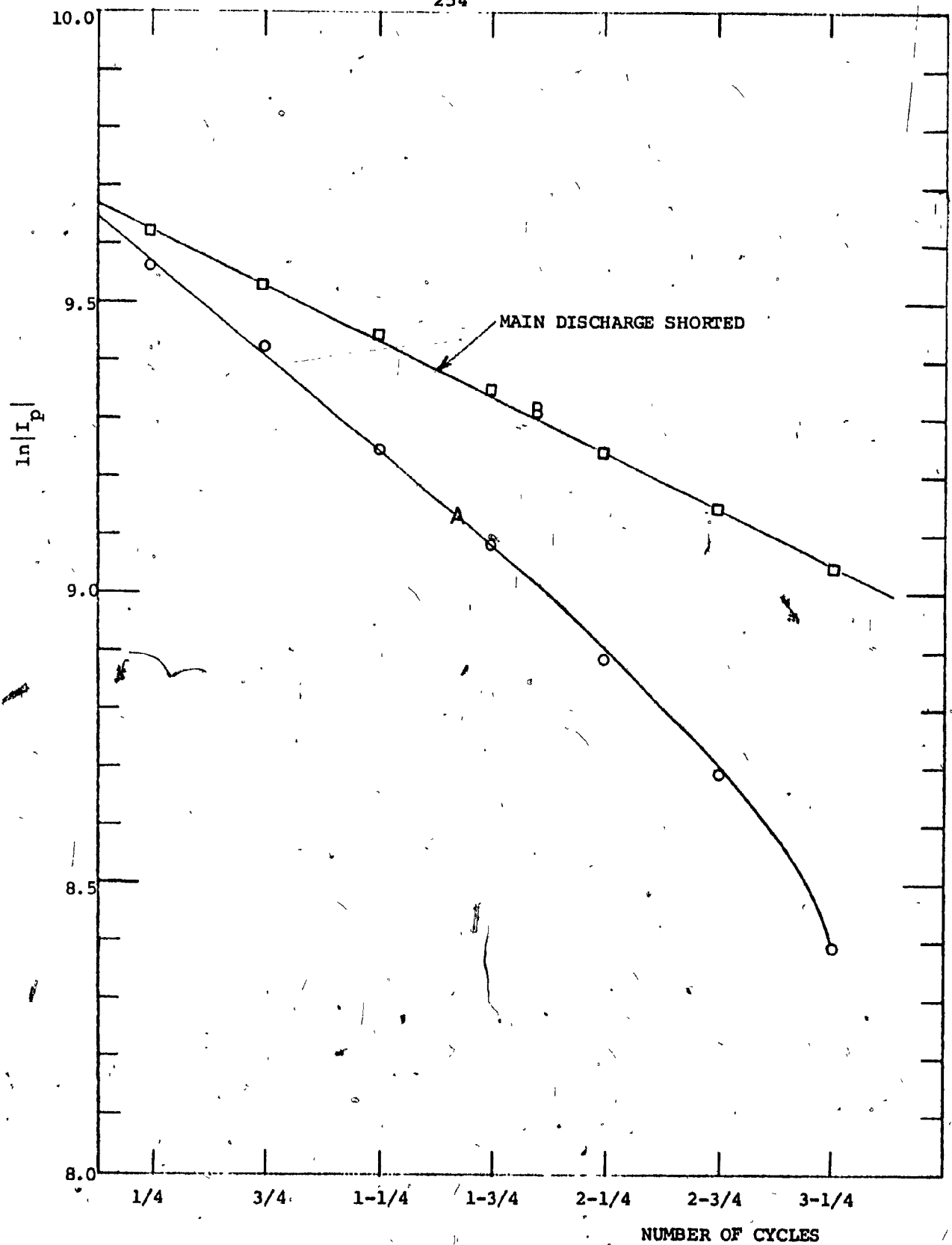
FIG. 52.   DETERMINATION OF THE RESISTANCE OF THE ELECTRICAL SPARK
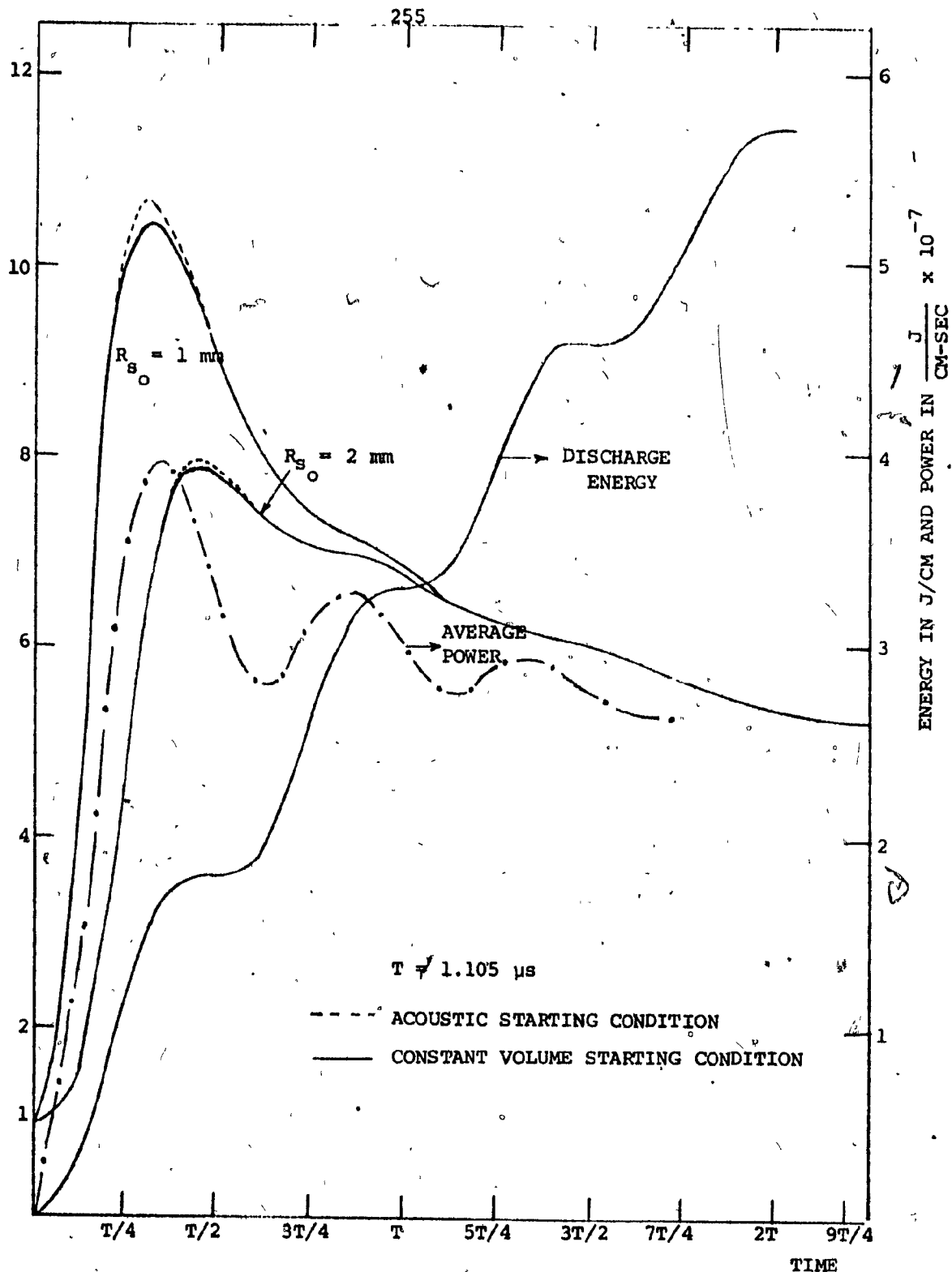
FIG. 53. VARIATION OF SHOCK MACH NUMBER WITH TIME FOR AN
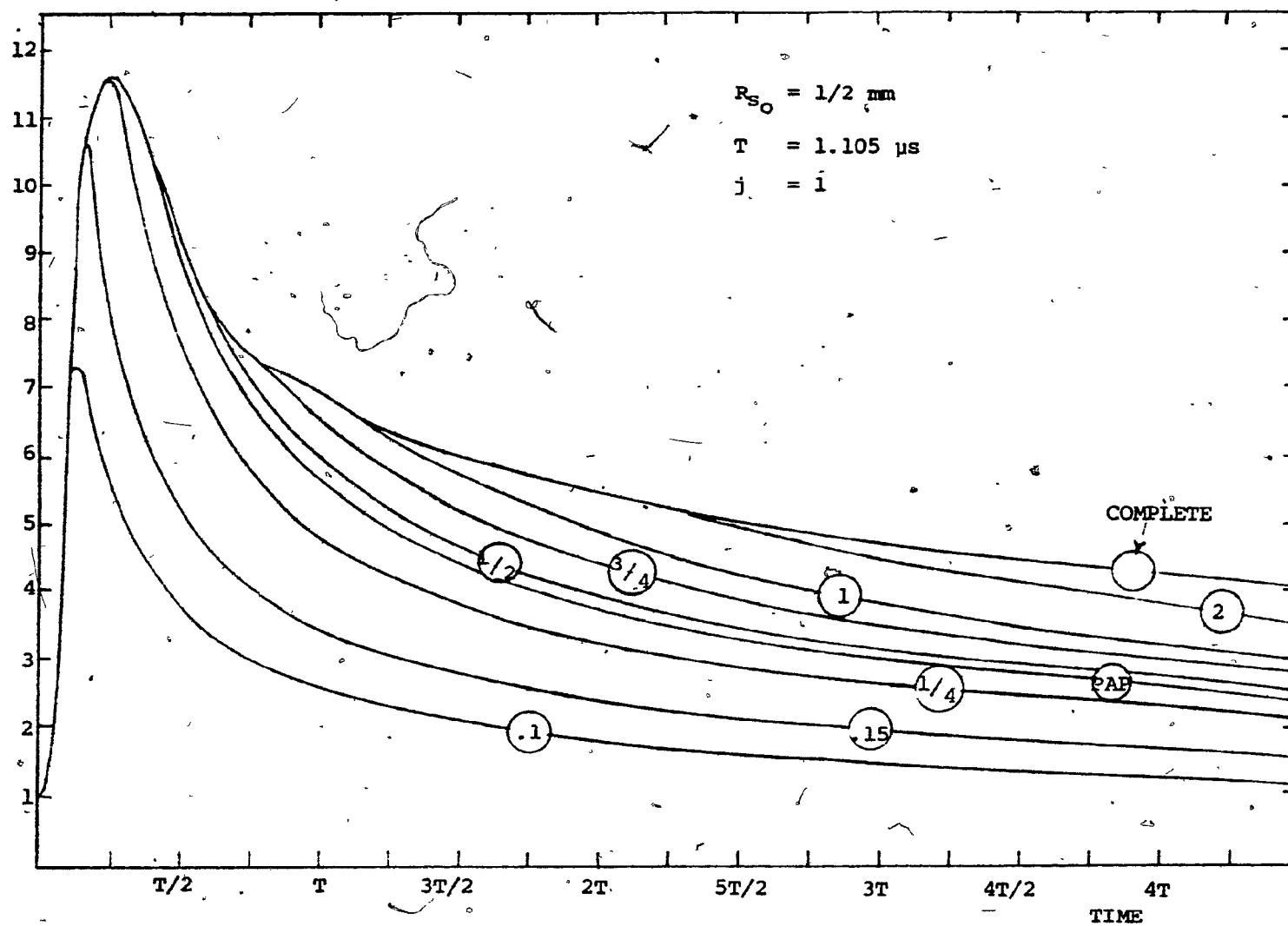OSCILLATORY ELECTRICAL DISCHARGE IN CYLINDRICAL
GEOMETRY

FIG. 54. EFFECT OF TRUNCATING THE DISCHARGE AT VARIOUS TIMES
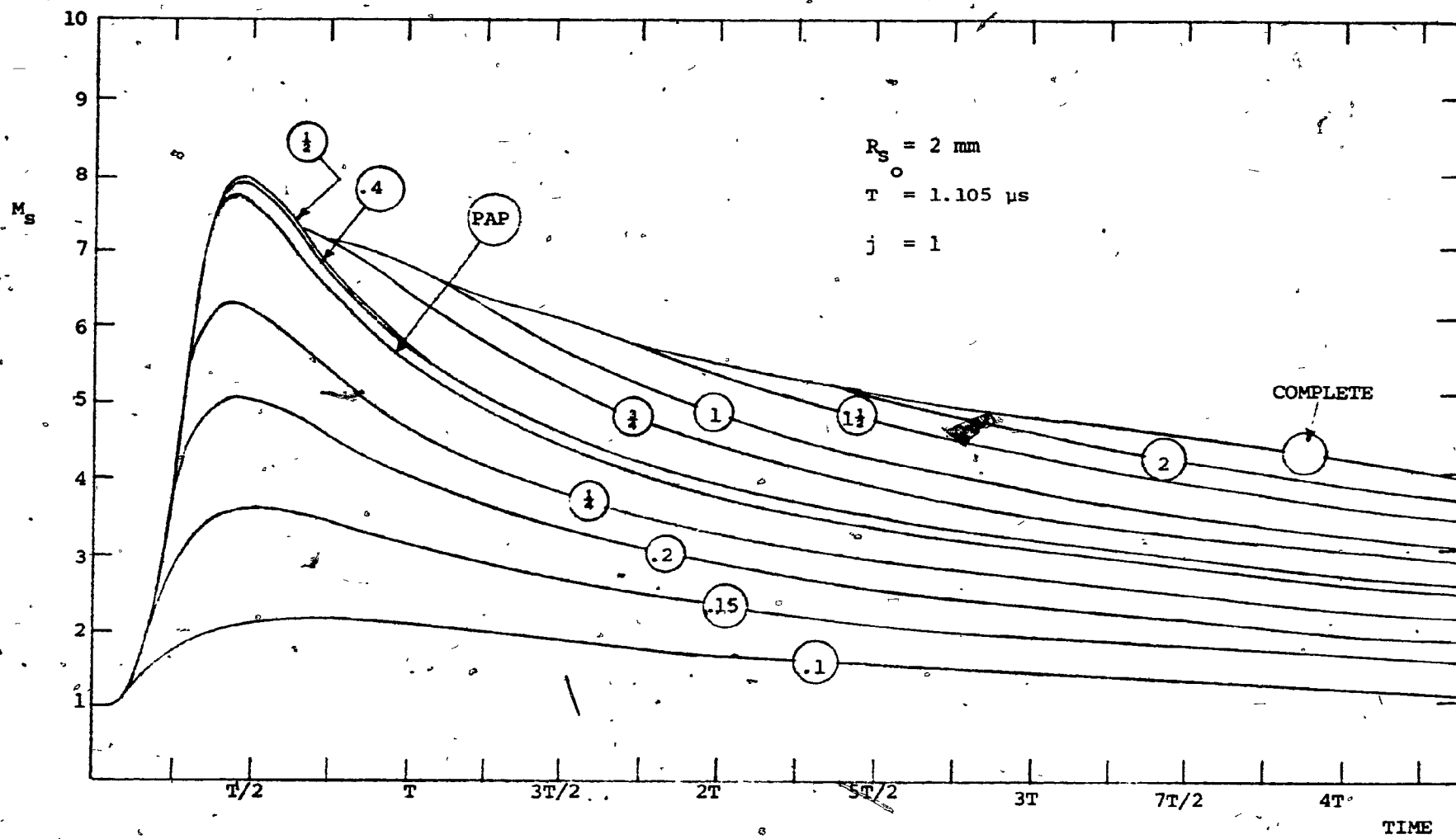
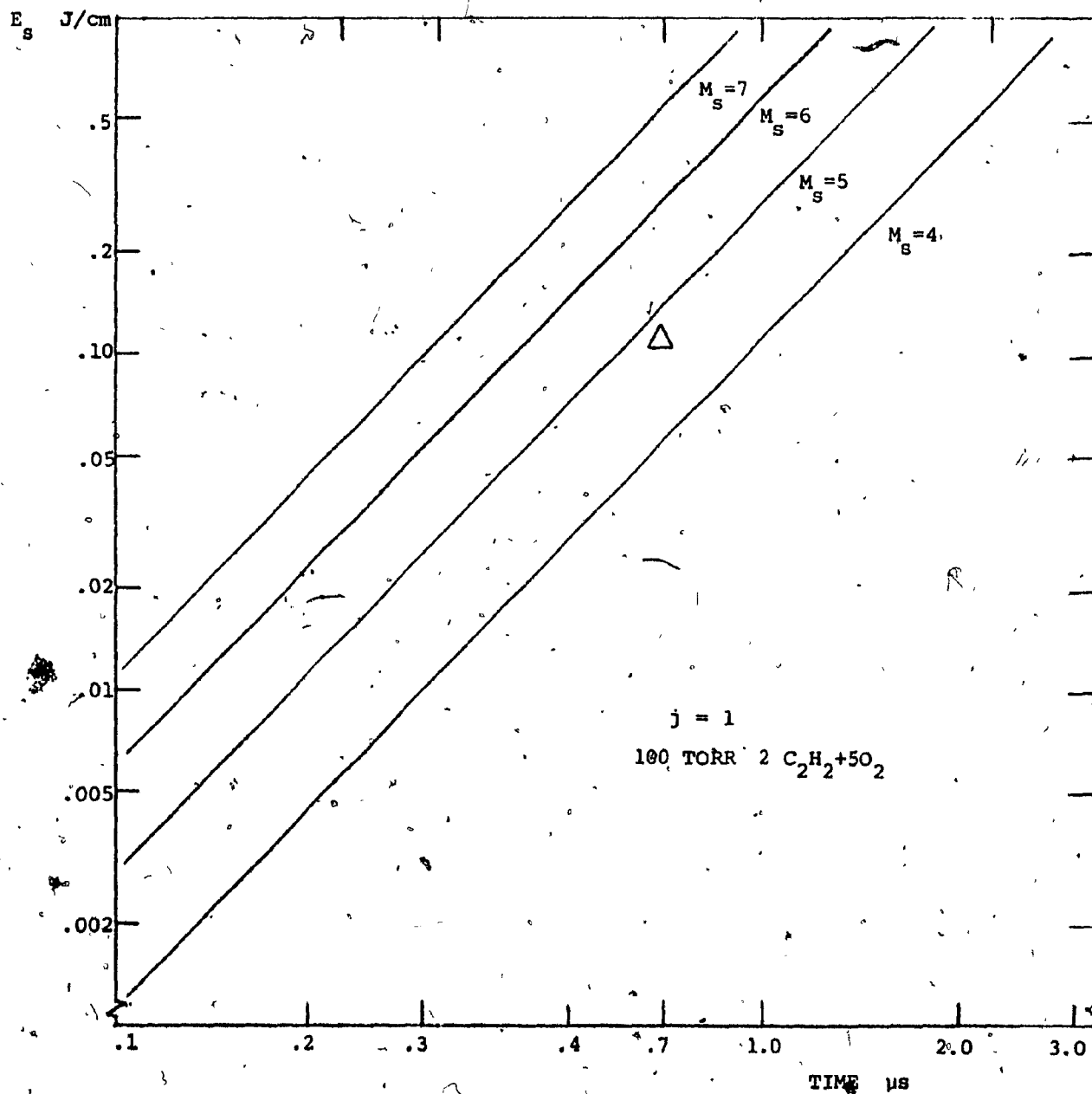FIG. 55. EFFECT OF TRUNCATING THE DISCHARGE AT VARIOUS TIMES

FIG. 56.   ESTIMATION OF MINIMUM SHOCK STRENGTH FROM THE MINIMUM
POWER REQUIREMENT